PHENOMENOLOGICAL STUDY OF SUBSONIC TURBULENT FLOW OVER A SWEPT REARWARD-FACING STEP

by

Gregory Vincent Selby

PHENOMENOLOGICAL STUDY OF SUBSONIC TURBULENT FLOW OVER A SWEPT REARWARD-FACING STEP

By

Gregory Vincent Selby

A dissertation submitted to the Faculty of the University of Delaware in partial fulfillment of the requirements for the degree of Doctor of Philosophy in Applied Science.

June, 1982

No. of Vols. (This Title) 1 of 3 | Cust. ☐ | Adh. ☐ | Standard ☐ | Spec ☐ | Job Ticket No. 17554

SIZE BOOK

"PLEASE CHECK"

COLOR NO: 990

BUCK

FABR.

RUB:

- NEW ☐
- ON FILE ☐
- ENCLOSED ☐
- SAMPLE ☐

COLLATE:

- INDEX FRONT ☐
- " BACK ☐
- " IN 2ND PART ☐
- " NOT REQ'D. ☐
- COVERS IN ☐
- " FRONT (ONLY) ☐
- COVERS OUT ☐
- ADS IN ☐
- ADS OUT ☐
- TEXT IN ADS ☐
- BIND ENTIRE ☐
- BIND INCOMP. ☐

STAMPING:

- HORIZONTAL XXX
- VERTICAL ☐
- GOLD XXXX
- WHITE ☐
- BLACK ☐

H & T LINES: YES ☐ NO ☒

IMPRINTS: YES ☐ NO ☒

LETTER AS FOLLOWS (EXACT LINE UP)

PHENOMENOLOGICAL STUDY
OF SUBSONIC TURBULENT
FLOW OVER A SWEPT REARWARD
FACING STEP

BY
GREGORY VINCENT SELBY

SPECIAL INSTRUCTIONS:
STAMP ON FRONT COVER

NAME OF LIBRARY:
NASA #115

SEND TO STAMPING

PHENOMENOLOGICAL STUDY OF SUBSONIC TURBULENT

FLOW OVER A SWEPT REARWARD-FACING STEP

By

Gregory Vincent Selby

Approved: _____

J. E. Danberg, Ph.D.
Professor in charge of dissertation on behalf of the Advisory Committee

Approved: _____

F. A. Kulacki, Ph.D.
Chairman of Department of Mechanical and Aerospace Engineering

Approved: _____

J. R. Vinson, Ph.D.
Chairman of the Applied Sciences Committee

Approved: _____

I. G. Greenfield, Ph.D.
Dean of College of Engineering

Approved: _____

R. B. Murray, Ph.D.
University Coordinator for Graduate Studies

ACKNOWLEDGEMENT

I am deeply indebted to Mr. Dennis M. Bushnell, Head, Viscous Flow Branch, NASA Langley Research Center and my present supervisor, who assisted me in all stages of the present research. I am also extremely grateful for the general guidance received from Dr. James E. Danberg, my dissertation advisor, who has superbly and successfully "led me through the maze."

I would like to acknowledge the invaluable support received from personnel in NASA Langley Research Center's Viscous Flow Branch, especially Mrs. Carolyn V. Snead for her expert general secretarial assistance, Ms. Jodi S. Rogers for efficiently typing the rough draft, Dr. Leonard M. Weinstein for his inventive genius and Mr. J. Ben Anders for generous general technical assistance. My gratitude is also expressed to Mr. Floyd D. Backley of the Advanced Machining Development Section for his conscientious supervision of model fabrication and to personnel of Technical Support Section C (Mr. Thomas L. Smith, group leader) for their skillful technical support.

I wish to thank my wife, Barbara, and older son, Gregory II (Vinny), for their patience and moral support - especially during these last few months. Though my second son, Gevell (Van), is not old enough now (11 months) to share this experience, it is my prayer that

my life and achievements will provide him with a positive role model. Hopefully, Vinny and Van will come to realize that "no mountain is too high to climb."

I am grateful to my parents, Mr. Hilbert C. and Mrs. Hattie N. Selby, who made many personal sacrifices for the benefit of their four children. Though hot dogs and beans became the "Selby Saturday Special," I didn't mind eating this meal on Monday, Tuesday and Wednesday nights also, that we might have enough money for other meaningful pursuits.

Finally, I thank my Heavenly Father through His Son, Jesus Christ, for all that I am and ever hope to be. It is through them that I have learned to patiently endure all things confronting me in this present life and gain hope for a life to come. I pray that my Father will continue to use me to convince others that the universe displays evidence of an intelligent Architect and Engineer - the omnificent, omnipresent, omniscient God of Heaven, who is solely responsible for instituting the complex laws of nature that scientists labor to elementarily understand. With His help I have endeavored to phenomenologically investigate three-dimensional separated flows and use any knowledge gained to the benefit - not detriment - of man.

TABLE OF CONTENTS

LIST OF FIGURES

ABSTRACT

This paper presents a phenomenological study of turbulent, subsonic flow over a swept, rearward-facing step. Effects of variations in step height, sweep angle, base geometry and end conditions on the 3-D separated flow were examined. The separated flow was visualized using smoke wire, oil drop and surface tuft techniques. Measurements include surface pressure, reattachment distance and swirl angle. Results indicate: (1) model/test section coupling affects the structure of the separated flow, but spanwise end conditions do not; (2) the Independence Prinicple is evidently valid for sweep angles up to 38^{o}; (3) a sweep angle/swirl angle correlation exists and (4) base modifications can significantly reduce the reattachment distance.

NOMENCLATURE

Ar	area ratio defined as ratio of area downstream of step to upstream area
AR	aspect ratio defined as ratio of model span to step height
C_p	pressure coefficient, $C_p \equiv (P - P_{ref})/\frac{1}{2}\rho V_\infty^2$
C_p[B-C]	Broda-Carnot pressure coefficient defined by $C_p[B\text{-}C] \equiv 2/Ar(1 - 1/Ar)$
C_p[base]	base C_p
C_p[max]	maximum midspan C_p
C_p[min]	minimum midspan C_p
ΔC_p	defined by $\Delta C_p \equiv C_p - C_p[min]$
ΔC_p[max]	defined by $\Delta C_p[max] \equiv C_p[max] - C_p[min]$
C_p^*	defined by $C_p^* \equiv \Delta C_p/(C_p[B\text{-}C] - C_p[min])$
C_p^{**}	defined by $C_p^{**} \equiv (\Delta C_p/\cos\Lambda + 1.274)/Ar$
C_p^+	defined by $C_p^+ \equiv \Delta C_p/\cos\Lambda$
C_p'	defined by $C_p' \equiv \Delta C_p/(1 - C_p[min])$
C_p''	defined by $C_p'' \equiv \Delta C_p/\Delta C_p[max]$
h	step height
h_w	height of smoke wire above model surface
l_w	streamwise distance (in X-direction) of smoke wire from model base
L	streamwise distance (in X-direction) from leading edge at midspan

L_a	spanwise distance (in Y'-direction) to asymptotic value of R' (Figure 37)
P	static pressure
R	reattachment distance in X-direction (Figure 37)
R'	reattachment distance in X'-direction (Figure 37)
Re	Reynolds number, $Re \equiv V_\infty L_{sep}/\nu$
Re_θ	momentum Reynolds number, $Re_\theta \equiv V_\infty \theta/\nu$
t	thickness of model at base (= .5" for LE1, = 1" for LE2)
u	streamwise component of flow velocity
u^+	defined by $u^+ \equiv u/v^*$
v^*	defined by $v^* \equiv \sqrt{\tau_w/\rho}$
V_∞	freestream velocity
X	coordinate in streamwise direction (Figure 37)
X'	coordinate normal to step (Figure 37)
y	distance normal to model surface
y^+	defined by $y^+ \equiv yv^*/\nu$
Y	coordinate normal to streamwise direction (Figure 37)
Y'	coordinate parallel to step (Figure 37)
Z'	distance in base plane normal to top edge
α	component of flow angle in vertical plane (Figure 16)
β	component of flow angle in horizontal plane (Figure 16)
β'	slant angle at base of bluff body
δ	boundary-layer thickness
δ^*	displacement thickness
θ	momentum thickness
θ'	total flow angle

Λ	sweep angle (Figure 37)
ν	kinematic viscosity
ρ	density
τ_w	wall shear stress
ϕ	swirl angle (Figure C1)

Subscripts

crit	critical value
ref	reference value
sep	value at the location of flow separation

1.0. INTRODUCTION

1.1. Background

Many problems encountered in flight vehicle design and development, as well as design problems in several other engineering disciplines, involve flow separation. Examples of separated flows of interest in the subsonic flow regime are: the flow ahead of deflected control surfaces, the flow over airfoils and bodies of revolution at high angles of attack, the flow behind bluff bodies and the flow over forward- and rearward-facing steps. An additional consideration is that most turbulent shear flows contain three-dimensional effects. The separation of three-dimensional turbulent boundary layers, e.g., from the lee side of a flight vehicle at high angle of attack, often results in dominant, large-scale vortex flow systems that generally move in the freestream direction. [See Howe (1968) and Peake and Tobak (1982).]

Much information presently exists for separated flows dominated by three-dimensional effects. For example, Peake and

---

Howe, John T., Some Fluid Mechanical Problems Related to Subsonic and Supersonic Aircraft, NASA SP-183, 1968.

Peake, D. J. and Tobak, M., Three-Dimensional Separation and Reattachment, AGARD Lecture Series No. 121 on High Angle-of-Attack Aerodynamics, Paper #1, NASA Langley Research Center, 10-11 March 1982.

Tobak (1980) discussed three-dimensional vortical flow structures shed by diverse lifting aerodynamic configurations immersed in flows from subsonic to hypersonic speeds. They applied simple topology laws to surface skin-friction lines obtained from oil flow patterns in order to deduce mean characteristics and structures of complex three-dimensional flows. While most "practical" separated flows are highly three-dimensional, research studies of separated flows generally consider only two-dimensional geometries. Between these two extremes of separated flows - two-dimensional and fully three-dimensional with complex vortical structures - there exist flows which are neither two-dimensional, nor completely vortex dominated, but which are worthy of investigation, e.g., turbulent, subsonic flow over a swept, rearward-facing step. Flow over rearward-facing step geometries is of considerable importance in several branches of engineering. Examples include:

(1) the flow of air over spanwise joints on airfoils and launch vehicles;

(2) flow in channels with a sudden enlargement;

(3) wind flow around buildings and

(4) the flow of water over an excrescence (roughness element) on the surface of a submarine.

Often, swept surface roughness elements are encountered in practice - as on the surface of swept airfoils and fins. The swept

---

Peake, D. J. and Tobak, M., Three-Dimensional Interations and Vortical Flows With Emphasis on High Speeds, NASA TM-81169, March 1980.

rearward-facing step may be included in this category. Data presented by Young and Patterson (1981) for gap drag show a tremendous (uncorrelated) variation due to sweep angle. Typical pressure drag data obtained by Czarnecki (1966) for a single 45° swept roughness element disagrees markedly with theory. Such swept excrescences can make significant contributions to aircraft drag.

Swept excrescences are also encountered on automobiles. The A-pillar (the windshield-sideglass junction) is one example. [See Hucho (1978).] Carr (1969, 1973) determined that the various protuberances and cavities essential to a practical ground vehicle increase overall drag by approximately 10%.

During the development of the wings for the Lockheed C-5A Galaxy, it was discovered on the final configuration that the flap-track

---

Young, A. D. and Patterson, J. H., Aircraft Excrescence Drag, AGARDograph No. 264, 1981.

Czarnecki, K. R., "The Problem of Roughness Drag at Supersonic Speeds," Conference on Aircraft Aerodynamics, NASA Langley Research Center, 23-25 May, 1966, pp. 455-468.

Hucho, W. "The Aerodynamic Drag of Cars - Current Understanding, Unresolved Problems and Future Prospects," Aerodynamic Drag Mechanisms of Bluff Bodies and Road Vehicles, Plenum Press, 1978, pp. 7-44.

Carr, G. W., "The Study of Road Vehicle Aerodynamics Using Wind Tunnel Models," Proceedings of Symposium on Road Vehicle Aerodynamics, City University, London, Paper 14.

Carr, G. W., "Aerodynamic Lift Characteristics of Cars," Proc. I. Mech. E., Vol. 187 30/73, p. 333.

fairings improved the wing drag characteristics [Patterson (1968)] - wind tunnel data indicated that the wing with fairings produced a four to six count reduction in drag relative to the clean wing.

The oil flow photographs presented in Figure 1 for flow over the upper surface of a C-5A wing (swept lifting surface) give some indication of the presence of a spanwise vortex in the three-dimensional separated-flow region at the trailing edge. This vortex is probably produced by the skewness of the velocity profile at the trailing edge resulting from the differences in the pressure distribution on the upper and lower surfaces of the wing and may be attenuated by the flap-track fairings. Young and Patterson (1981) have suggested that there is a need for systematic experimental studies on the effects of excrescences in three-dimensional flows involving large sweep angles.

These studies and experiences indicate a need for studies of the genesis and possible attenuation and control of spanwise (vortex?) flow. Along with pressure drag minimization, results of such studies could be practically applied to the design of lifting surfaces in order to optimize the effect of spanwise flow control on wing drag due to lift.

Patterson, J. H., "Aerodynamic Design Features of the C-5A," Aircraft Engineering, June Issue, pp. 8-15, 1968.

Figure 1.

EFFECT OF FLAP-TRACK FAIRINGS ON FLOW
OVER UPPER SURFACE OF C-5A WING

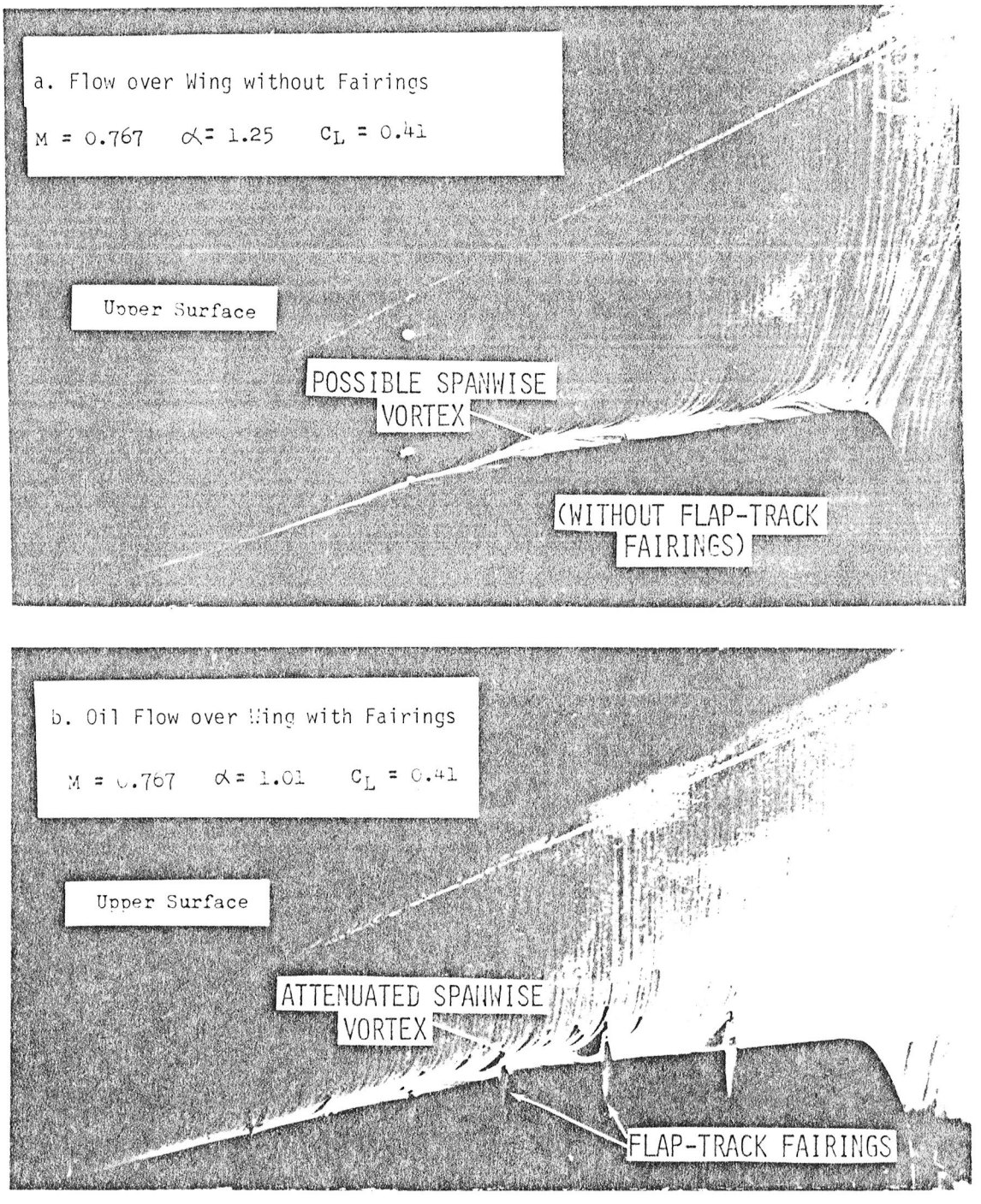

A considerable amount of information is available on the unswept rearward-facing step geometry - as the following literature review indicates.

1.2. Literature Review

Recent reviews of research on subsonic unswept rearward-facing step flows were performed by Eaton and Johnston (1980) and Bradshaw and Wong (1972). No mention was made in either review of swept rearward-facing step experiments.

Eaton and Johnston (1980) have indicated that the reasons for the proliferation of research in the area of two-dimensional rearward-facing step flow are:

(1) among two-dimensional flows, the rearward-facing step is the simplest reattaching flow;

(2) the separation line is straight and fixed at the edge of the step;

(3) there is only one primary separated zone, instead of two, as in the flow over an obstacle and

(4) the streamlines are nearly parallel to the wall at the separation point.

Eaton J. K. and Johnston, J. P., A Review of Research on Subsonic Turbulent Flow Reattachment, AIAA 13th Fluid and Plasma Dynamics Conference, 14-16 July, Snowmass, Colorado, AIAA 80-1438, 1980.

Bradshaw, P. and Wong, F. Y. F., "The Reattachment and Relaxation of a Turbulent Shear Layer," Journal of Fluid Mechanics, Volume 52, Part I, pp. 113-135, 1972.

These comments generally apply to the three-dimensional (or swept) rearward-facing step flow also. In the previous unswept rearward-facing step studies, five main parameters were typically varied:

(1) initial boundary-layer state,

(2) initial boundary-layer thickness,

(3) free-stream turbulence level,

(4) streamwise pressure gradient in the reattachment zone and

(5) step aspect ratio.

Additional aspects of two-dimensional rearward facing step flows have also been examined. Kim, Kline and Johnston (1979) investigated the flow characteristics in the relaxation region downstream of reattachment. Mullin, Greated and Grant (1980) studied pulsating flow over a step. Kangovi and Page (1978) conducted an experiment for flow past an annular step. Abbott and Kline (1962) experimentally investigated flow

---

Kim, J., Kline, S. J. and Johnston, J. P., "Investigation of a Reattaching Turbulent Shear Layer: Flow Over a Backward-Facing Step," Proceedings of the Winter Annual Meeting, American Society of Mechanical Engineers, pp. 41-48, 1979.

Mullin, T., Greated, C. A. and Grant, I., "Pulsating Flow Over a Step," The Physics of Fluids, Vol. 23, No. 4, pp. 669-674, 1980.

Kangovi, S. and Page, R. H., "Subsonic Turbulent Flow Past a Downstream Facing Annular Step," Proceedings of the Winter Annual Meeting, American Society of Mechanical Engineers, No. 78-WA/FE15, 1978.

Abbott, D. E. and Kline, S. J., "Experimental Investigation of Subsonic Turbulent Flow Over Single and Double Backward Facing Steps," Journal of Basic Engineering, No. 9, pp. 317-325, 1962.

over double steps, and Nice, Tseng and Moses (1965) examined flow over a curved step. These are only a few examples of the diversity of flow conditions studied during the past two decades in the area of two-dimensional, subsonic, turbulent, rearward-facing step flow.

Researchers usually employ the same basic theoretical model for two-dimensional, backward-facing-step flow. However, a few conceptual differences exist regarding detailed aspects of the flow. [See, for example, Bradshaw and Wong (1972), Crawford (1967), Eaton and Johnston (1980), Aung and Goldstein (1972) and Ram and Wauschkuhn (1975).]

The flow model shown in Figure 2(a) is the one generally accepted. Turbulent, two-dimensional, subsonic, boundary-layer flow is shown approaching a rearward-facing step. The fluid is unable to negotiate the sharp corner and therefore separates from the surface, splitting into the two regions shown. Part of the fluid is entrained

---

Nice, G. R., Tseng, W. and Moses, H. L., Separation of Turbulent, Incompressible Flow From a Curved, Backward-Facing Step, Gas Turbine Laboratory, Massachusetts Institute of Technology, Report No. 87, 1965.

Crawford, D. R., Supersonic Separated Flow Downstream of a Backward-Facing Step, Ph.D. Dissertation, University of California at Berkeley, University Microfilms, Inc., Ann Arbor, Michigan, 1967.

Aung, W. and Goldstein, R. J., "Heat Transfer in Turbulent Separated Flow Downstream of a Rearward-Facing Step," Israel Journal of Technology, Vol. 10, No. 1-2, pp. 35-41, 1972.

Ram, V. V. and Wauschkuhn, P., "Turbulent Flow Connected with Separation and Reattachment," Boundary Layer Effects: Proceedings of the Fourth Data Exchange Agreement Meeting, Gottingen, West Germany, 2-3 June, pp. 96-103, 1975.

a. General Model

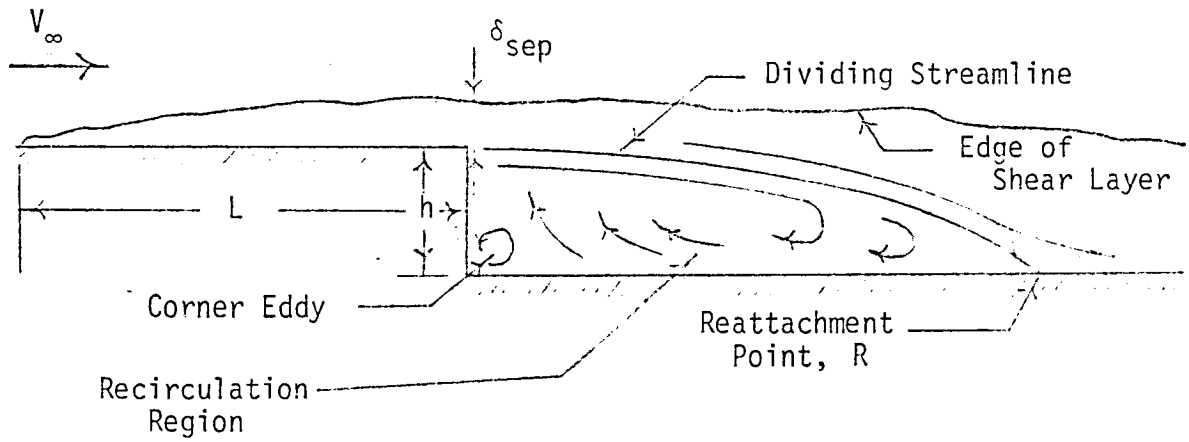

b. Axial Velocity Distribution

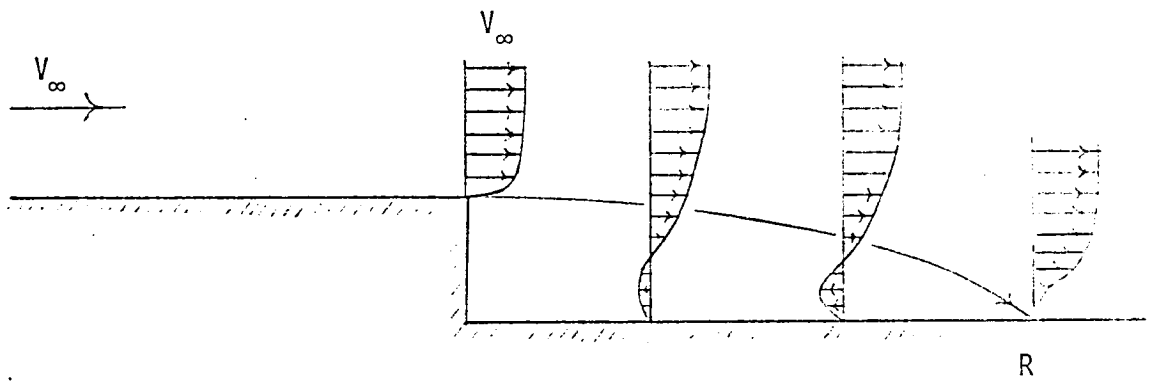

Figure 2. Flow With Separation Past a Rearward-Facing Step

by the recirculating flow near the step. The remaining fluid continues downstream—forming a separated shear layer. The streamline that separates the two flow regions is called the dividing streamline. The separated shear layer curves sharply downwards several step heights downstream of the step and reattaches to the downstream surface. Eaton and Johnston (1980) have stated that the length of the separation region fluctuates so that the reattachment point of the shear layer moves up and downstream. They also mentioned that the maximum measured backflow velocity in the separated-flow region is approximately 20% of the freestream velocity, so that this region cannot be accurately called a dead-air region. In addition to the primary stationary vortex in the separated-flow region, a secondary stationary vortex exists in the corner between the step wall and the downstream surface. This has been labeled "corner eddy" in Figure 2(a). Figure 2(b) qualitatively illustrates the axial velocity distribution [Aung and Goldstein (1972)].

Bradshaw and Wong (1972) have defined three strengths of perturbations to a boundary layer based on the ratio of the step height, h, to the boundary layer thickness at separation, δ_{sep}.

(1) A weak perturbation, in which the velocity and length scales of the flow are altered without significant change in the dimensionless properties of the turbulence structure, such as the ratio of one intensity component to another, $(h/\delta \ll 1)$.

(2) A strong perturbation, in which the turbulence structure is significantly altered but the flow is recognizable throughout as a perturbed form of a specific kind of shear layer. An example is a boundary layer flowing over a cavity only a few boundary-layer thicknesses in length in the streamwise direction ($h/\delta = O(1)$).

(3) An overwhelming perturbation, in which the shear layer changes to one of a different species, as in the mutation of a boundary layer into a wake or mixing layer ($h/\delta >> 1$).

In the subject research program, h/δ_{sep} was varied between 0.1 and 1.2.

One interesting feature of two-dimensional flow over a rearward-facing step is the existence of longitudinal vortices. This phenomenon has received considerable attention in recent years. Kasagi, Hirata and Hiraoka (1977) confirmed the presence of longitudinal, vortex-like structures in the reattaching region and in the region just behind a two-dimensional step in subsonic, turbulent flow. They visually analyzed instantaneous photographic records of the flow using the smoke-wire technique. Rockwell and Knisely (1980) examined

---

Kasagi, N., Hirata, M. and Hiraoka, H., Large-Eddy Structures in Turbulent, Separated Flow Downstream of a Rearward-Facing Step, Symposium on Turbulent Shear Flows, University Park, Pennsylvania, 18-20 April 1977.

Rockwell, D. and Knisely, C., "Observations of the Three-Dimensional Nature of Unstable Flow Past a Cavity," The Physics of Fluids, Vol. 23, No. 3, pp. 425-431, 1980.

the spanwise structure of the free-shear layer along the periphery of a cavity in a water channel using the hydrogen bubble technique. During the time of Ginoux (1961) and Browand (1966), this question was unsettled, though Ginoux observed a regular pattern of three-dimensional perturbations at reattachment behind a two-dimensional step in supersonic flow. Roshko (1980) examined the periodic spanwise structure in a subsonic, turbulent mixing layer downstream of transition. Inger (1974) theoretically studied possible causes of the periodic spanwise disturbances that are observed in nominally two-dimensional reattaching laminar and turbulent separated flows. de Brederode and Bradshaw (1972) concluded that the longitudinal vortices were caused by pressure gradients arising from a nonstraight

---

Ginoux, J. J., Leading Edge Effect on Separated Supersonic Flows, Training Center for Experimental Aerodynamics, Belgium, Technical Note NR.4, May 1961.

Roshko, A., The Plane Mixing Layer-Flow Visualization Results and Three-Dimensional Effects, International Conference on the Role of Coherent Structures in Modelling Turbulence and Mixing, Madrid, Spain, 25-27 June, 1980.

Inger, G. R., Three-Dimensional Disturbances in Reattaching Separated Flows, Department of Aerospace and Ocean Engineering, Virginia Polytechnic Institute and State University, Blacksburg, Virginia, 1974.

Browand, F. K., "An Experimental Investigation of the Instability of an Incompressible, Separated Shear Layer," Journal of Fluid Mechanics, Vol. 26, Part 2, pp. 281-307, 1966.

de Brederode, V. and Bradshaw, P., Three-Dimensional Flow in Nominally Two-Dimensional Separation Bubbles-Flow Behind a Rearward-Facing Step, Imperial College of Science and Technology, I. C. Aero Report 72-19, 1972.

transition line and not from three-dimensional effects in the separation bubble itself. An alternate explanation is that the concavely curved streamlines near reattachment generate Gortler vortices. This additional feature of subsonic flow over a rearward-facing step is depicted in Figure 3.

To the best of the present author's knowledge, results of research relating to flow over a simple swept rearward-facing step have not yet been reported. It is therefore concluded that a detailed systematic study of the problem has not been undertaken up to the present time. However, flow visualization studies for subsonic flow over chevron-shaped rearward-facing steps have been made by Werle (1980) and Mirande and Quelin (1977). In addition, Billet (1980) has written a computer code to calculate the flow studied by Mirande and Quelin (1977). Presently, at least one study is being undertaken that relates more directly to the present research. Mirande and LeBalleur (ONERA) are currently studying reattachment behind a swept step (single sweep angle) of varying height (private communication).

Werle, H., "Transition and Separation - Visualizations in the ONERA Water Tunnel," LaRecherche Aerospatiale (English Edition), No. 5, pp. 35-49, 1980.

Mirande, J. et Quelin C., Analyse detailee de la structure d'un ecoulement tridimensionnel, Rapport Technique 07-1977, ONERA, 1977.

Billet, G., "Numerical Simulation of a Three-Dimensional Wall Separation," La Recherche Aerospatiale (English Edition), No. 4, pp. 11-23, 1980.

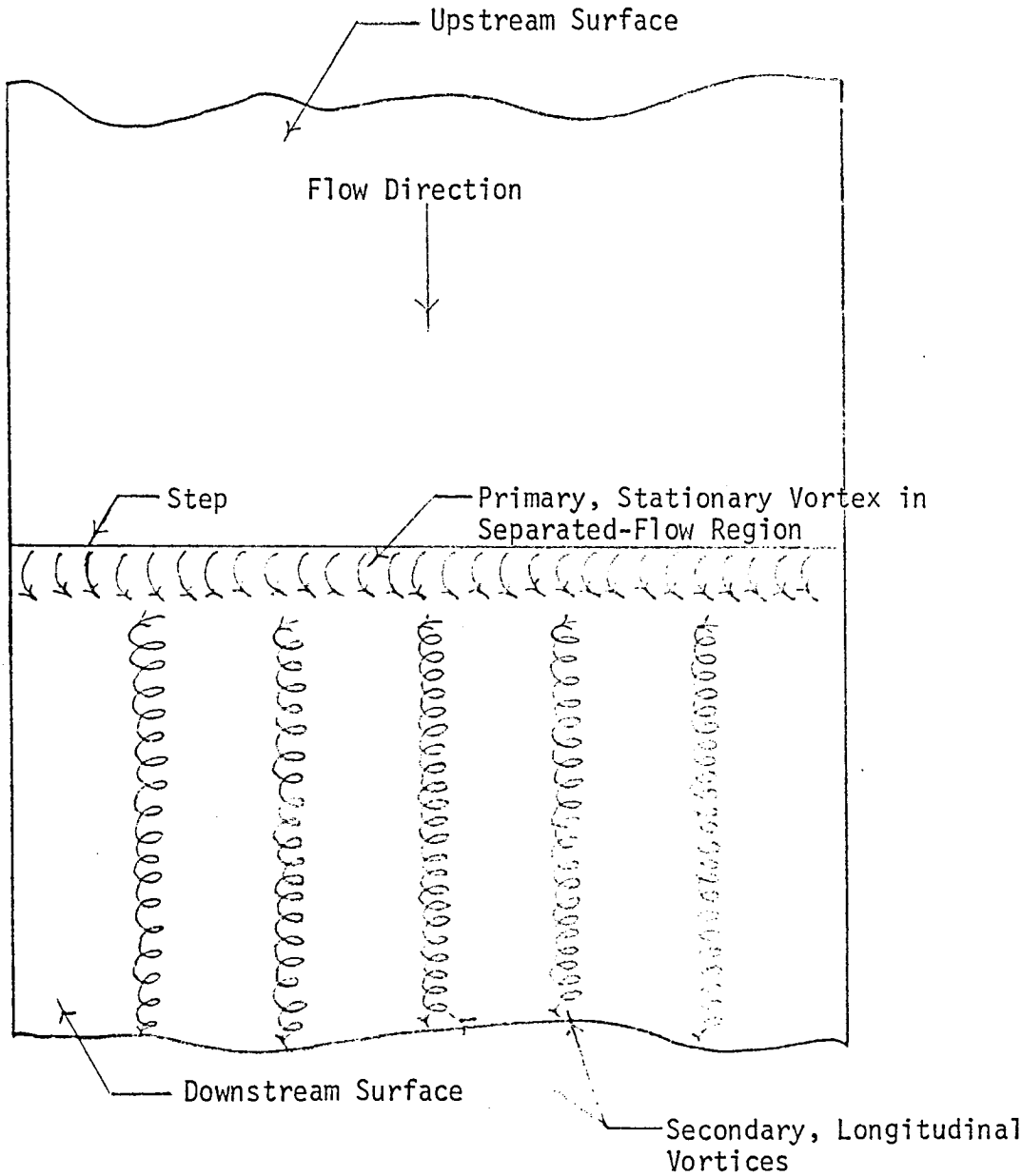

Figure 3. Subsonic Flow over a Rearward-Facing Step with Zero Sweep (Top View)

1.3. Research Objectives

The overall objective of the present research was to try to at least partially bridge the informational gap that exists between two-dimensional and fully three-dimensional, vortex-dominated separated flows by a phenomenological examination of sweep (or 3-D) effects on subsonic, turbulent flow over a rearward-facing step. Specifically, it was intended that the results of this research provide knowledge relative to:

(1) general flow physics in the three-dimensional separated-flow region, including the occurrence, characteristics and control of organized spanwise vorticity (spanwise vortices);
(2) three-dimensional shear-layer reattachment and
(3) the effect of base geometry on the three-dimensional separated flow and consequently, on base pressure.

The most significant difference that was expected (in the present work) between the relatively well-studied two-dimensional case and the present three-dimensional flow was the existence of a spanwise velocity component in the separated-flow region, which could result in a separated flow composed of spanwise vortices as shown in Figure 4.

Figure 4. Subsonic Flow over a Rearward-Facing Step

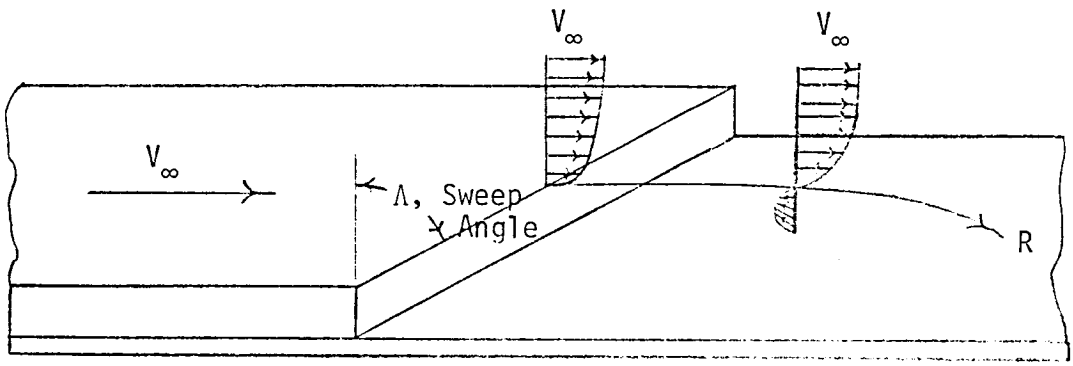

a. Skewed Velocity Profile in Separated-Flow Region

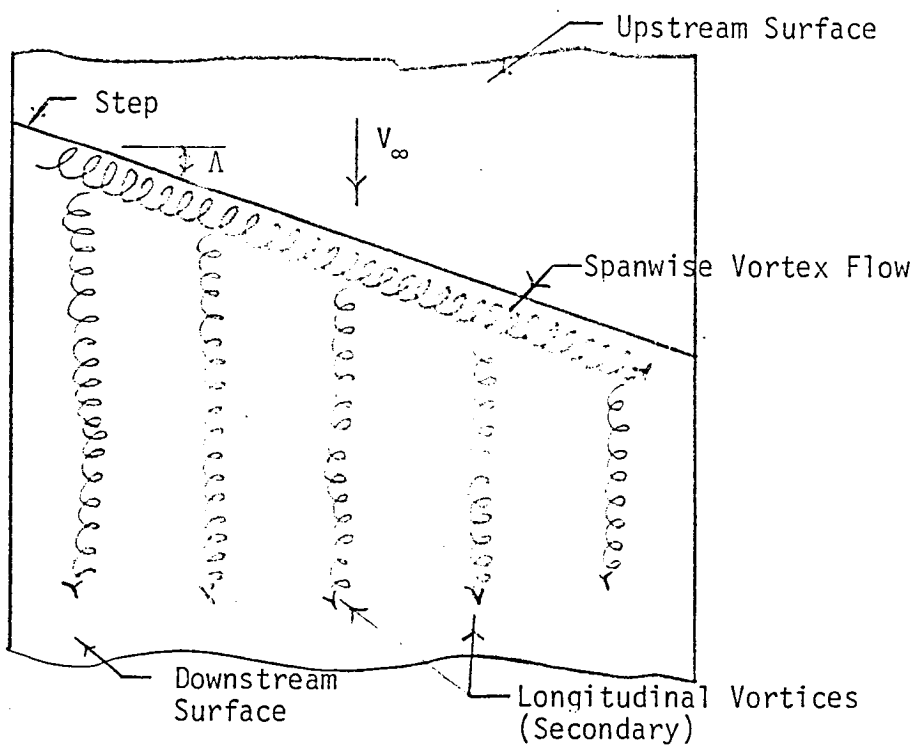

b. Other Principal Flow Features (Top View)

1.4. An Application - Airfoil with Swept, Blunt Trailing Edge

Upon removing the splitter plate at the base of the swept, rearward-facing step model, it is effectively transformed into an airfoil with a thick, swept trailing edge.

1.4.1. Background

There has been considerable interest in the past in the use of blunt trailing-edge wings for subsonic and supersonic aircraft. Chapman and Kester (1952) and Chapman (1955) have pointed out that a supersonic wing section with a blunt trailing edge could make possible a decrease in the section wave drag. In some cases, the decrease in wave drag was sufficient to offset the base-drag penalty. The higher structural integrity of wings with a blunt trailing edge is an additional advantage.

Whitcomb (1974) traced the evolution of the general shape of the NASA supercritical airfoil from a configuration with a thin trailing edge, which had structural problems, to one with a thickened trailing edge. This change improved not only the structure, but also the high

---

Chapman, D. R. and Kester, R. H., Effect of Trailing Edge Thickness on Lift at Supersonic Velocities, NACA RM A 52D17, 1952.

Chapman, D. R., Reduction of Profile Drag at Supersonic Velocities by the use of Airfoil Sections Having a Blunt Trailing Edge, NACA TN 3503.

Whitcomb, R. T., Review of NASA Supercritical Airfoils, Presented at the 9th Congress of the International Council of the Aeronautical Sciences, Haifa, Israel, 25-30 August, ICAS Paper 74-10, 1974.

speed aerodynamic characteristics at lifting conditions with very little increase in the basic subsonic drag level.

1.4.2. Advantages of a Blunt Trailing Edge

Holder (1964) discussed the advantages of thickened trailing edges for transonic airfoils in general. He indicated that the purpose of using a thick trailing edge is to reduce the strength of the shock on the upper airfoil surface in order to delay the onset of drag rise and separation effects. Wing sweep also results in reduced shock strength. [See Hieser and Whitcomb (1948).] Therefore, it may be possible to reduce wing sweep through the use of airfoil sections with thickened trailing edge.

According to Pearcey (1962), a thick trailing edge can be used at subsonic and transonic speeds for the following purposes:

(1) to increase the thickness/chord ratio without any increase in upper-surface slopes [see Figure 5(a)];

Holder, D. W., "The Transonic Flow Past Two-Dimensional Aerofoils," Journal of the Royal Aeronautical Society, Vol. 68, No. 644, pp. 501-516, 1964.

Hieser, G. and Whitcomb, C. F., Investigation of the Effects of a Nacelle on the Aerodynamic Characteristics of a Swept Wing and the Effects of Sweep on a Wing Alone, NACA TN 1709, 1948.

Pearcey, H. H., "The Aerodynamic Design of Section Shapes for Swept Wings," Advances in Aeronautical Sciences: Proceedings of the Second International Congress in the Aeronautical Sciences (Zurich, 12-16 September 1960), Pergamon Press, pp. 277-322, 1962.

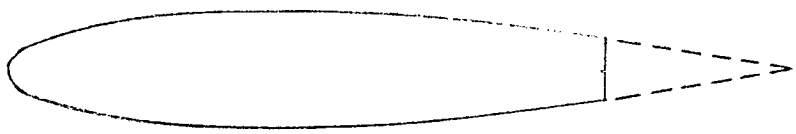

(a) Thickness/Chord Ratio Is Increased

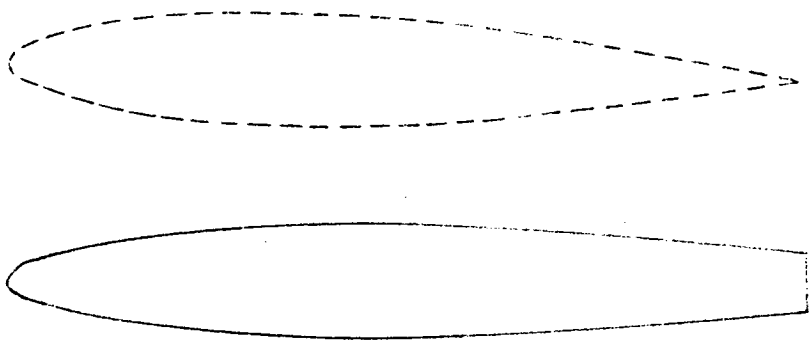

(b) Surface Slopes Are Reduced

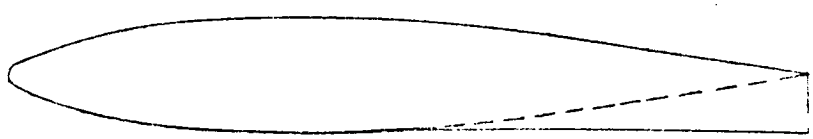

(c) Camber Is Increased Without Changing Upper Surface

Figure 5. The Use of Thick Trailing-Edges in Airfoil Section Design (Pearcey(1962))

(2) to reduce the surface slopes on the upper surface alone or on both the upper and lower surfaces for a given thickness/chord ratio [see Figure 5(b)] and

(3) to increase camber without changing the upper surface slope profile [see Figure 5(c)].

Modification (1) effects a structural advantage without changing the conditions for the onset of drag rise and separation effects. Modification (2) delays the onset of drag rise and separation effects. Modification (3) provides lift with smaller upper surface velocities than would be possible with a sharp trailing edge. In addition, Pearcey (1958) has stated that another advantage gained from a thick trailing edge is a delay in the initiation of separation resulting from the interaction of the upper-surface and lower-surface flows, due to the shielding provided by the thick trailing edge.

1.4.3. Disadvantage of a Thick Trailing Edge

Any increased base drag could be a strong disadvantage confronting the designer of an airfoil shape with a thick trailing edge. This disadvantage must be considered along with the advantages to be gained.

An accurate prediction of base drag must be available in order to evaluate the thick trailing edge option. An example of a method to

---

Pearcey, H. H., A Method for the Prediction of the Onset of Buffeting and Other Separation Effect from Wind Tunnel Tests on Rigid Models, ARC 20, 631, AGARD Report No. 223, 1958.

predict base drag in two-dimensional flow is the one developed by Nash (1962). Other two-dimensional methods were later reviewed by Nash (1965). Chang (1970) has indicated that there are two-dimensional geometries for which the prediction of base pressure is still not satisfactory. In addition, no three-dimensional problems are examined in his chapter on "Base Pressure." An unavoidable conclusion is that the experimental determination and theoretical prediction of base pressures in three-dimensional flows are still in their infancy—though considerable work has been done on axisymmetric bodies at angle-of-attack and on specialized three-dimensional configurations, e.g., the Space Shuttle.

Along with understanding the flow physics in the base region and accurately determining the base drag of a thick trailing-edge airfoil section, methods for reducing the base drag at subsonic and transonic speeds are needed. Considerable research has been accomplished in this area (for two-dimensional configurations) according to Hefner and Bushnell (1977). Since base drag occurs because of the presence

---

Nash, J. F., An Analysis of Two-Dimensional Turbulent Base Flow Including the Effect of the Approaching Boundary Layer, London, England: Ministry of Aviation, Aeronautical Research Council Reports and Memoranda No. 3344, 1962.

Nash, J. F., A Discussion of Two-Dimensional Turbulent Base Flows, London, England: Ministry of Aviation, Aeronautical Research Council Reports and Memoranda No. 3468, 1965.

Chang, Paul K., Separation of Flow, Peragamon Press, Inc., 1970.

Hefner, Jerry N. and Bushnell, Dennis M., "An Overview of Concepts for Aircraft Drag Reduction," Special Course on Concepts for Drag Reduction, NATO Advisory Group for Aerospace Research and Development, AGARD Report No. 654, 1977.

of a viscosity-induced low-speed layer of fluid near the wall of a body, they indicate that the basic philosophy for two-dimensional base drag reduction is to thin the low-momentum boundary-layer flow to the maximum extent possible. Alternatively, other flow structures, such as longitudinal vortices, can be introduced into the low momentum region in order to pump in high momentum air (which offers more resistance to adverse-pressure-gradient influences). Methods listed by Hefner and Bushnell which apply specifically to reducing base drag are:

(1) boattailing (reduces adverse pressure gradient),
(2) concave surface curvature (generates longitudinal vortices),
(3) splitter plates (reduces occurrence of Karman vortex street),
(4) base bleed (energizes shear layer),
(5) solid and ventilated recessed base geometry (may produce splitter-plate effect) and
(6) serrated trailing edges (may introduce longitudinal vortices).

A few of these methods are also discussed by Nash (1965) and Chang (1976). Some of these techniques are illustrated in Figure 6.

Chang, Paul K., Control of Flow Separation, Hemisphere Publishing Corporation, 1976.

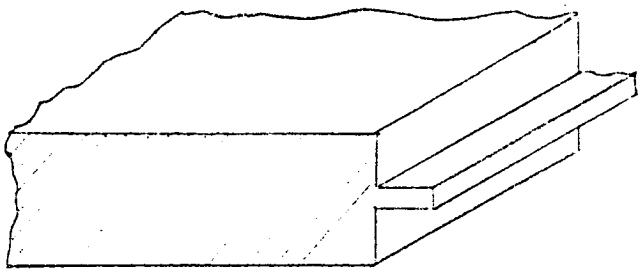

Splitter Plate

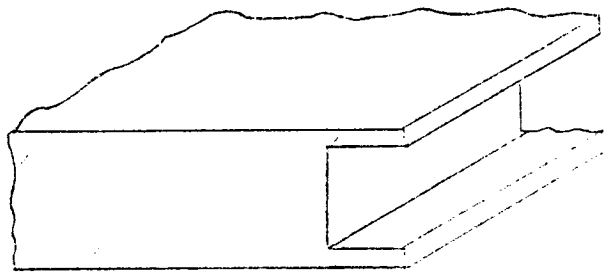

Simple Base Cavity

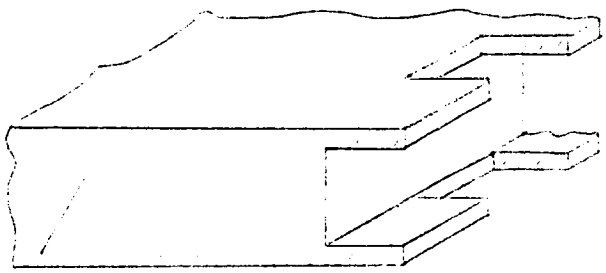

Serrated Base Cavity

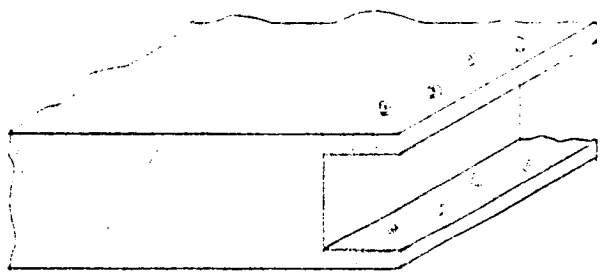

Perforated Base Cavity

Figure 6. Devices for Increasing Base Pressure at Subsonic Speeds (Nash(1965))

Nash, Quincey and Callinan (1963) examined the effect of splitter-plate length on base pressure. They found that at subsonic speeds the effect of a splitter plate is to reduce that part of the base drag which can be attributed to the existence of the vortex street. Harrawood (1967) varied the distance of a constant-length splitter plate from a horizontal cylinder (angle of attack = 90°) and concluded that interference is effective only in the region where vortices form. Holder (1964) has suggested that the effect of base bleed and splitter plates is to move the point where periodic flow begins in the wake farther downstream from the trailing edge. The vorticity shed from the airfoil thus becomes more diffuse before periodic flow begins and the strengths of the vortices in the vortex street are therefore reduced. This results in a reduction in the exchange of momentum between the wake fluid and the outside flow, consequently yielding a reduction in drag. Hoerner (1965) has shown that the drag of a cylinder in cross-flow can be reduced by 40% upon placing a splitter plate in the wake region. In addition, Nash et al. (1963) have indicated that the base drag on a two-dimensional rearward-facing step may be one-third the value measured on the equivalent two-dimensional airfoil with thick trailing edge.

Nash, J. F., Quincey, V. G. and Callinan, J., Experiments on Two-Dimensional Base Flow at Subsonic and Transonic Speeds, National Physical Laboratory, Aerodynamics Division, NPL Aero. Report 1070 - A.R.C. 25 070, 1963.

Harrawood, Paul, Study of Vortex Motions in Wake Flows, Ph.D. Dissertation, North Carolina State University, University Microfilms, Inc., Ann Arbor, Michigan, 1967.

Hoerner, S. F., Fluid-Dynamic Drag, Hoerner Fluid Dynamics, 1965.

1.4.4. Literature Review

In the supersonic flow regime, experimental investigations have been performed on two-dimensional blunt-trailing-edge airfoils by Nash, Quincey and Callinan (1963), Badrinarayanan (1961) and Rom, Kronzon and Seginer (1968). Nash (1967) published a literature survey of experimental and theoretical investigations of two-dimensional turbulent base flows (supersonic and subsonic). Nash, Quincey and Callinan (1963) studied the subsonic problem also for a flat plate model. Goradia, Mehta and Shrewsbury (1977) experimentally examined turbulent subsonic flow over a blunt trailing-edge airfoil.

No works were uncovered which examined the flow over a flat plate or an airfoil shape with a swept, blunt trailing edge. However, it is likely that the wealth of information that exists pertaining to flow over swept and unswept circular cylinders will be useful in understanding the three-dimensional wakes shed from swept, blunt

---

Badrinarayanan, M. A., "An Experimental Investigation of Base Flows at Supersonic Speeds," Journal of the Royal Aeronautical Society, Vol. 65, pp. 475-482, 1961.

Rom, J., Kronzon, Y. and Seginer, A., "The Velocity, Pressure and Temperature Distribution in the Turbulent, Supersonic, Near Wake Behind a 2-D Wedge-Flat Plate Model," Israel Journal of Technology, Vol. 6, pp. 84-94, 1968.

Goradia, S. H., Mehta, J. M. and Shrewsbury, G. S., Analysis of the Separated-Boundary-Layer Flow on the Surface and in the Wake of Blunt Trailing Edge Airfoils, NASA CR-145202 Prepared by Lockheed-Georgia Company, 1977.

trailing edges. [See, e.g., Morkovin (1964) and Thompson and Morrison (1971).] Of course, many investigations have been conducted for flow over an airfoil shape with a swept, sharp trailing edge.

1.4.5. The Flat Plate with Swept Trailing Edge

Swept, blunt trailing edge models were included in the present research program in order to:

(1) provide models which generate flow with characteristics which are more similar to the flow over blunt trailing-edge airfoils and

(2) provide preliminary base pressure measurements for comparison with the rearward-facing step measurements to show the effect of the periodic phenomenon present.

Since the same models could be used in both cases, the swept-wake problem was investigated simultaneously with the swept-step problem, primarily to determine any influence of sweep upon the Karman vortex street.

Morkovin, M. V., "Flow Around Circular Cylinder-A Kaleidoscope of Challenging Fluid Phenomena," Symposium on Fully Separated Flows, ASME Fluids Engineering Division Conference, Philadelphia, Pa., May 18-20, pp. 102-118, 1964.

Thompson, K. D. and Morrison, D. F., "The Spacing, Position and Strength of Vortices in the Wake of Slender Cylindrical Bodies at Large Incidence," Journal of Fluid Mechanics, Vol. 50, Part 4, pp. 751-783, 1971.

2.0. THE EXPERIMENTAL PROGRAM

2.1. Description of Test Facility

Tests were conducted in the NASA Langley Subsonic Low-Turbulence Open-Loop Wind Tunnel, which is best described as being composed of three separate sections: a settling chamber, a test section and a downstream section which includes a diffuser and a blower/motor unit. These sections are shown in Figure 7(a), in the order listed above, from right to left.

The settling chamber consists of an inlet, a honeycomb, screens and a contraction. The inlet provides a direct opening to the honeycomb section and is located away from obstructions since the laboratory space provides the return loop of the open-circuit wind tunnel. The honeycomb is utilized as a flow-straightening device. It aids in breaking up large-scale eddies and swirls which may be present at the inlet. The screens also help remove large-scale eddies. Geometrically, the contraction section is designed so that separation does not occur along the walls.

The test section shown in Figure 7(b) is 15 by 15 inches and 10 feet long. The free-stream velocity can effectively be varied between 20 and 150 feet per second. The turbulence level is less than

Figure 7.

NASA LANGLEY FLUID MECHANICS BRANCH
15" LOW TURBULENCE WIND TUNNEL

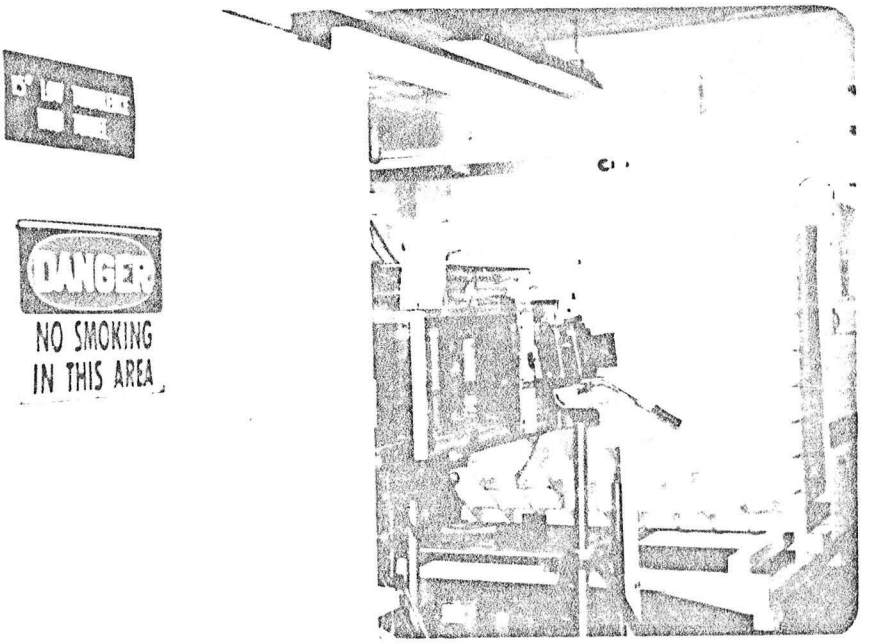

A. View of Diffuser, Test Section and Settling Chamber

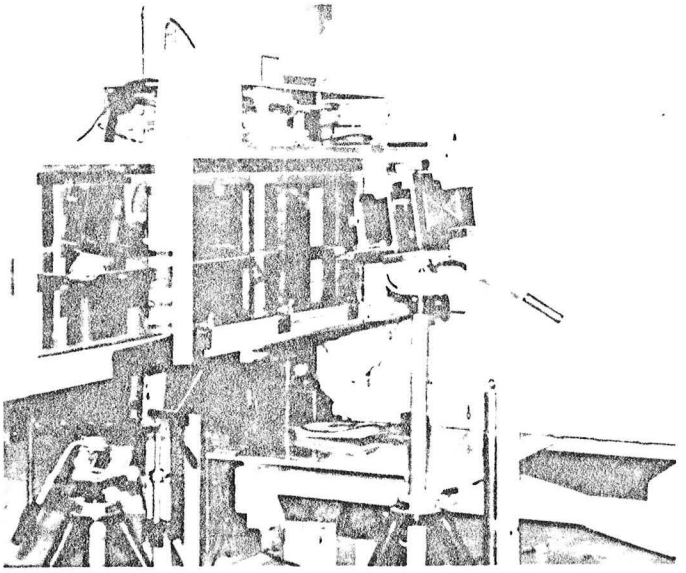

B. View of Test Section Showing Arrangement of Photographic Equipment

0.1% at 70 feet per second. The walls of the test section are made of plexiglas to allow flow visualization. Additional information for a similar tunnel has been presented by Hanson (1969).

2.2. Test Configurations

A pictoral summary of the experimental program is given in Figure 8. Step height, h, and sweep angle, Λ, were the major geometric variables in the present experiment. Models with step heights of .12, .31, .50 and .94 in. and sweep angles of 0, 15, 30, 37.5, 45 and 60° were tested. As previously discussed, the swept-step models can be converted to swept-trailing edge models by removing the splitter plate downstream of the step.

Base geometry was modified, as shown in Figure 8(c), in order to determine the effect on the flow in the separated region and on base pressure. The various geometries considered represent extensions of work performed by Nash et al. (1968), Zumwalt (1980) and Wilson et al. (1979).

Hanson, C. E., The Design and Construction of a Low-Noise, Low Turbulence Wind Tunnel, Department of Mechanical Engineering, Massachusetts Institute of Technology, Report No. DSR 79611-1, 1969.

Zumwalt, G. W., The Vortex Trough and Its Use as an Igniter for Supersonic Burning, Report to NASA Langley Research Center, Hypersonic Propulsion Branch, 1980.

Wilson, D. J., Winkel, G. and Neiman, O., "Reynolds Number Effects on Flow Recirculation Behind Two-Dimensional Obstacles in a Turbulent Boundary Layer," Proceedings of the Fifth International Conference on Wind Engineering, Fort Collins, Colorado, July, pp. 965-974, 1979.

Figure 8.

THREE-DIMENSIONAL, SUBSONIC, BASE FLOW EXPERIMENTAL PROGRAM

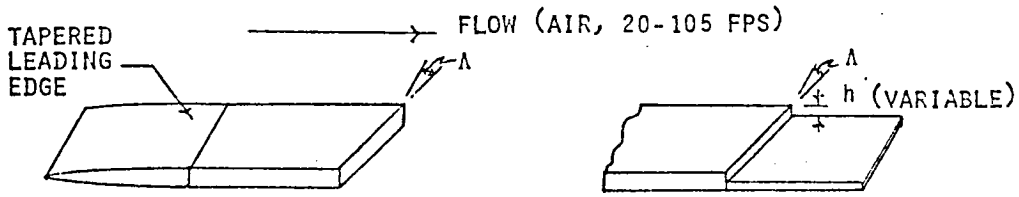

A. BASIC WAKE MODEL WITH SWEPT TRAILING EDGE (Λ = 0,15, 30, AND 60 DEG.)

B. BASIC SWEPT, REARWARD-FACING-STEP MODEL (Λ = 0, 15, 30, 37.5, 45, & 60 DEG.)

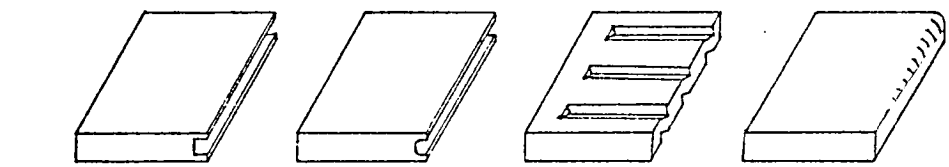

RECTANGULAR SLOT CIRCULAR SLOT VORTEX TROUGHS CONICAL LIP

C. BASE MODIFICATIONS

D. OTHER DETAILS

1. QUALITATIVE MEASUREMENTS
   - *SMOKE WIRE
   - *OIL DROP
   - *TUFTS

2. QUANTITATIVE MEASUREMENTS
   - *SURFACE PRESSURE
   - *VELOCITY PROFILE
   - *FLOW ANGLE
   - *REATTACHMENT LENGTH
   - *SWIRL ANGLE

3. CHANGES TO INITIAL, LATERAL, AND DOWNSTREAM END CONDITIONS
   - *FREE AND FIXED FLOW TRANSITION
   - *TUNNEL ROOF STEP
   - *VARIABLE LATERAL END CONDITIONS
   - *FLOW RESTRICTOR IN RELAXATION REGION

The configurational codes used to describe the models tested are listed in Table 1. Contained in Table 2 is a summary of the configurations and measurements. Figures 9 through 11 indicate model sketches of the basic 1-in. leading edge (LE2), the 30° swept base section with circular base cavity (CC30) and the splitter plate placed downstream of the 30° swept step. These sketches provide the dimensions used for typical model components and also an indication of typical pressure orifice placement. The basic model with zero sweep (LE1-BB0-DS0.31) is shown in Figure 12 mounted in the tunnel on rails attached to the test section side walls. The overall model essentially constitutes a splitter plate in the tunnel test section.

Several changes were made to the nominal test conditions in order to evaluate the effect of various initial, lateral and downstream end conditions on the flow. The state of the oncoming boundary layer was varied during the tests by removing the .039-in. trip wire located 2 in. downstream of the leading edge—thus providing for free transition. A swept model was tested with and without a tunnel roof step in order to determine the effect of the three-dimensional area expansion aft of the step. A honeycomb flow restrictor was placed in the relaxation region so that the effect of a favorable pressure gradient several step heights downstream of the step might be examined. The upstream step-wall junction angle was varied to determine the effect of various initial conditions on the three-dimensional separated flow.

Table 1.

Configurational Codes

Configuration	Code
Forebody	
½-in. thickness	LE1
1-in. thickness	LE2
Basic Trailing Edges (TE)	BBΛ (where Λ ≡ sweep angle)
TE with Rectangular Base Cavity	RCΛ (e.g., RC30 for $\Lambda = 30^{o}$)
TE with Semi-circular Base Cavity	CCΛ
TE with Vortex Troughs	VTΛ
TE with Conical Step Lip	CLΛ
Downstream Splitter Plate	DSΛ.h (where h ≡ step height; e.g., DS 30.5 for $\Lambda = 30^{o}$ & h = .5")

Table 2.

3-D SEPARATED-FLOW RESEARCH PROGRAM

	Configuration	Flow Visualization				Measurements		
		Smoke		Oil Drops	Tufts	Surface Pressure	B. L. Vel. Survey	Flow Angle Checks
		Hor.	Vert.					
1.	LE1-BB0	Ø	Ø					
2.	LE1-BB15	X	X					
3.	LE1-BB30	Ø	Ø					
4.	LE1-BB38	X						
5.	LE1-BB60	Ø	Ø					
6.	LE1-BB0-DS0.12			X				
7.	-DS0.31	X	X	X				
8.	-DS0.50	X	X	X				
9.	LE1-BB15-DS15.12			X				
10.	-DS15.31	X	X	X				
11.	-DS15.50			X				

*Note: Configurations were tested at one or more velocities in the range 25 - 105 fps. (X ≡ turbulent flow only; Ø ≡ laminar and turbulent flow)

3-D SEPARATED-FLOW RESEARCH PROGRAM CONT'D

	Configuration	Flow Visualization				Measurements		
		Smoke		Oil Drops	Tufts	Surface Pressure	B. L. Vel. Survey	Flow Angle Checks
		Hor.	Vert.					
12.	LE1-BB30-DS30.12			X				
13.	-DS30.31	X	X	X				
14.	-DS30.50	Ø	Ø	X				
15.	LE1-BB38-DS38.12			X				
16.	-DS38.50			X				
17.	LE1-BB45-DS45.12			X				
18.	-DS45.50			X				
19.	LE1-BB60-DS60.12			X				
20.	-DS60.31	X	X	X				
21.	-DS60.50	Ø	Ø	X				
22.	LE2-BB0					X		
23.	LE2-BB15					X		
24.	LE2-BB30					X		
25.	LE2-BB60					X		
26.	LE2-BB0-DS0.50					X	X	X

3-D SEPARATED-FLOW RESEARCH PROGRAM CONT'D

	Configuration	Flow Visualization				Measurements		
		Smoke		Oil Drops	Tufts	Surface Pressure	B. L. Vel. Survey	Flow Angle Checks
		Hor.	Vert.					
27.	-DS0.94			X	X	X		
28.	LE2-BB15-DS15.50					X		
29.	-DS15.94			X	X			
30.	LE2-BB30-DS30.50	X				X		
31.	-DS30.94			X	X	X		
32.	LE2-BB60-DS60.50			X		X		X
33.	-DS60.94			X	X	X		
34.	LE2-RC0					X		
35.	-RC0-DS0.94			X	X	X		
36.	LE2-RC30					X		
37.	-RC30-DS30.94			X		X		
38.	LE2-CC0					X		
39.	-CC0-DS0.94			X	X	X		
40.	LE2-CC30					X		

3-D SEPARATED-FLOW RESEARCH PROGRAM CONT'D

	Configuration	Flow Visualization				Surface Pressure	Measurements B. L. Vel. Survey	Flow Angle Checks
		Smoke Hor.	Smoke Vert.	Oil Drops	Tufts			
41.	-CC30-DS30.94			X		X		
42.	LE2-VT0					X		
43.	-VT0-DS0.5			X		X		
44.	LE2-VT30	X				X		
45.	-VT30-DS30.5	X		X		X		
46.	LE2-CL30					X		
47.	-CL30-DS30.50			X		X		
48.	-DS30.94			X		X		

Figure 9.

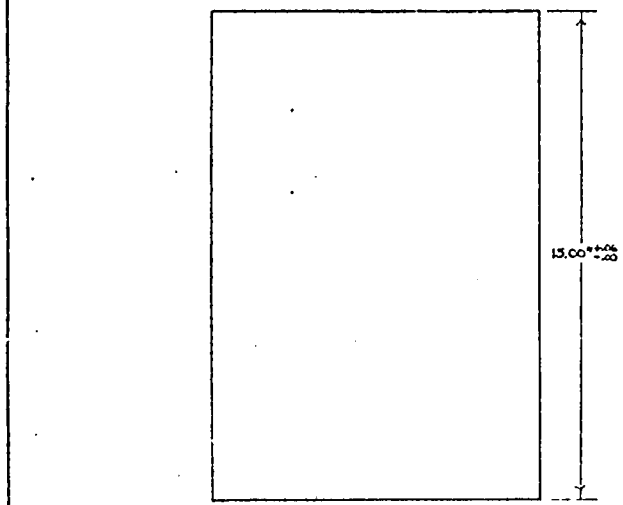

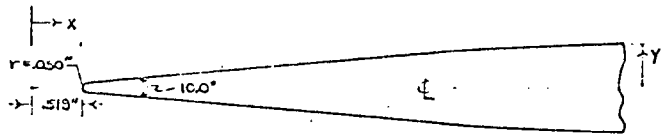

Leading Edge Detail (Scale: Full)

X(in)	Y(in)	
0.000	0.000	10° wedge
3.614	0.316	
3.614	0.316	elliptical surface: $y = .5\sqrt{1-.2241(x-3.614)^2}$
4.000	0.347	
5.000	0.403	
6.000	0.451	
7.000	0.478	
8.000	0.494	
9.000	0.500	
9.036	0.500	
9.036	0.500	flat plate
10.519	0.500	

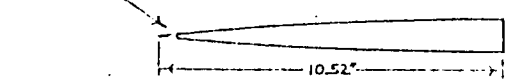

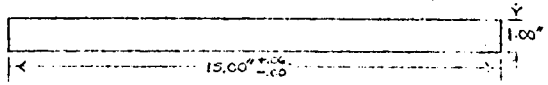

DATE	LET	FREQ.	REVISIONS	BY	CK.	APPD.

MATERIAL: Hardened Aluminum or Steel

SCALE: 1"=3"

TOLERANCE ON DIMENSIONS UNLESS SHOWN OTHERWISE: XX (1 DECIMAL PLACES) ± .1; XXX (2 DECIMAL PLACES) ± .02; XXXX (3 DECIMAL PLACES) ± .005; ANGULAR ± .1°

SURFACE FINISH IN MICROINCHES RMS UNLESS SHOWN OTHERWISE

EST. FIN. WEIGHT

DR. [illegible] STARTED

DES. " APPD.

CHK. [illegible] APPD.

NATIONAL AERONAUTICS AND SPACE ADMINISTRATION
LANGLEY RESEARCH CENTER
HAMPTON, VIRGINIA 23665

PROJECT TITLE: 3-D BASE FLOW

DRAWING TITLE: Basic Leading Edge Coordinates for Elliptical Nose Section

PROJECT NO. | BLDG. NO. | JOB ORDER NO. | SHEET NO.

DRAWING NO. LB-GVSC1

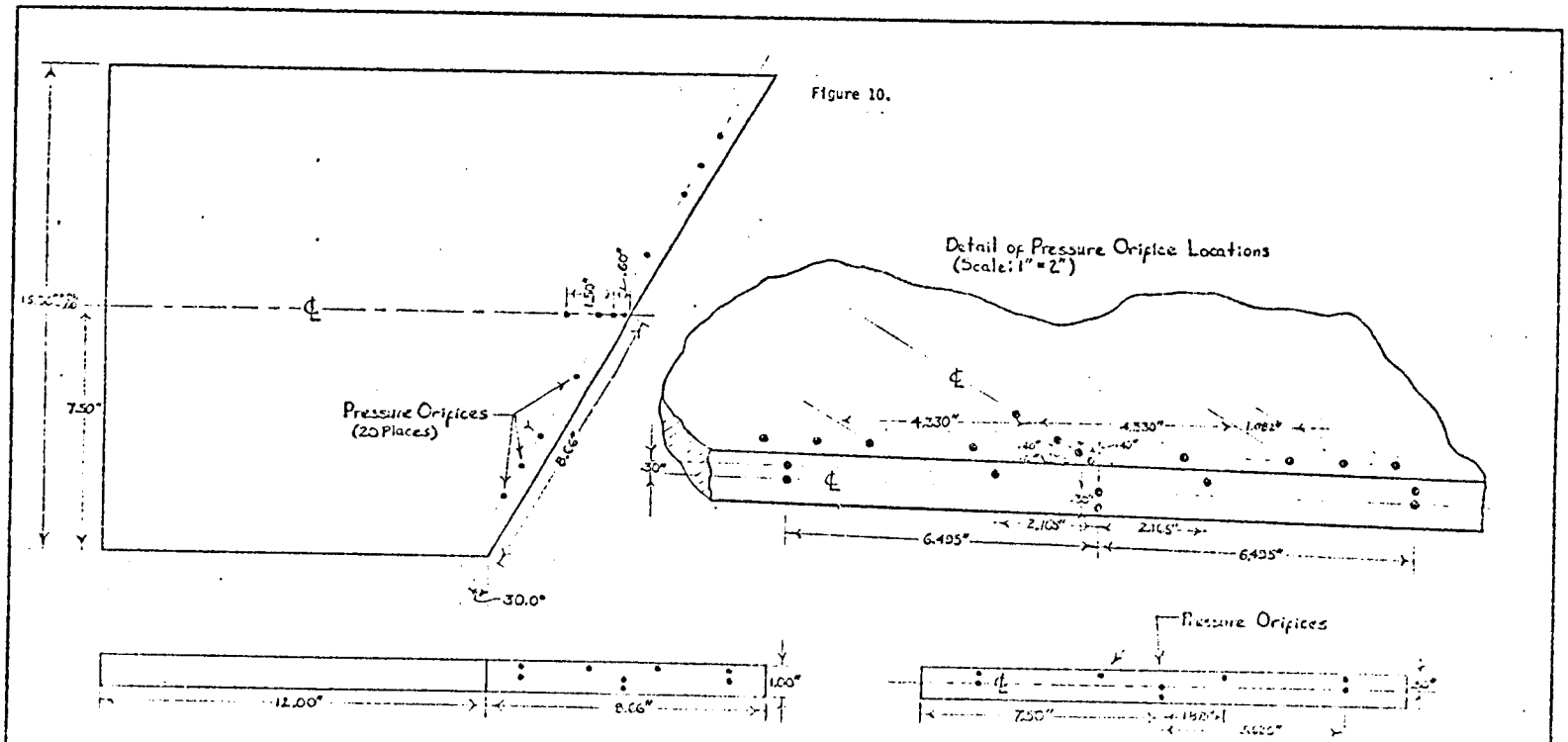
Figure 10.
Detail of Pressure Orifice Locations
(Scale: 1" = 2")
Pressure Orifices
(20 Places)
7.50"
30.0°
8.66"
4.330"
2.165"
6.495"
12.00"
1.00"
Pressure Orifices
7.50"
MATERIAL
Smooth Plywood
SCALE
1"=3"
TOLERANCE ON DIMENSIONS UNLESS SHOWN OTHERWISE
ANGULAR ± 1°
SURFACE FINISH IN MICROINCHES RMS UNLESS SHOWN OTHERWISE
EST. FIN. WEIGHT
DR.
DES.
CHK.
STRESS
APPD.
DATE
LET
FREQ.
REVISIONS
BY
CK.
APPD.
NATIONAL AERONAUTICS AND SPACE ADMINISTRATION
LANGLEY RESEARCH CENTER
HAMPTON, VIRGINIA 23665
PROJECT TITLE
3-D EASE FLOW
DRAWING TITLE
Trailing Edge with 30° Sweep Angle
PROJECT NO.
JOB ORDER NO.
SHEET NO.
LB-GV30-1
DRAWING NO.

Figure 11.

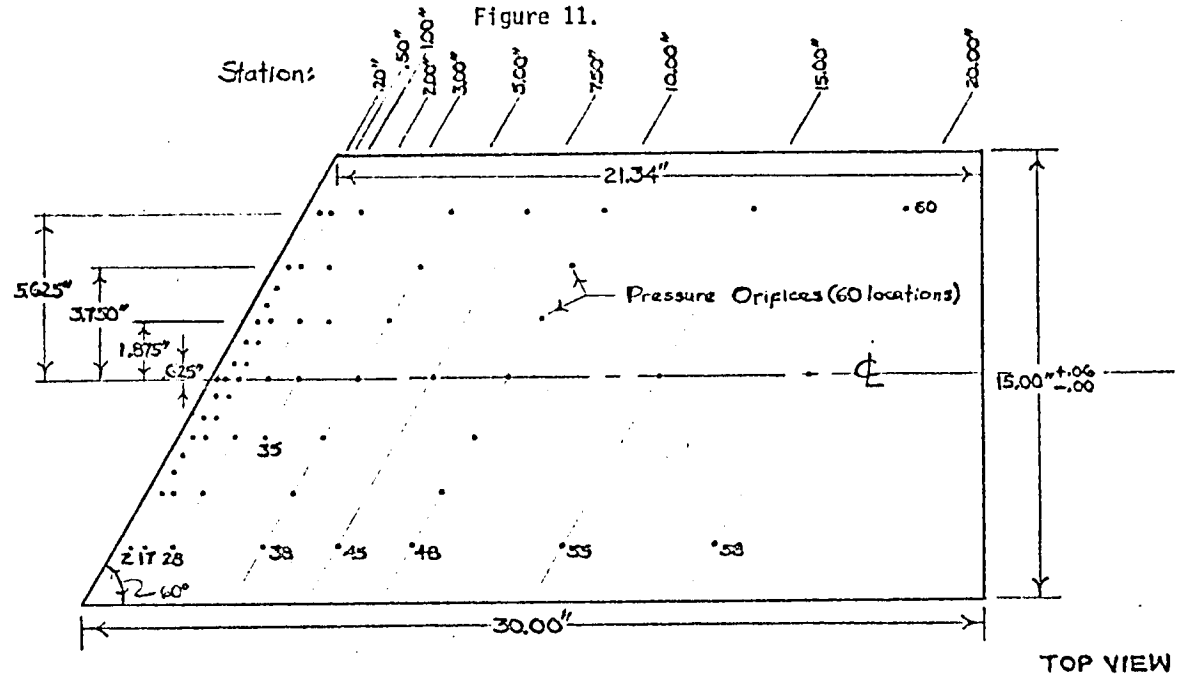

	DATE	LET.	REVISION	BY		
	UNIT OR PROJECT	SCALE	MATERIAL	HEAT TREAT	DR.	[illegible] 2 Sept. 80
NEXT ASSEMBLY	3-D BASE FLOW	1"=5"	V16" Aluminum; V2" Plywood		DES.	"
TOLERANCE ON DIMENSIONS UNLESS SHOWN OTHERWISE: X.X (1 DECIMAL PLACE) ±.1; X.XX (2 DECIMAL PLACES) ±.02; X.XXX (3 DECIMAL PLACES) ±.005; ANGULAR ± .1°			NATIONAL AERONAUTICS AND SPACE ADMINISTRATION LANGLEY RESEARCH CENTER LANGLEY FIELD, VA.		CHK.	[illegible] 11 Sept. 80
					GL.	
SURFACE FINISH IN MICROINCHES RMS UNLESS SHOWN OTHERWISE: V	EST. FIN. WEIGHT		Surface Downstream of 30° Swept Step Code: DS30		AP.	
					SHEET SIZE: LA	GVS16

Figure 12.
REARWARD-FACING STEP MODEL IN
15" LOW-TURBULENCE WIND TUNNEL

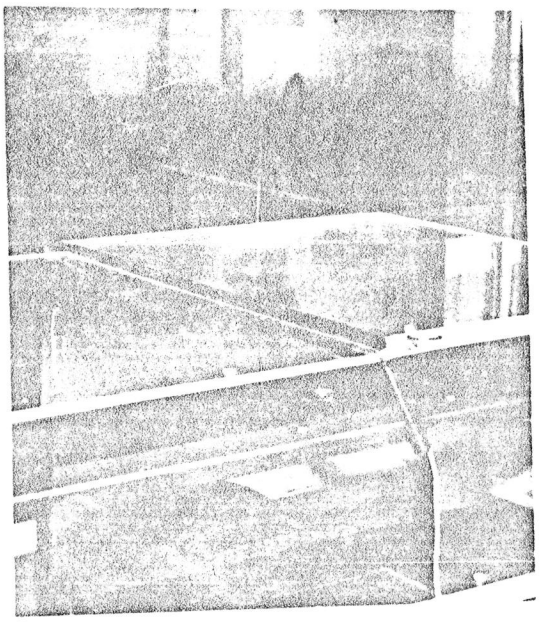

A. Rail-Mounted Rearward-Facing Step Model

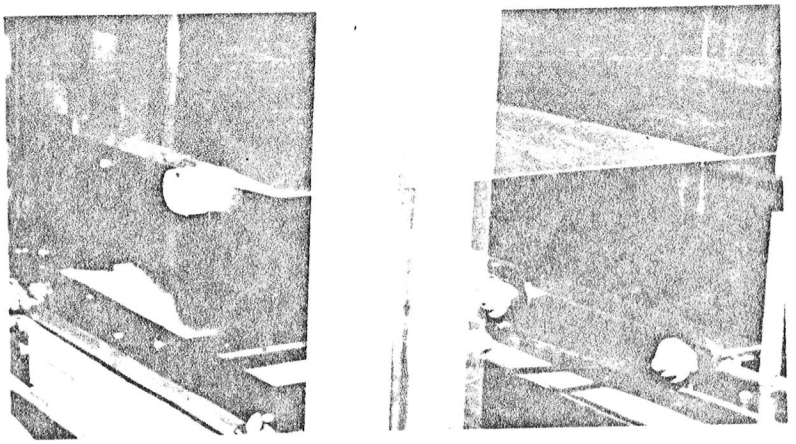

B. Elliptical Leading Edge

Various flow visualization techniques were utilized in obtaining a qualitative understanding of the general physics of the subject three-dimensional separated flow. These include the smoke wire, oil drop and surface tuft techniques.

The quantitative data obtained include surface pressure, boundary-layer velocity surveys upstream of separation, mean flow angularity, reattachment distance and swirl angle.

The diversity of test configurations allowed a systematic study of various effects on the three-dimensional separated flow. As a result, the general flow model introduced in Figure 4 was modified as described in Chapter 3.

2.3. Qualitative Measurements--Flow Visualization

Rows of acrylic fiber tufts were attached to sheets of stiff paper and placed downstream of the 1.0-in. step models. The distance between tuft rows was 1.0 in. and the tufts were .75-in. long. The tufts were expected to show the flow reattachment line by giving a visual indication of general flow direction in the region from 0 to 12 in. downstream of the step for the four sweep angles: 0, 15, 30, and 60°. Appropriate photographs were taken to document the results.

Black artist's oil-based paint thinned with linseed oil was applied to the surface downstream of the step in the form of droplets. Prior to this, a thin film of lightweight oil was spread over the

downstream surface, which had been painted white to provide a good contrast. This method allowed a determination of surface shear stress lines, reattachment distance and swirl angle. Photographs were taken to record the results.

A vertical smoke wire located at the inlet of the test section and a horizontal smoke wire located at the base of the model were used to provide an indication of the flow pattern of the entire flow over specific models. The presence of the turbulent boundary layer, the flow separation and reattachment points and the Karman vortex street were observable through the use of this technique. The arrangement of the photographic equipment to record the smoke flow is shown in Figure 7(b). Graflex 4" × 5" cameras were used with Kodak Tri-X Ortho film. The pulsing of the smoke wire with an electric current was appropriately synchronized with the firing of one of two high intensity strobe lamps. One lamp was located above the test section to give a sheet of light in a vertical plane at midspan when the vertical smoke wire was used. The other lamp was located in the test section downstream of the step to give a sheet of light in a horizontal plane when the horizontal smoke wire was used. The camera in Figure 7(b) recording the side view was used in conjunction with the vertical smoke wire and the other camera was used with the horizontal smoke wire.

2.4. Quantitative Measurements

Surface pressure was measured for the swept-step configurations with the 1-in. leading edge at various spanwise locations upstream of

the step, on the step base and in the separated flow, reattachment and relaxation regions. Typical placement of pressure orifices is shown in Figures 10 and 11. All pressure orifices were .020-in. in diameter. Surface pressure and base pressure were also measured for selected swept-wake configurations.

The pressure orifices on a given model were connected to a 48-port Scanivalve via metal and plastic tubing. The Scanivalve output was input to a Datametrics, Inc., Barocel Pressure Sensor/Manometer unit which converted the pressure differential to a DC voltage level. The pressure difference measured was between the surface pressure and the static pressure at an orifice located on the side wall of the test section about 2 feet downstream of the leading edge. The voltage signal was received by a Hewlett-Packard 2052A Automatic Data Acquisition System which included a 9825A Desktop Computer for Scanivalve control and data storage.

Boundary-layer velocity surveys were performed using a conventional pitot-static probe. Typical data are presented in Chapter 3 for a position upstream of the basic two-dimensional rearward-facing step model with LE2. Boundary-layer thickness and other conventional boundary-layer parameters were determined from the conventional velocity profiles, as well as the velocity profile in law-of-the-wall coordinates. The HP 9825A computer was used for velocity data acquisition and control of probe location.

The angularity of the mean flow was checked near the centerline of the test section. A four-element constant-temperature, "X," hot-film, flow-angle probe built by TSI (Model 1294CF) was used in conjunction with a flow angle analog computer designed and built by NASA personnel for another project. The system, however, had not been previously used until the present checks were conducted. Vertical probe location in the tunnel was controlled by the HP 9825A computer, which was also used for flow-angle data acquisition.

2.5. Measurement Accuracy

The uncertainty in swirl angle and reattachment distance measurements from oil flow patterns was estimated to be ±3° and approximately ±.2 step heights, respectively. In most instances, actual reattachment-distance measurements were repeatable within ±.5 step heights. This is typical of the accuracy obtainable using current flow-visualization techniques [Eaton (1980)].

Manufacturer's specifications for the Barocel Pressure Sensor/Manometer unit indicate a maximum uncertainty of approximately ±0.5% of the pressure reading. This corresponds to a ±1% error in C_p from instrumentation sources, since similar instrumentation is used in measuring freestream velocity. These estimates do not consider instrument drift which might have occurred between calibrations (up to 8 hours apart).

Since the calibration curves (Figure 17) for the flow angle probe indicated only small differences between actual and measured values, the measured values are reported herein. This results in a .2° to .3° error in flow angle (θ) for $|\theta| < 8°$ and an error $\simeq .5°$ at $|\theta| = 10°$, which increases almost linearly to a value $\simeq 4°$ at $|\theta| = 30°$.

3.0. PRESENTATION OF EXPERIMENTAL RESULTS

3.1. Incoming Turbulent Boundary-Layer Characteristics

Boundary-layer velocity profiles were obtained at locations 33.0 and 42.5 in. downstream of the leading edge (10.0 and 0.5 in. upstream of two-dimensional step, respectively) on the centerline of the model. The table below contains typical values obtained for the boundary layer (δ), momentum (θ) and displacement (δ^*) thicknesses.

Table 3

Boundary Layer Characteristics

L (in. from L.E.)	V_∞ (fps)	Re	δ (in.)	θ (in.)	δ^* (in.)	Re_θ
33.0	35	5.2×10^5	.72	.084	.120	1.5×10^3
33.0	70	1.0×10^6	.66	.072	.102	2.5×10^3
42.5	35	6.7×10^5	.88	.096	.136	1.7×10^3
42.5	70	1.4×10^6	.79	.090	.127	3.2×10^3

A pitot probe/pitot-static probe arrangement was used in surveying the boundary layer. Fifty data samples were averaged at each y-position to define the local boundary-layer velocity. The upper probe (pitot-static) measured freestream total minus static

pressure which defined the freestream velocity, while the lower probe (pitot) measured total boundary-layer pressure. This value of the total pressure was combined with the static pressure from the upper probe to define the boundary-layer velocity at a point. A typical velocity profile at L = 33 in. is presented in Figure 13 using conventional variables and in Figure 14 using the inner law variables $u^+ \equiv u/v^*$ and $y^+ \equiv yv^*/\nu$ with $v^* \equiv \sqrt{\tau_w/\rho}$ (τ_w from the Ludwieg-Tillmann incompressible empirical relation). It can be observed in Figure 13 that the measured profile has the shape usually characteristic of turbulent boundary layers—high velocity gradients near the wall. In Figure 14 the measured velocity profile is compared with the generally accepted empirical relation for the turbulent overlap layer. It can be seen that good agreement exists. Velocity profiles at V_∞ = 35 fps show similar agreement.

3.2. Freestream Flow Angularity Checks

As previously stated, the constant-temperature hot-film probe included four sensing elements. These elements were located 90° apart circumferentially and set at an angle of 45° from the probe axis. The two mutually perpendicular sensing elements in the vertical plane measured the flow angle in that plane as did the pair of sensing elements in the horizontal plane. These flow angle components could then be combined to give a total flow angle. A sketch of the probe is shown in Figure 15. The flow angles are defined in Figure 16.

FIGURE 13. TYPICAL BOUNDARY-LAYER VELOCITY PROFILE AT L=33 in. WITH V_∞=70 fps (Re=1.4X10^6)

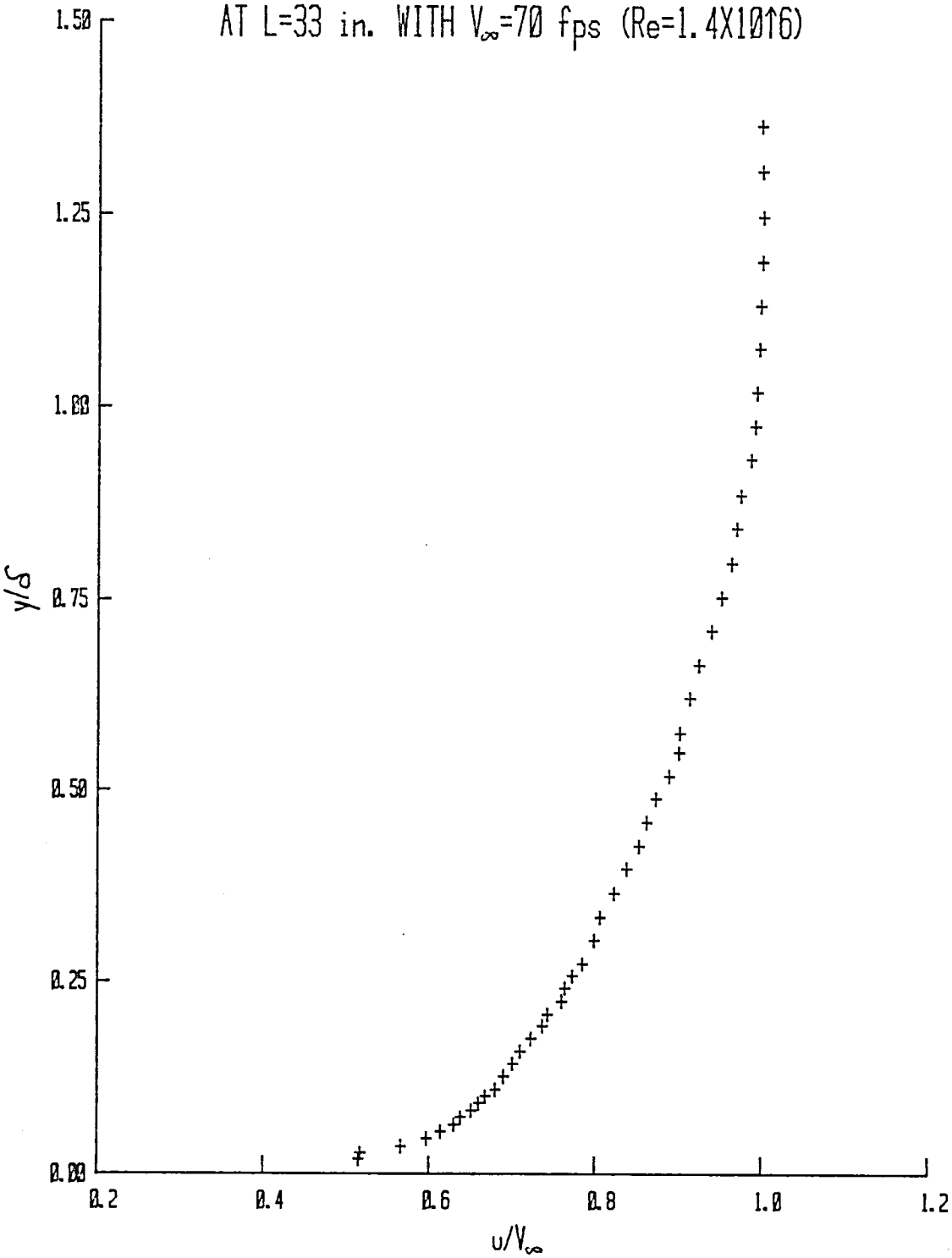

Figure 14. Boundary Layer Velocity Profile Using Inner-Law Variables at L = 33 in. with Re = 1.4×10^6

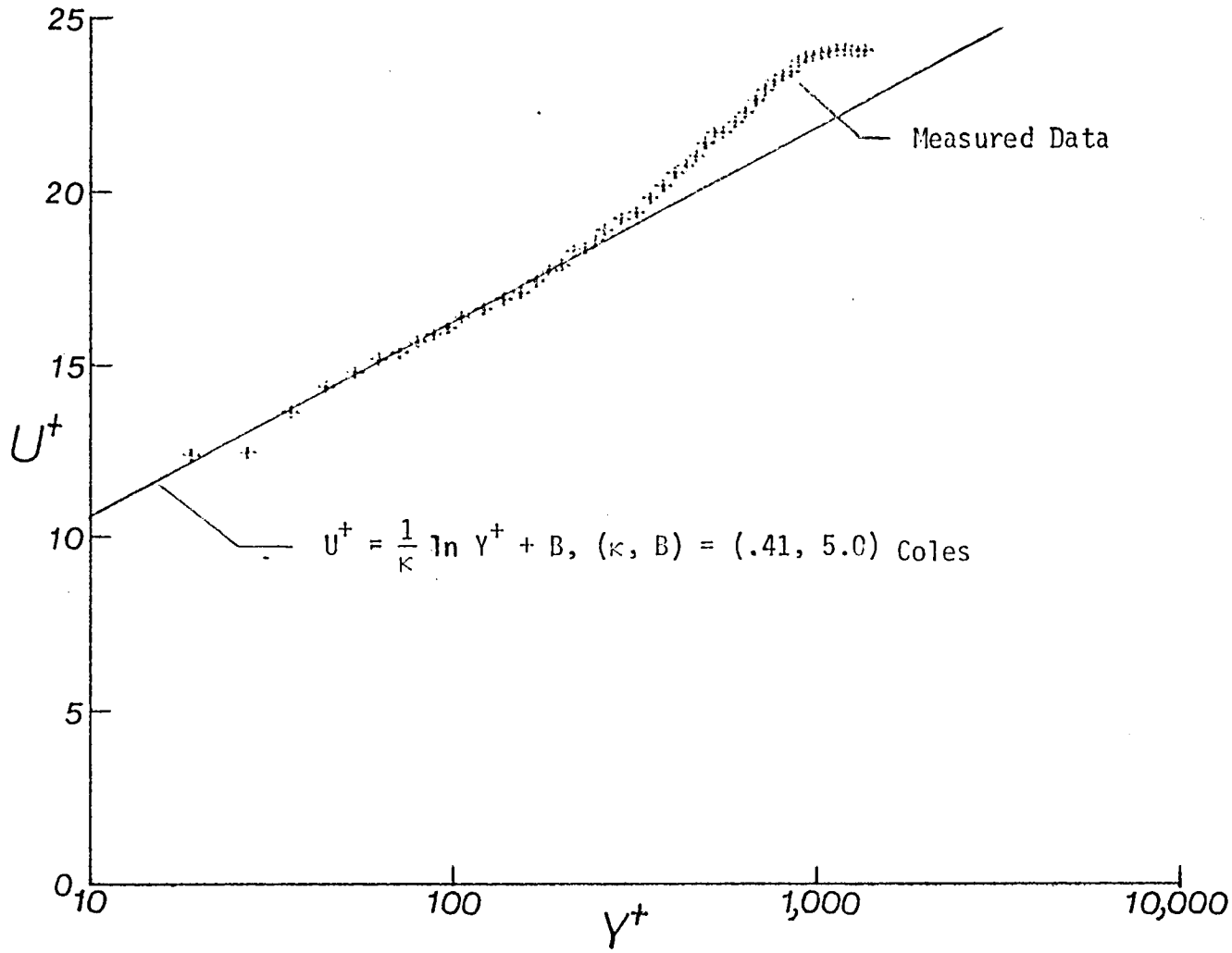

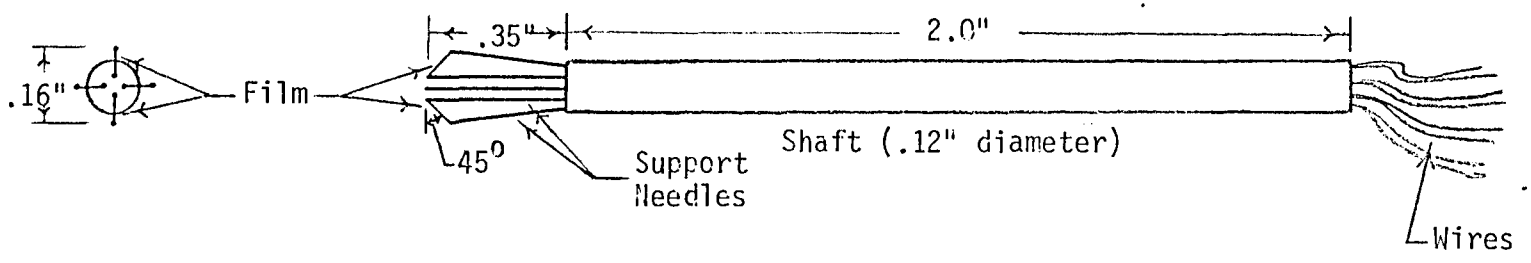

Figure 15. Sketch of Four-Element Flow Angle Probe.

Figure 16. Coordinate System for Flow Angle Measurements

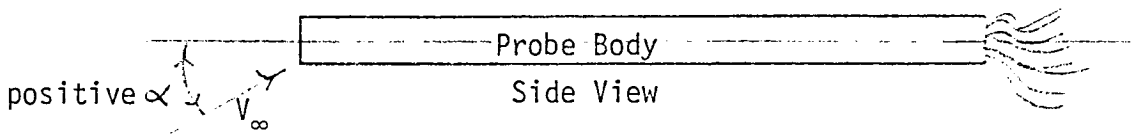

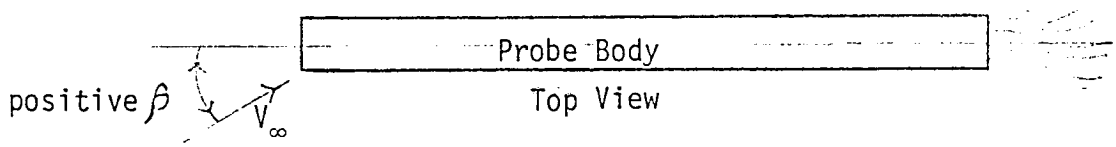

$$\vartheta' \equiv \text{Total Flow Angle} \equiv \tan^{-1}\sqrt{\tan^2\alpha + \tan^2\beta}$$

Measurements made with a dual-sensor probe in supersonic and hypersonic flow using a similar technique have been discussed by Helms (1979).

The hot-film probe was calibrated in the two planes over a range of angles from -30° to 30° and at freestream velocities of 15 and 40 fps. The resulting calibration curves of Figure 17 were essentially velocity-independent and the output of the four-channel constant temperature anemometer was scaled to give .1° = .001 volt.

Total flow angle measured with respect to the test section centerline for V_∞ = 35 fps is presented in Figure 18 at a spanwise position 1 in. from midspan and 14 in. forward of the step face at midspan. Step sweep angles were 0° and 60°. The results show that the flow was essentially parallel to the test section walls. Total flow angle as a function of height above the model surface is again presented in Figure 19, but now at a position 0.4 in. forward of the step face near midspan for a sweep angle of 60°. For comparison purposes, the data are presented at the same location without the step. Again, it can be concluded at this location also, the flow is essentially parallel to the test section walls, though for both cases at Λ = 60°, the flow angles are slightly greater than for the zero-sweep and no-step cases. This is to be expected due to the large spanwise velocity component and significant spanwise pressure gradient present in the separated-flow region aft of the step.

Helms, V. T. III, "Measuring Flow Angle and Mass Flow Rate in an Unknown Flowfield," Journal of Spacecraft and Rockets, Vol. 16, No. 1, January-February 1979, pp. 20-26.

FIGURE 17. CALIBRATION CURVES FOR FLOW ANGLE PROBE IN HORIZONTAL AND VERTICAL PLANES

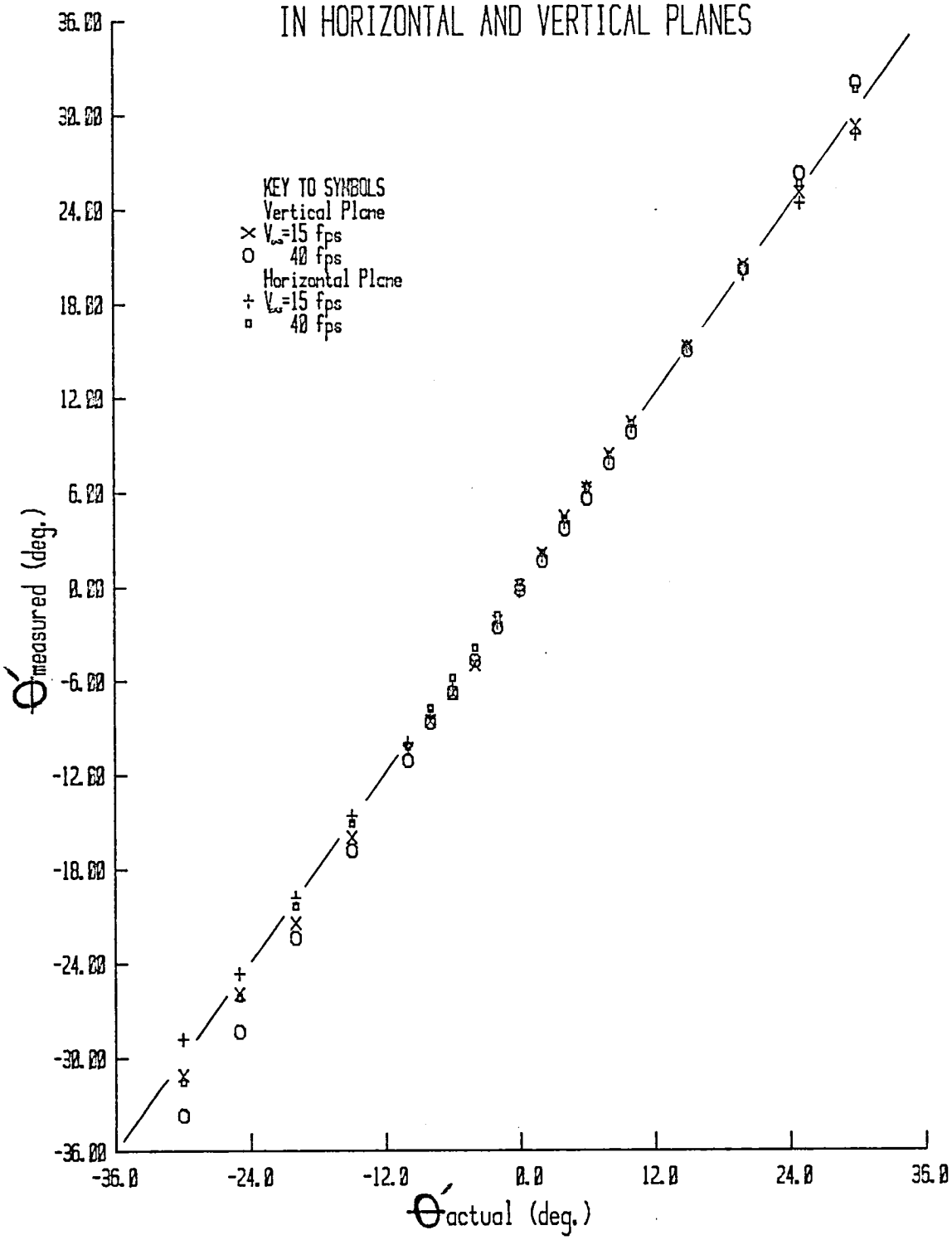

FIGURE 18. TOTAL FLOW ANGLE PROFILE AT L=29 in.
WITH V_∞=35 fps (Re=4.6X10↑5)

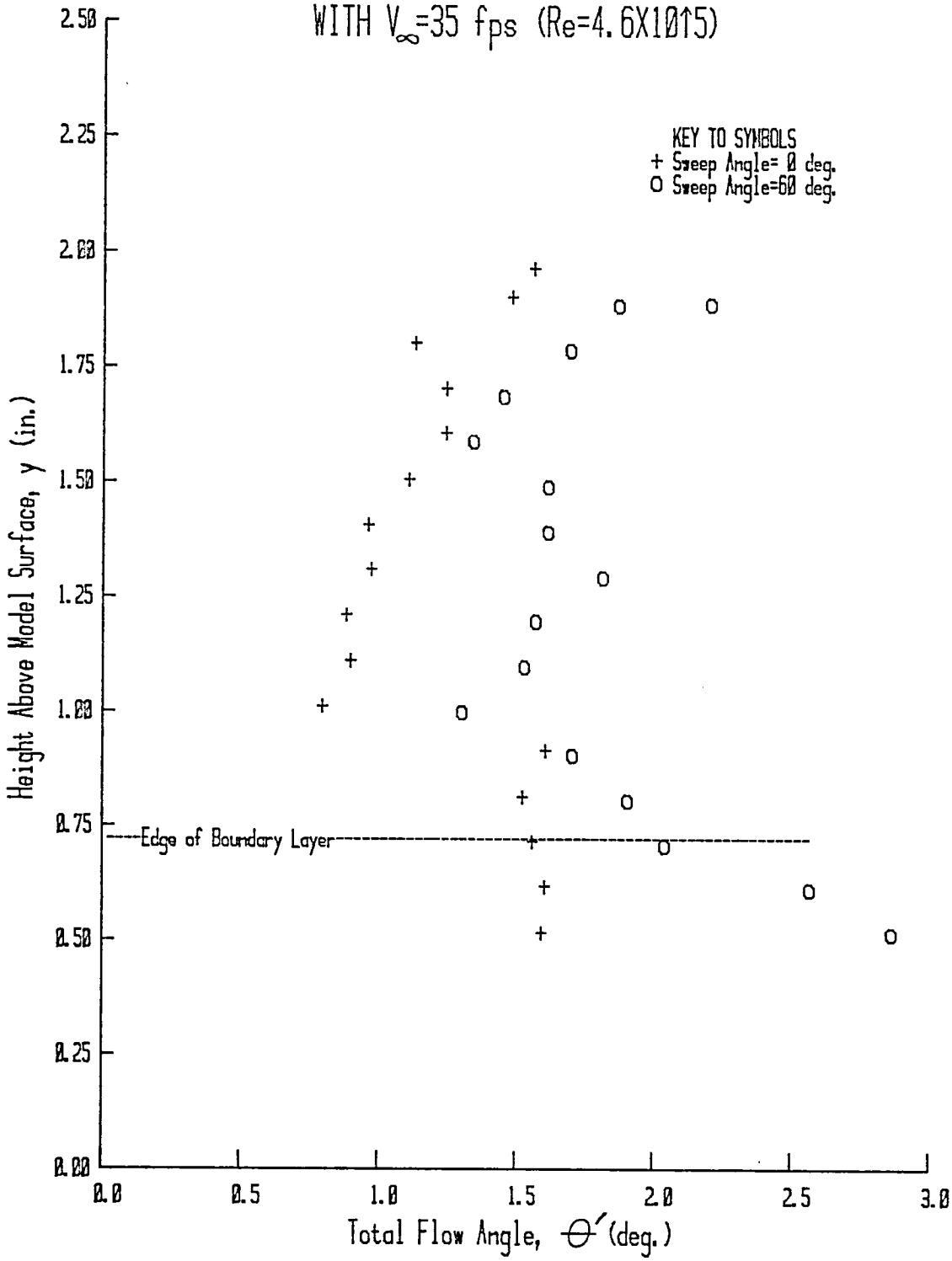

FIGURE 19. TOTAL FLOW ANGLE PROFILE AT L=42.6 in.
WITH V_∞=35 fps (Re=6.8X10↑5)

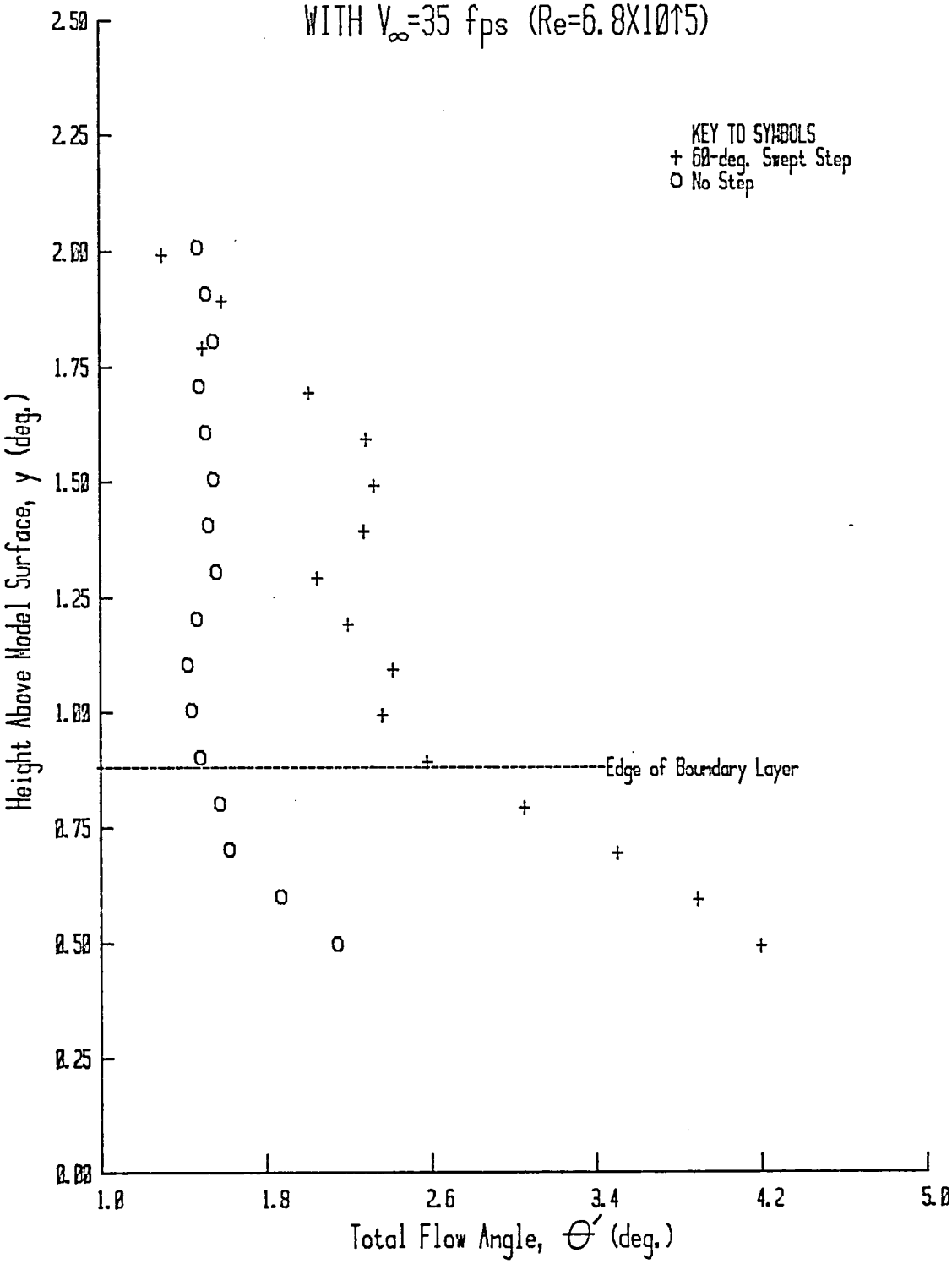

3.3. Qualitative Measurements (Basic Models)

3.3.1. Smoke Wire Photographs

A trip wire located on the surface of the model 2 in. aft of the leading edge ensured turbulent flow at the step. The turbulent nature of the oncoming boundary layer can be identified in the vertical smoke wire photos presented in this section. The smoke flow from the vertical and horizontal smoke wires was recorded as specified in Section 2.3. The freestream velocity was 25 fps for all smoke photos.

Turbulent boundary-layer flow approaching a 60° swept-step (h = .5") is shown in the vertical smoke-wire photo of Figure 20. Unfortunately, details of the flow in the separated-flow region are masked by the turbulence. Figure 20 is to be contrasted with Figures A1 through A4 of Appendix A, which depict laminar swept-step flow for Λ = 0, 30, and 60°. The smoke wire photo for turbulent flow over a two-dimensional step is similar to Figure 20; hence, it is not presented.

A series of horizontal smoke wire photos are presented in Figure 21 for the same 60° swept step as in Figure 20. The position of the horizontal smoke wire above the splitter plate was varied between 1/8 in. and 1/2 in. The smoke wire was placed parallel to the step base in the separated-flow region. The perpendicular distance of the wire from the step was 3.12 in. (approximately in the middle of

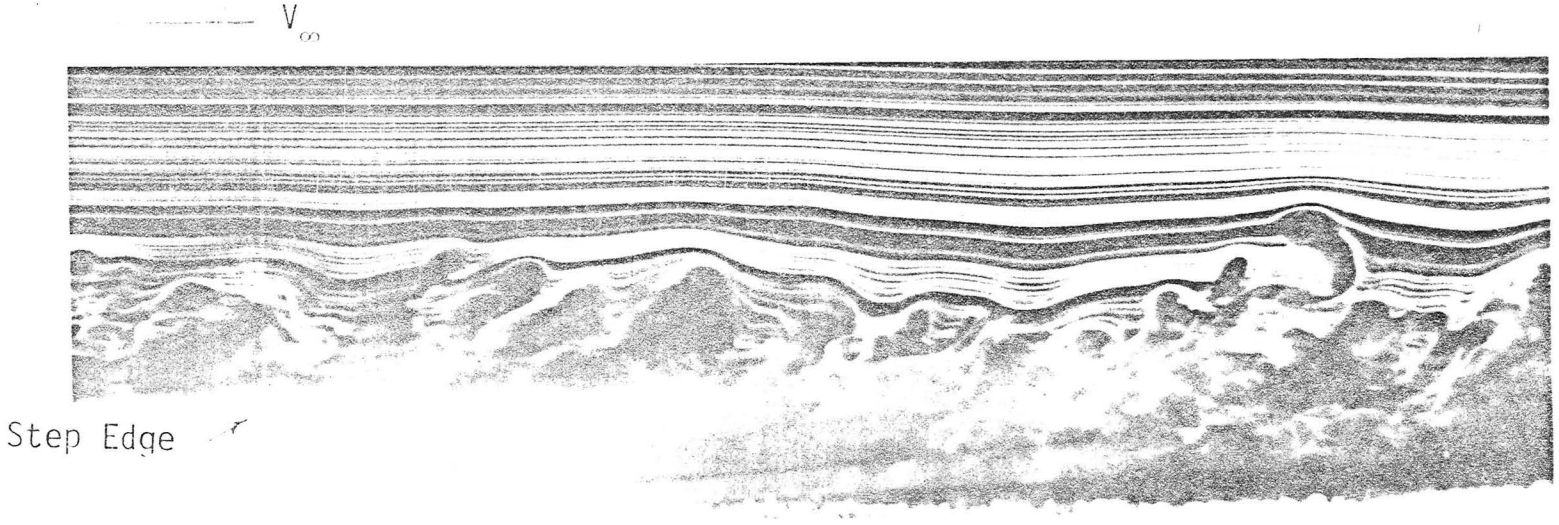

Figure 20. Smoke Visualization of Flow over a 60-deg. Swept Rearward-Facing Step with h=.5" and V_∞=25 fps Using a Vertical Smoke Wire

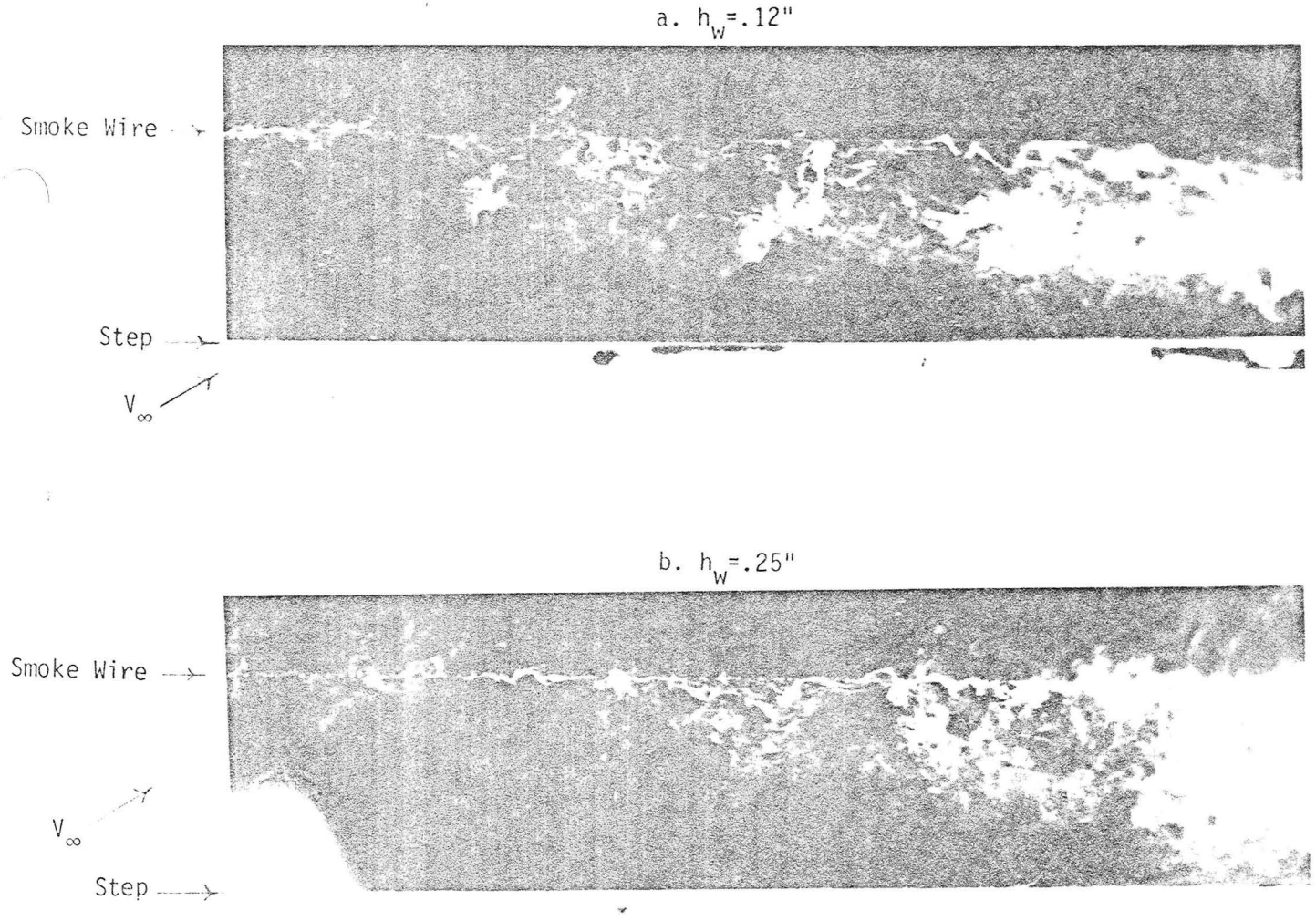

Figure 21. Smoke Visualization of the Separated-Flow Region aft of a 60-deg. Swept Rearward-Facing Step with h=.5", l_w=3.12" and V_∞=25 fps Using a Horizontal Smoke Wire

c. h_w=.38"

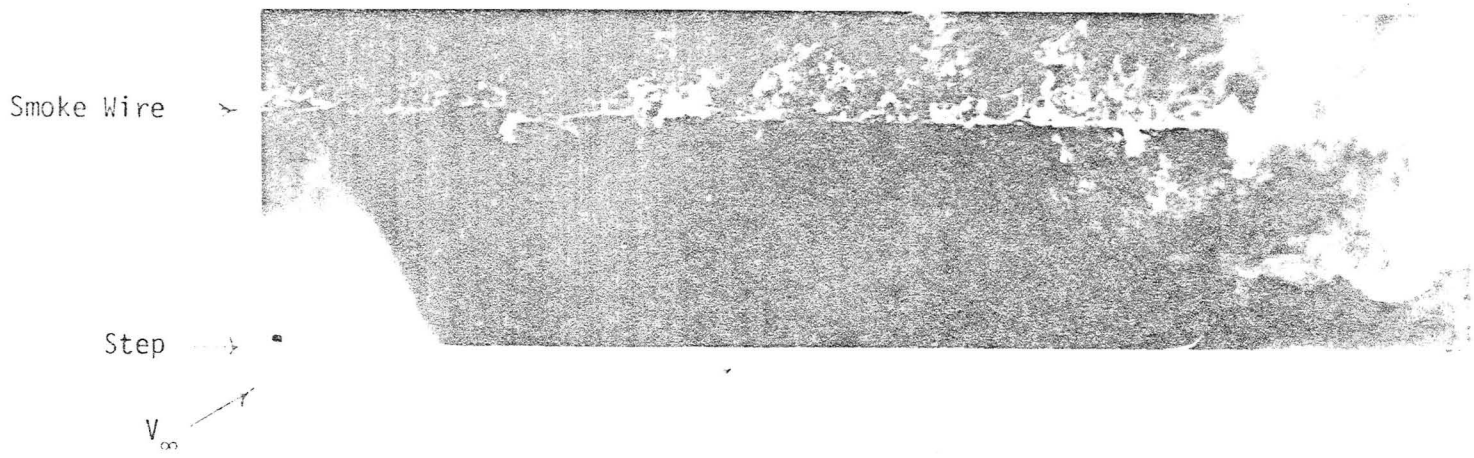

d. h_w=.50"

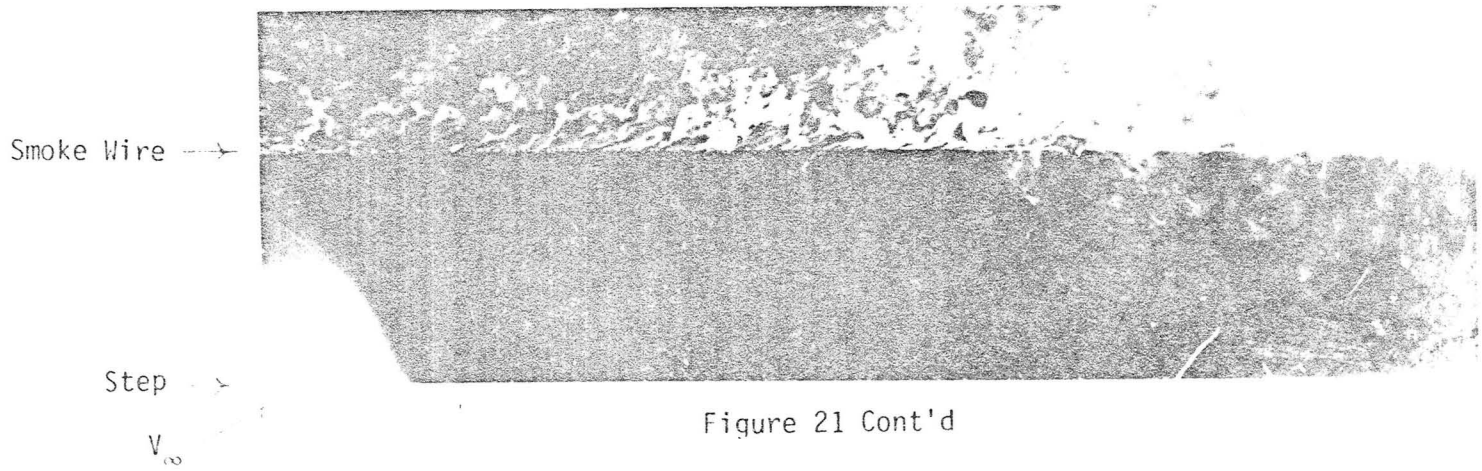

Figure 21 Cont'd

the separated-flow region). Figures 21(a) (wire height, h_w = 1/8"), 21(b) (h_w = 1/4"), 21(c) (h_w = 3/8") and 21(d) (h_w = 1/2") establish the recirculating nature of the three-dimensional separated-flow region as well as the presence of a strong spanwise flow component. The smoke flow in Figure 21(a) is shown to be predominately toward the step and in the expected spanwise direction for h_w = 1/8". When h_w is increased to 1/4 in., part of the smoke is periodically entrained by the freestream and is swept downstream. Also shown again is smoke movement in the upstream and spanwise directions. Upon increasing h_w to 3/8 in., vortical motion is experienced by several smoke filaments, but the smoke either is quickly entrained by the outer flow or rapidly diffuses before moving far in the spanwise direction. The rapid diffusion of the smoke is caused by the highly turbulent nature of the separated flow. Figure 21(d) (h_w = h = 1/2") shows the smoke predominately being swept downstream as expected.

Next, the distance of the smoke wire from the step, l_w, was varied. The two photos presented as Figure 22 also show the local spanwise vortical motion of several smoke filaments. The applicable values of l_w are 1.0 in. for Figure 22(a) and 3.5 in. for Figure 22(b) with h_w = .25", h = .50" and Λ = 60°.

The smoke wire photos are intended to give a nearly instantaneous view of the flow field as opposed to oil flow patterns which take several minutes to develop. The smoke patterns are recorded a few tenths of a second after the smoke wire is pulsed with current.

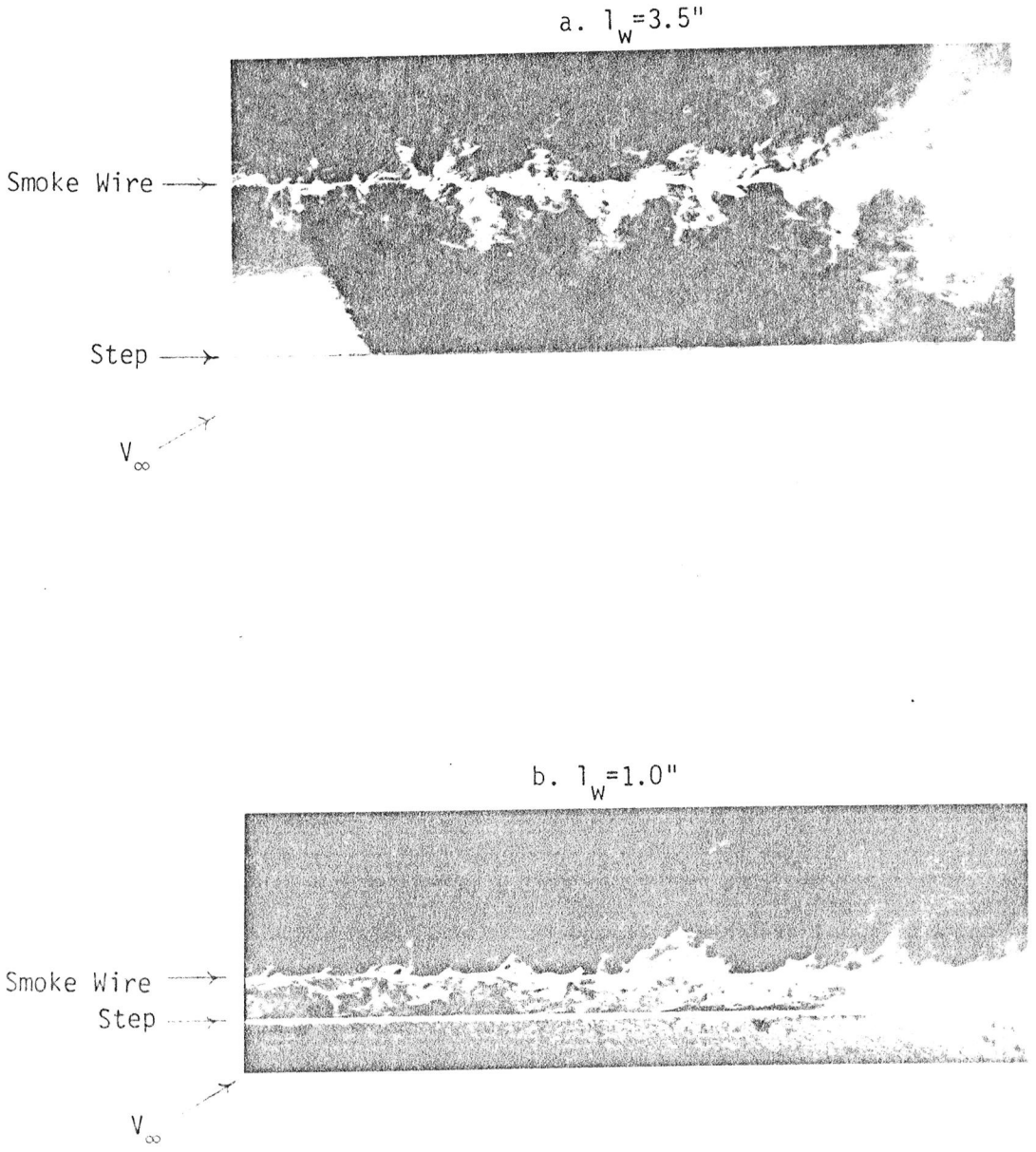

Figure 22. Smoke Visualization of the Separated-Flow Region aft of a 60-deg. Swept Rearward-Facing Step with h=.5", h_w=.25" and V_∞=25 fps Using a Horizontal Smoke Wire

Upon removing the splitter plate downstream of the step, swept wake flow ensues. The turbulent wake of a flat plate with a 60°, .5-in. thick trailing edge is presented in Figure 23(a). The oncoming boundary layer is turbulent. (Flow trips were placed at the same location on both sides of the plate.) As is the case in Figure 20, the turbulent nature of the flow masks the flow details in the vicinity of the base. Even the presence of a Karman vortex street cannot be determined in this view. However, as Figure 23(b) shows, several cores of the vortices in the Karman vortex street are distinguishable in this horizontal smoke wire photo for the same model. For this case, the horizontal smoke wire was placed at midbase with l_w = .25".

Based on the smoke-wire visualization studies for turbulent flow over swept rearward-facing steps and flat plates with swept trailing edges, it was not possible to substantiate or invalidate the flow features assumed in Figure 4. It was possible, however, to identify the Karman vortex street shed by the swept trailing-edge. In addition, it was possible to visually observe the spanwise motion of oil drops on the horizontal smoke wire when the wire was located in the vicinity of the base. This observation is indicative of a significant spanwise flow component.

3.3.2. Tufts

The tuft grids were installed downstream of the 0, 15, 30 and 60° swept rearward-facing step models. Tuft spacing was 1 in. along lines parallel to the tunnel walls. All photos were taken with a flow

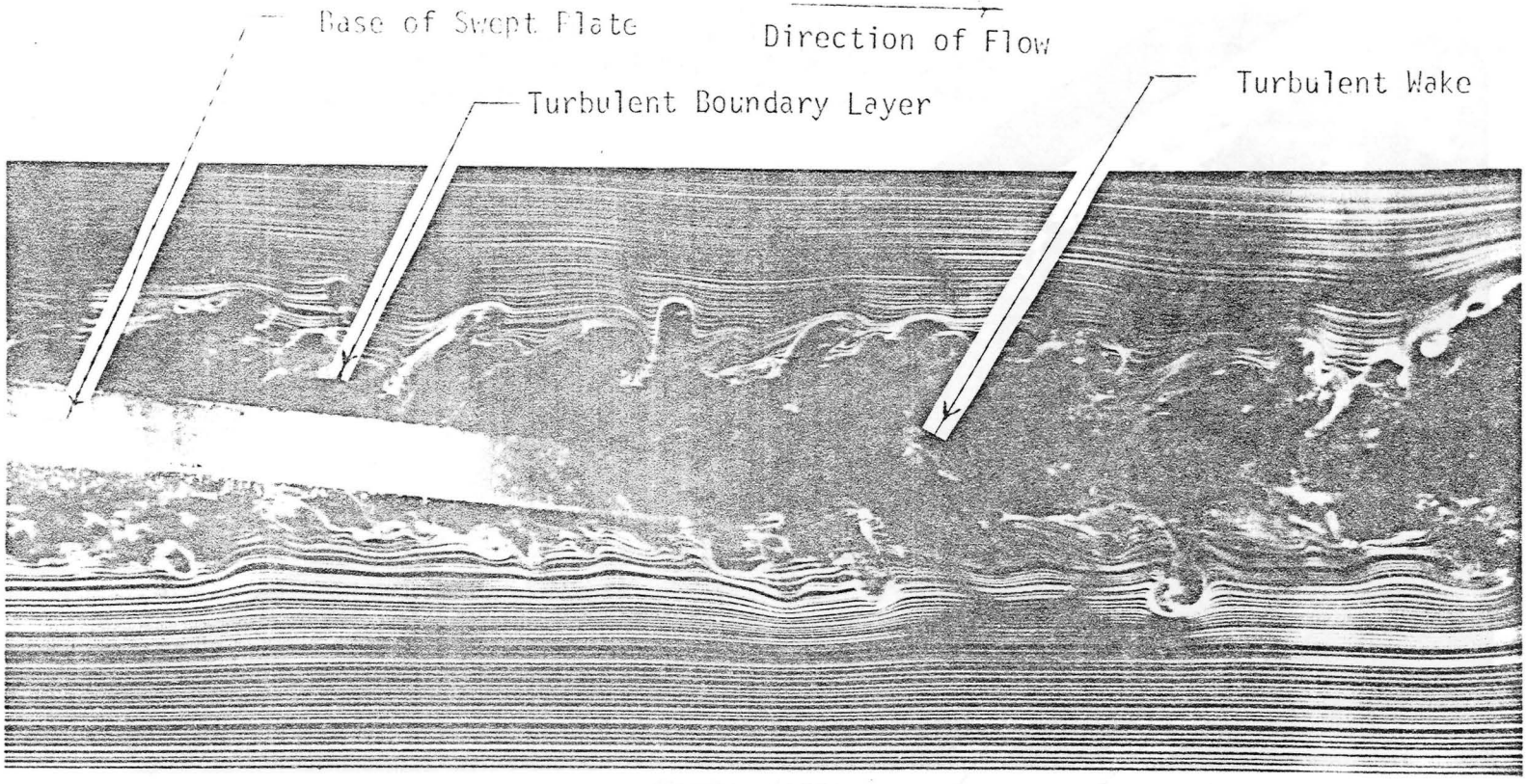

Figure 23a. Turbulent Wake of the Basic Model with 60-Degree Swept Trailing Edge Visualized Using a Vertical Smoke Wire ($t = .5"$, $V_\infty = 25$ fps, $Re = 5 \times 10^5$)

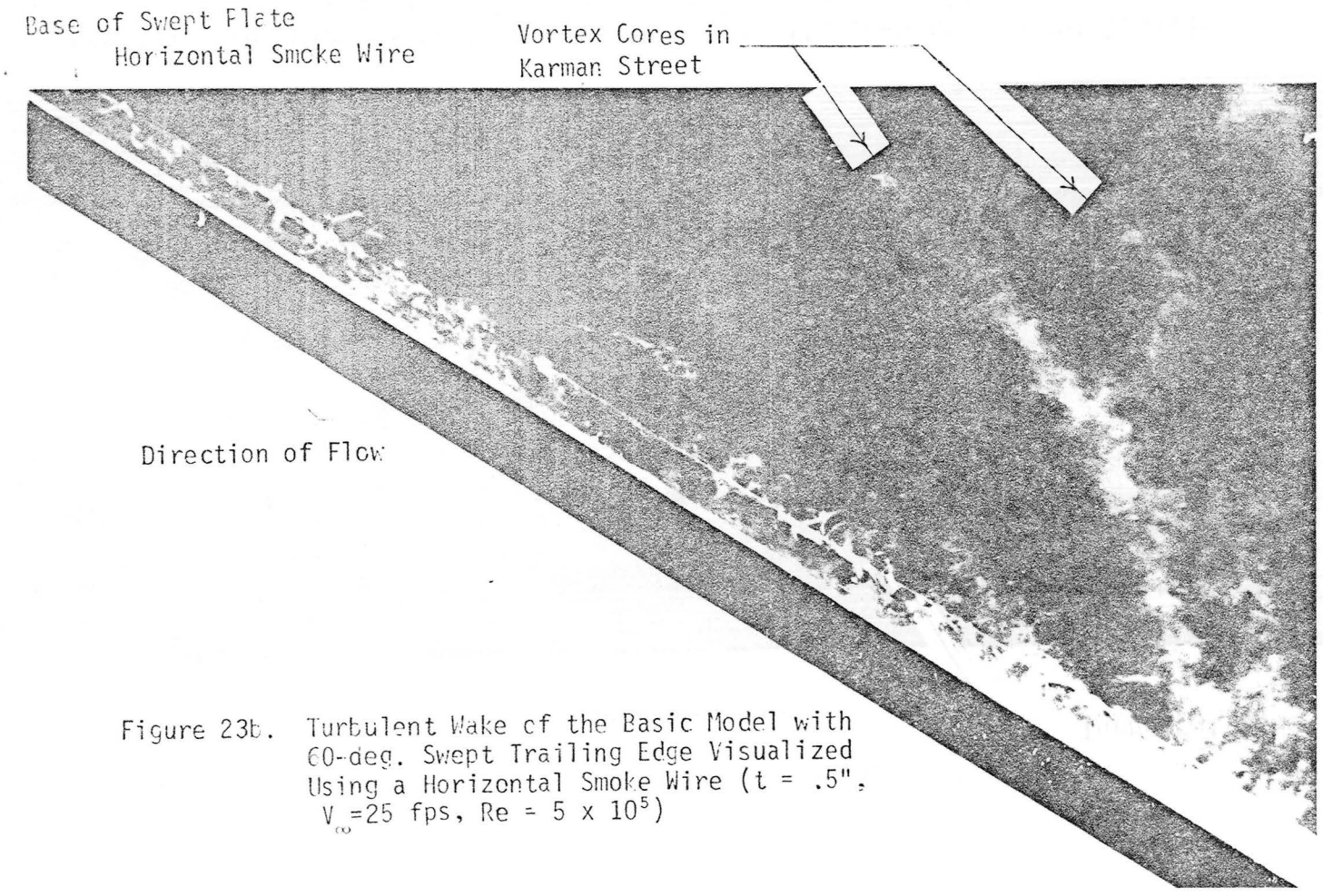

Figure 23b. Turbulent Wake of the Basic Model with 60-deg. Swept Trailing Edge Visualized Using a Horizontal Smoke Wire (t = .5", V_∞=25 fps, Re = 5 x 10^5)

speed of 70 fps which corresponds to $Re \approx 10^6$. All models had a constant step height of .88 in.

Figure 24 shows the random orientation of the tufts in the absence of flow.

Figure 25 indicates the occurrence of reattachment in the vicinity of row 5 ($R'/h = 5.7$). No appreciable spanwise tuft movement was either visually observed or in evidence from an examination of Figure 26(b)—another view of the 15° swept model.

Figures 27(a) and 27(b) pertain to the 30° swept-step model. These photos show that reattachment occurs between rows 5 and 6. In addition, the tufts in rows 2 to 4 are becoming noticeably oriented in the spanwise direction indicating the increased prominence of spanwise flow ($4.9 < R'/h < 5.9$).

Tuft dynamics for flow over a 60° swept-step model are shown in Figures 28(a) and 28(b). Figure 28(a) indicates that reattachment occurs in the region between rows 7 and 8 ($4.0 < R'/h < 4.5$). It can also be determined from tuft orientation in rows 1 through 6 that appreciable spanwise flow is present.

The reattachment distances determined from tuft motion generally agree well with the values determined using the oil drop method for $h = .94"$, as indicated by the comparisons below.

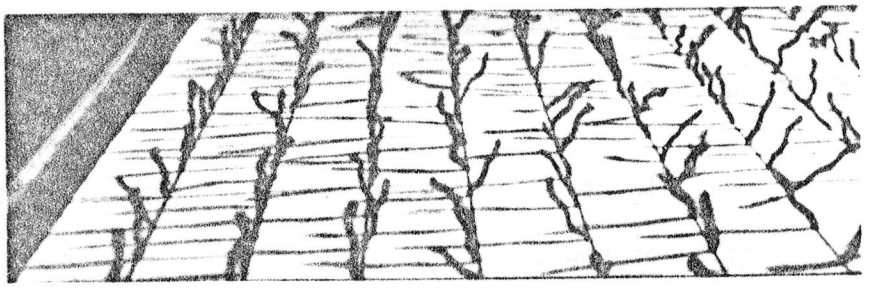

Figure 24. Random Tuft Orientation in the Absence of Flow

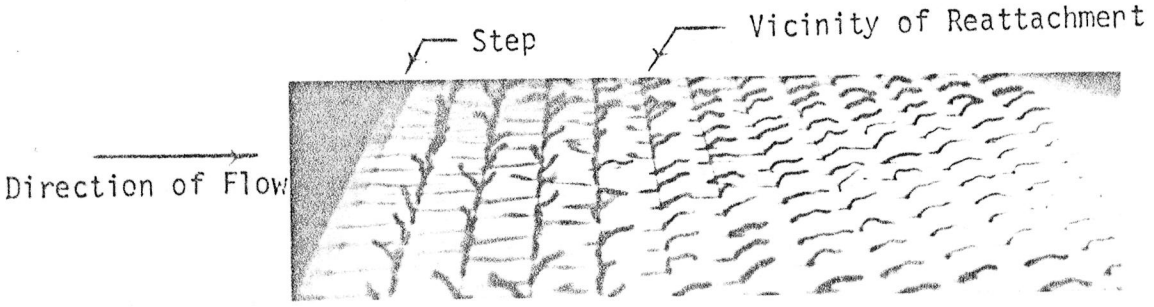

Figure 25. Visualization of the Flow Downstream of the Basic 2-D Step Using a Tuft Grid ($h = .88"$, $V_\infty = 70fps$, $Re = 1.4 \times 10^6$)

Figure 26.
Visualization of the Flow Downstream of the Basic 15-deg. Swept Step Using a Tuft Grid (h = .88", V_∞ = 70 fps, Re = 1.4 x 10^6)

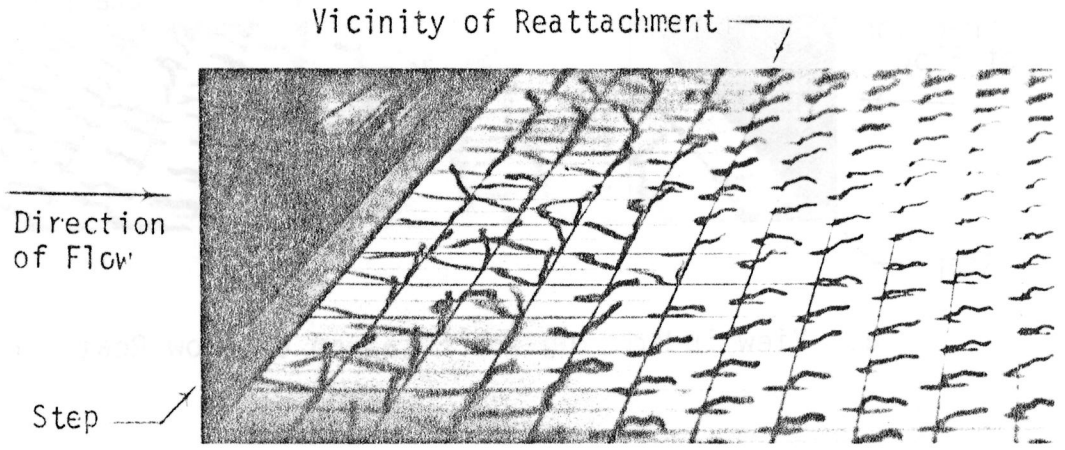

a. View Showing the Location of Flow Reattachment

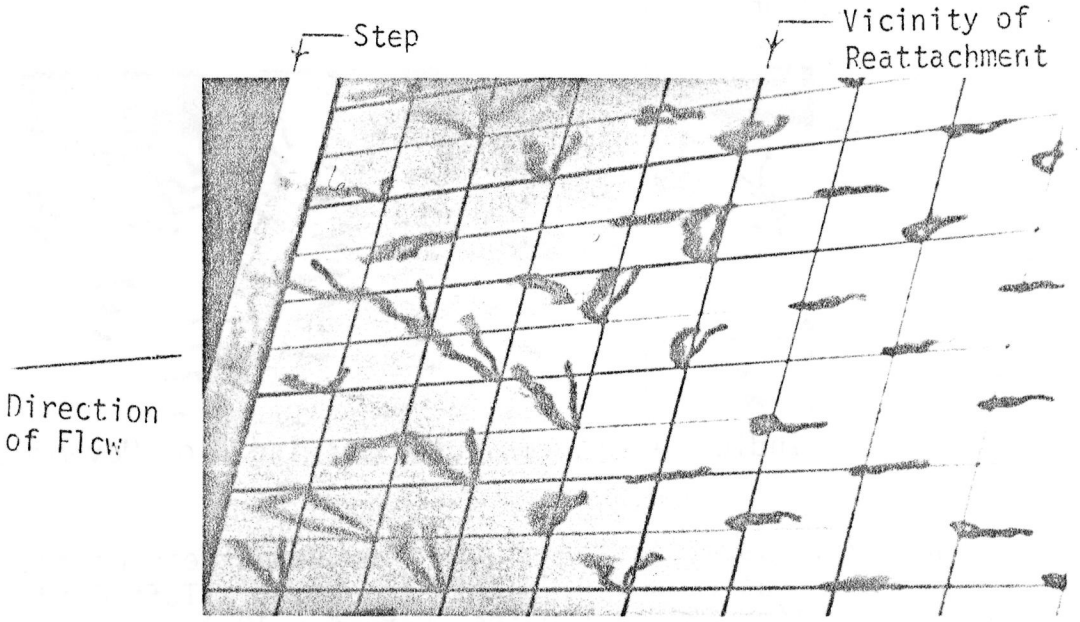

b. View Showing the Lack of Spanwise Flow Movement

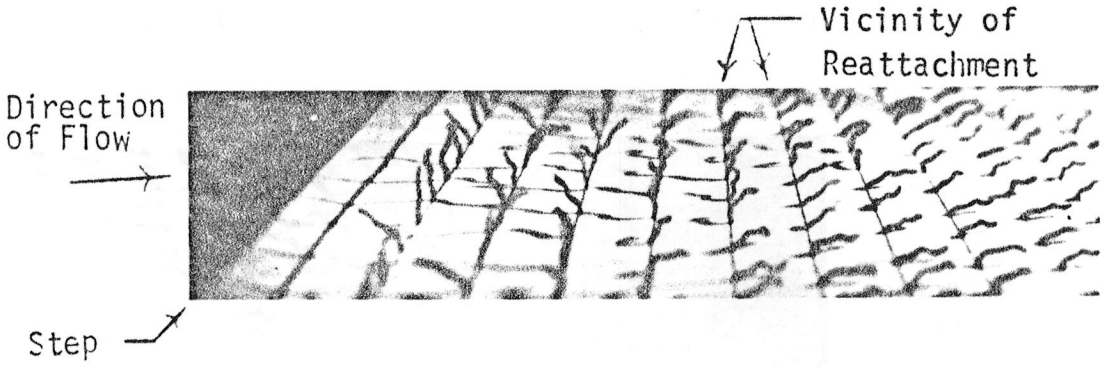

a. View Indicating the Location of Flow Reattachment

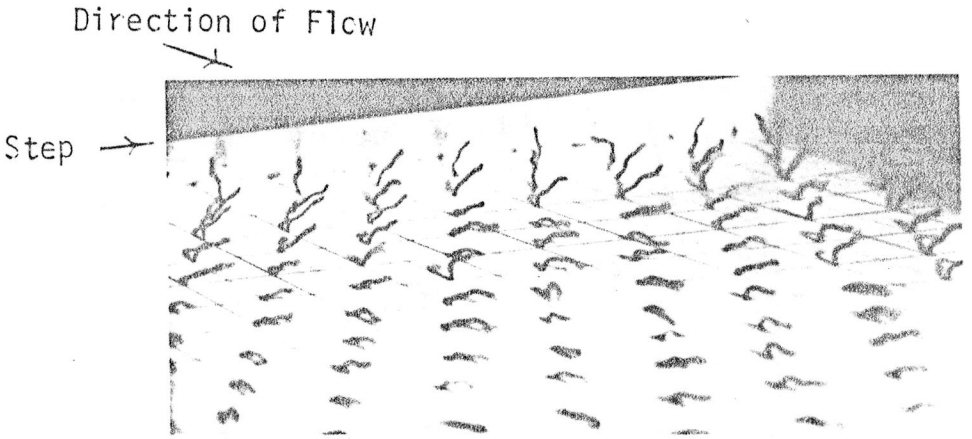

b. View Indicating Appreciable Spanwise Flow Movement

Figure 27. Visualization of the Flow Downstream of the Basic 30-deg. Swept Step Using a Tuft Grid ($h=.88"$, $V_\infty=70$ fps, $Re=1.4 \times 10^6$)

Figure 28. Visualization of the Flow Downstream of the Basic 60-deg. Swept Step Using a Tuft Grid ($h=.88"$, $V_\infty=70$ fps, $Re=1.4 \times 10^6$)

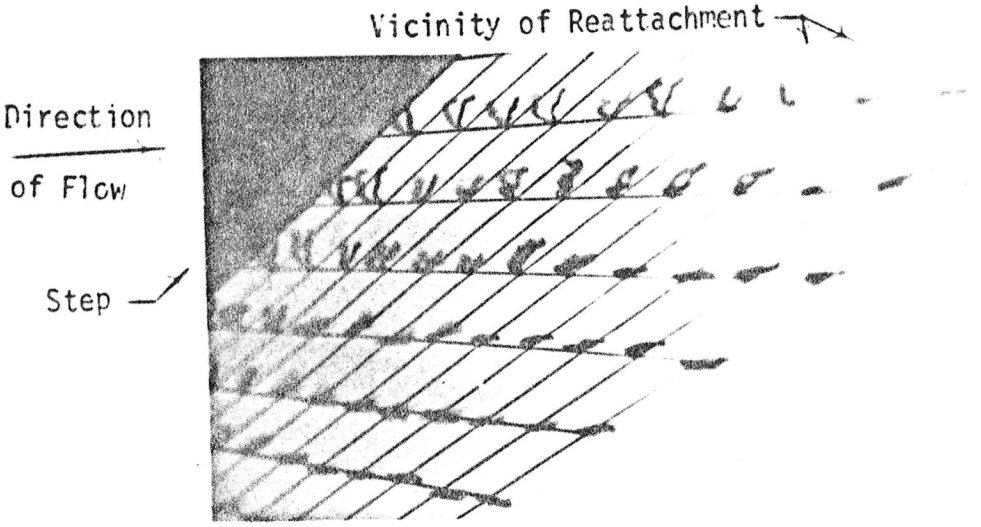

a. View Indicating the Location of Flow Reattachment

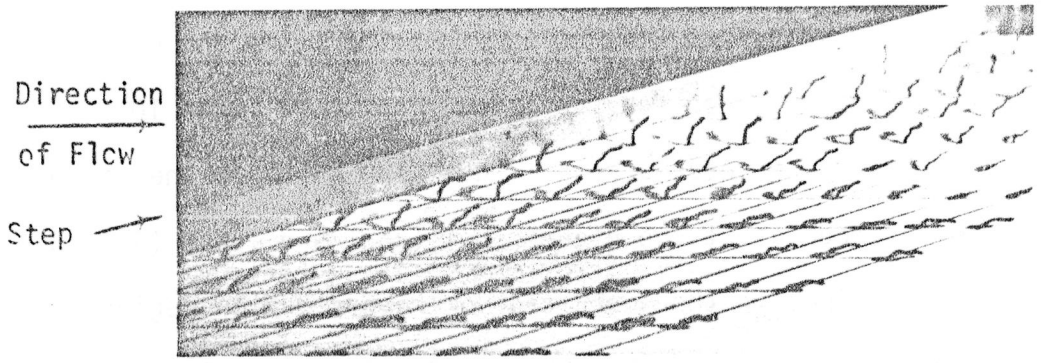

b. View Showing the Presence of Significant Spanwise Flow

Table 4

Reattachment Distances Based on Tuft and Oil Drop Methods

	R'/h	
Λ (deg.)	Tuft	Oil Drop
0	5.7	6.1 - 6.9
15	5.5	5.4
30	4.9 - 5.9	5.4
60	4.0 - 4.5	3.8

3.3.3. Oil Flow Photographs

The oil flow photographs were produced in the manner described in Section 2.3—the oil flow lines indicating the average local direction of the flow at the model surface.

Presented in Figures 29(a) and (b) are the oil flow photos for the unswept model with $h = .50"$ for $V_\infty = 35$ and 70 fps ($Re = 6.8 \times 10^5$ and 1.4×10^6), respectively. Figure 30 shows the oil flow pattern for the unswept step for $h = .94"$ and $Re = 1.4 \times 10^6$. At the lower Re, the surface shear stress is not very high, so the oil pattern is not as pronounced as at the higher Re. For $h = .50"$ (AR = 30) the oil flow lines in the separated- or reversed-flow region are generally perpendicular to the step, except near the side walls. This would suggest that the separated flow is two-dimensional over the interval $5 < Y'/h < 25$. The reattachment line is curved near the side walls—also

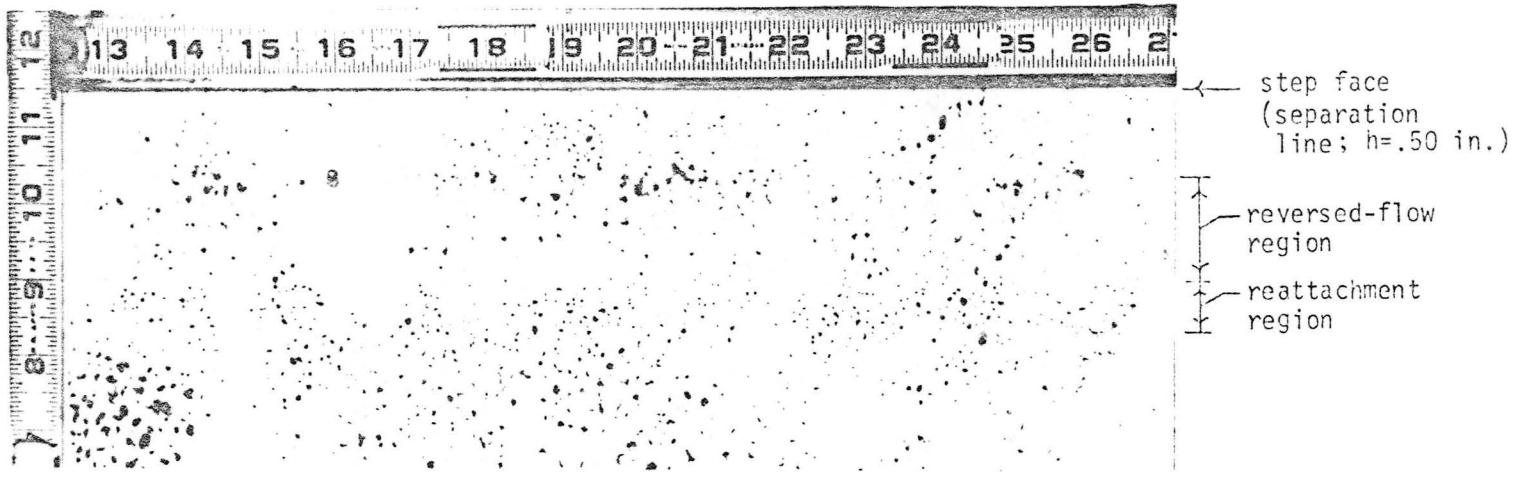

Figure 29a. Surface Oil Streak Patterns ($\Lambda=0^{\circ}$ and $V_{\infty}=35$ fps; flow from top to bottom)

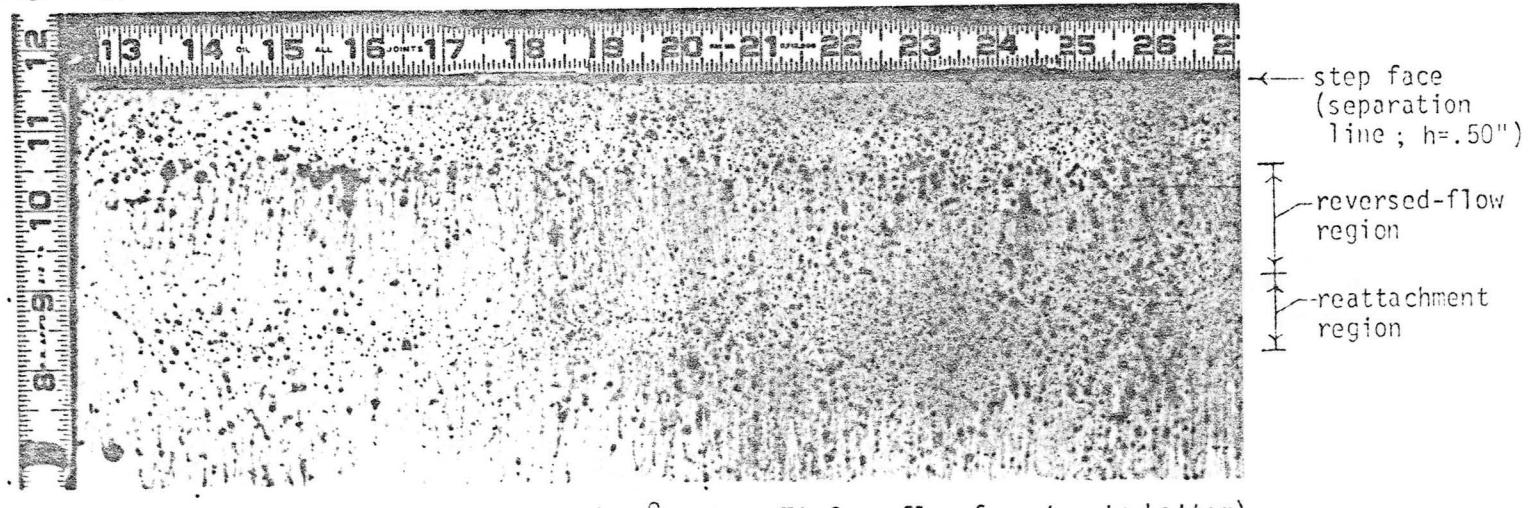

Figure 29b. Surface Oil Streak Patterns ($\Lambda=0^{\circ}$ and $V_{\infty}=70$ fps; flow from top to bottom)

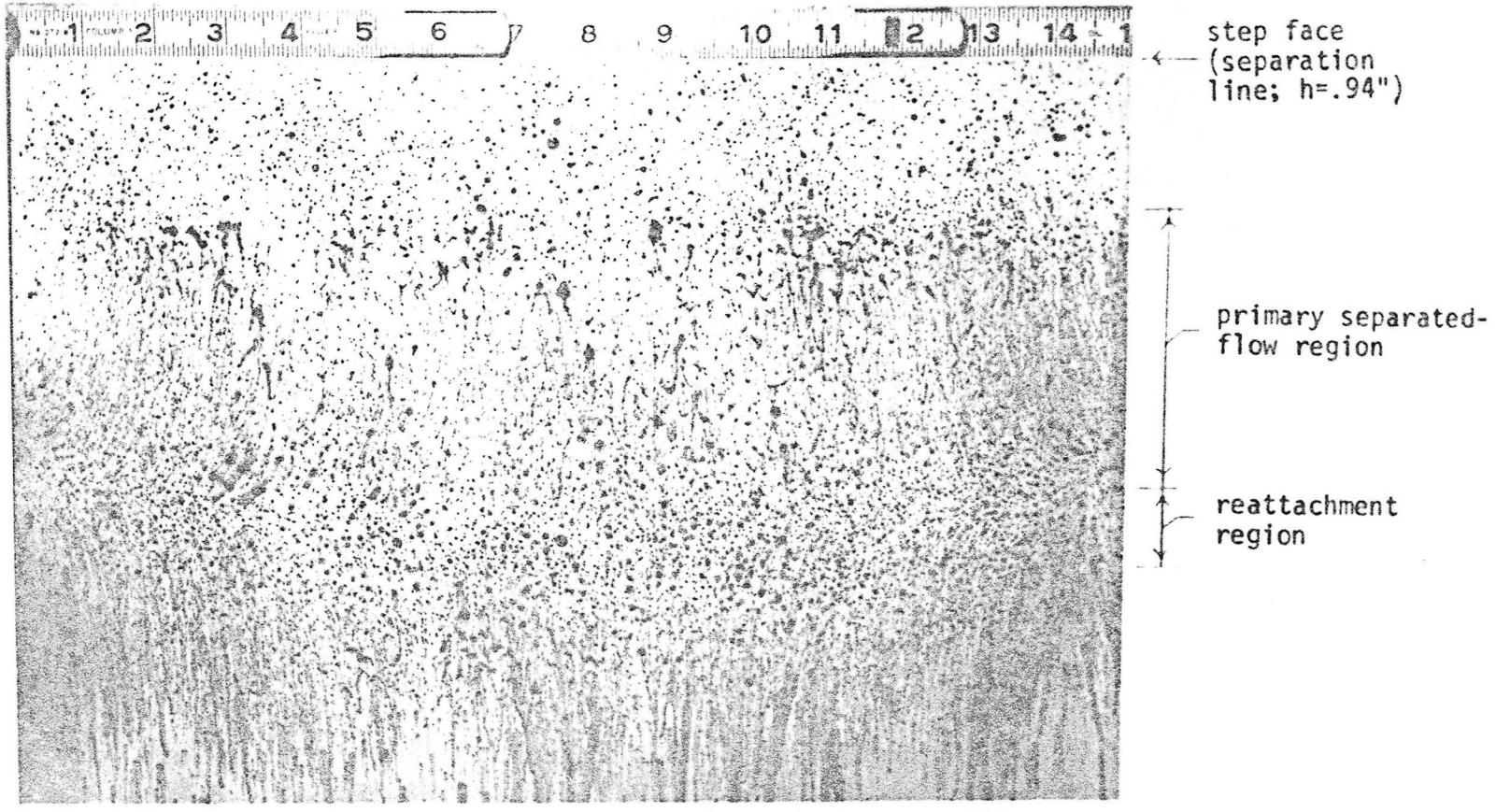

Figure 30. Surface Oil Streak Patterns (Λ=0°, V_∞=70 fps and h=.94"; flow from top to bottom)

due to end effects. The oil flow pattern for $h = .94"$ (AR = 16), however, indicates that the separated flow is two-dimensional only for a small region near midspan.

This observation for AR = 16 is inconsistent with the findings of de Brederode and Bradshaw (1972) who indicate that if AR > 10, the flow over an unswept rearward-facing step will be two-dimensional over most of the span—end effects being virtually negligible. Their conclusions were based on an examination of oil flow photos and representative base pressure measurements. The aspect ratio was varied from 3 to 30 by changing the position of end plates as opposed to changing step height and hence, area ratio (Ar), as in the present study. Another significant difference is that de Brederode and Bradshaw were working with a very thin sidewall boundary layer at the step in the turbulent case—$\delta = .16$ in. The sidewall boundary-layer thickness was not measured in the present study, however, it is expected to have been at least three or four times greater than the aforementioned value at the step for the flow conditions examined in Figure 30.

Early in the present study, the unswept model was inadvertently laterally misaligned which resulted in an appreciable spanwise pressure gradient. Under these conditions, the oil flow pattern for AR = 30 displayed no effect due to the pressure gradient, though three-dimensional flow was undoubtedly present to some degree across the entire span.

Surface oil flow patterns in the separated flow behind a 15° .5-in. swept step are shown in Figure 31 for $Re = 6.8 \times 10^5$. Just as in the preceding low Re case, the surface shear is not high enough to move the oil drops very far, however, certain prominent features can still be identified. The reattachment region, for instance, was of finite width in the two-dimensional case. For $\Lambda = 15°$, however, a distinct reattachment line can be observed. There is a reversed-flow region as in the two-dimensional case, but the oil flow lines are no longer generally perpendicular to the step being at an angle (Swirl Angle, ϕ) to the step normal. Instead of a transverse vortex being characteristic of the separated flow, it may now be characterized as spanwise vortex flow.

The surface oil flow patterns resulting from the spanwise vortex flow become more distinguishable as the sweep angle is increased. At $\Lambda = 30°$ and $h = .5"$ (Figure 32) the reattachment line is easily detected. The oil accumulation line observed in Figures 31, 32 and subsequent photos is apparently the location where the reversed flow separates from the surface. It was visually observed that the movement of oil within the oil accumulation line was spanwise in the same direction as that of the primary vortex. For all cases discussed up to this point, no movement of oil drops upstream of the oil accumulation line was observed.

For $\Lambda = 30°$ and $h = .94$, an interesting feature was observed at $Re = 1.4 \times 10^6$. The spanwise motion of the oil drops upstream of

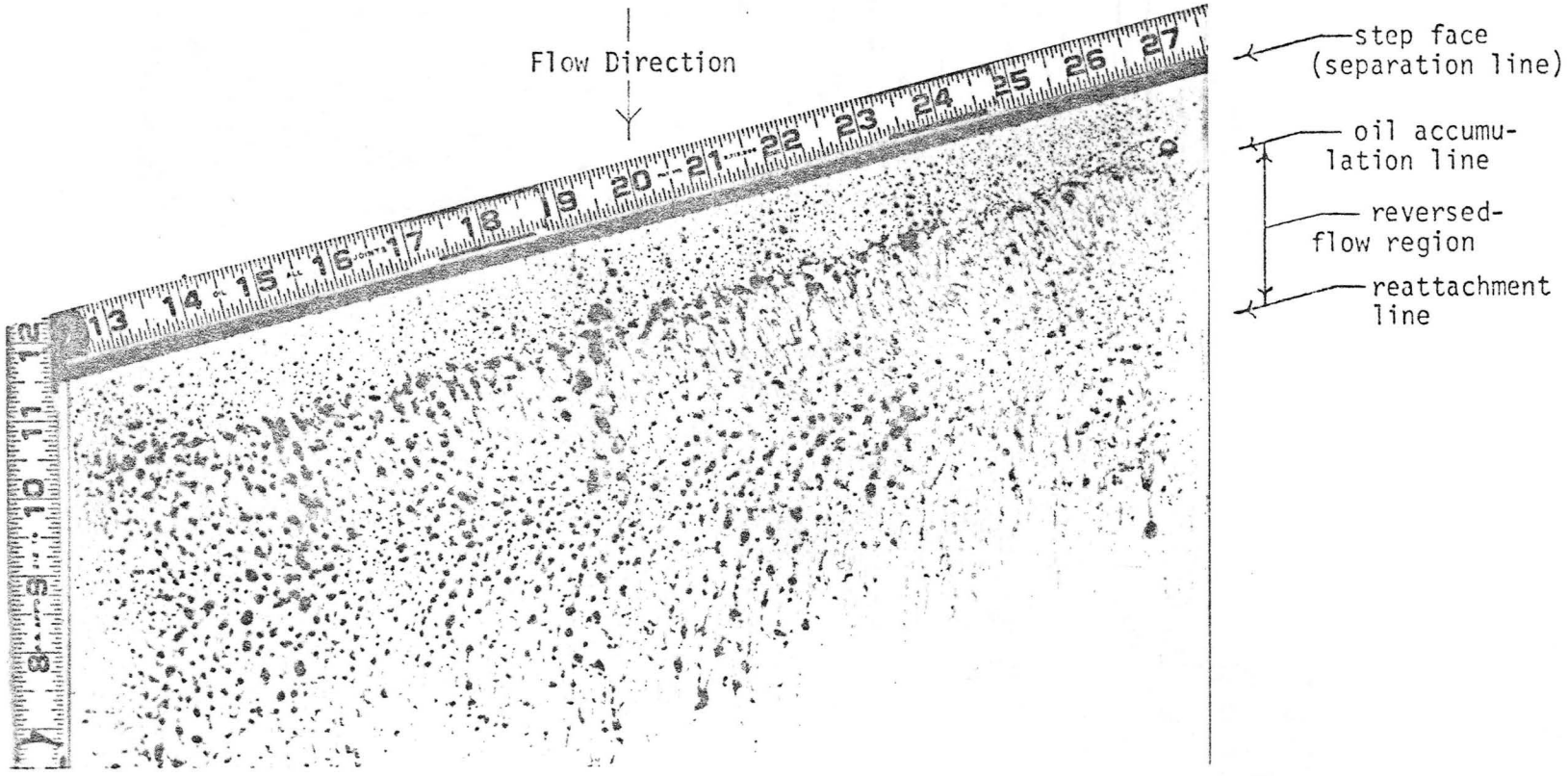

Figure 31. Surface Oil Streak Patterns ($\Lambda=15^{o}$, $V_{\infty}=35$ fps and h=.50 in.; flow from top to bottom)

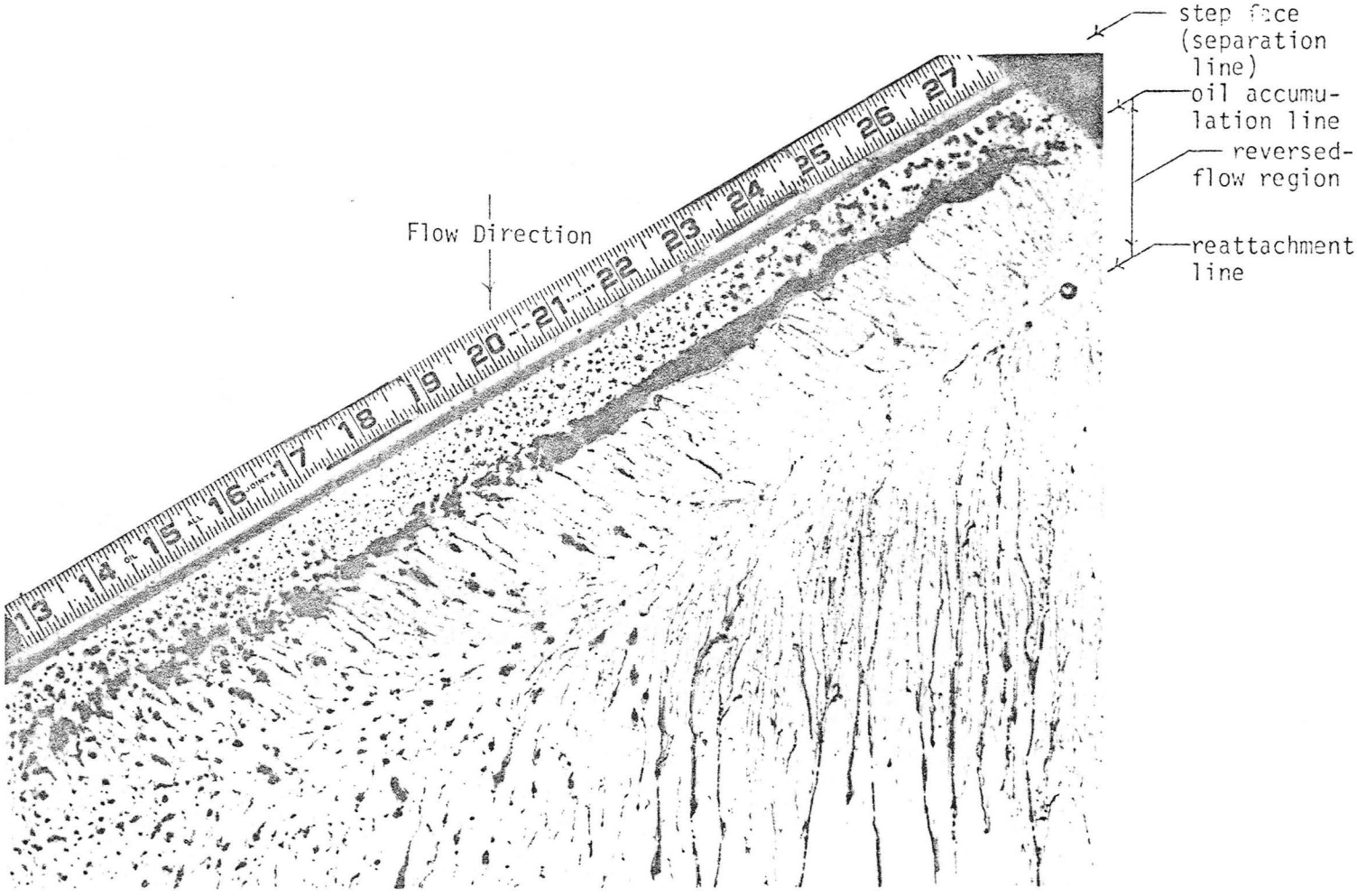

Figure 32. Surface Oil Streak Patterns ($\Lambda=30^{o}$, V_{∞}=70 fps and h=.50 in.; flow from top to bottom)

the oil accumulation line was opposite the motion in the primary reversed flow region. In other words, in Figure 33, the spanwise vortex flow in the primary separated-flow region is from left to right, while the flow in the secondary separated-flow region is from right to left. (This phenomenon may not be clearly distinguishable in the figure.) This feature is considered to be the effect of model-test section coupling as discussed in Appendix B—primarily a geometric consideration which results in a spanwise pressure gradient in the direction of the secondary vortex flow. It is recalled that the two-dimensional rearward-facing step model presented in Figure 3 included a "corner eddy" as a flow feature. The secondary vortex flow is apparently an extension of the two-dimensional corner eddy to three-dimensional flow.

Secondary vortex flow and secondary separation regions are not unique—being encountered in many three-dimensional flows. Griffin and Ramberg (1974) reported secondary vortex formation in the wake of a vibrating cylinder. Peake and Tobak (1980) have postulated the existence of secondary vortex flow structures on the leeward side of blunt and sharp cones—as have other researchers. Mirande and Quelin (1977) also found secondary vortex flow (same direction as primary flow)

Griffin, O. M. and Ramberg, S. E., "The Vortex Street in the Wake of a Vibrating Cylinder," Journal of Fluid Mechanics, Vol. 66, pp. 553-578, 1974.

Peake, D. J. and Tobak, M., Three-Dimensional Interactions and Vortical Flows with Emphasis on High Speeds, NASA Ames Research Center, NASA TM 81169, 1980.

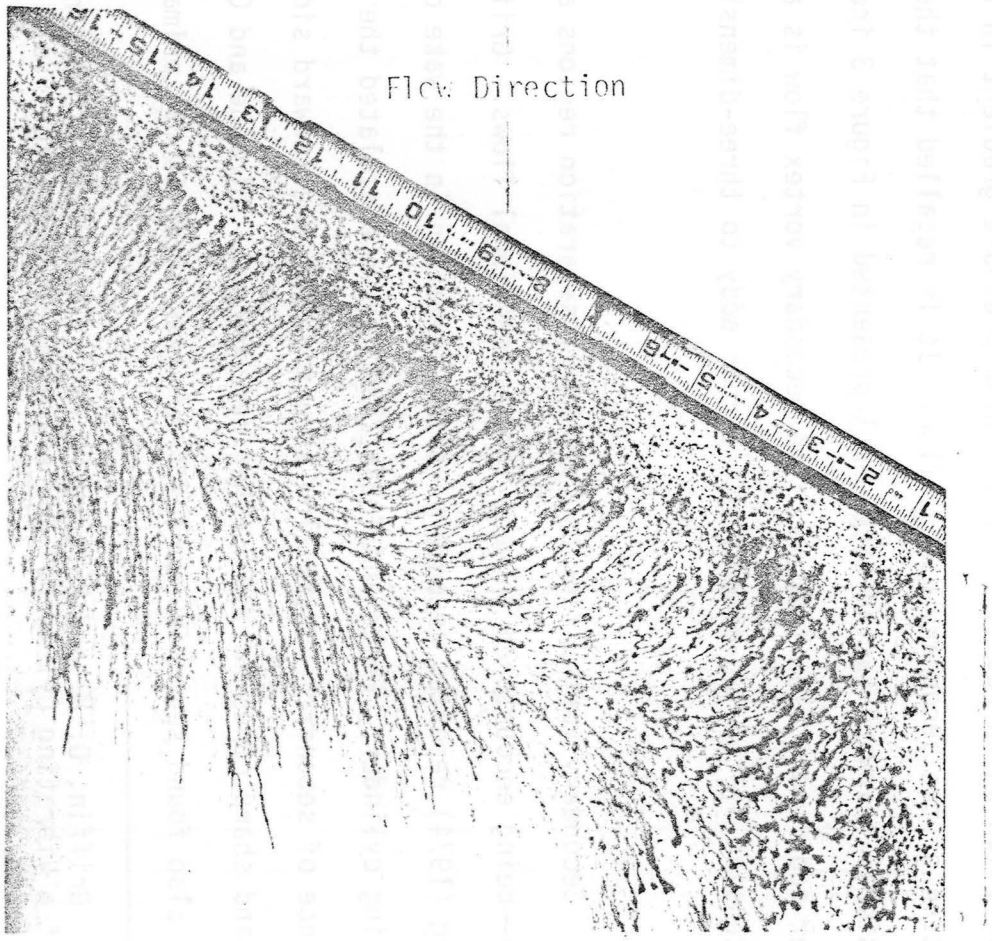

Figure 33. Surface Oil Streak Patterns ($\Lambda = 30^{0}$, V_{∞} = 70 fps and h = .94 in.)

in their oil drop visualization studies of flow over a swept, chevron-shaped (maximum step height at midspan) step with a double sweep angle of 45°.

Figure 34 again shows a secondary separated-flow region for $\Lambda = 60°$, $h = .5$ in. and $Re = 1.4 \times 10^6$ (70 fps). However, in this case, the primary and secondary vortex flows are in the same directions. At this large sweep angle, it is apparent that the strong primary vortex has a greater effect on driving the secondary flow than does the geometrically induced spanwise pressure gradient, or it is simply due to the fact that this gradient becomes smaller as Λ is increased, as shown in Appendix B. The secondary vortex flow is clearly shown in Figure 35, which is at the same sweep angle (60°) but with a larger step height (.94 in.).

It should be pointed out that the oil droplets do not interfere appreciably with the flow [Maltby (1962) and Merzkirch (1974)], but produce an average view of the surface flow phenomena. Therefore, this method cannot give an instantaneous view of an unsteady flow pattern.

The surface flow features observable in the oil flow photos presented in this section are summarized in Figure 36. These features

---

Maltby, R. L., Flow Visualization in Wind Tunnels Using Indicators, NATO Advisory Group for Aeronautical Research and Development, AGARDograph 70, 1962.

Merzkirch, W., Flow Visualization, Academic Press, Inc., p. 53, 1974.

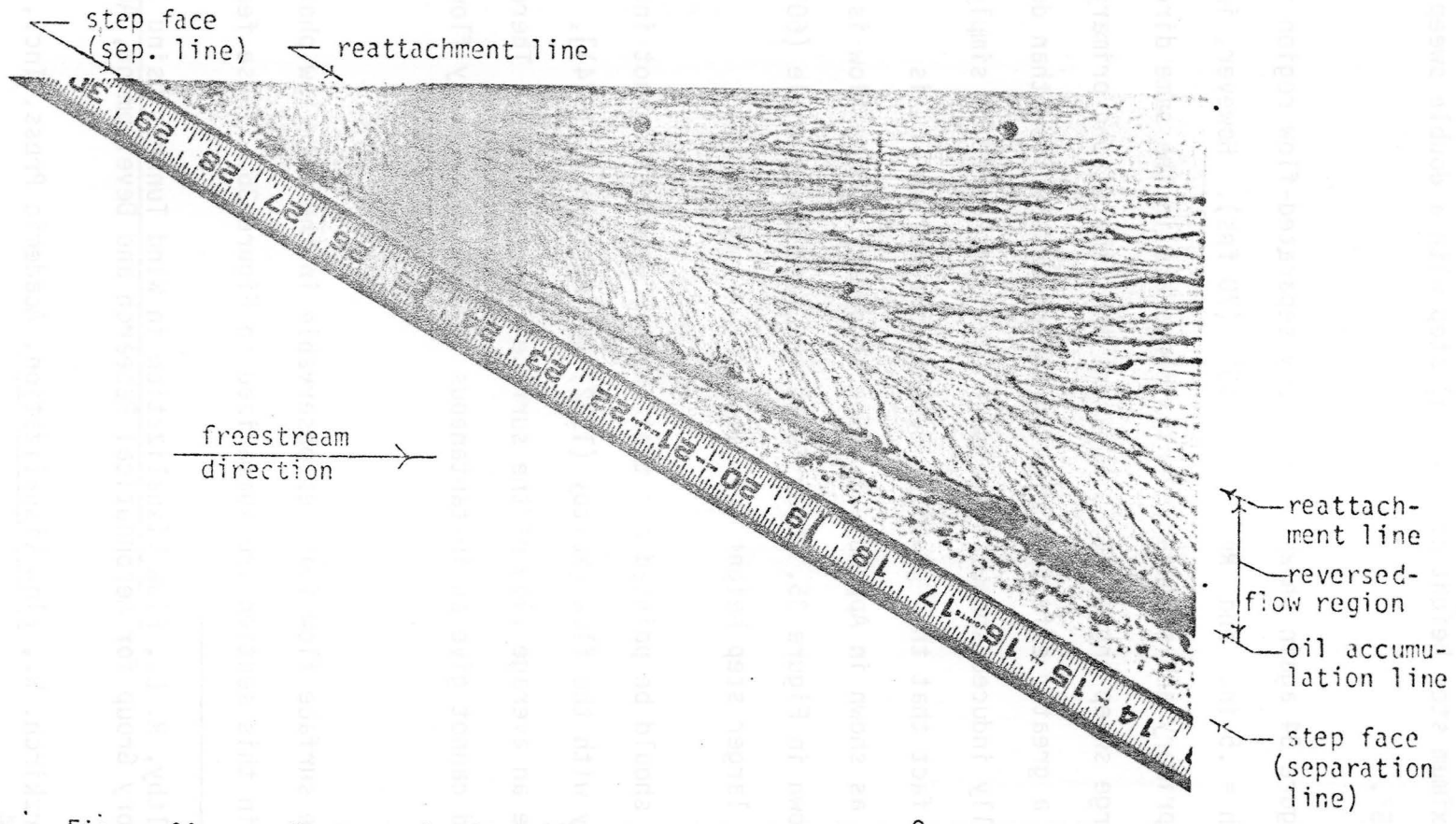

Figure 34a. Upstream Surface Oil Streak Patterns ($\Lambda=60^{o}$, $V_{\infty}=70$ fps and $h = .50$ in; flow from left to right)

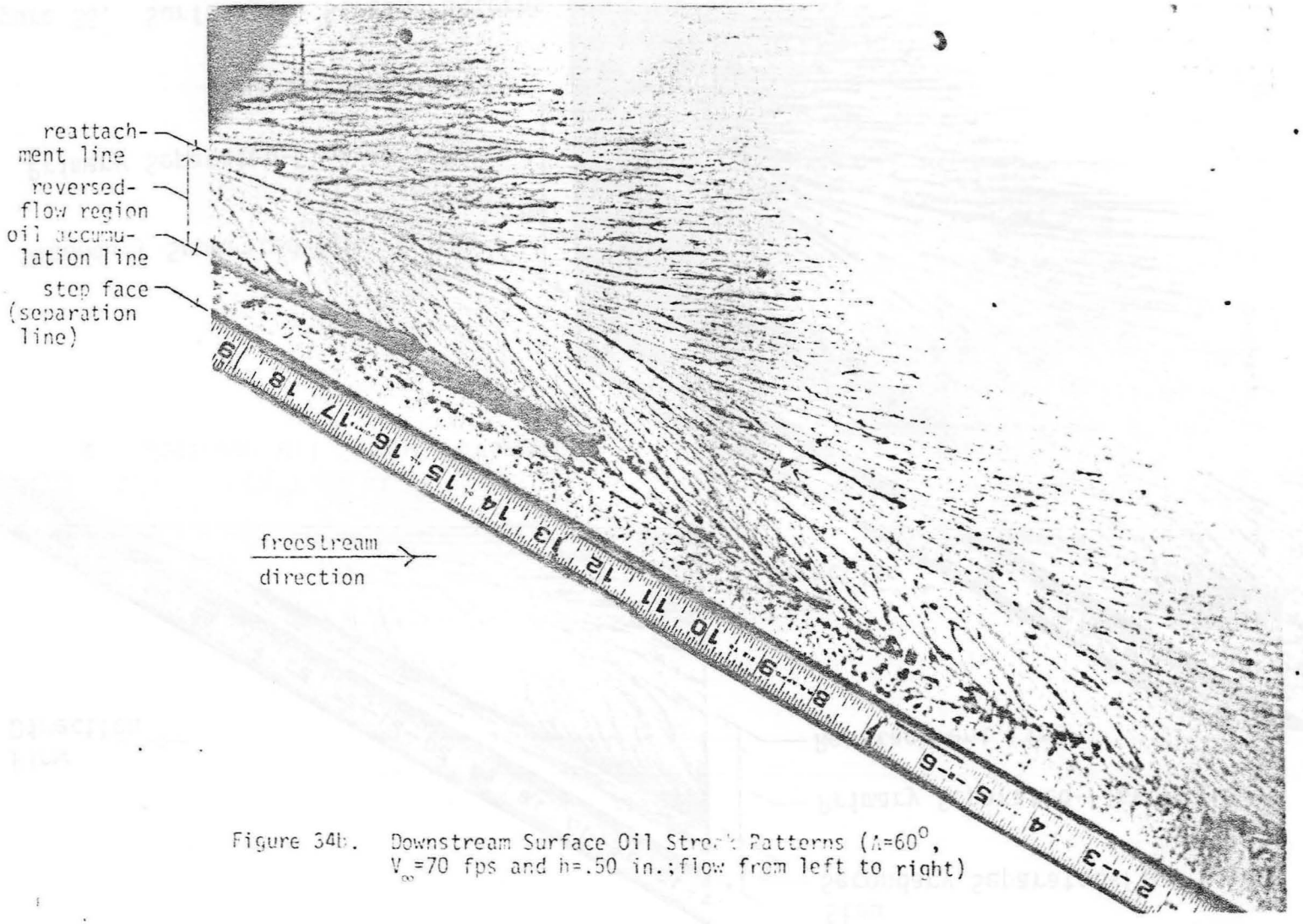

Figure 34b. Downstream Surface Oil Streak Patterns ($\Lambda=60^{o}$, $V_{\infty}=70$ fps and $h=.50$ in.; flow from left to right)

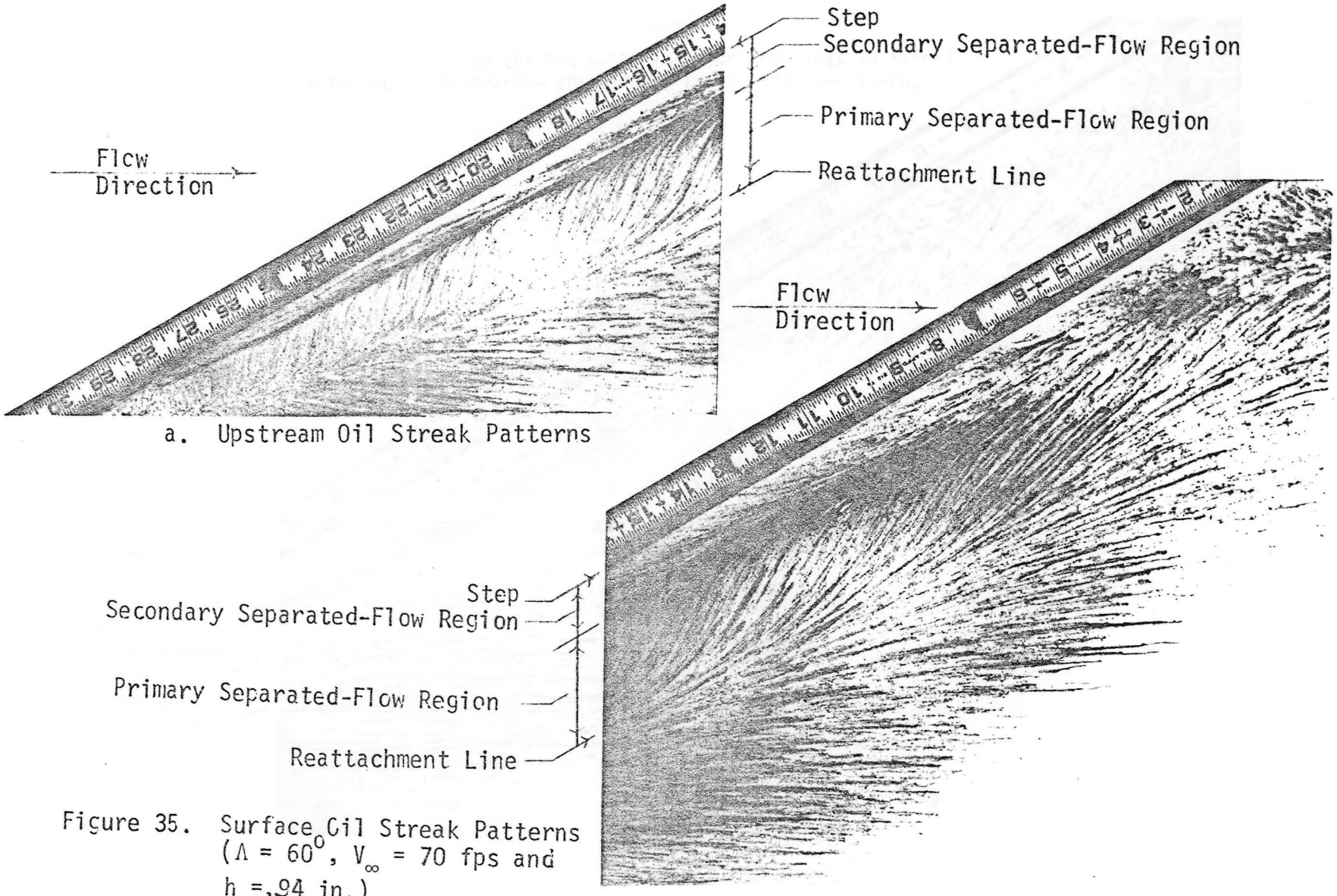

Figure 35. Surface Oil Streak Patterns ($\Lambda = 60^{0}$, V_{∞} = 70 fps and h = .94 in.)

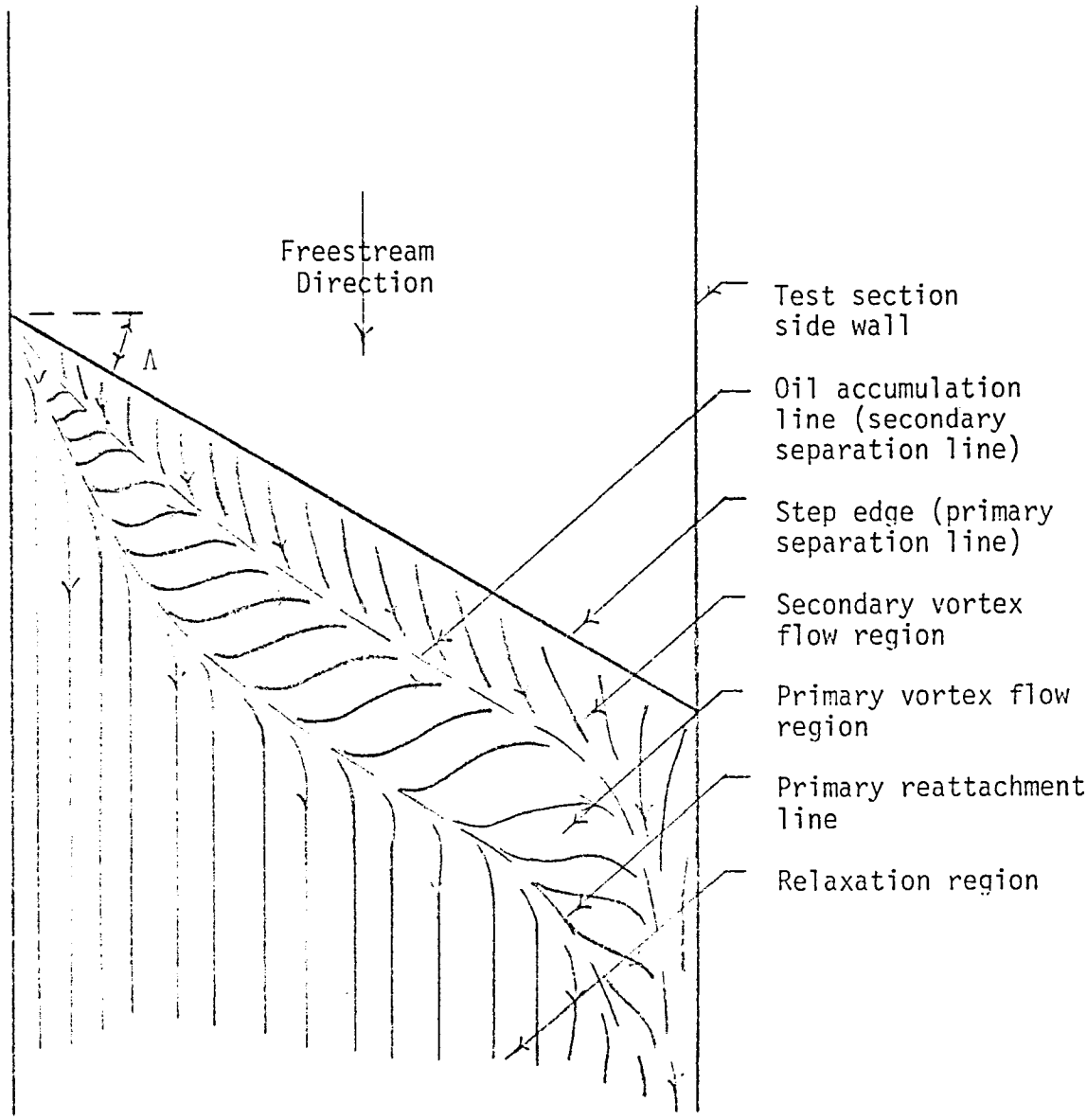

Figure 36. Pictorial Summary of Surface Flow Features Determined from Oil Flows Downstream of a Swept, Rearward-Facing Step.

include the secondary vortex flow region shown to be present in the higher sweep cases ($\Lambda > 30°$). As previously stated, the direction of the secondary vortex flow depends on the value of Λ. The critical value of Λ at which the spanwise direction of the secondary flow changes lies somewhere between 30° and 60°. The primary and secondary vortex flows are shown in the same direction in Figure 36.

The flow model for the swept rearward-facing step as presented in Figure 4(b) includes secondary longitudinal vortices which the flow visualization methods employed in the subject research program failed to uncover. Hopkins et al. (1960) and Ginoux (1958) have indicated that for two-dimensional compressible rearward-facing step flow, striations in the surface oil flow patterns are indicative of the existence of streamwise vortices. Similar striations appear to be present in the relaxation region of the oil flow patterns examined in this section. However, a different oil flow method than that employed by Hopkins et al. (1960) and Ginoux (1958) was used—oil droplet versus oil film. It is probable that the method of applying the oil in the present study is partially responsible for the striations observed, thereby masking the striations produced by the longitudinal vortices.

Hopkins, E. J., Keating, S. J., Jr. and Bandettini, A., Photographic Evidence of Streamwise Arrays of Vortices in Boundary-Layer Flow, NASA Ames Research Center, TW D-32G, 1960.

Ginoux, J. J., Experimental Evidence of Three-Dimensional Perturbations in the Reattachment of a Two-Dimensional Laminar Boundary Layer at M = 2.05, Training Center for Experimental Aerodynamics (Belgium), Tech. Note 1, 1958.

The oil droplet method was chosen over the oil film method because it was found to work better for the low flow velocities of the present research.

3.4. Quantitative Measurements (Basic Models)

3.4.1. Surface Pressure for the Basic Unswept Model

Pressure on the surfaces upstream and downstream of the rearward-facing step configurations listed in Table 2 was measured in accordance with Section 2.4. The pressure data were validated by obtaining favorable comparisons between the surface pressure measured in the present study and the data reported by various investigators for flow over the two-dimensional rearward-facing step. The two-dimensional investigations used for comparison purposes are listed in Table 5 along with the values of pertinent parameters. The coordinate system used in reporting the surface pressures is shown in Figure 37.

Surface pressures measured along the centerline of configurations LE2-BB0-DS0.50 and DS0.94 are compared with the data of Kim et al. (1980) in Figure 38 in the form $C_p - C_p[\text{min}] \equiv \Delta C_p$. $C_p[\text{min}]$ is the minimum measured pressure along the centerline. Comparing ΔC_p instead of C_p is one way of obtaining better agreement between independent experiments since factors, such as instrument drift, which would contribute to differing values for C_p would cancel upon computing ΔC_p. The agreement obtained is generally good, except possibly in the cases with $h = .50$ in the relaxation region. The differences observed in

Figure 37.

Coordinate System for Surface Pressure Measurements

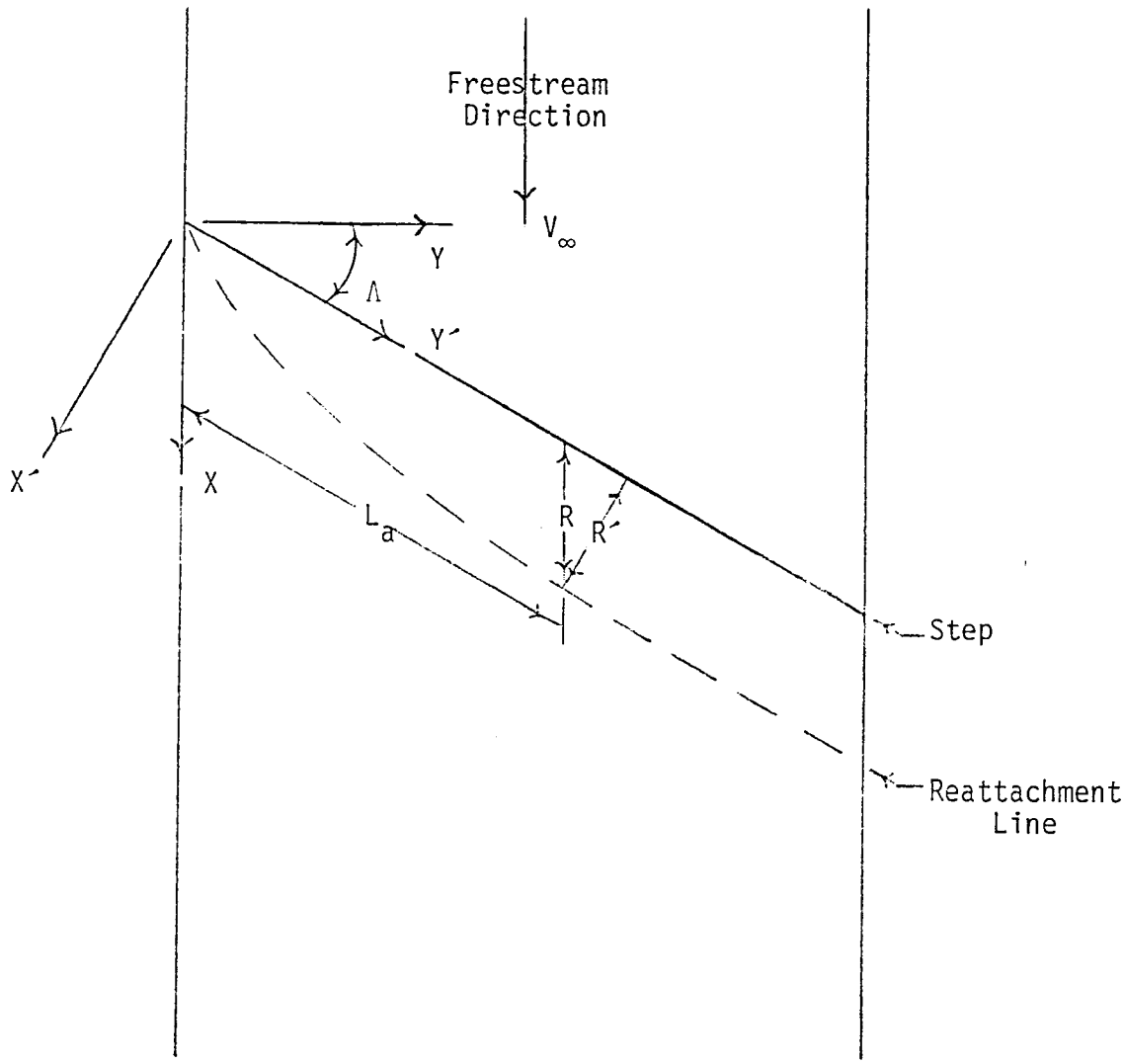

FIGURE 38. Cp-Cp[min] AT ZERO SWEEP
COMPARED TO KIM ET AL(1980)

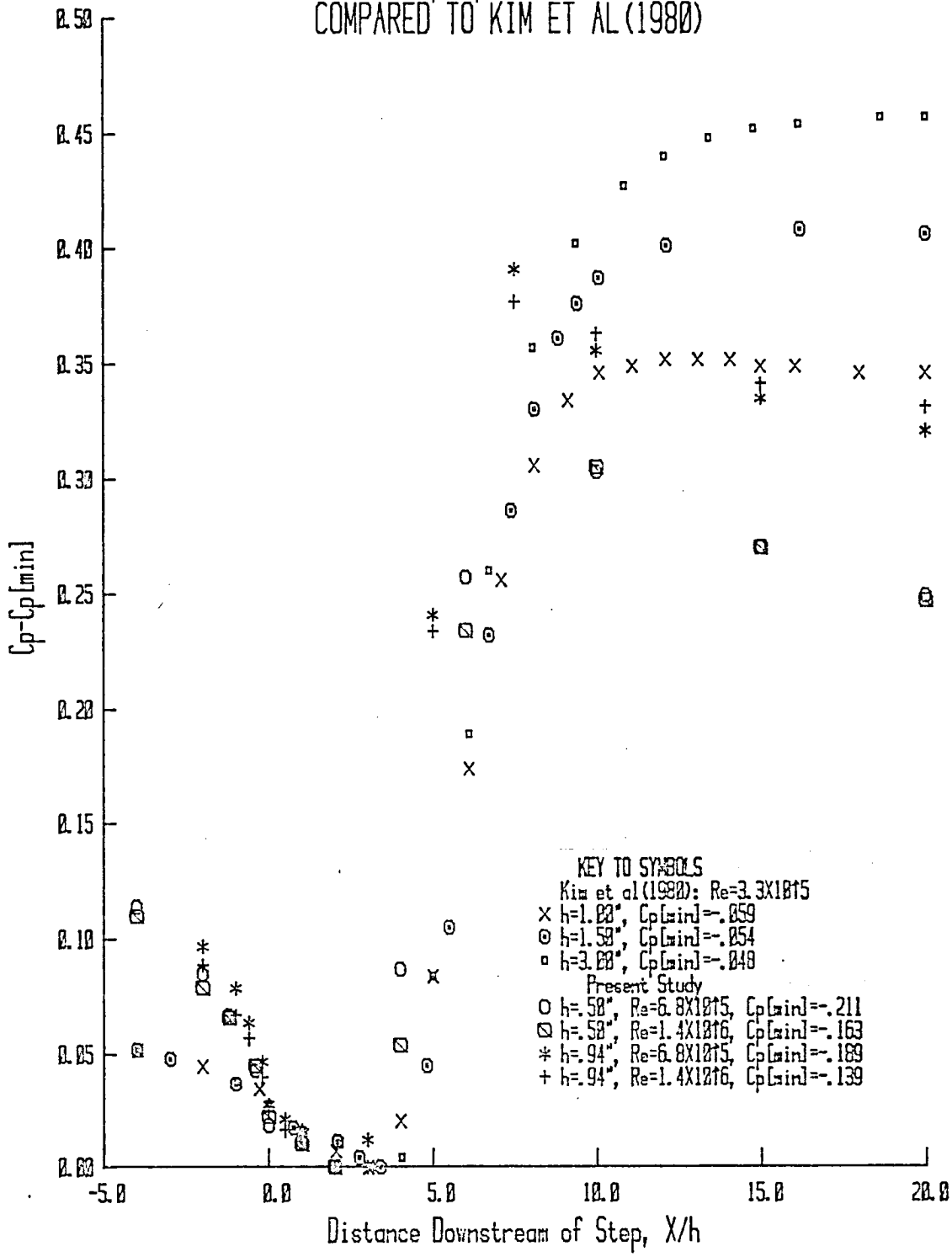

Table 5

Summary of 2-D Rearward-Facing Step Investigations Used for Surface Pressure Comparisons

Author(s)	h (in.)	h/δ_{sep}	Ar	AR	L_{sep}(in.)	Re	State of B.L. at Separation
Kim et al. (1980)	1.00	2.2	1.33	24	12	3.3×10^5	Turbulent
	1.50	3.3	1.50	16	12	3.3×10^5	"
	3.00	6.6	2.00	8	12	3.3×10^5	"
Eaton (1980)	2.00	4.5	1.67	12	12	1.3×10^5	Turbulent
	2.00	4.5	1.67	12	12	2.2×10^5	"
Moss & Baker (1980)	3.00	1.4	1.10	18	36	6.3×10^5	Turbulent
Narayanan et al. (1974)	0.75	1.9	1.06	26	24	6.3×10^5	Turbulent
	0.98	2.5	1.08	20	24	6.3×10^5	"
	1.48	3.8	1.12	13	24	6.3×10^5	"
Present Study	0.50	0.6	1.06	30	43	6.8×10^5	Turbulent
	0.50	0.6	1.06	30	43	1.4×10^6	"
	0.94	1.1	1.12	16	43	6.8×10^5	"
	0.94	1.2	1.12	16	43	1.4×10^6	"

Eaton, John K., Turbulent Flow Reattachment: An Experimental Study of the Flow and Structure Behind a Backward-Facing Step, Ph.D. Dissertation, Stanford University, University Microfilms International, Ann Arbor, Michigan, 1980.

Moss, W. D. and Baker, S., "Re-Circulating Flows Associated with Two-Dimensional Steps," The Aeronautical Quarterly, Vol. 31, Part 3, pp. 151-172, 1980.

Narayanan, M. A., Khadgi, Y. N. and Viswanath, P. R., "Similarities in Pressure Distribution in Separated Flow Behind Backward-Facing Steps," Aeronautical Quarterly, Vol. 25, pp. 305-312, 1974.

the values of $\Delta C_p[max] \equiv C_p[max] - C_p[min]$ are generally due to the differences in area ratio from one case to the next. The differences in the slopes of the pressure curves (longitudinal pressure gradient) upstream of the step and in the relaxation region are generally due to differences in the rate of growth of the shear layer (hence, the displacement thickness) between experiments. This relates to different values of L_{sep}, length from inlet to step, in different experiments. In addition, the rate of relaxation of a shear layer after reattachment to pre-separation characteristics depends heavily on the ratio h/δ_{sep}, as alluded to in Section 1.2 [Bradshaw and Wong (1972)]. This is the primary reason for the differences in the longitudinal pressure gradient in the relaxation region between the cases at $h = .50"$ ($h/\delta_{sep} \approx .6$) and $h = .94"$ ($h/\delta_{sep} \approx 1.2$) of the present study and the other results to be examined presently.

The conventional pressure coefficient reported in Figure 38 is defined by the relation

$$C_p \equiv \frac{P - P_{ref}}{1/2\ \rho V_\infty^2} \tag{3.1}$$

where P_{ref} in the present study is measured on the side wall at $L = 2'$ and $y = 4"$. Kim et al. (1980) used a normalized pressure coefficient defined as

$$C_p^* \equiv \frac{\Delta C_p}{C_p[B\text{-}C] - C_p[min]} \tag{3.2}$$

where $C_p[B\text{-}C]$ is the Broad-Carnot pressure coefficient defined by the relation

$$C_p[B\text{-}C] \equiv 2\frac{1}{Ar}\left(1 - \frac{1}{Ar}\right) \tag{3.3}$$

Use of the normalized pressure coefficient C_p^* was an attempt by Kim et al. (1980) to reduce their three sets of pressure data to a single curve. Presented in Figure 39 is C_p^* as a function of the distance from the step along the centerline of the model. Although the data measured by Kim et al. (1980) are normalized, the data from the present study are not.

Two-dimensional surface pressure measurements from the present study are compared to the data collected by Eaton (1980) in Figure 40. The agreement obtained with the data of Eaton (1980) is essentially the same as obtained with the data of Kim et al. (1980). One reason may be that these investigators used essentially the same tunnel/test section arrangement, although different step heights were examined.

Better agreement in the region upstream of the step and in the separated-flow region was obtained with the data of Moss and Baker (1980) than with the data of the previous investigators mentioned, as shown in Figure 41. The excellent agreement in these regions is due primarily to the presence of similar values of entry length (L_{sep}), AR and h/δ_{sep} in the present study and that of Moss and Baker (1980).

FIGURE 39.
Cp* AT ZERO SWEEP COMPARED TO KIM ET AL(1980)

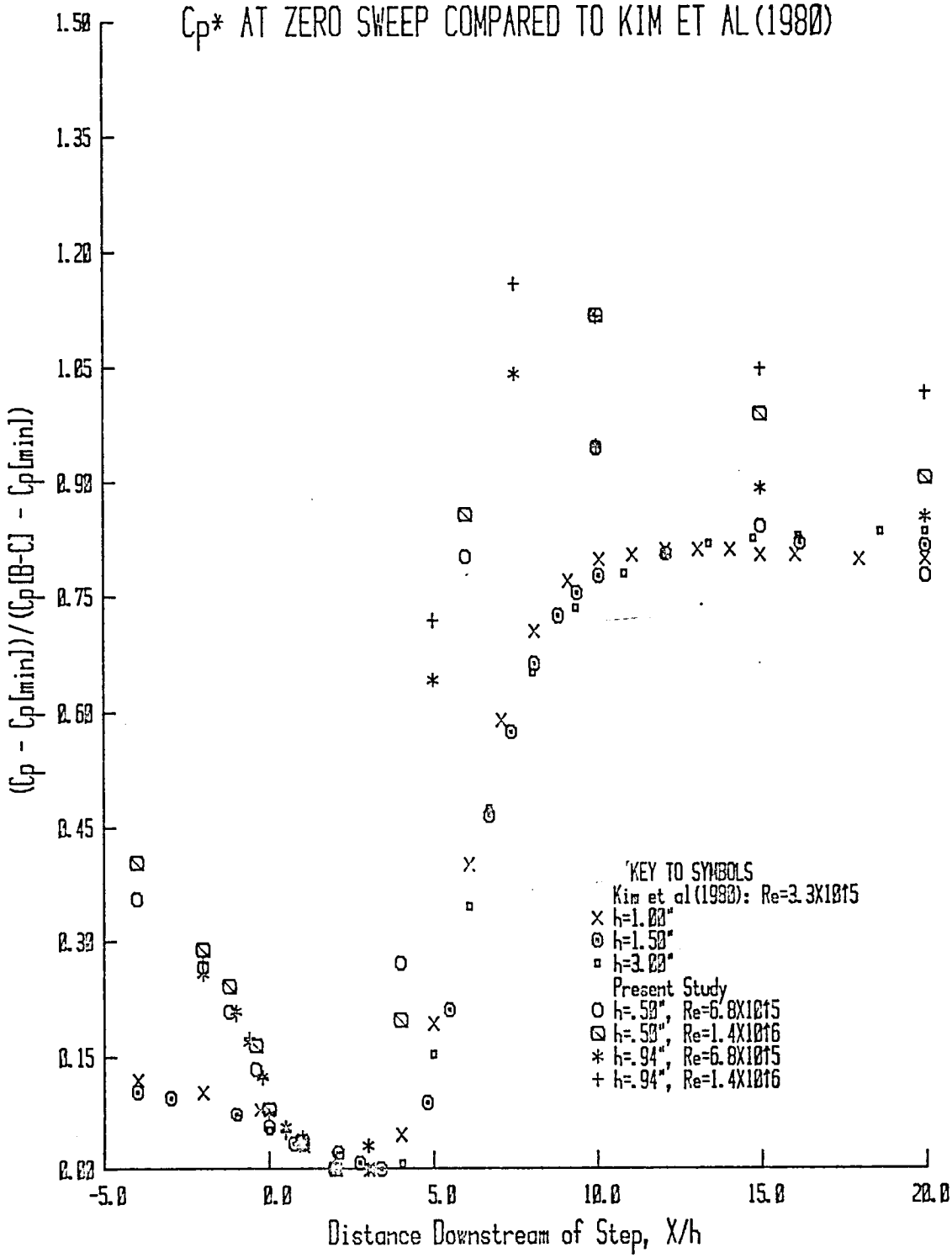

FIGURE 40.

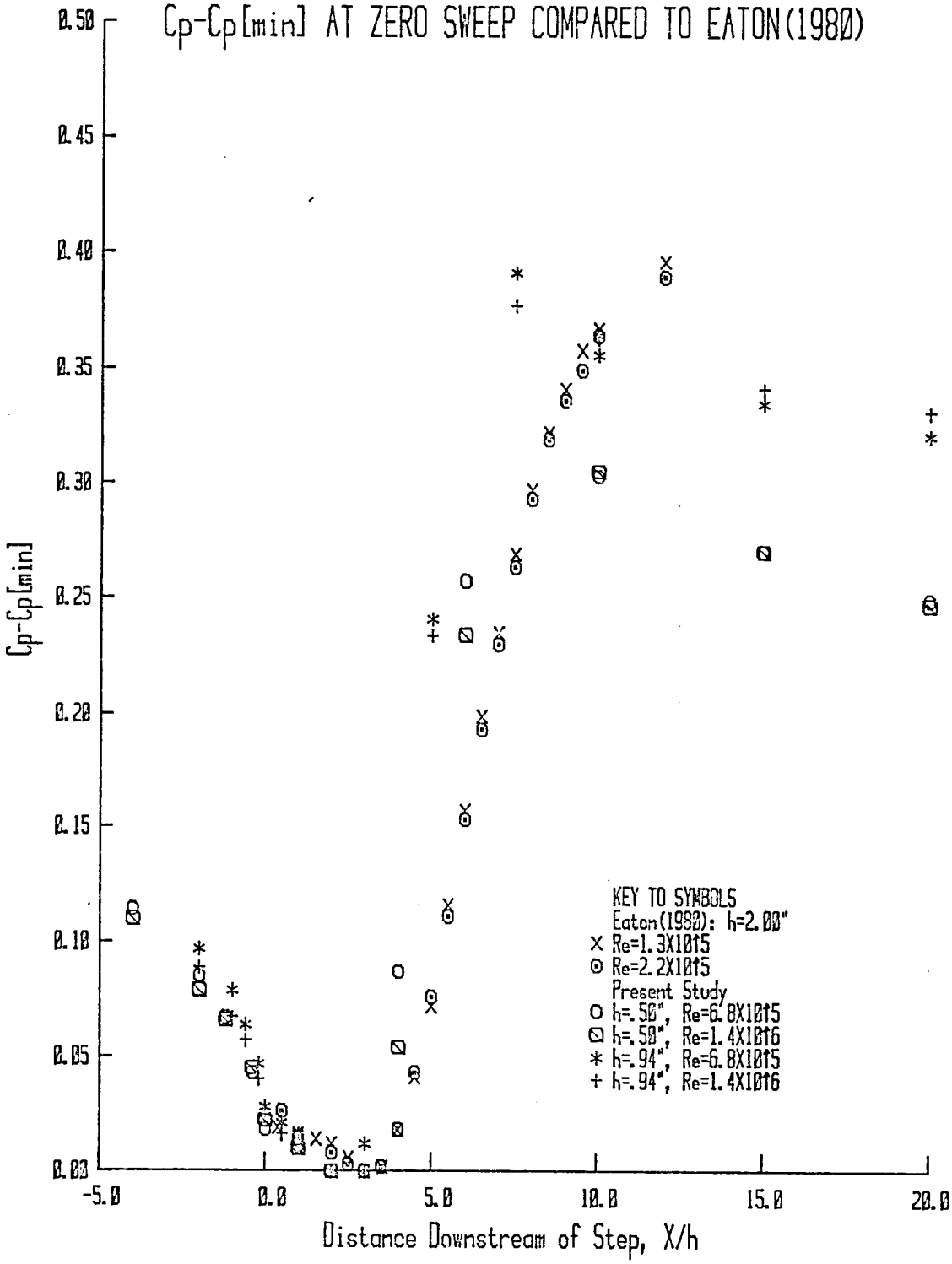
Cp-Cp[min] AT ZERO SWEEP COMPARED TO EATON(1980)
0.50
0.45
0.40
0.35
0.30
0.25
0.20
0.15
0.10
0.05
0.00
Cp-Cp[min]
-5.0
0.0
5.0
10.0
15.0
20.0
Distance Downstream of Step, X/h
KEY TO SYMBOLS
Eaton(1980): h=2.00"
× Re=1.3X1015
⊙ Re=2.2X1015
Present Study
O h=.50", Re=6.8X1015
⊠ h=.50", Re=1.4X1016
* h=.94", Re=6.8X1015
+ h=.94", Re=1.4X1016

FIGURE 41.

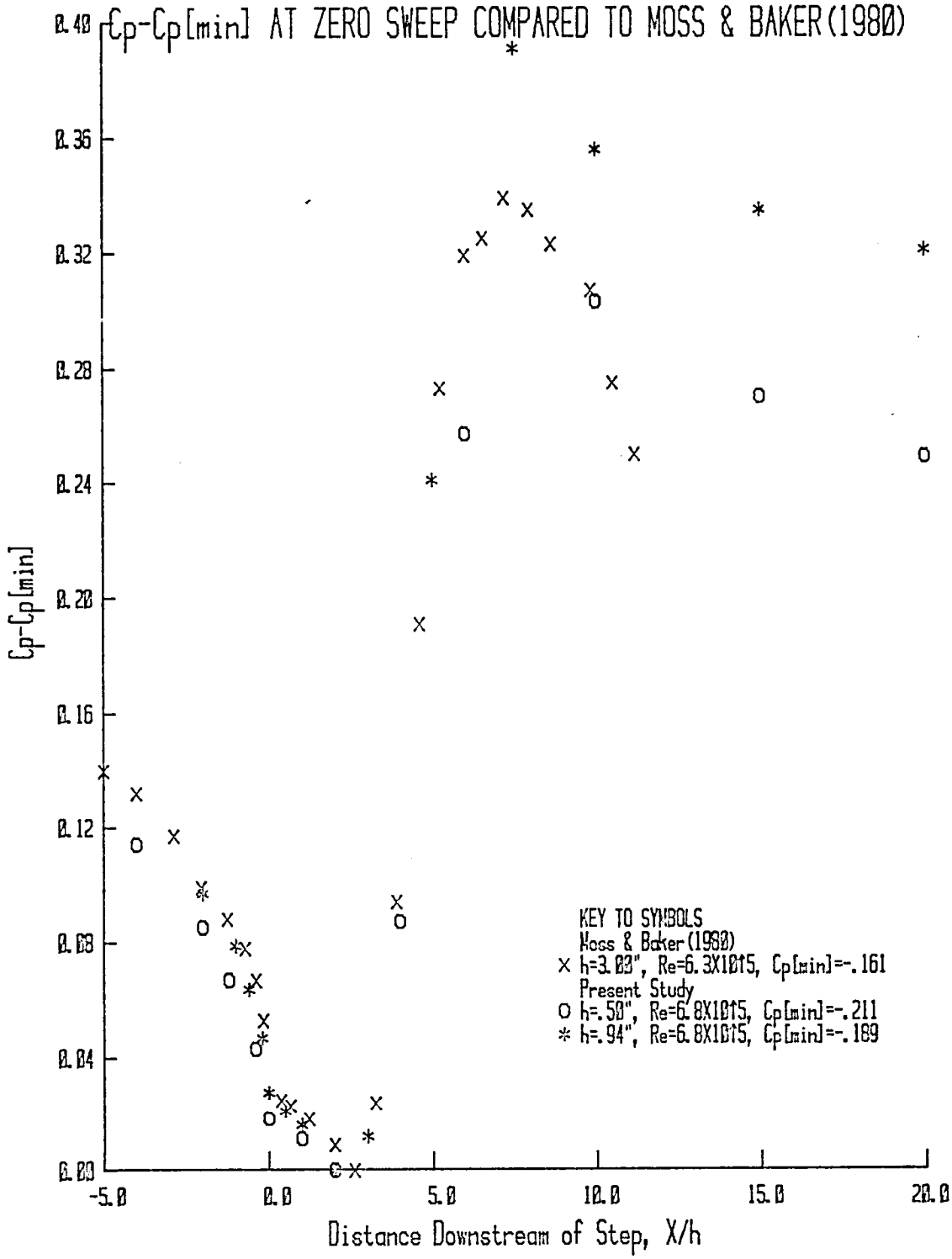
Cp-Cp[min] AT ZERO SWEEP COMPARED TO MOSS & BAKER(1980)
0.40
0.36
0.32
0.28
0.24
0.20
0.16
0.12
0.08
0.04
0.00
Cp-Cp[min]
-5.0
0.0
5.0
10.0
15.0
20.0
Distance Downstream of Step, X/h
KEY TO SYMBOLS
Moss & Baker(1980)
x h=3.03", Re=6.3X10↑5, Cp[min]=-.161
Present Study
o h=.50", Re=6.8X10↑5, Cp[min]=-.211
* h=.94", Re=6.8X10↑5, Cp[min]=-.189

The normalized pressure coefficient used by Moss and Baker (1980) in their comparisons similar to Equation (3.2), being:

$$C_p' \equiv \frac{\Delta C_p}{1 - C_p[min]} \tag{3.4}$$

This normalized pressure coefficient data are presented in Figure 42 for the same sets of data of Figure 41. The agreement between the sets of data in Figure 42 in terms of C_p' is similar to that observed in the preceding figure in terms of the conventional pressure coefficient.

The two-dimensional pressure data of the present study are in fair agreement with the data of Narayanan et al. (1974) in the relaxation region as shown in Figure 43. Narayanan et al. (1974) have introduced a third normalized pressure coefficient—herein referred to as C_p'' and defined by the relation

$$C_p'' \quad \frac{\Delta C_p}{\Delta C_p[max]} \tag{3.5}$$

Pressure coefficient is presented in terms of C_p'' as a function of X/h in Figure 44 for the data from the present study along with the data of Narayanan et al. (1974), Kim et al. (1980) and Moss and Baker (1980). The normalized pressure coefficient C_p'' appears to be more successful than the other two normalized pressure

FIGURE 42.
C_p' AT ZERO SWEEP COMPARED TO MOSS & BAKER(1980)

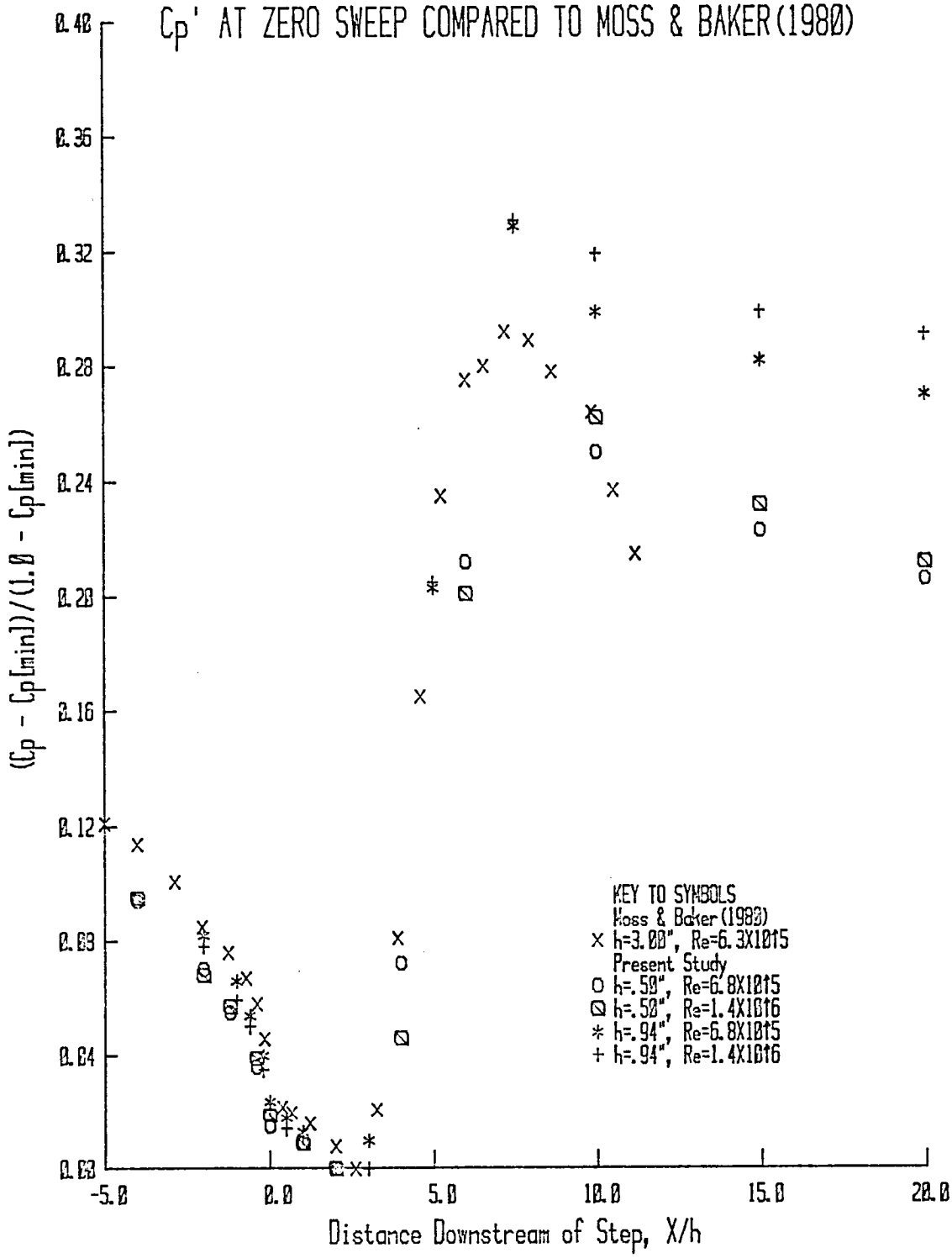

FIGURE 43. Cp-Cp[min] AT ZERO SWEEP
COMPARED TO NARAYANAN ET AL(1974)

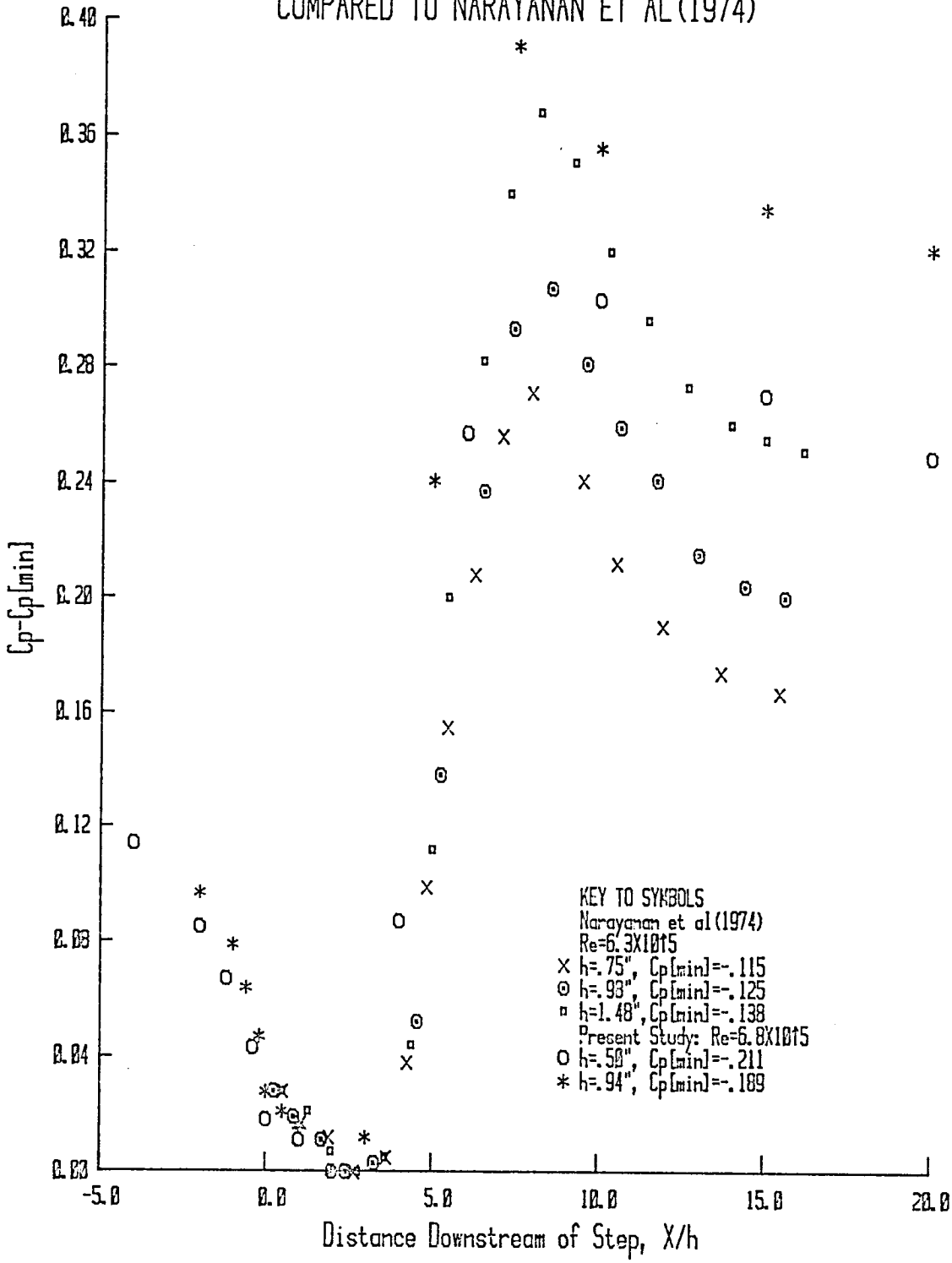

FIGURE 44. C_p" AT ZERO SWEEP COMPARED TO NARAYANAN ET AL(1974), KIM ET AL(1980) AND MOSS & BAKER(1980)

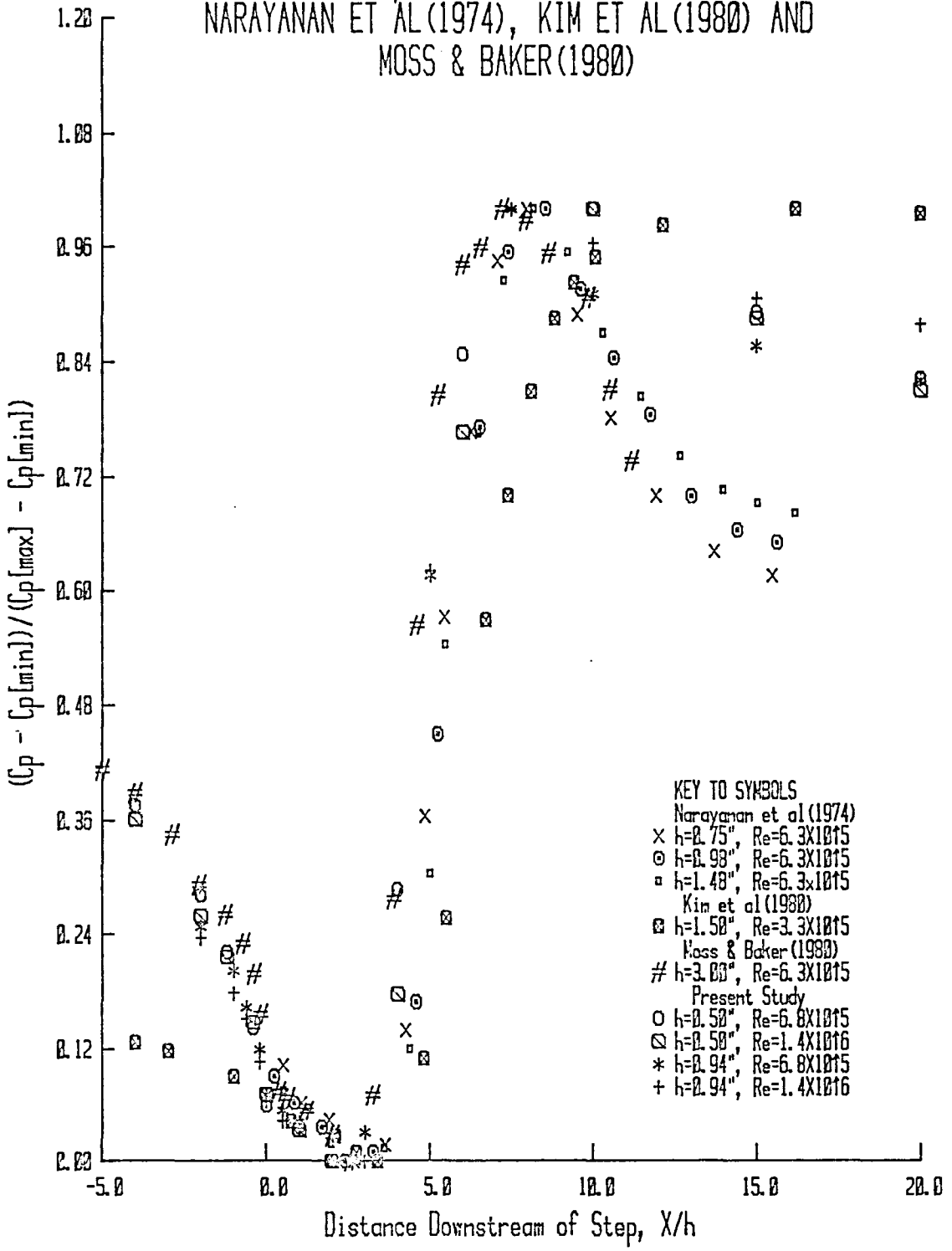

coefficients defined by Equations (3.2) and (3.4) in reducing all data to a single curve. The same normalized pressure coefficient has been used later in this section in an attempt to normalize the surface pressure data collected as a function of sweep angle. The pressure parameter ΔC_p in the separated-flow region as a function of longitudinal distance downstream of the unswept model at midspan is presented in Figures 45 and 46 for all the sets of data listed in Table 5.

In summary, it has been shown that the pressure data collected along the centerline of the unswept model is in general agreement with the data gathered by other researchers. These comparisons represent a means of validating the present data on unswept models.

It appears apparent from a casual examination of the two-dimensional surface pressure data previously presented that there exists some relationship between the total pressure rise at midspan, $\Delta C_p[\max]$, and the change in cross-section area across the step. Accordingly, $\Delta C_p[\max]$ as a function of area ratio is presented in Figure 47. Based on these data—though limited—it is possible to determine a linear relationship between $\Delta C_p[\max]$ and Ar depending on the value of Ar. These relationships are

$$\Delta C_p[\max] = 1.48\ Ar - 1.27 \quad \text{for} \quad 1.0 < Ar < 1.12 \tag{3.6}$$

$$\Delta C_p[\max] = 0.11\ Ar + 0.23 \quad \text{for} \quad Ar > 1.33 \tag{3.7}$$

FIGURE 45. Cp-Cp[min] IN SEPARATED-FLOW REGION AT ZERO SWEEP COMPARED TO KIM ET AL(1980) AND EATON(1980)

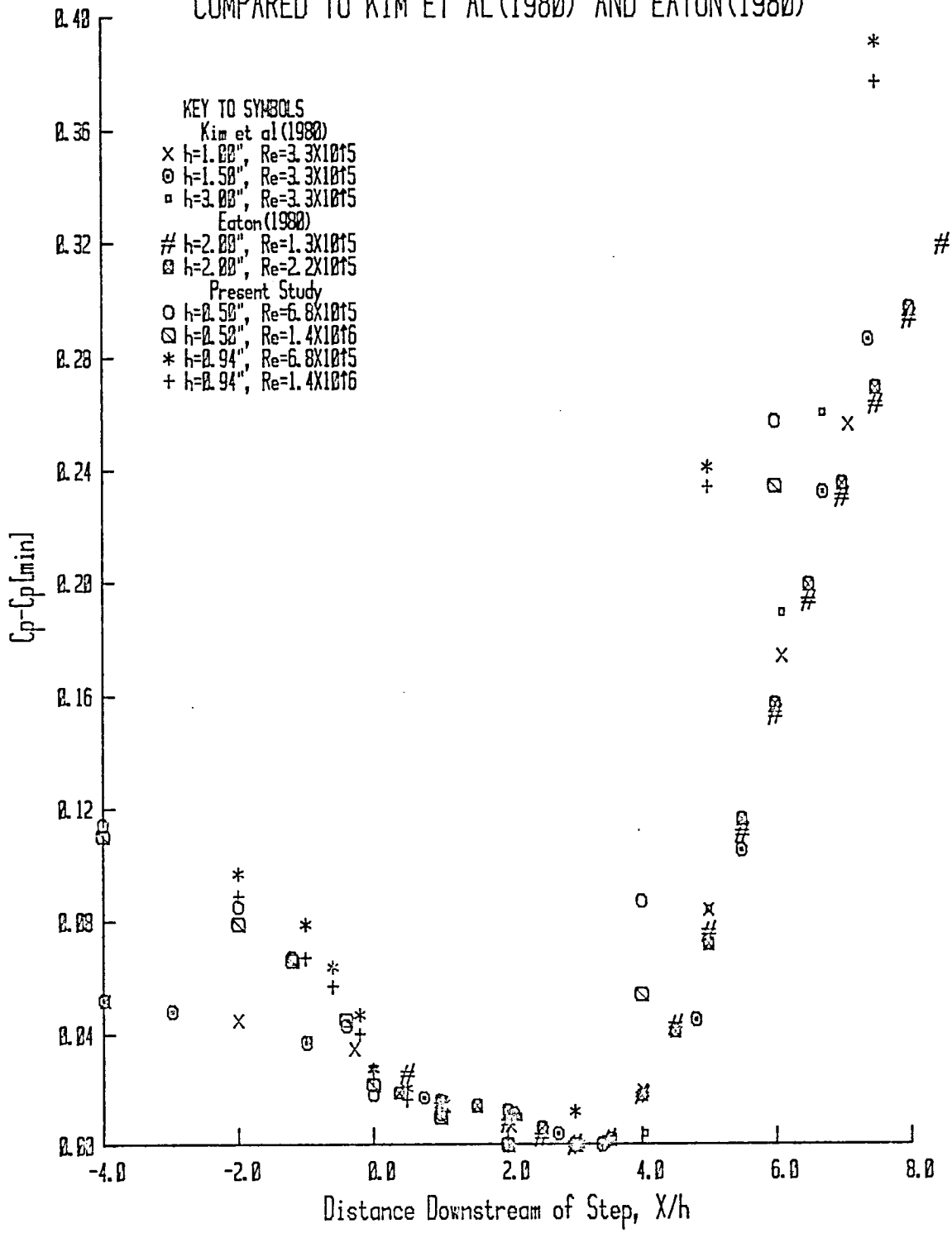

FIGURE 46. Cp-Cp[min] IN SEPARATED-FLOW REGION AT ZERO SWEEP COMPARED TO NARAYANAN ET AL(1974) AND MOSS & BAKER(1980)

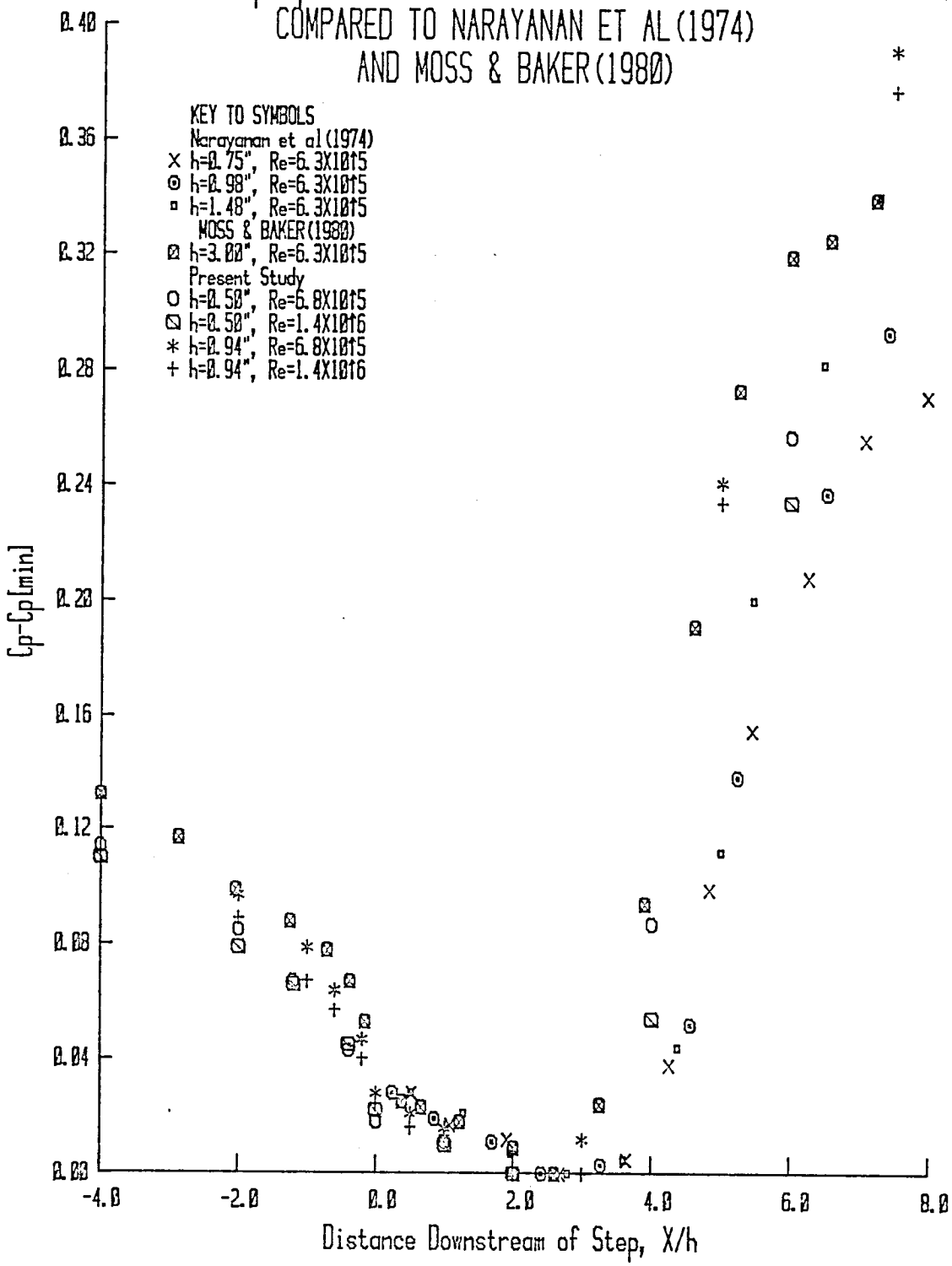

FIGURE 47. $C_p[max]-C_p[min]$ VS. RATIO OF DOWNSTREAM TO UPSTREAM AREAS AT ZERO SWEEP

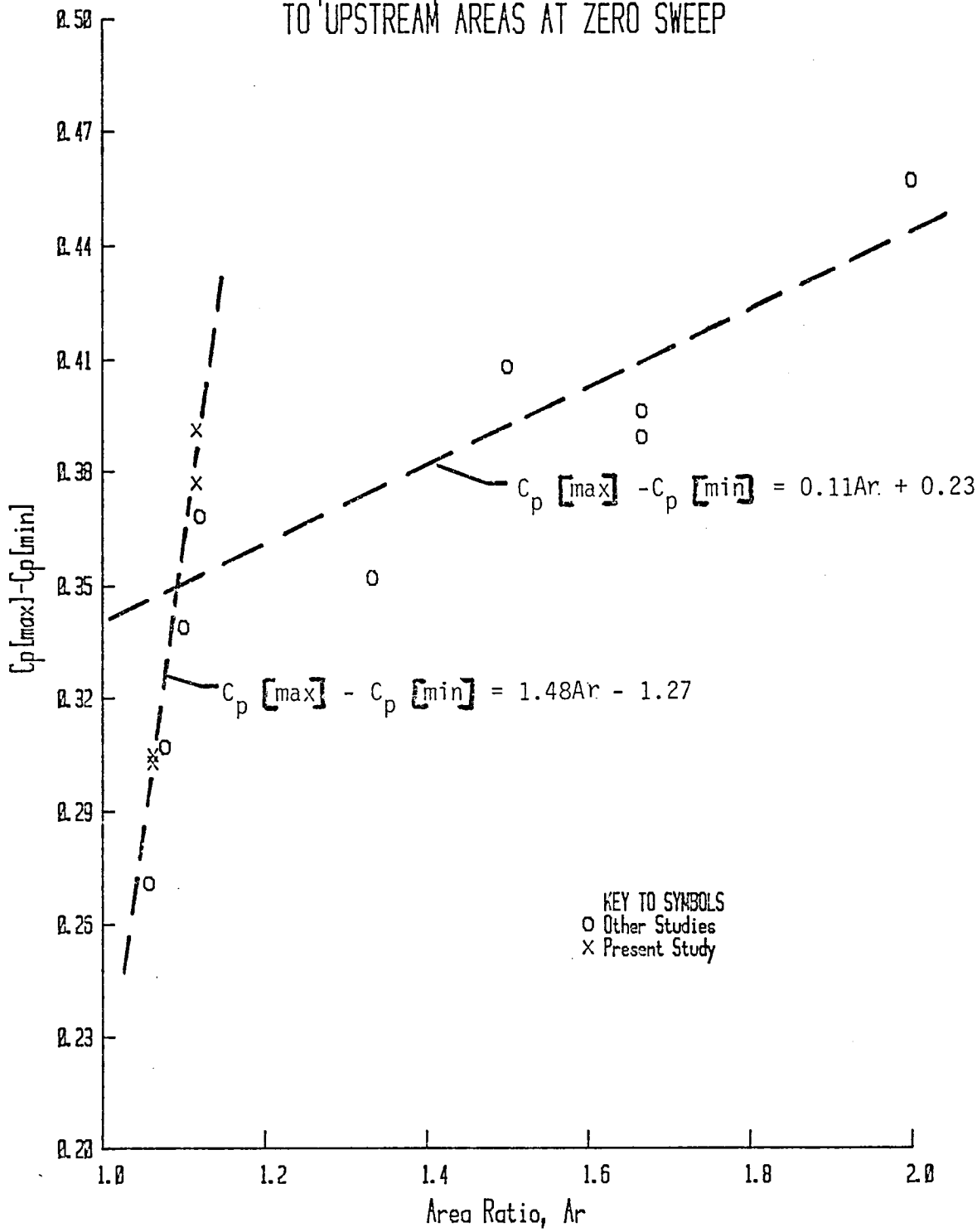

An examination of the data contained in Table 5 was fruitless in terms of yielding a single parameter, such as h/δ_{sep}, that more objectively defined the extent of these two intervals in area ratio. Nevertheless, these relationships were advantageously used in normalizing the pressure data obtained as a function of h and Λ, as presented in the next section.

3.4.2. Surface Pressures for the Basic Swept Models

Midspan ΔC_p as a function of perpendicular distance from the basic swept step is presented in Figure 48 for the sweep angles of 0, 15, 30 and 60° at $h = .50$ and .94".

$\Delta C_p[max]$ noticeably decreases with increasing sweep angle at both step heights, yet, the pressure profiles at a given step height for various sweep angles are similar. This similarity in profiles is indicative of the possibility of finding a normalized pressure coefficient, similar to those presented in Section 3.4.1, which results in the definition of a single curve by the four sets of data. The normalized pressure coefficient decided upon is simply

$$C_p^+ \equiv \frac{\Delta C_p}{\cos \Lambda} \tag{3.8}$$

The pressure parameter defined in Equation (3.8) is presented as a function of X'/h in Figure 49 for $h = .50$". The normalized pressure coefficient C_p^+ adequately collapses the swept-step midspan

FIGURE 48. MIDSPAN Cp-Cp[min] AT VARIOUS SWEEP ANGLES FOR THE BASIC MODEL AT Re=1.4X10↑6

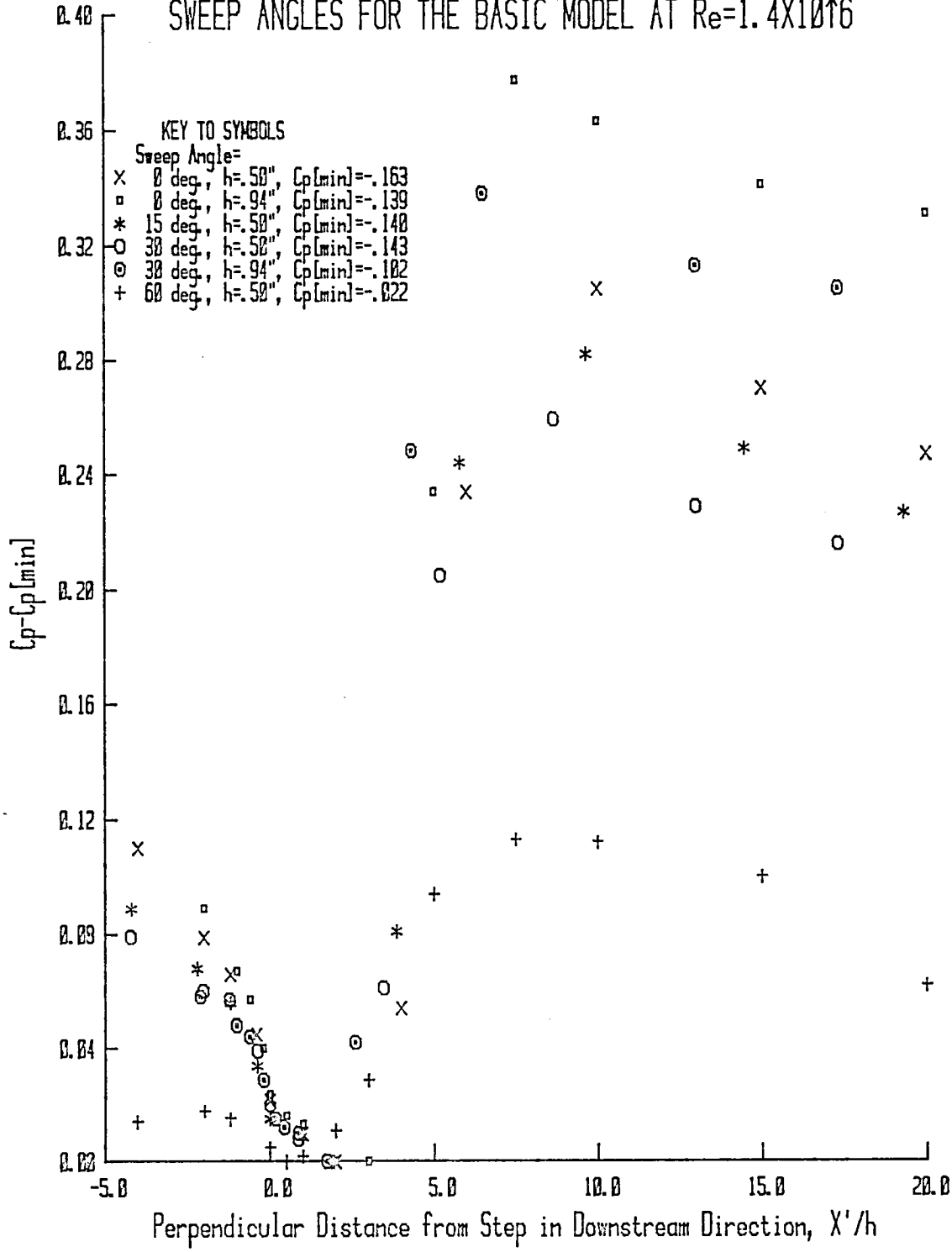

FIGURE 49. MIDSPAN Cp+ AT VARIOUS SWEEP ANGLES FOR THE BASIC MODEL AT h=.50" AND Re=1.4X10↑6

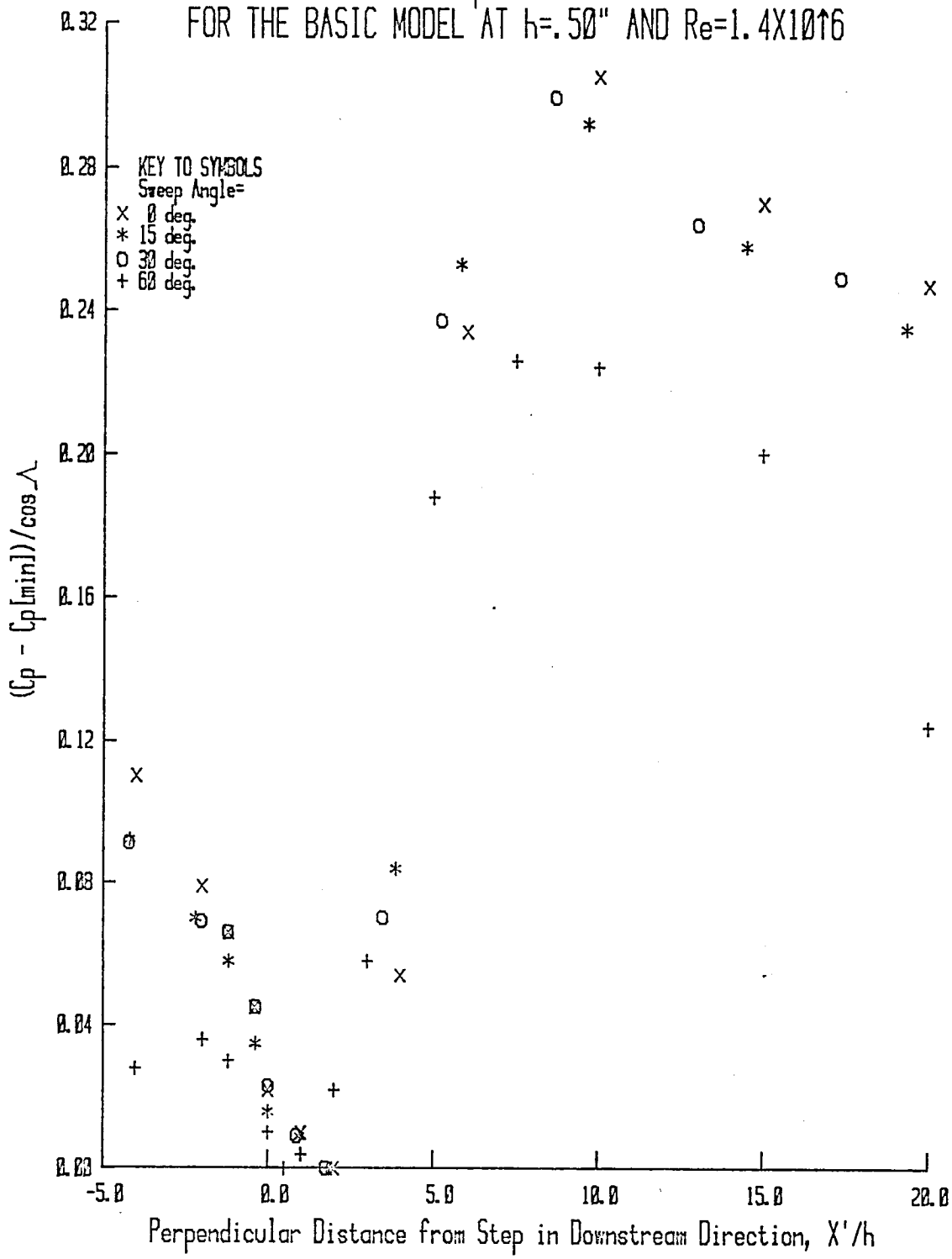

pressure profiles onto a single profile at a given value of h, with the exception of the data at $\Lambda = 60°$. The pressure parameter C_p'' as a function of X'/h is presented in Figure 50 for the same cases of Figure 49. This parameter essentially collapses all data onto a single curve. Another parameter which has been defined as

$$C_p^{**} \equiv \left(\frac{\Delta C_p}{\cos \Lambda} + 1.274\right) \frac{1}{Ar} \tag{3.9}$$

satisfactorily collapses all the data in Figure 48 onto a single curve independent of Λ and h, with the exception of the data at $\Lambda = 60°$, as shown in Figure 51. Equation (3.9) is based on Equations (3.6) and (3.8).

The empirical relation included below as Equation (3.10) can be used to calculate $\Delta C_p[max]$ to within 3% of the values measured at $h = .50"$ or $.94"$ and $0 \leq \Lambda \leq 30°$ for $Re = 1.4 \times 10^6$.

$$\Delta C_p[max] = (1.482\ Ar - 1.274) \cos \Lambda \tag{3.10}$$

Furthermore, given the curve for midspan ΔC_p at $\Lambda = 0°$ and $h = .50"$ or $.94"$, the profile for midspan ΔC_p can be computed for any case reported herein within the intervals $.50" < h < .94"$ and $0° \leq \Lambda \leq 30°$ using the relation

$$(\Delta C_p)_{\Lambda \leq 30°} = \left[(\Delta C_p)_{\Lambda=0°} + (Ar_{\Lambda \leq 30} - Ar_{\Lambda=0})\ 1.482\right] \cos \Lambda \tag{3.11}$$

FIGURE 50. MIDSPAN Cp" AT VARIOUS SWEEP ANGLES FOR THE BASIC MODEL AT h=.50" AND Re=1.4X10↑6

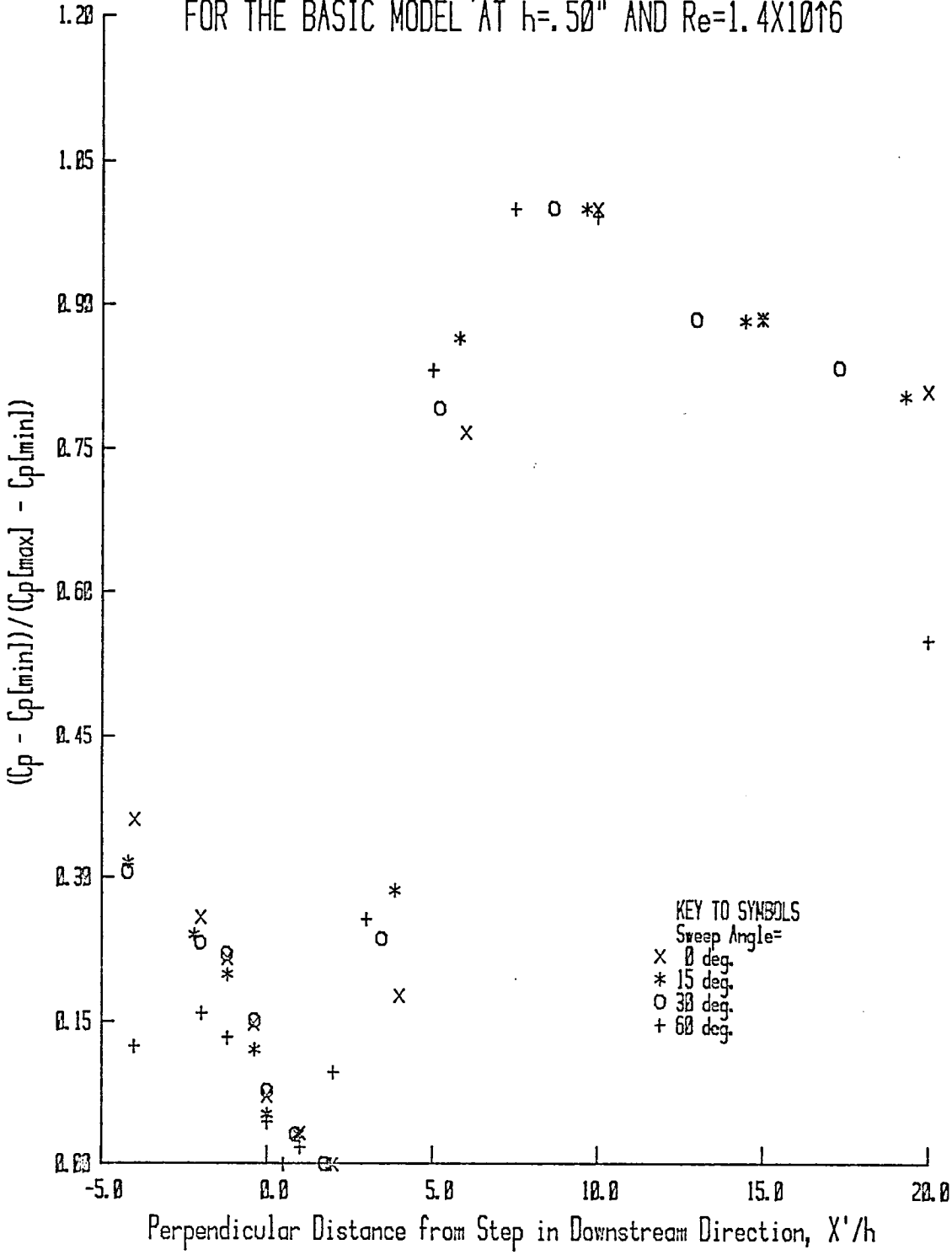

FIGURE 51. MIDSPAN Cp** AT VARIOUS SWEEP ANGLES FOR THE BASIC MODEL AT Re=1.4X10↑6

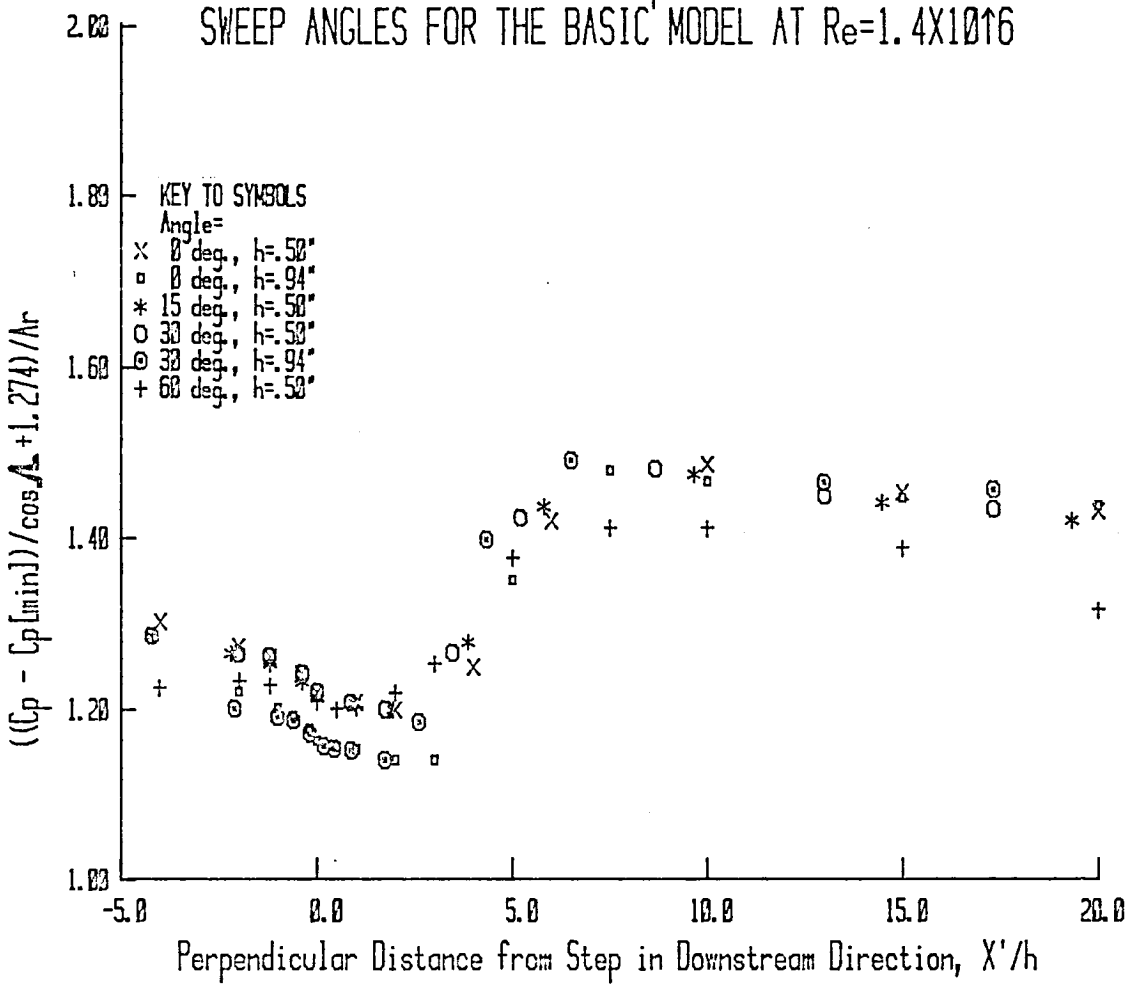

which is based on the facts that the pressure distributions examined exhibit similarity with respect to the parameter C_p^+ and that there exists a relationship between $\Delta C_p[max]$ and Ar, hence, also between ΔC_p and Ar.

ΔC_p as a function of the spanwise coordinate Y'/h (as defined in Figure 37) is presented in Figures 52 and 53 for configurations LE2-BBO-DSO.50 and DSO.94, respectively. There is little change in pressure with respect to Y'/h as would be expected in a two-dimensional flow. However, as the sweep angle is increased to 15°, three-dimensional effects become noticeable, as observed in Figure 54 for h = .50".

At Λ = 30°, an appreciable adverse pressure gradient exists in the Y' direction in the separated-flow at both h = .50" and h = .94", as seen in Figures 55 and 56, respectively. The basis for this adverse pressure gradient is examined in Appendix B. Figures 55 and 56 also show that the pressure becomes invariant with Y' in the relaxation region not far from the reattachment line, though the pressure there has not relaxed to pre-separation values. The same observations made for the 30° swept-step case apply to the 60° swept-step case as well, as can be determined from a comparison of Figures 55 through 57—Figure 57 being for Λ = 60° and h = .50". Pressure in the separated-flow region as a function of Y'/h is presented in Figure 58 for comparison purposes for the cases referred to in Figures 52 through 57. Spanwise pressure gradients computed graphically from Figure 58 are compared to theoretical values in Appendix B. As previously mentioned in Section 3.3.3, the spanwise

FIGURE 52. SPANWISE VARIATION IN C_p AT VARIOUS LONGITUDINAL LOCATIONS FOR THE BASIC UNSWEPT MODEL WITH h=.50"

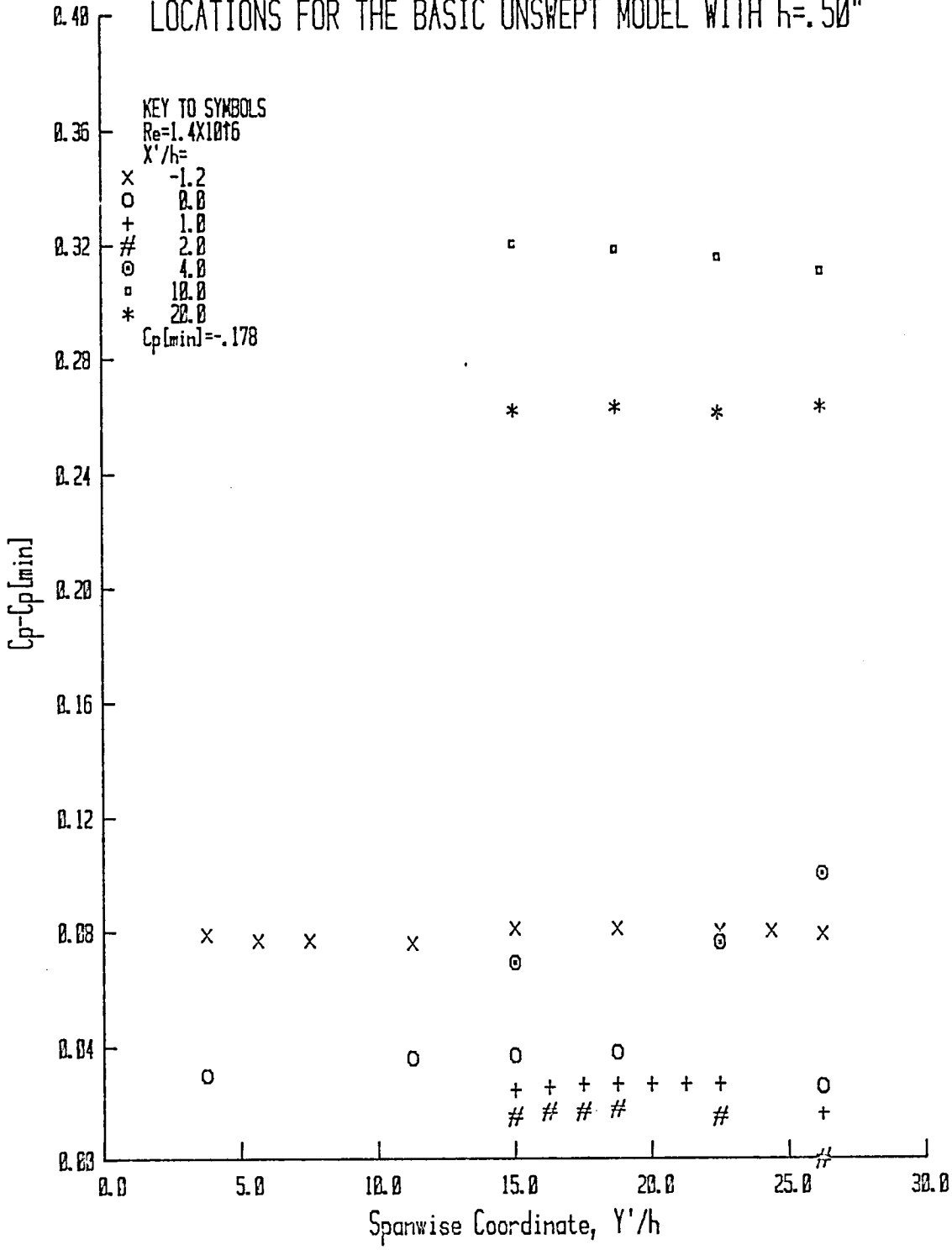

FIGURE 53. SPANWISE VARIATION IN C_p AT VARIOUS LONGITUDINAL LOCATIONS FOR THE BASIC UNSWEPT MODEL WITH h=.94"

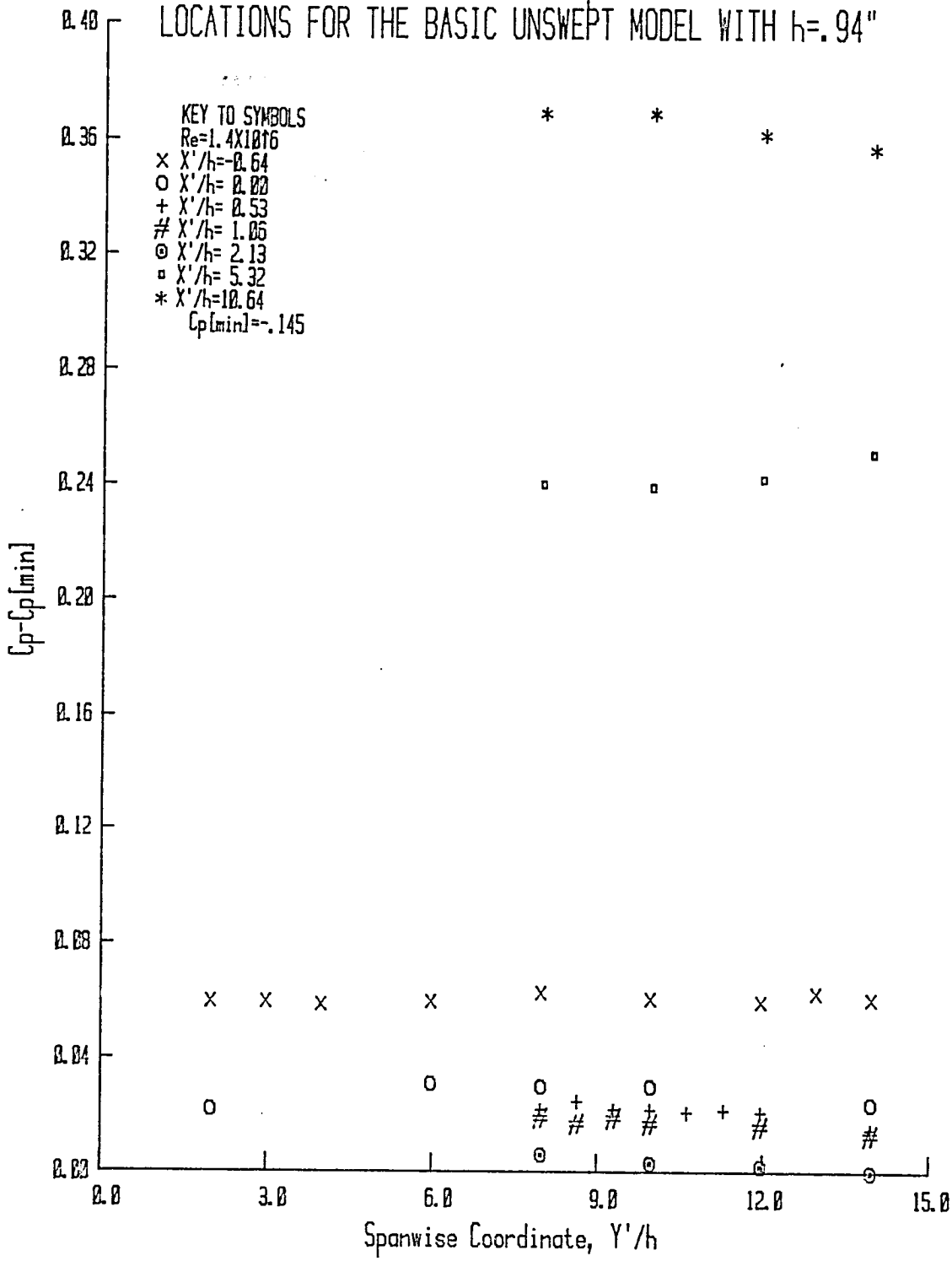

FIGURE 54. SPANWISE VARIATION IN C_p AT VARIOUS LONGITUDINAL LOCATIONS FOR THE BASIC 15-DEG. SWEPT STEP MODEL WITH h=.50"

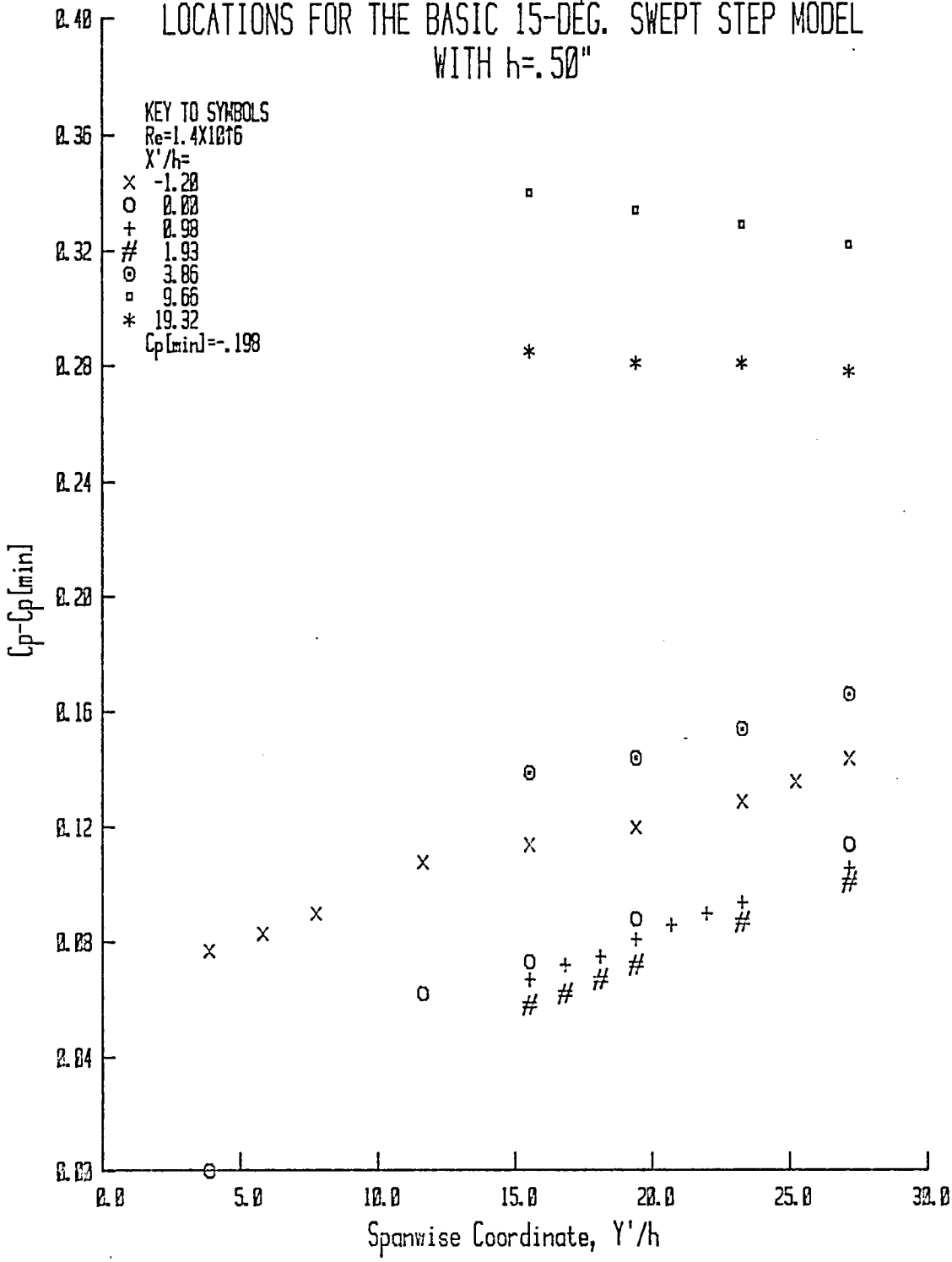

FIGURE 55. SPANWISE VARIATION IN C_p AT VARIOUS LONGITUDINAL LOCATIONS FOR THE 30-DEG. BASIC SWEPT-STEP MODEL WITH h=.50"

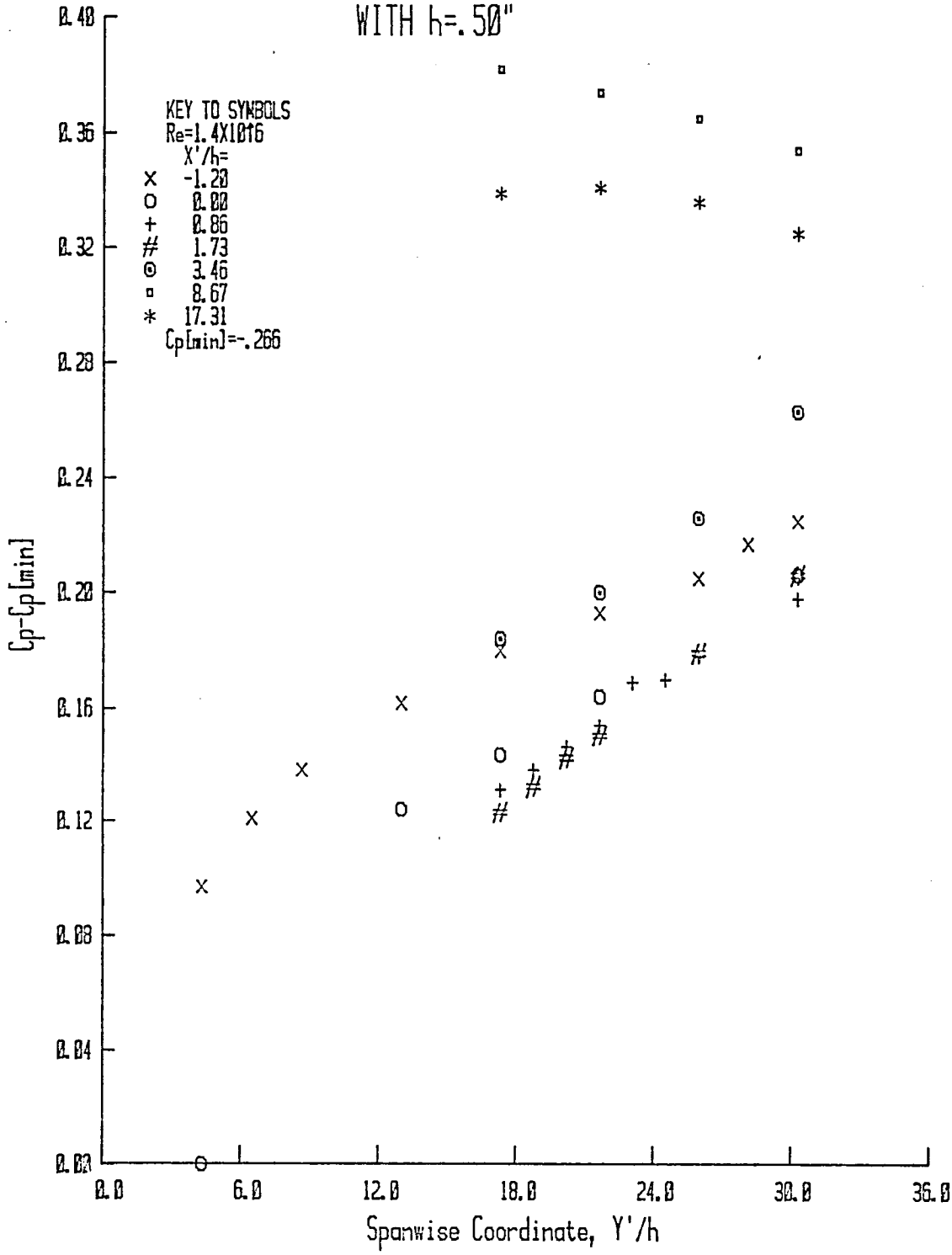

FIGURE 56. SPANWISE VARIATION IN C_p AT VARIOUS LONGITUDINAL LOCATIONS FOR THE 30-DEG. BASIC SWEPT-STEP MODEL WITH h=.94"

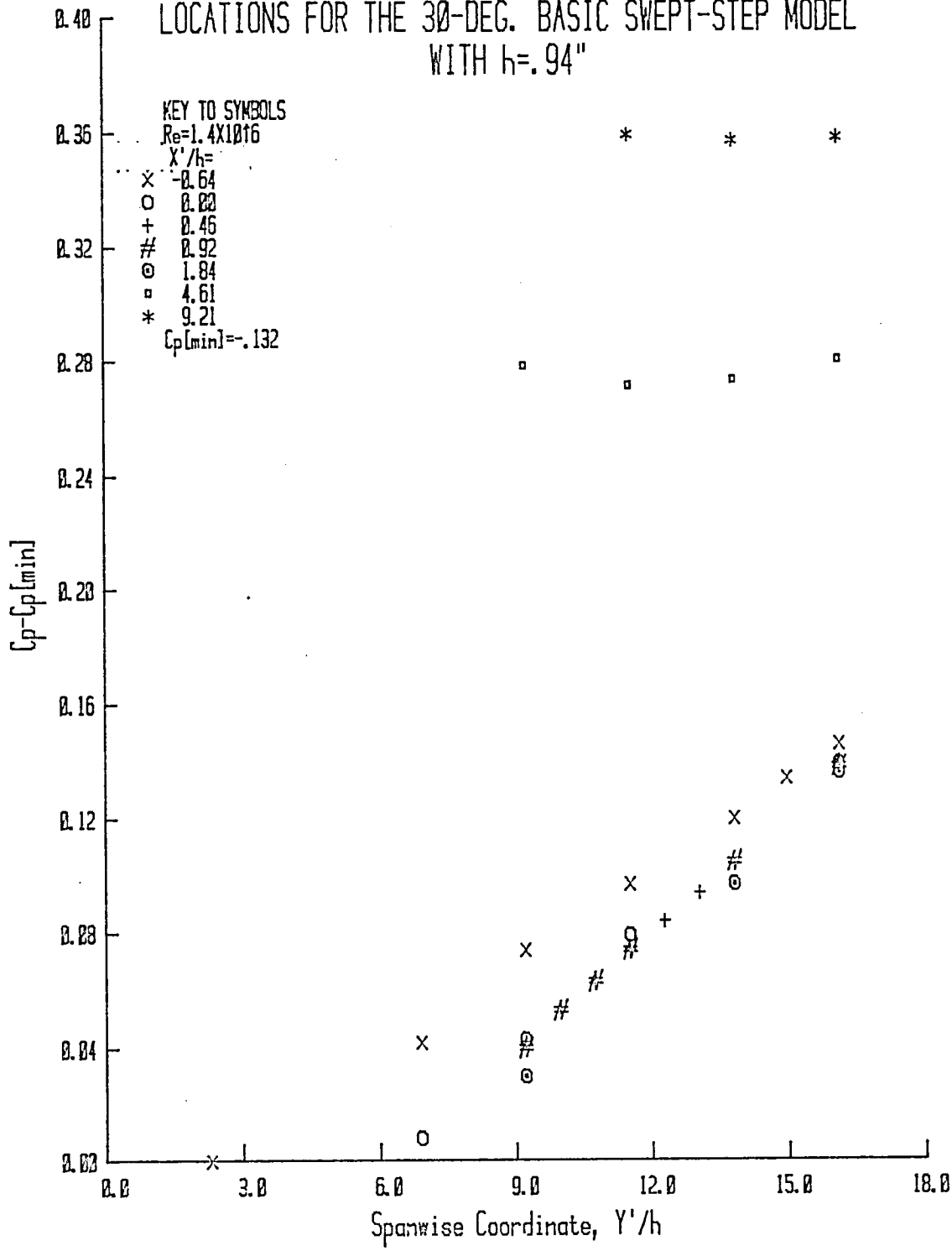

FIGURE 57. SPANWISE VARIATION IN C_p AT VARIOUS LONGITUDINAL LOCATIONS FOR THE 60-DEG. BASIC SWEPT-STEP MODEL WITH h=.50"

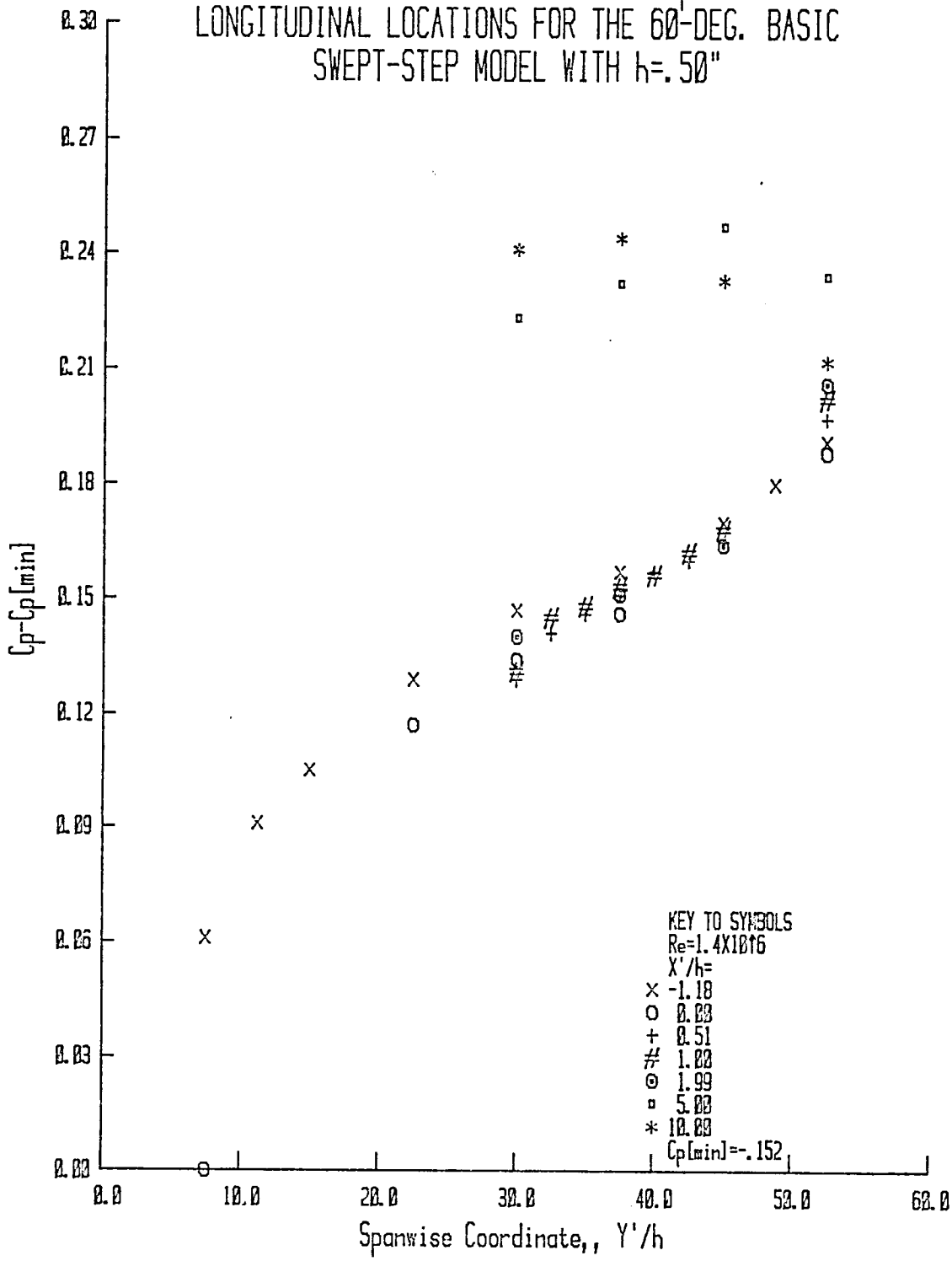

FIGURE 58. SPANWISE VARIATION IN C_p IN THE SEPARATED-FLOW REGION AT X'/h=1 FOR THE BASIC SWEPT-STEP MODEL WITH VARIOUS SWEEP ANGLES

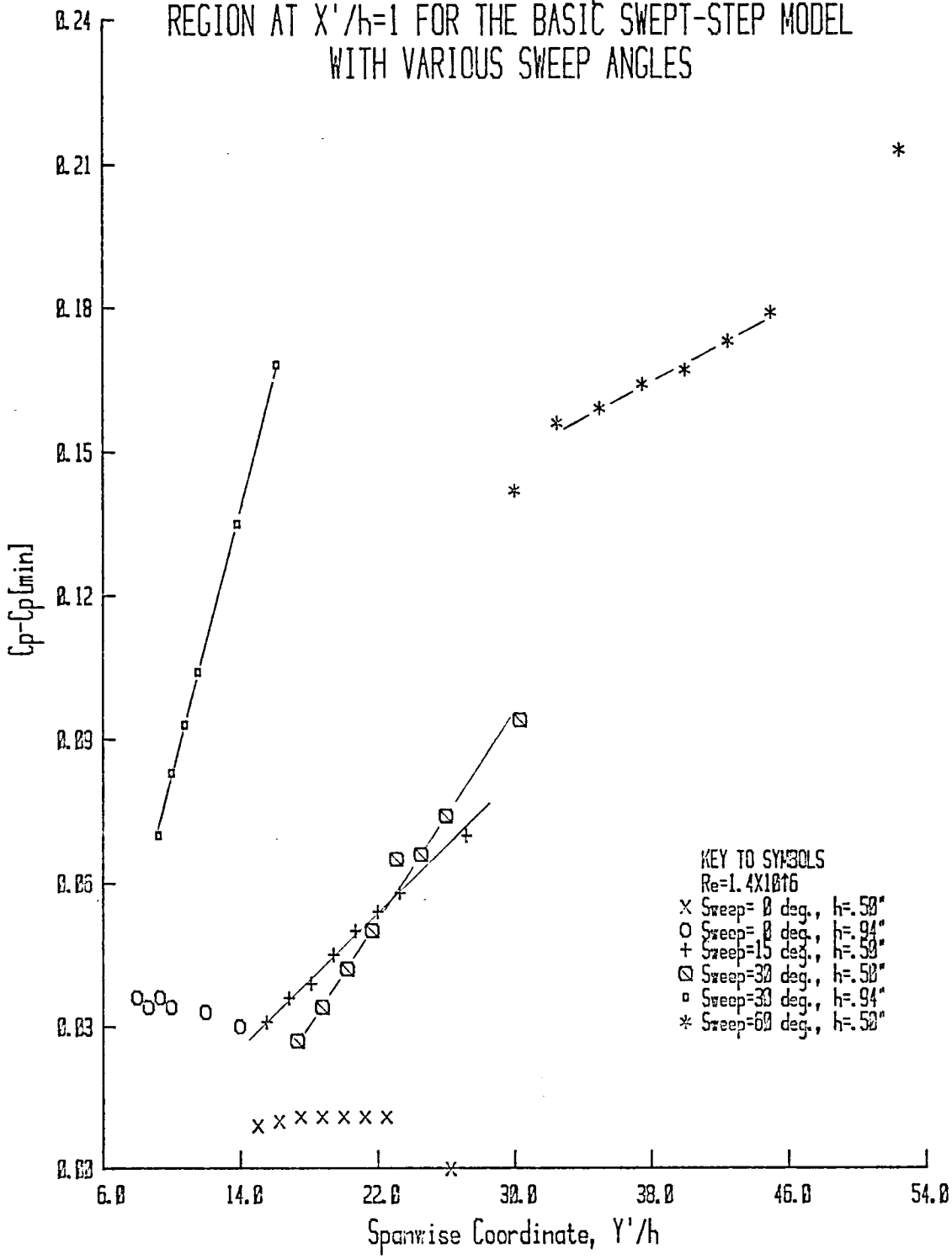

pressure gradient presently under discussion is the cause of the secondary vortex flow discernible in the flow visualization photographs obtained using the oil drop method.

It was previously observed, based on data presented in Figures 49 and 51, that the parameters C_p^+ and C_p^{**} failed to collapse the data for $\Lambda = 60°$ onto the curve for $\Lambda = 0$ to 30°. In the interval $0 < \Lambda < 30°$, the Independence Principle (Jones (1947)) appears to be valid—hence, the reason for the "cos Λ" term in Equations (3.8) and (3.9). This finding will be discussed further in the next section with regards to reattachment distance.

3.4.3 Reattachment Distance

Reattachment distances were deduced from the oil flow patterns produced as described in Section 2.3. Figure 36 shows that the reattachment line is well defined in the oil flow pattern. A review of the oil flow photographs of Section 3.3.3 shows that the reattachment line is easily distinguishable. The distance of the reattachment line from the step in terms of R or R', as defined in Figure 37, was measured without disturbing the oil pattern produced by the surface flow. These data were recorded as a function of Y or Y'—also defined in Figure 37. Reattachment distance as a function of a spanwise coordinate is herein reported for several sweep angle-step height permutations.

Reattachment distance, in terms of R (or R') was measured as a function of Y (or Y') for the unswept rearward-facing step at several values of h. The reattachment line becomes curved near the

side walls of the test section—insteady of being equidistant from the step across the entire span—giving an indication of the extent of the step-wall interaction; hence, of the two-dimensionality of the flow. It was found, based on the linearity of the reattachment line, that the worst case was for $h = .94"$—as expected. For this step height, the oil flow pattern indicated that two-dimensional flow prevailed across the span except within a 4" region near the side walls; thus, yielding two-dimensional flow in the region $4.2 < Y/h < 11.7$. This two-dimensional region has extent $12.9 < Y/h < 35.5$ and $8.0 < Y/h < 22.0$ for $h = .31"$ and $.50"$, respectively, for three-dimensional step-wall interaction regions of equal extent. The extent of the step-side wall interaction regions was found to be independent of step height over the range of values for h considered.

There was no well-defined reattachment line for $\Lambda = 0°$ at the values of Re tested. The reattachment point varied in the streamwise direction defining a reattachment region as described in Section 3.3.3. The general extent of this reattachment region at midspan over the range of values tested for h and Re was $4.5 < R'/h < 7.0$. This range of values in R'/h compares well with the range reported by Eaton and Johnston (1980) in their survey of rearward-facing step research ($4.9 < R'/h < 8.2$).

Reattachment distance, in terms of R'/h, is presented in Figure 59 as a function of the spanwise coordinate, Y'/h, for the 15°

FIGURE 59. REATTACHMENT DISTANCE PERPENDICULAR TO STEP VS. SPANWISE COORDINATE FOR THE 15-DEGREE BASIC SWEPT-STEP MODEL

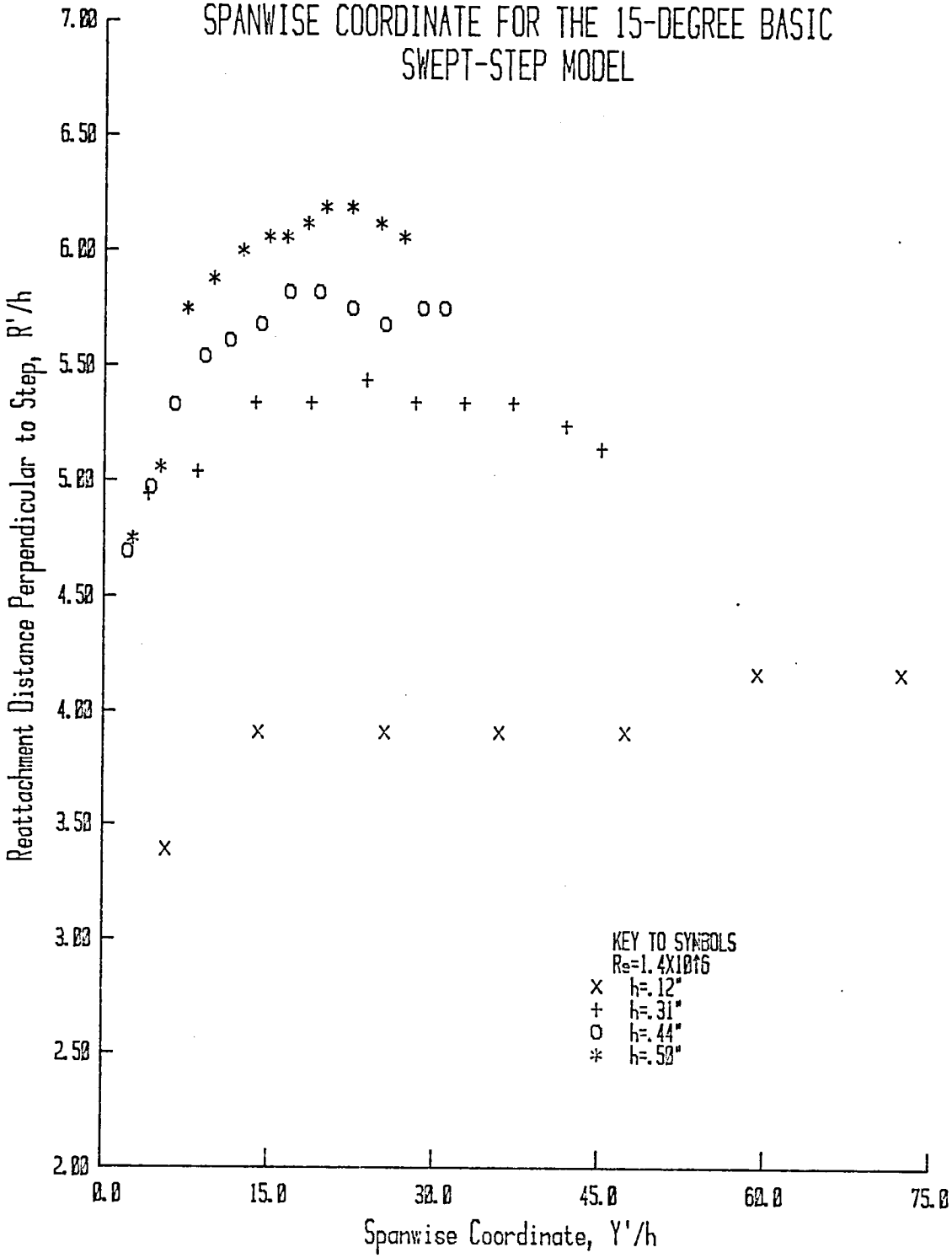

basic swept-step model for values of h of .12, .33, .44 and .50". It can be seen that asymptotic values of R'/h increase with Ar over the range of step heights examined at $\Lambda = 15°$, for which upstream area was held constant. This is the same general relationship that has been observed at $\Lambda = 0°$ as reported by Eaton and Johnston (1980).

The effect of boundary-layer thickness on reattachment length can also be extracted from Figure 59, which shows that R'/h decreases for increasing δ_{sep}/h. This general trend was also observed in the present data at $\Lambda = 0°$. These observations are in agreement with the relationship between these parameters as cited by Eaton and Johnston (1980).

Reattachment distance data are shown in Figures 60 and 61 for $\Lambda = 30°$ and 60°, respectively. It can be concluded from these data that the effect of changes in the parameter δ_{sep}/h on R'/h is not apparent at $\Lambda = 30°$ and greater. In particular, at these two step heights, the asymptotic value of R'/h for $h = .94"$ is less than that for smaller step heights. This suggests that there was insufficient span for the actual asymptotic value of R'/h to have been reached before end effects were encountered.

The spanwise distance to asymptote, L_a/h, lies between 20 and 30 for $\Lambda = 15°$, 30°, and 60° as determined from Figures 59 through 61. This observation validates the conclusion that asymptotic values of R'/h were not reached for $h = .94"$.

Generally, the data in Figures 59 through 61 indicate that the effect of Re on R' is small. This finding agrees with the

FIGURE 60. REATTACHMENT DISTANCE PERPENDICULAR TO STEP VS. SPANWISE COORDINATE FOR THE 30-DEGREE BASIC SWEPT-STEP MODEL

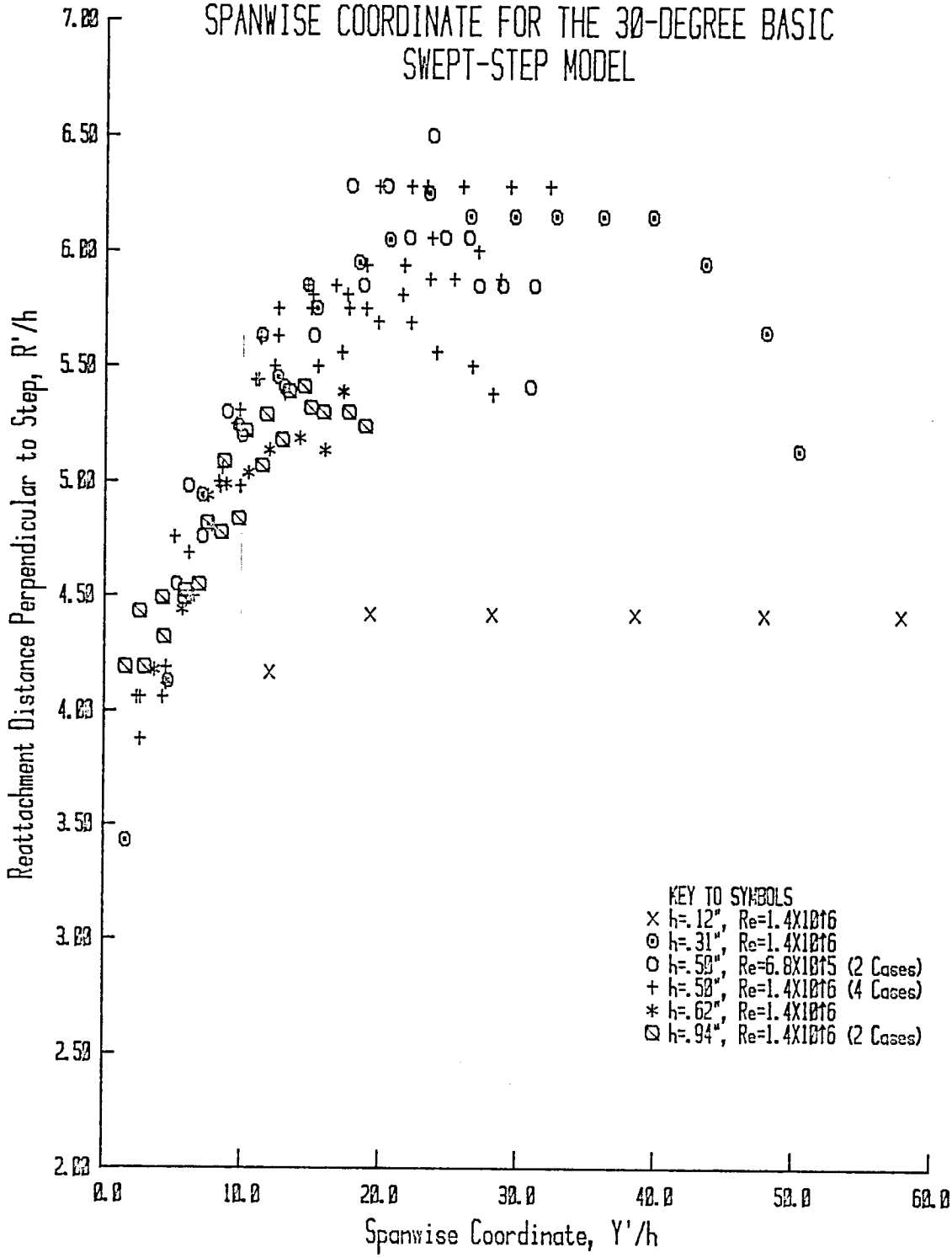

FIGURE 61. REATTACHMENT DISTANCE PERPENDICULAR TO STEP VS. SPANWISE COORDINATE FOR THE 60-DEGREE BASIC SWEPT-STEP MODEL

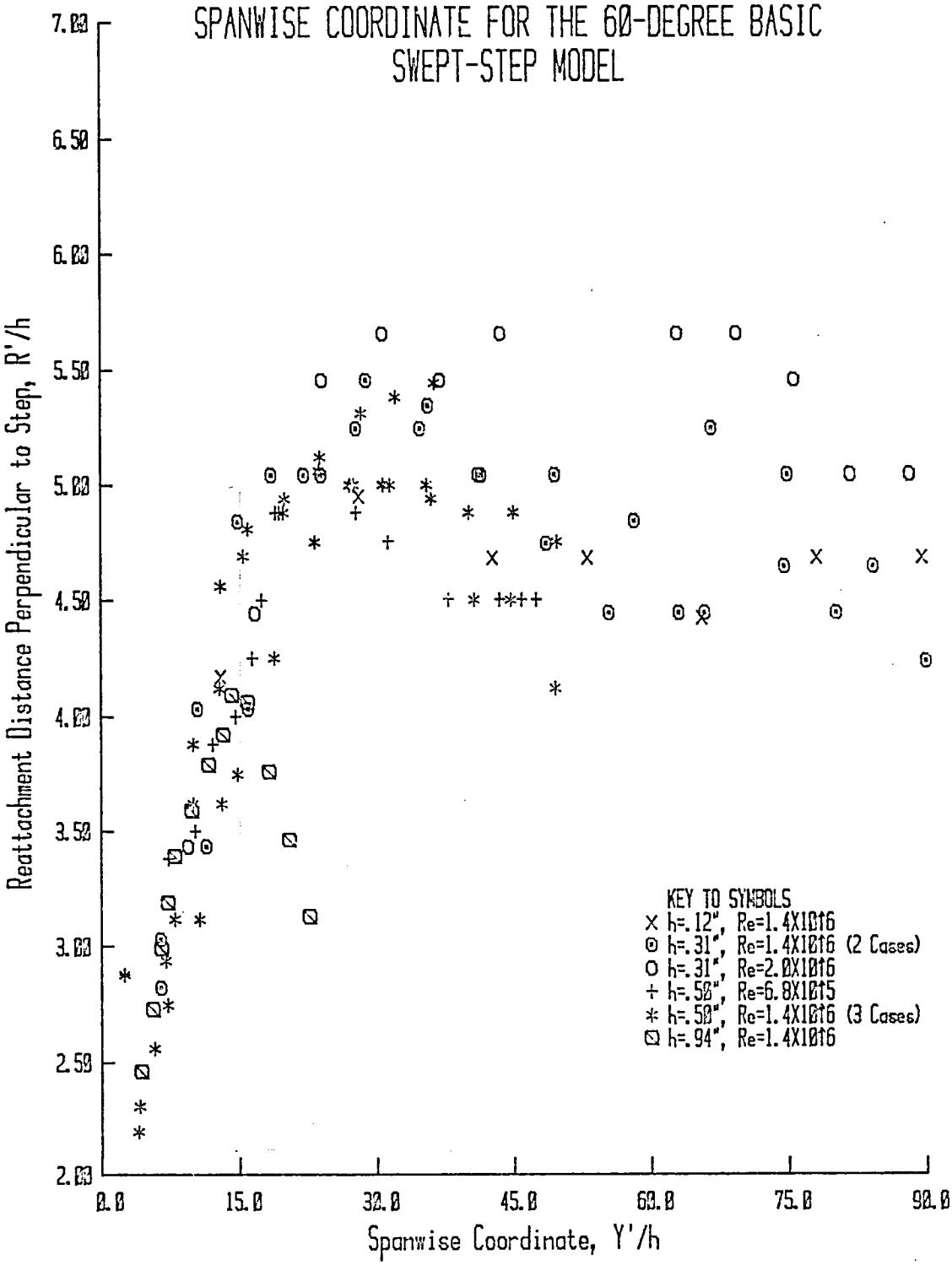

relationship between these two parameters as reported by Eaton and Johnston (1980), who have indicated that R'/h varies weakly with Re_θ in the turbulent flow regime for unswept steps. This is likely a consequence of the weak variation of mixing length with Re_θ for $Re_\theta \approx 4 \times 10^3$ and larger [Bushnell and Morris (1971)].

Reattachment distance as a function of Y'/h is displayed in Figures 62 through 65 for $h = .12$, .31, .50 and .94", respectively. Presenting the data in this form is conducive to the determination of sweep effects at constant h. It is observable that sweep effects become more pronounced as h increases—being negligible at $h = .12$" and appreciable at $h = .50$". The data for $h = .94$" is presented for comparison, although it is understood that maximum R'/h values had not been reached. Still, considerable sweep effects are shown to be present.

It has previously been shown that separated flows can be highly sensitive to sweep effects. Typical studies in which this has been

---

Bushnell, D. M. and Morris, D. J., Shear-Stress, Eddy-Viscosity, and Mixing-Length Distributions in Hypersonic Turbulent Boundary Layers, NASA TM X-2310, 1971.

FIGURE 62. REATTACHMENT DISTANCE PERPENDICULAR TO STEP VS. SPANWISE COORDINATE FOR THE BASIC SWEPT-STEP MODEL AT VARIOUS SWEEP ANGLES WITH h=.12"

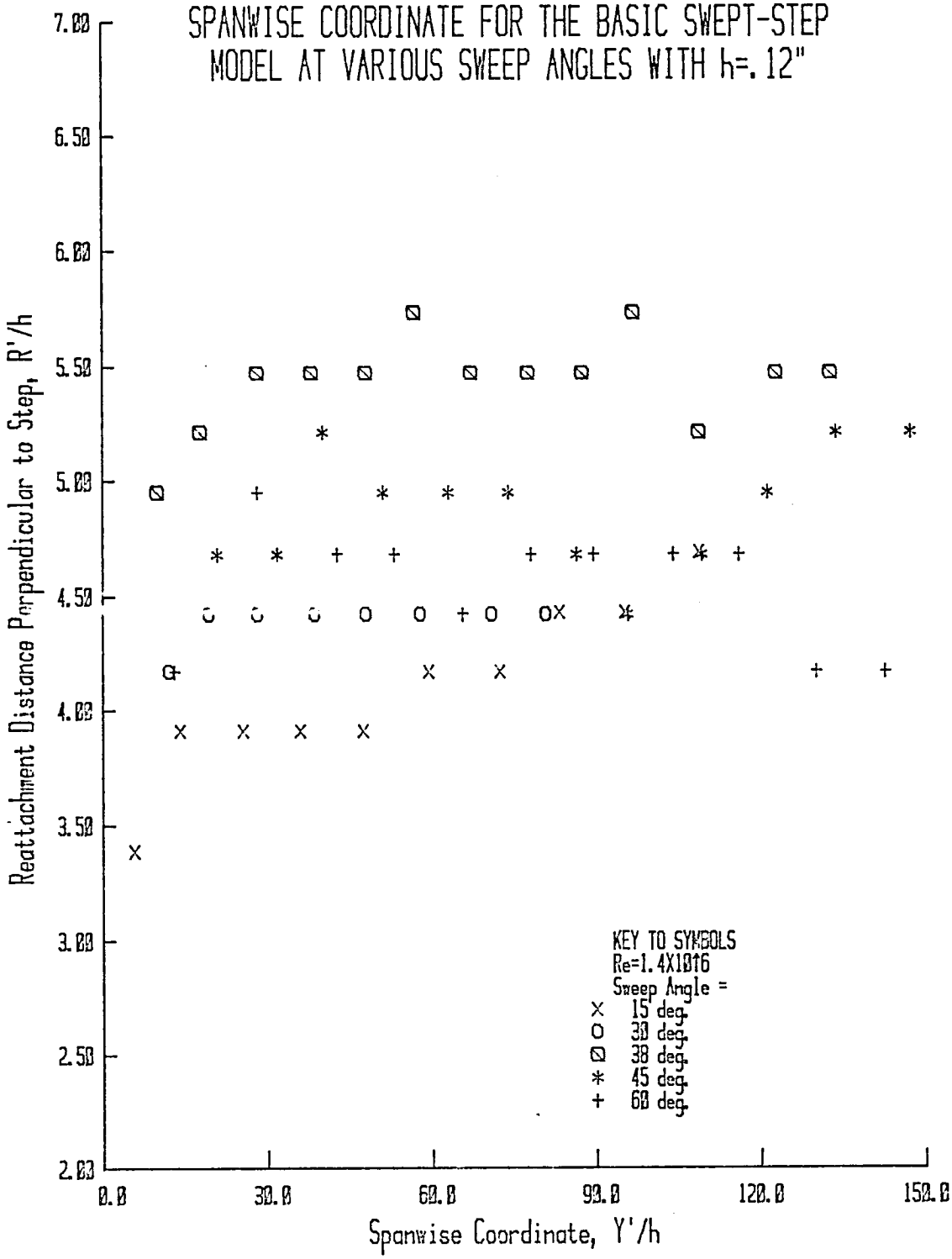

FIGURE 63. REATTACHMENT DISTANCE PERPENDICULAR TO STEP VS. SPANWISE COORDINATE FOR THE BASIC SWEPT-STEP MODEL AT VARIOUS SWEEP ANGLES WITH h=.31"

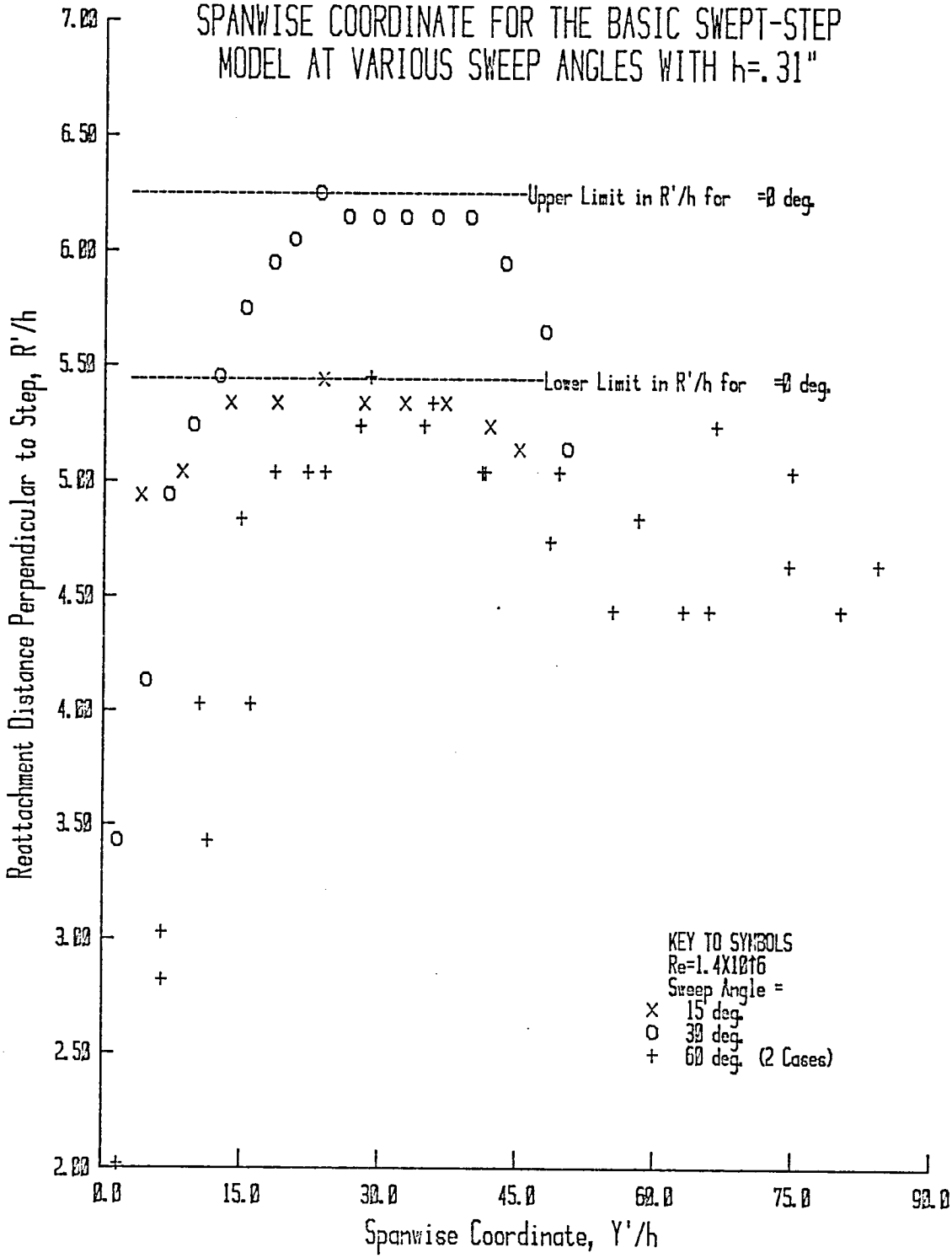

FIGURE 64. REATTACHMENT DISTANCE PERPENDICULAR TO STEP VS. SPANWISE COORDINATE FOR THE BASIC SWEPT-STEP MODEL AT VARIOUS SWEEP ANGLES WITH h=.50"

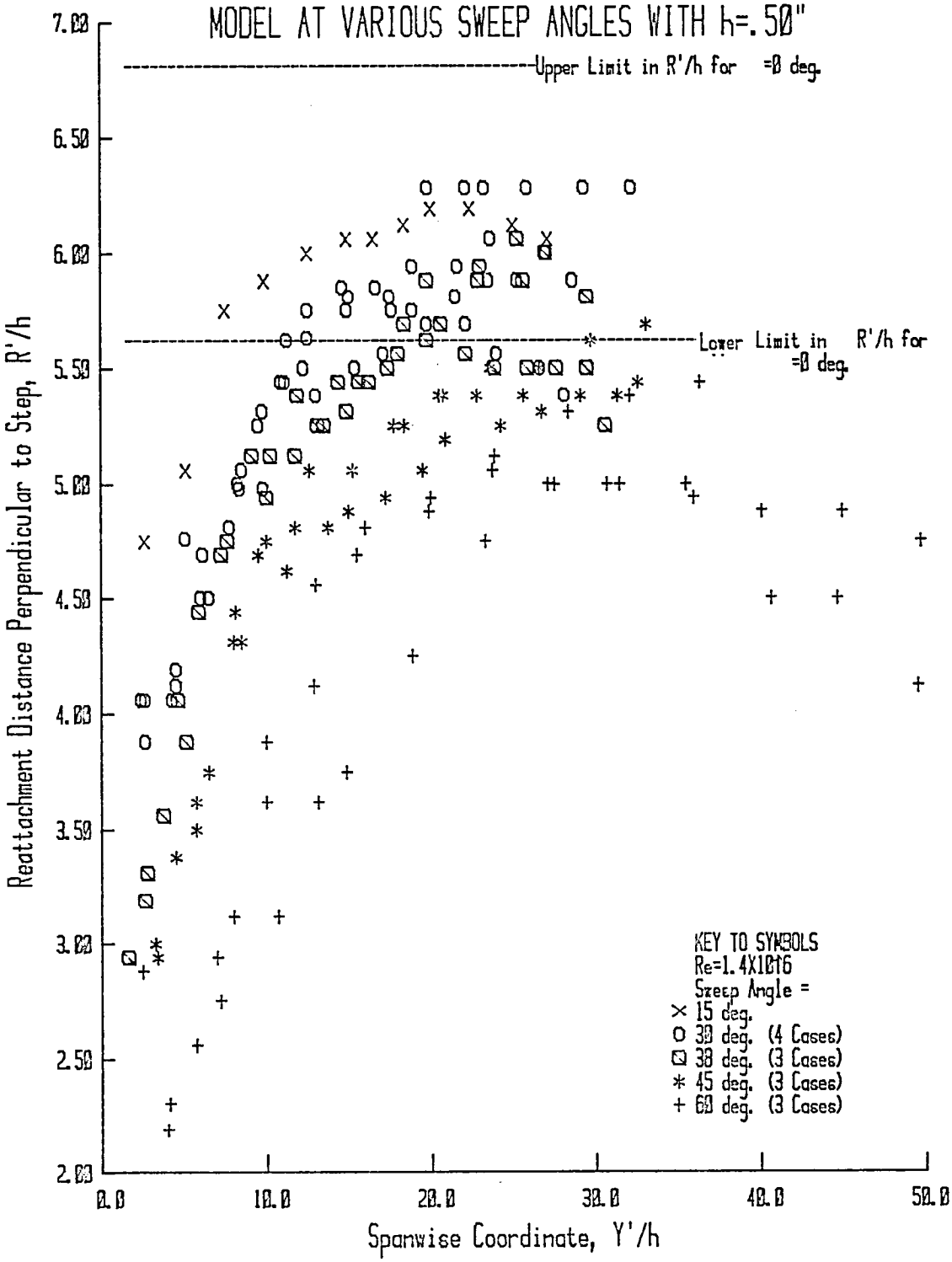

FIGURE 65. REATTACHMENT DISTANCE PERPENDICULAR TO STEP VS. SPANWISE COORDINATE FOR THE BASIC SWEPT-STEP MODEL AT VARIOUS SWEEP ANGLES WITH h=.94"

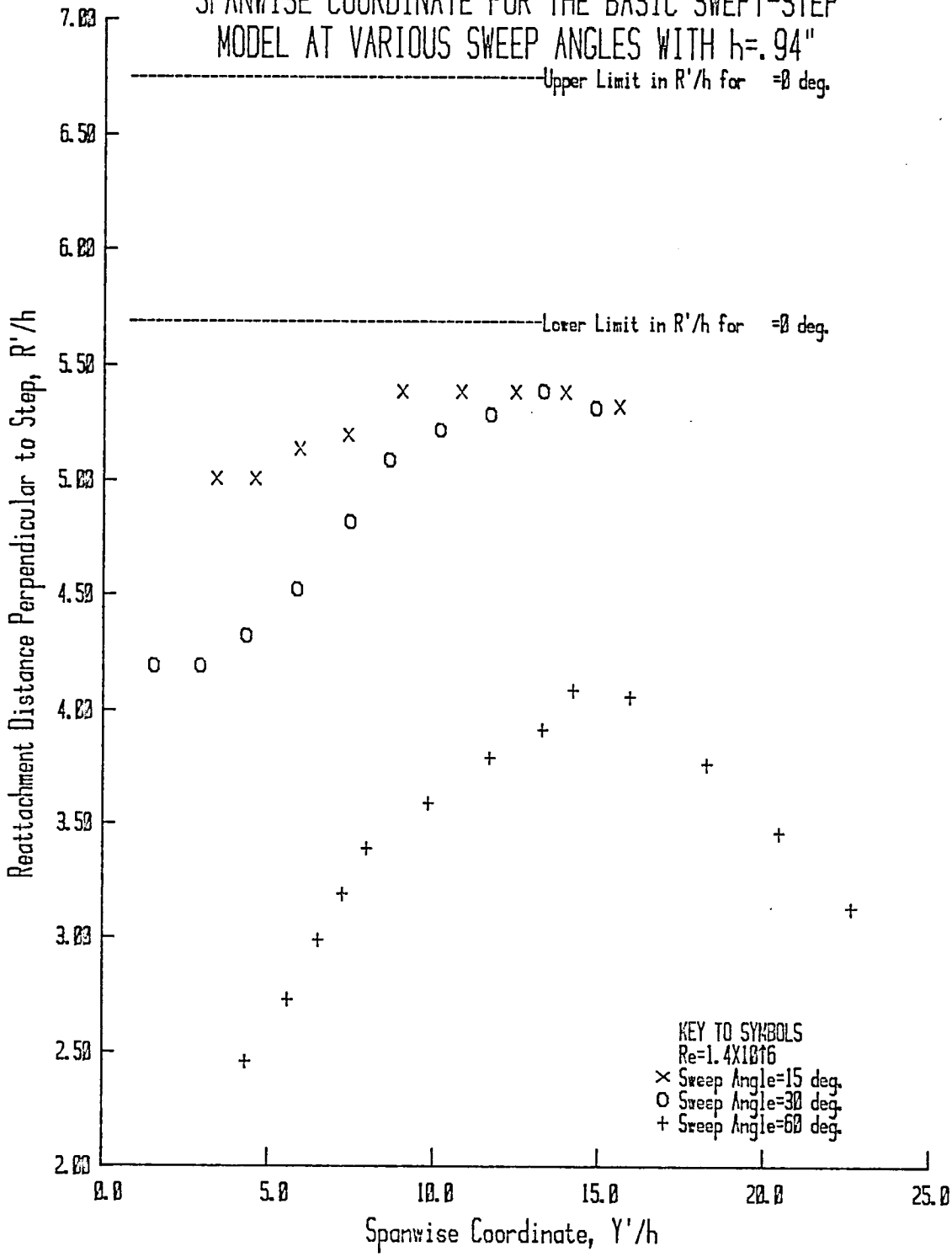

demonstrated have been conducted by Werle et al. (1973), Yevenko and Anisin (1978) and Settles and Perkins (1979).

In the present situation, at a given step height, it is possible to determine the range of sweep angles over which sweep effects dominate by identifying when the R' measurements fail to satisfy the Independence Principle. According to Jones (1947), the Independence Principle—as applied to the present problem—states that if R is observed in a plane perpendicular to the step face (R'), its value is determined solely by the component of velocity in that plane. Therefore, flow in the direction normal to the step face is independent of the spanwise flow whenever this principle is satisfied.

Using as an example the data of Figure 64, it can be observed that for $\Lambda > 38° = \Lambda_{crit}$, the R'/h data primarily fall outside the reattachment region defined by $\Lambda = 0°$. The conclusion reached is that for $\Lambda > 38°$, the Independence Principle becomes invalid

---

Werle, M. J., Vatsa, V. N. and Bertke, S. D., "Sweep Effects on Supersonic Separated Flows—A Numerical Study," AIAA Journal, Vol. 11, No. 12, pp. 1763-1765, 1973.

Yevenko, V. I. and Anisin, A. K., "Effect of Surface Orientation on the Characteristics of Separated Flow," Heat Transfer—Soviet Research, Vol. 10, No. 5, pp. 16-19, 1978.

Settles, G. S. and Perkins, J. J., Investigation of Three-Dimensional Shock-Boundary Layer Interactions at Swept Compression Corners, Paper 79-1498, AIAA 12th Fluid and Plasma Dynamics Conference, July 23-25, Williamsburg, VA, 1979.

Jones, R. T., Effects of Sweepback on Boundary Layer and Separation, NACA TN 1402, 1947.

so that the two aforementioned components of the freestream velocity can no longer be considered independently. The fact that the Independence Principle applies, though the flow is turbulent, is contrary to conclusions drawn by Ashkenas and Riddell (1955) and Bradshaw (1971), who found that the Independence Principle did not apply to yawed flat plates in turbulent flow. Ashkenas and Riddell (1955) further concluded that this principle did not apply to turbulent flows in general.

Practical implications of the applicability of the Independence Principle include the tentative assertion that three-dimensional separated regions on swept wings, unless subjected to strong airfoil pressure gradients, act essentially as two-dimensional flows (in a suitable coordinate system) for sweep angles less than Λ_{crit}.

Morel (1978) slanted the base of a bluff body, which resembled a ground vehicle, and of an ogive cylinder. For each model he found a critical slant angle, β'_{crit} (corresponds to Λ_{crit}), for which the drag changed discontinuously. This phenomenon was explained by a change in the type of base flow. For $\beta < 30°$, vortex flow was detected

---

Ashkenas, H. and Riddell, F. R., Investigation of the Turbulent Boundary Layer on a Yawed Flat Plate, NACA TN 3383, 1955.

Bradshaw, P., "Calculation of Three-Dimensional Turbulent Boundary Layers," Journal of Fluid Mechanics, Vol. 46, p. 417, 1971.

Morel, T., Aerodynamic Drag of Bluff Body Shapes Characteristic of Hatch-Back Cars, Research Publication GMR-2581, General Motors Research Laboratories, 1977.

along the base of the bluff-body model. The value of β'_{crit} was 43° for the ogive-cylinder model. These values of β'_{crit} are similar in magnitude to the value of $\Lambda_{crit} = 38°$ as previously discussed.

Carr (1974) performed oil flow studies on a bluff body similar to Morel's with $\beta' = 25°$. The surface flow pattern obtained indicated the presence of "side-edge" vortices.

Sedney (1981) examined these experimental findings and found them to be compatible with theory upon (1) invoking the Independence Principle for turbulent flow, (2) assuming $\beta' = O(\phi)$ and (3) using experimentally observed values for ϕ for vortex breakdown ($\approx 30°$). (Swirl angle, ϕ, is defined in the next section.)

The "side-edge" vortices examined by Morel (1978), Carr (1974) and Sedney (1981) are related to the spanwise vortices presently under examination. The assumption made by Sedney (1981) of the equality of β' and ϕ is substantiated in the next section (in terms of Λ and ϕ) and theoretically examined in Appendix C.

3.4.4. Swirl Angle

Swirl angle, ϕ, as defined in Figure C-1 of Appendix C, was extracted from the oil flow photographs of Section 3.3.3. Swirl angle

---

Carr, G. W., Influence of Rear Body Shape on the Aerodynamic Characteristics of Saloon Cars, Motor Industry Research Association, Nuneaton, Warwickshire, Report No. 2, 1974.

Sedney, R., A Flow Model for the Effect of a Slanted Base on Drag, Ballistic Research Labs., Aberdeen Proving Ground, MD, Technical Report ARBRL-TR-02341, 1981.

data are exhibited in Figures 66 through 68 for Λ = 15°, 30° and 60°, respectively. In each case, the swirl angle data are clustered around the appropriate value of Λ. In addition, it is shown that ϕ is independent of h. The same data are presented in Figure 69 without regards to h, with data included at Λ = 45° also. It can be concluded that some correlation exists between ϕ and Λ such that $\phi \approx \Lambda$. This correlation is developed in Appendix C.

The values of ϕ measured in the separated-flow region downstream of the swept steps often exceed the maximum value quoted by Sedney (1981) and by Hall (1972) of 40°, which is a prerequisite to vortex breakdown. The necessary conditions for breakdown given by Hall (1972) are: (1) maximum $\phi > 40°$, (2) an adverse pressure gradient and (3) stream tube divergence in the vortex core. Conditions (1) and (2) are generally satisfied by the spanwise vortex flow behind swept steps, but condition (3) is not since R' generally reaches some asymptotic value impeding the radial growth of the region of vortex flow.

Flow angles α and β, as functions of Y, were measured in the separated-flow region of configuration LE2-BB60-DS60.5, according to the coordinate system defined in Figure 16(b). Surveys were performed at midspan locations X = 0.5, 2.0 and 3.1 in., in order to determine the inviscid cross-flow angle (β) just above the plane of dividing

---

Hall, M. G., "Vortex Breakdown," Annual Review of Fluid Mechanics, Annual Review, Inc., Vol. 4, 1972.

FIGURE 66.
SWIRL ANGLE VS. SPANWISE COORDINATE
FOR THE 15-DEGREE BASIC SWEPT-STEP MODEL

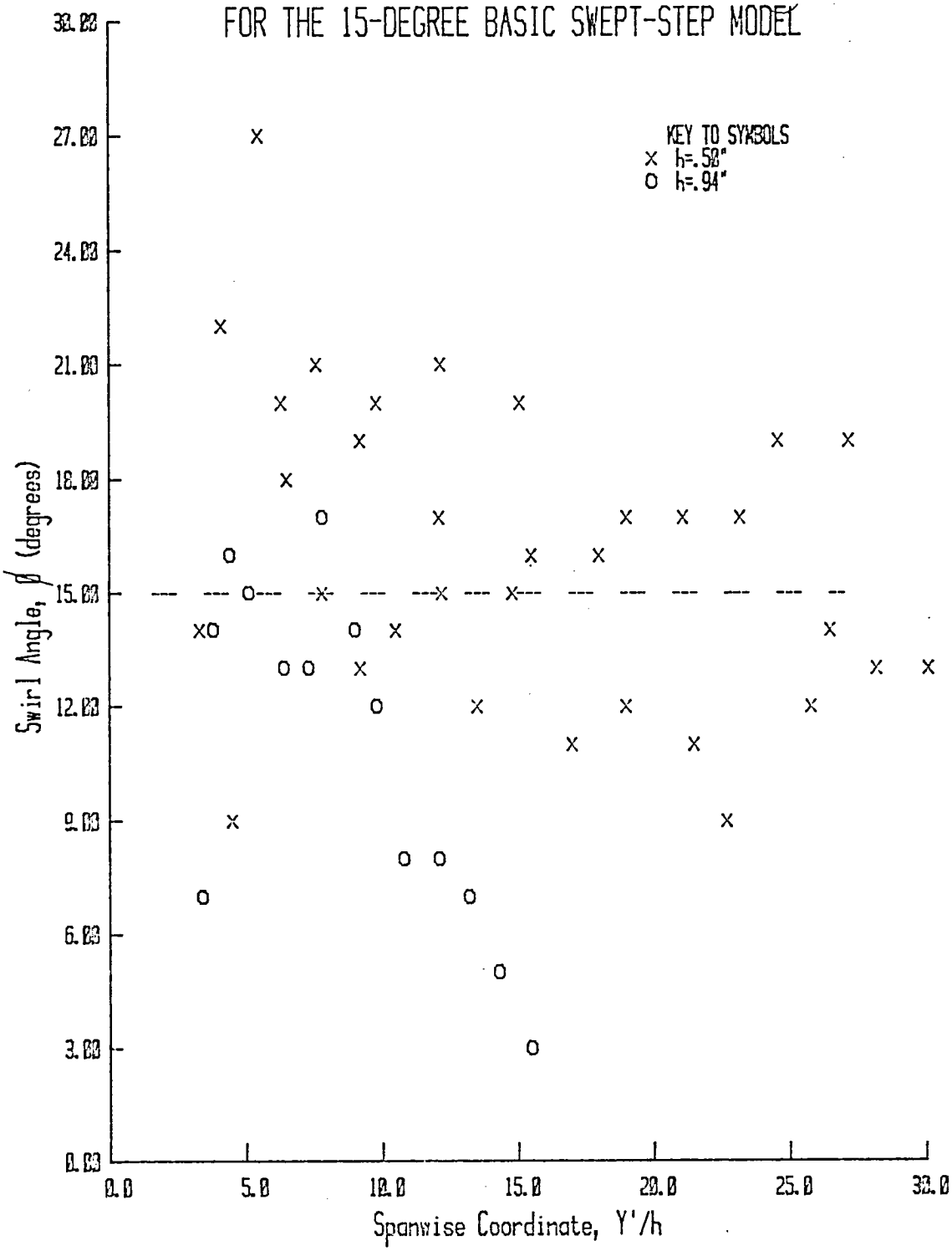

FIGURE 67.
SWIRL ANGLE VS. SPANWISE COORDINATE
FOR THE 30-DEGREE BASIC SWEPT-STEP MODEL

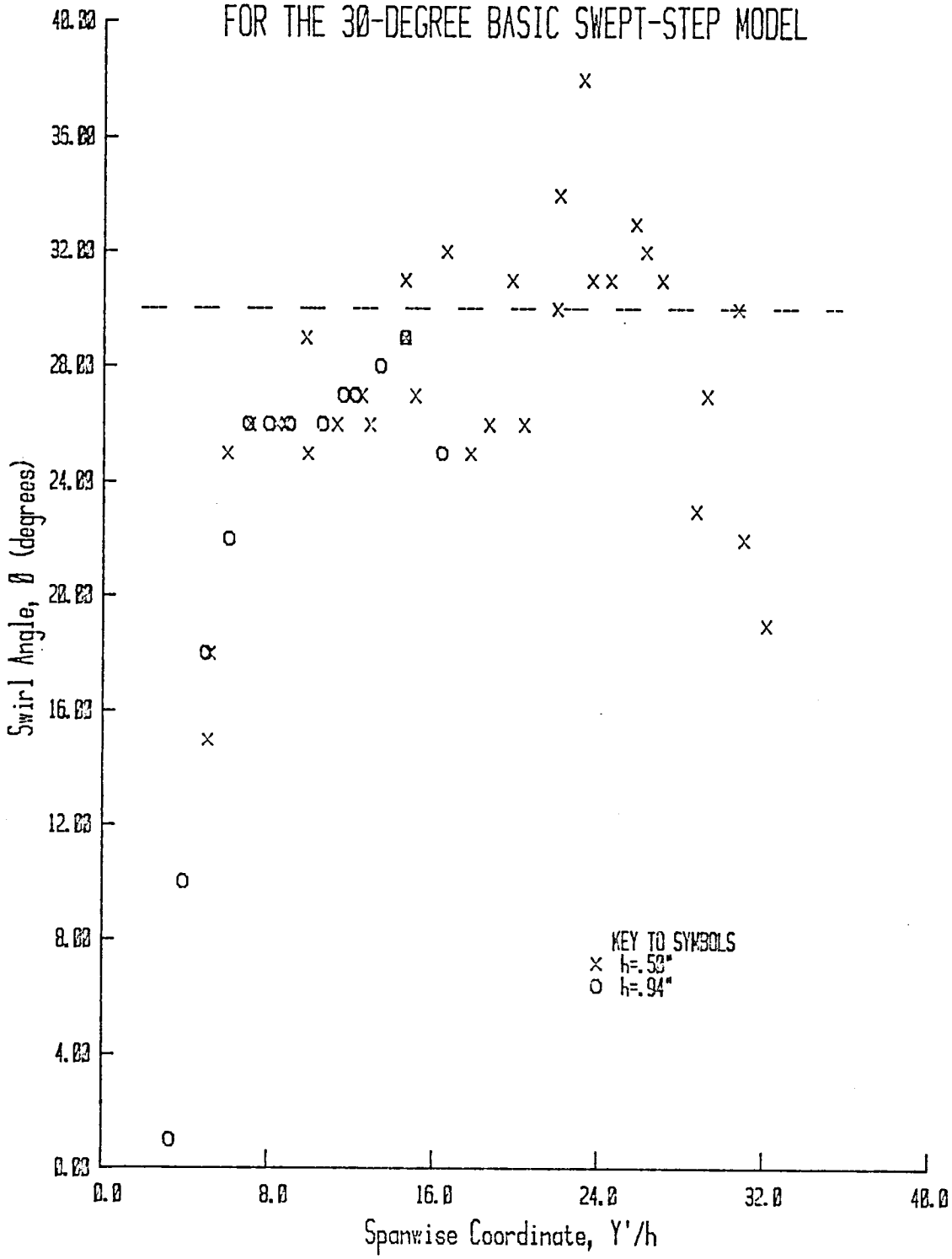

FIGURE 68.
SWIRL ANGLE VS. SPANWISE COORDINATE FOR THE 60-DEGREE BASIC SWEPT-STEP MODEL

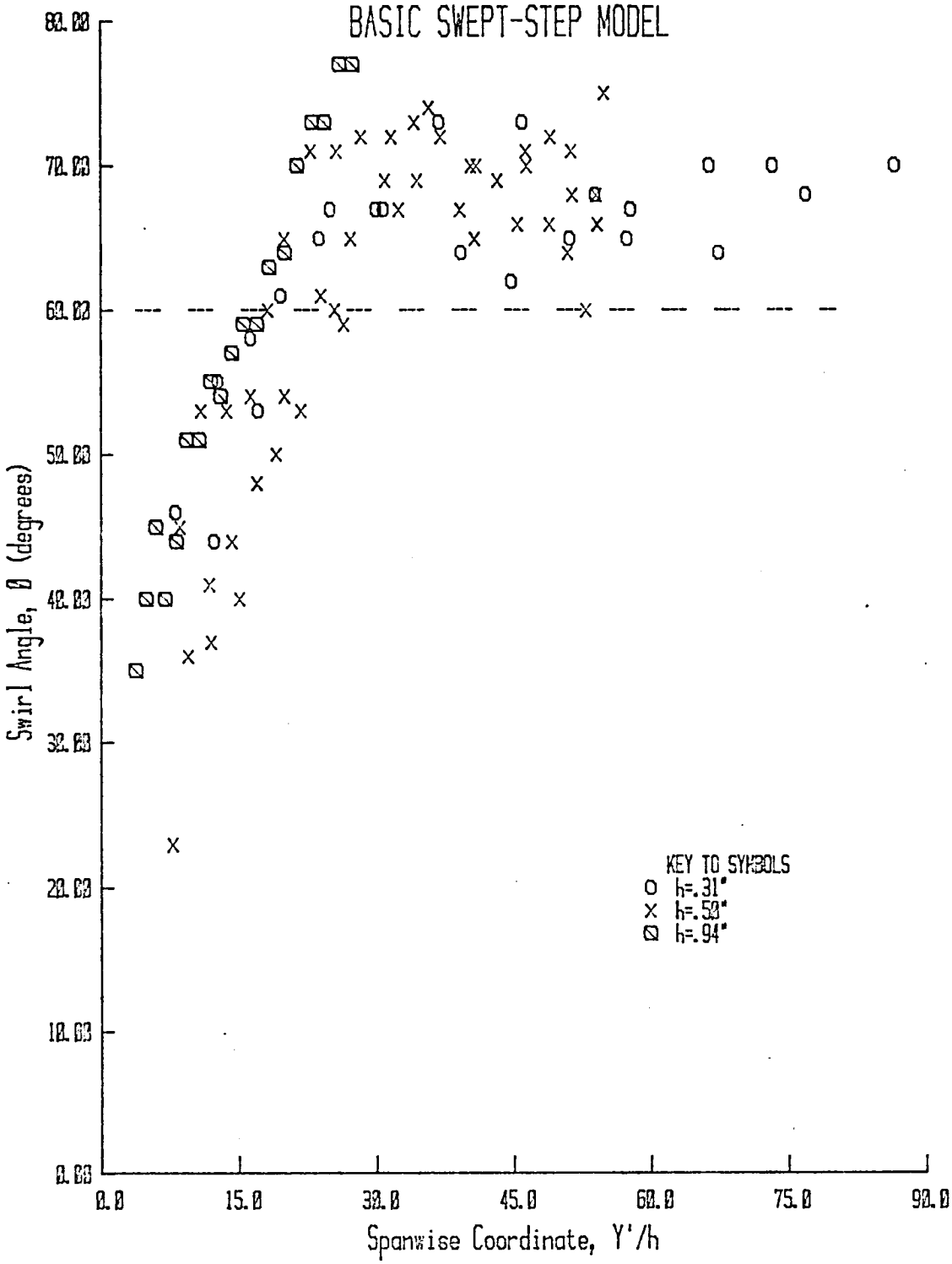

FIGURE 69.
SWIRL ANGLE VS. SPANWISE COORDINATE FOR THE BASIC SWEPT-STEP MODEL AT VARIOUS SWEEP ANGLES, STEP HEIGHTS AND REYNOLDS NUMBERS

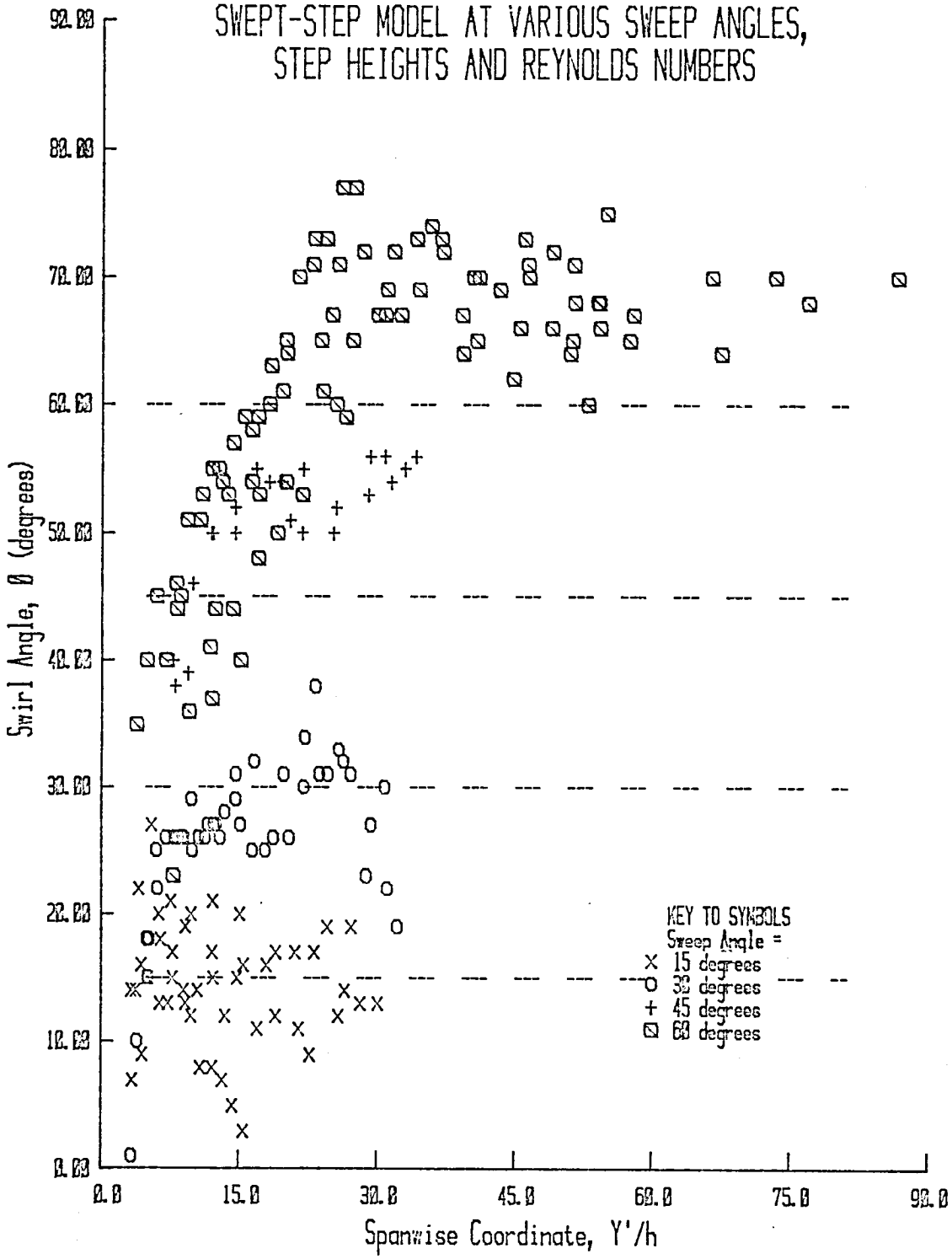

streamlines. Using assumptions discussed in Appendix C, this angle can then be related to ϕ.

The measured flow angle data are displayed in Figures 70 through 72 at X = 0.5, 2.0, and 3.1 in., respectively. The height of the dividing streamline above the surface cannot be exactly determined, but can be estimated using appropriate bounds. For example, at X = 3.1", the actual height is between y = .19"—obtained assuming the linear streamline profile of Figure 73—and that value of y corresponding to α = -.57°—y = .37". Assuming that the probable profile of Figure 73 is valid, the measured value of α at X = 3.1" should be greater than -5.7°. Values of the swirl angle determined from the measured flow angle data in this manner are contained in Table 6 below.

Table 6

Swirl Angles Determined from Flow Angle Data

X (in.)	Y [div. s.l.] (in.)	β (deg.)	ϕ (deg.)
0.5	.45	21 - 22	81 - 82
2.0	.30 - .42	9 - 23	69 - 83
3.1	.19 - .37	14 - 28	74 - 88

The values of ϕ reported in Table 6 are in the same range (60° to 80°) as the data in Figure 68, as measured from oil flow patterns, and Figure C-2, as calculated from surface pressure measurements. These independent measurements have served to validate the analysis of Appendix C, in addition to the swirl angle measurements.

FIGURE 70. MEASURED FLOW ANGLE PROFILES ABOVE SEPARATED FLOW AT X/h=1.0 FOR THE BASIC 60-DEG. SWEPT-STEP MODEL WITH h=.50"

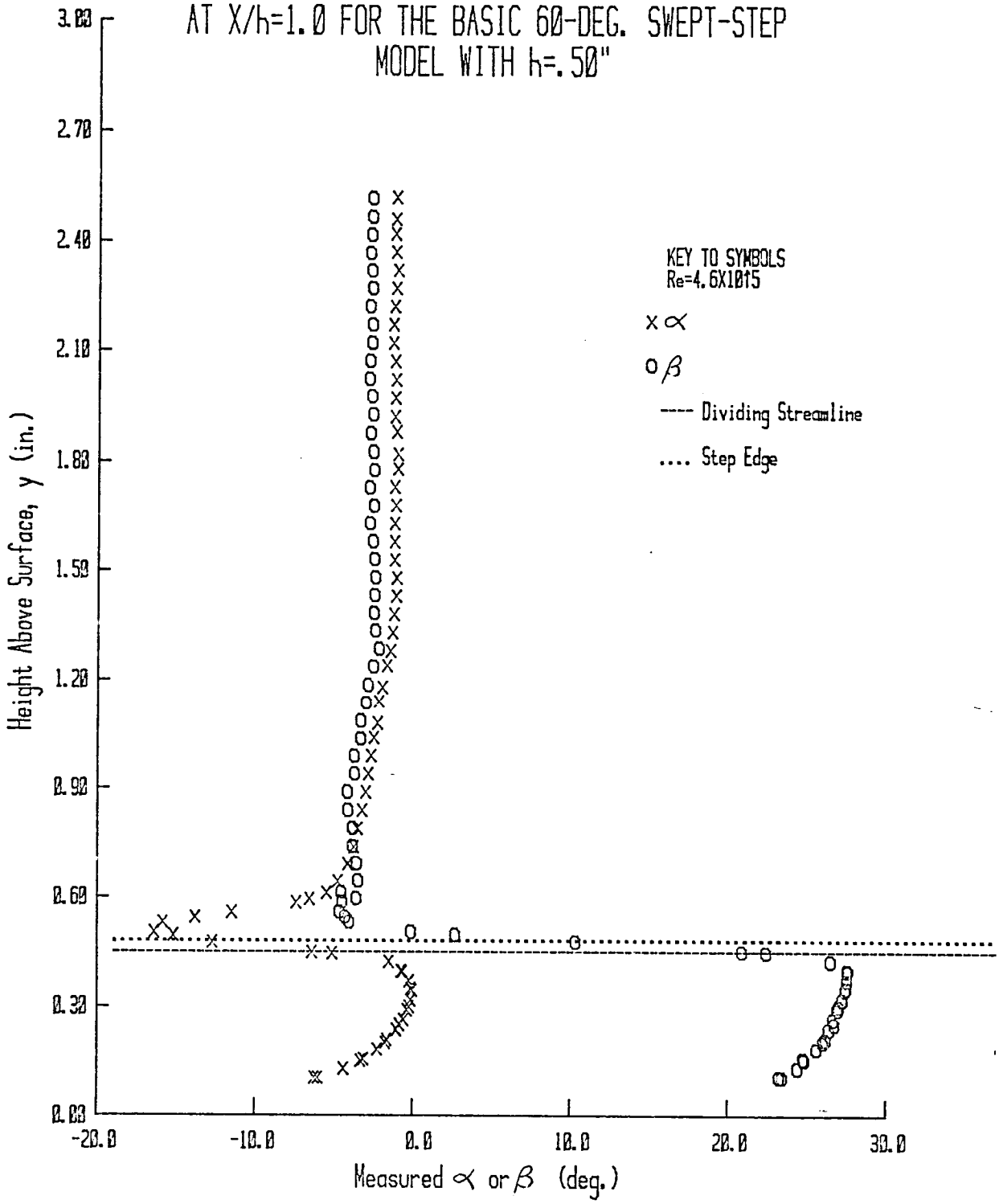

FIGURE 71. MEASURED FLOW ANGLE PROFILES ABOVE SEPARATED FLOW AT X/h=4.0 FOR THE BASIC 60-DEG. SWEPT-STEP MODEL WITH h=.50"

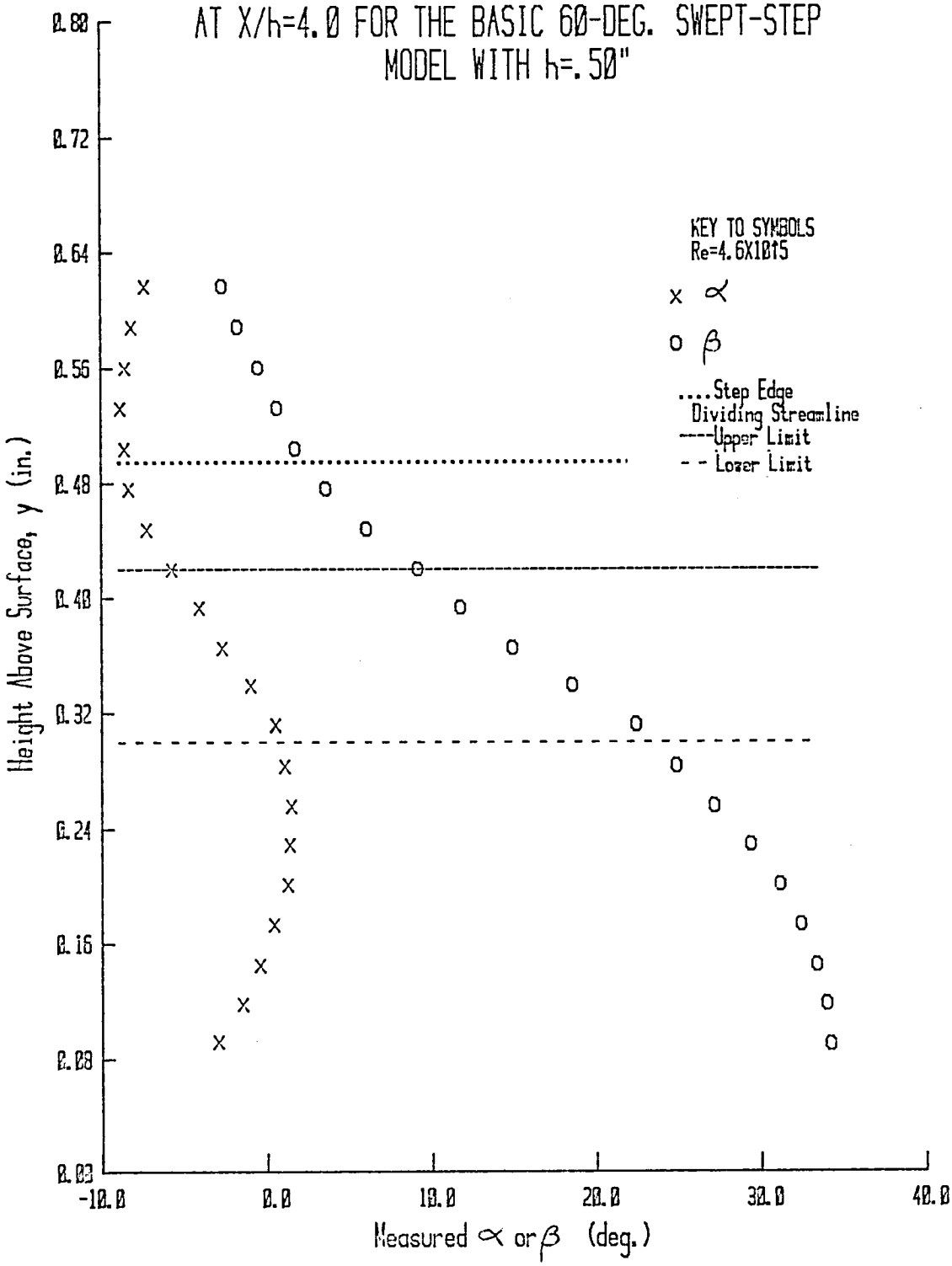

FIGURE 72. MEASURED FLOW ANGLE PROFILES ABOVE SEPARATED FLOW AT X/h=6.2 FOR THE BASIC 60-DEG. SWEPT-STEP MODEL WITH h=.50"

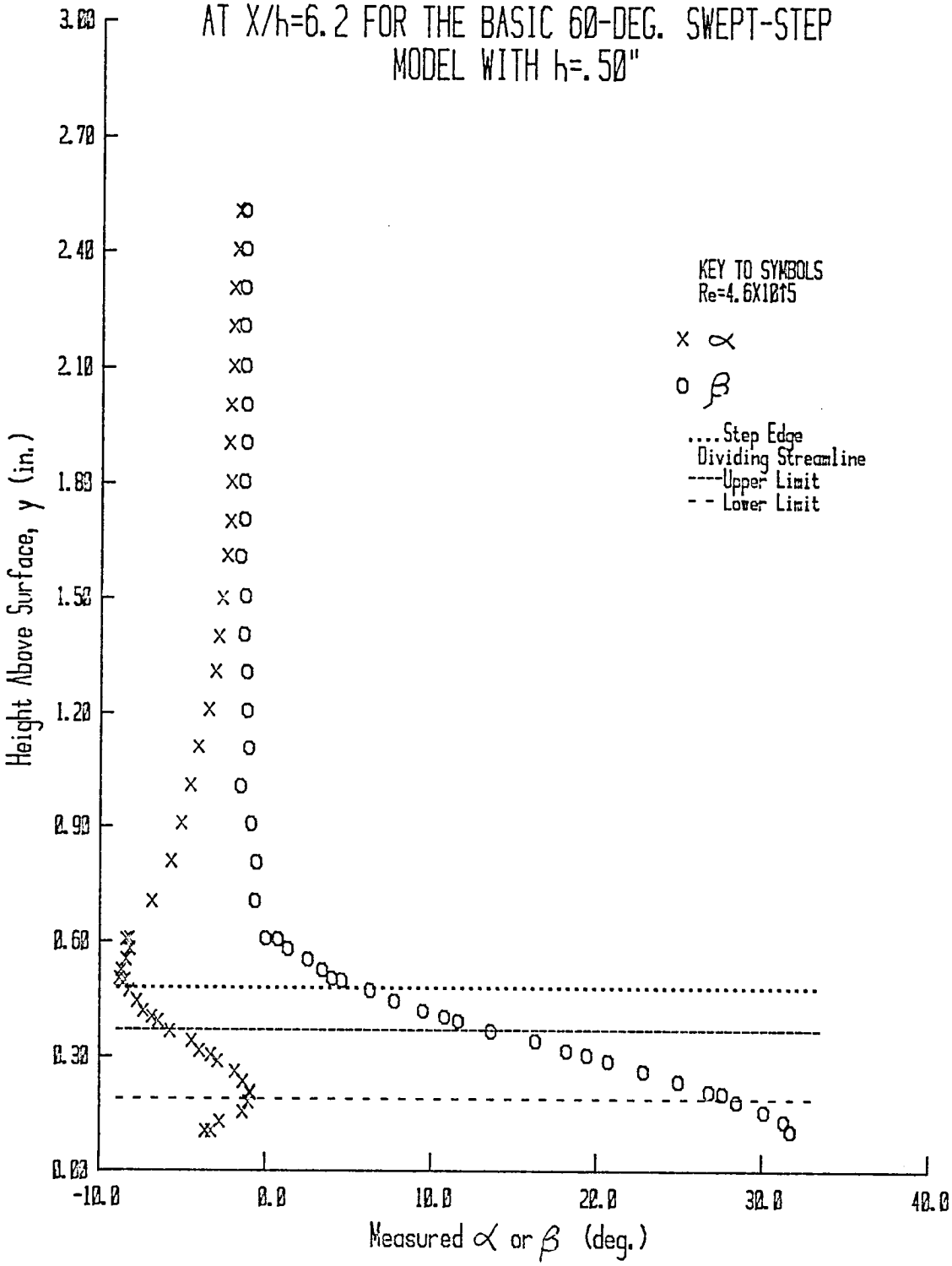

Figure 73. Dividing Streamline Profiles for $\Lambda = 60^{0}$ and h = .50"

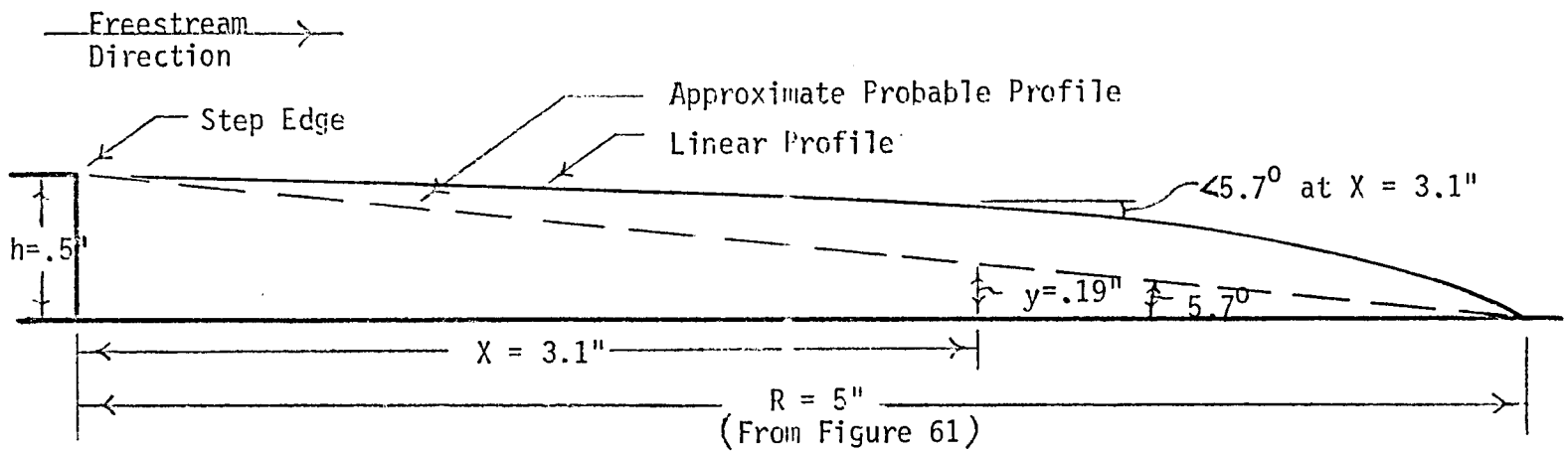

3.5. Effects of Modifications to Basic Models

The effect on the separated flow of physical modifications to the basic model geometry and test section will now be discussed. These modifications are listed in Figure 8.

3.5.1. Free Transition

The effect of variations in the state of the boundary layer approaching the step was determined by examining surface pressures measured with and without the .039-in. diameter trip wire in position. Since surface pressure varies weakly with X' in the upstream portion of the separated-flow region, the value of the base pressure is indicative of the surface pressure level in the near-separated region. The applicable base pressure and midspan surface pressure measurements are presented in Figures 74 and 75. It can be concluded from the data displayed in Figures 74 and 75 that the manner of flow transition (free or fixed) has little effect on the static pressure in the separated-flow region and probably no significant effect on the flow physics there.

3.5.2. Addition of Compensating Swept Roof Step

Most rearward-facing step experiments more accurately correspond to channel flow with an abrupt increase in flow cross-section area. In order to realistically simulate flow over such excrescences on airfoils, where the inviscid region extends infinitely in the y direction, a compensating roof step is needed in the test section. Due to the

FIGURE 74. SPANWISE VARIATION IN Cp[base] FOR THE 60-DEGREE BASIC SWEPT-STEP MODEL WITH AND WITHOUT TRIP WIRE

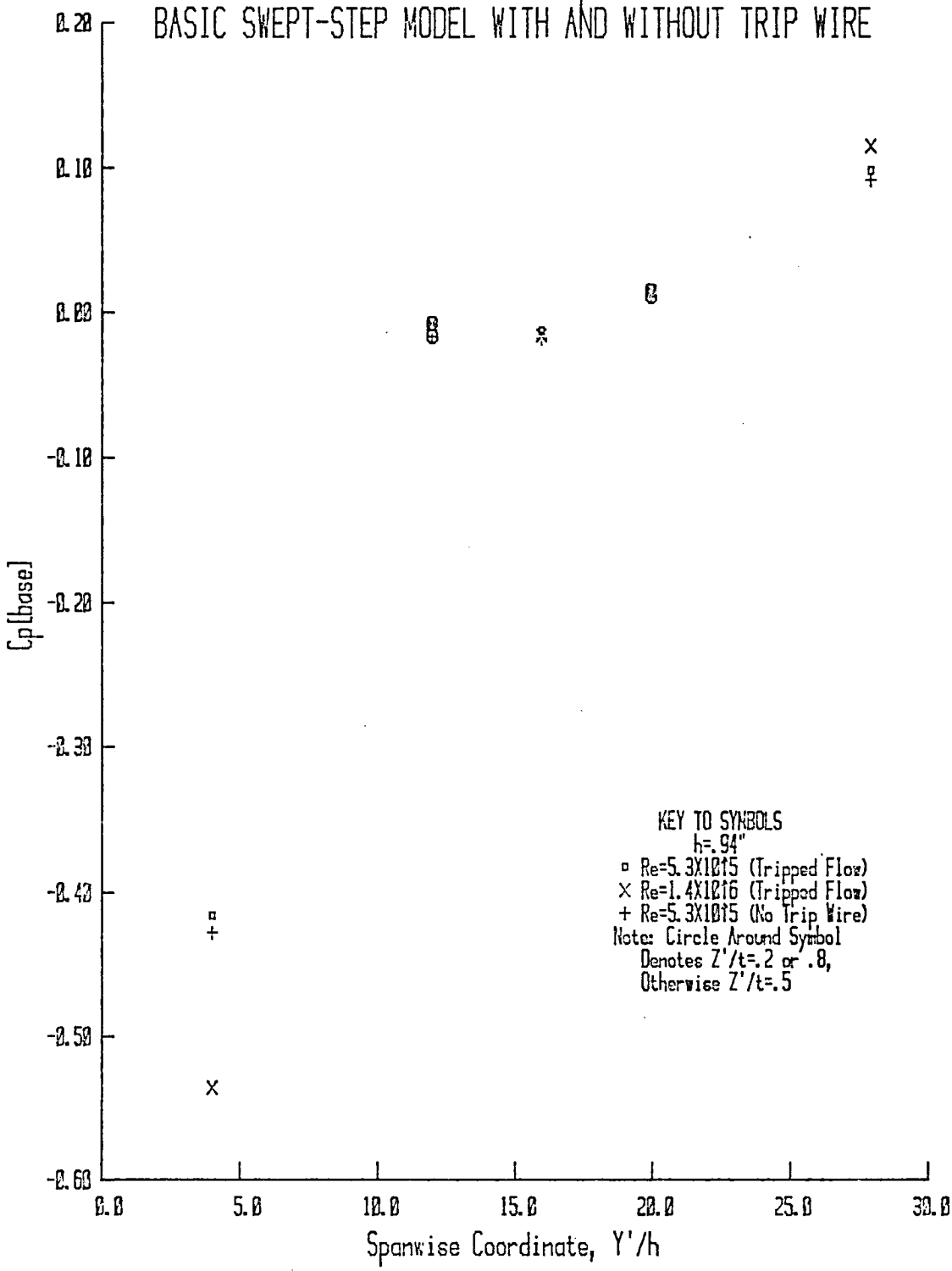

FIGURE 75.

MID-SPAN Cp-Cp[min] FOR 60-DEGREE BASIC SWEPT-STEP MODEL WITH AND WITHOUT TRIP WIRE

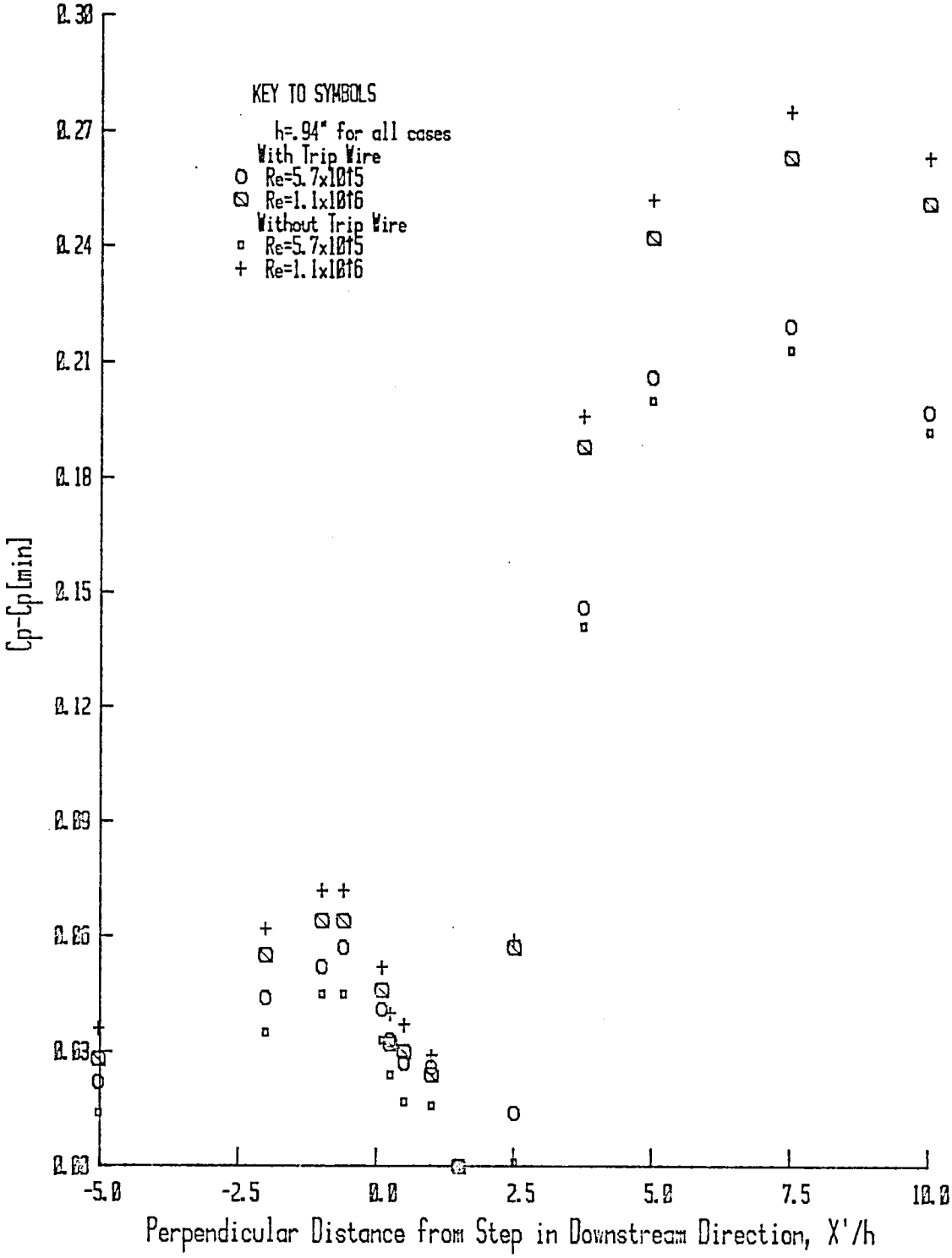

increase in area downstream of the step, the surface pressure does not reach the freestream value far upstream of the step. The resulting change in surface pressure has an appreciable effect on the overall pressure distribution, according to results obtained by Narayanan (1974) for two-dimensional steps, and present results obtained for the 30° swept-step model with h = .94".

In the present research, a compensating 30°, swept step was attached to the test section roof, directly opposite the step in the model. The height of the forward-facing roof step was also .94". A swept ramp immediately upstream of the roof step compensated for the area change due to the presence of the separated-flow region. Surface pressure is shown in Figure 76 for the swept model with roof step. A comparison of the surface pressures with (Figure 76) and without (Figure 56) the roof step indicated a 25% reduction in $\Delta C_p[max]$ at midspan with the roof step present. In addition, the base pressure data presented in Figure 77 indicate a reduced spanwise pressure gradient in the separated-flow region with the roof step attached (≈50% reduction).

This latter observation is an indication of the strong coupling that exists between the model and test section. Using a local one-dimensional analysis, it is shown in Appendix B that the spanwise pressure gradient in the separated-flow region is primarily due to the area expansion at the step. Therefore, theoretical models of the swept-step problem must include the test-section walls as the appropriate boundaries when attempting to match experimental results.

FIGURE 76.
SPANWISE VARIATION IN C_p AT VARIOUS LONGITUDINAL LOCATIONS FOR THE 30-DEGREE BASIC SWEPT-STEP MODEL WITH ROOF STEP AND h=.94"

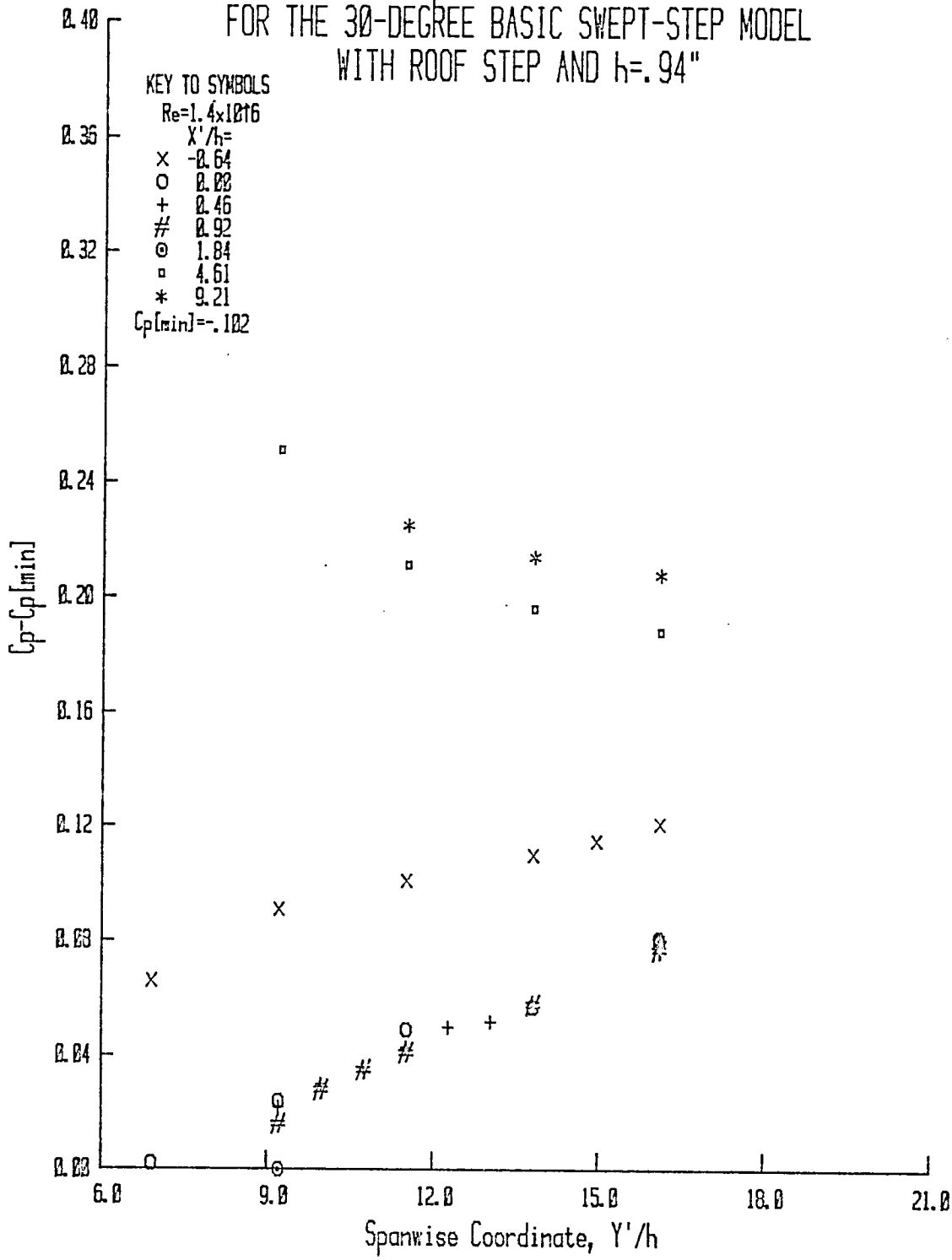

FIGURE 77. SPANWISE VARIATION IN Cp[base] FOR THE 30-DEGREE BASIC SWEPT-STEP MODEL WITH AND WITHOUT ROOF STEP

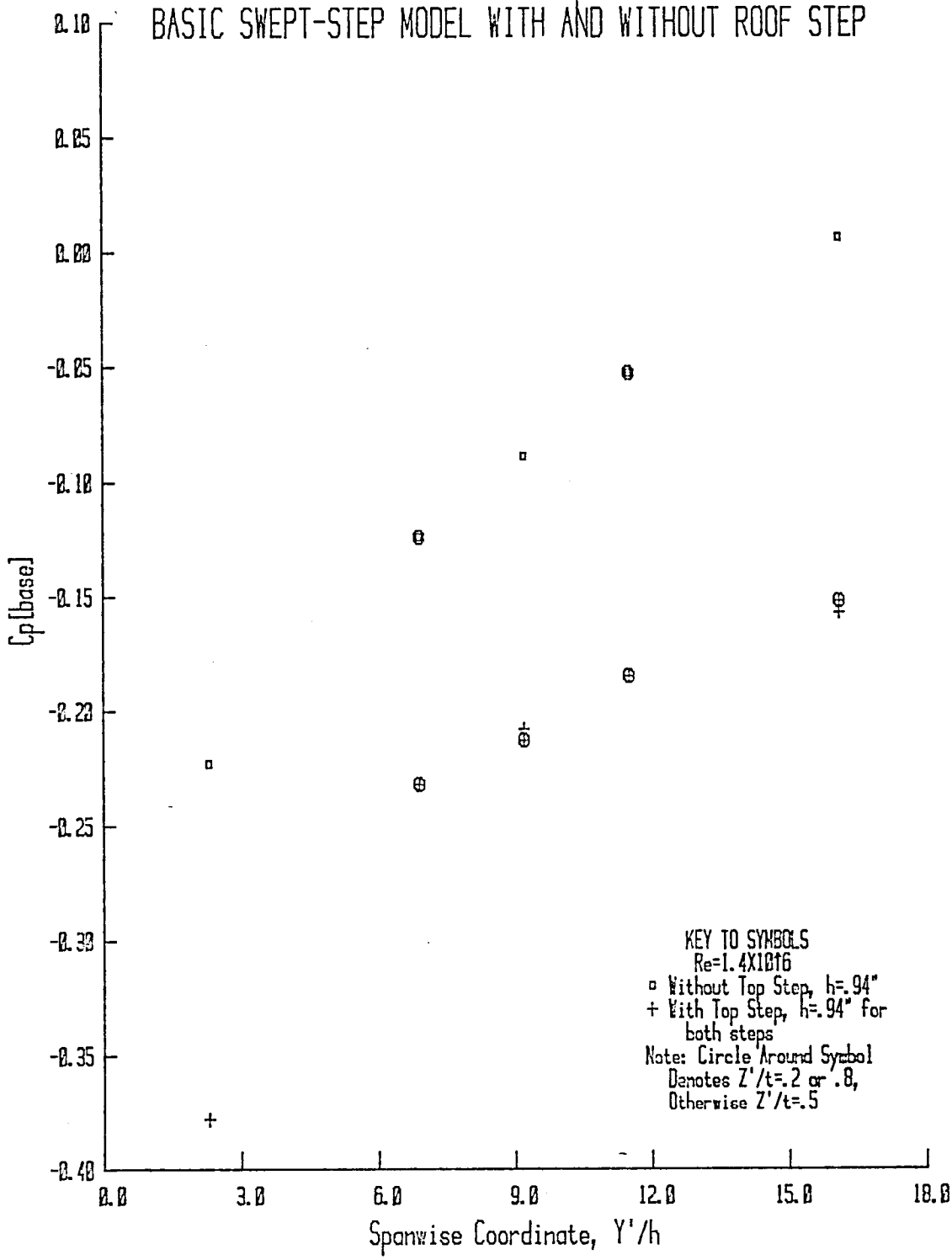

Further evidence of model/test section coupling has been experimentally observed by Armaly and Burst (1980) in laminar incompressible flow over a two-dimensional rearward-facing step. An additional recirculating region was observed at the test section roof downstream of the step. This region was present for Reynolds numbers coresponding to laminar flow but disappeared near the end of the transitional flow regime; therefore, it is not thought to be present in turbulent flows. This recirculating region at the roof is thought to be created by the adverse pressure gradient caused by the sudden area expansion and its existence is believed to depend largely on area ratio. According to Armaly and Burst (1980), studies to confirm these observations are currently underway.

3.5.3. Installation of Flow Restrictor in Relaxation Region

A honeycomb flow restrictor was placed in the relaxation region of the basic 30°, swept-step model (h = .94) 27 step heights downstream of the step face at midspan. This honeycomb section was approximately the same dimensions as the flow cross-section area. The purpose of this modification was to determine the effect of downstream end conditions on the separated-flow region. The pressure coefficient data presented in Figure 78 was collected with the roof step attached with and without the downstream flow disturbance present. The resultant midspan

---

Armaly, B. F. and Durst, F., "Reattachment Length and Circulation Regions Downstream of a Two-Dimensional Single Backward-Facing Step," Momentum and Heat Transfer Processes in Recirculating Flows, ASME Winter Annual Meeting, Chicago, Illinois, 16-21 November, HTD-Vol. 13, 1980.

FIGURE 78. MID-SPAN Cp-Cp[min] FOR THE 30-DEGREE BASIC SWEPT-STEP MODEL WITH AND WITHOUT DOWNSTREAM FLOW DISTURBANCE

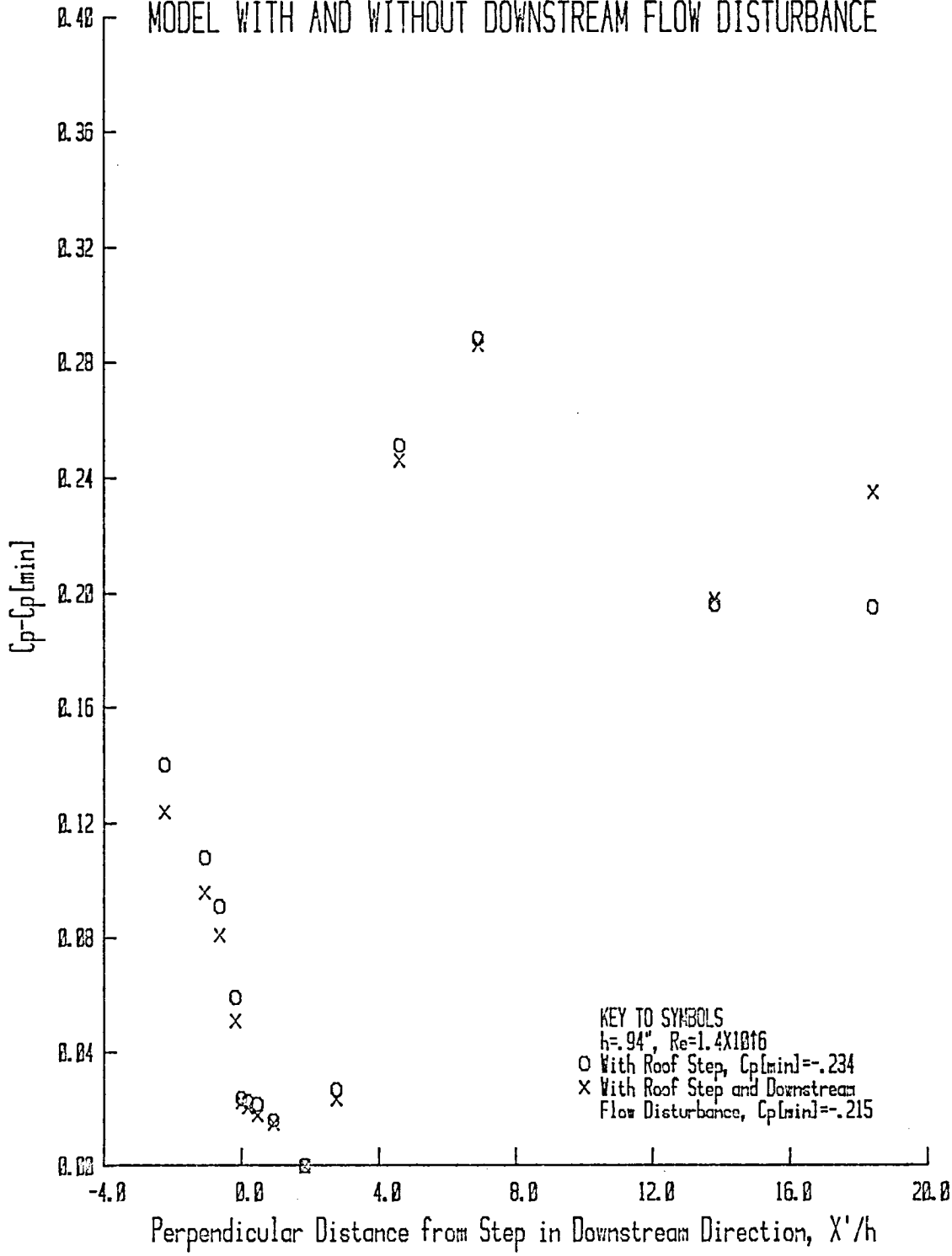

longitudinal pressure distribution (Figure 78) measured in the presence of the flow restrictor shows no change due to this modification except at the orifice nearest the restrictor ($X'/h = 18$). Therefore, it is concluded that physical changes (of the type utilized herein) in the downstream end conditions do not significantly effect the separated flow.

3.5.4. Geometric Modifications at Location of Vortex Formation

The upstream swept step-wall junction angle was varied to determine the effect on flow parameters in the separated-flow region of geometric modifications to initial conditions at the location of vortex genesis. The junction angle at this spanwise end condition (E.C.) was varied as shown in Figure 79. The separated-flow parameters examined were reattachment distance, swirl angle and base C_p. These comparisons are presented in Figures 80 through 82, respectively, for the basic 60° swept step with $h = .50"$. The origin for the pressure measurements is the same for all end conditions—the step-wall junction for the nominal end condition. The origin for the other measurements is at the respective junction.

An examination of Figures 80 and 81 indicates that R'/h and ϕ are independent of the "vortex formation condition." The base pressures as shown in Figure 82 are essentially equal for $Y'/h \leq 30$ (at and beyond midspan).

It can be concluded that the values of these pertinent parameters that characterize the three-dimensional separated flow are

Figure 79a. Imposed Spanwise End Conditions

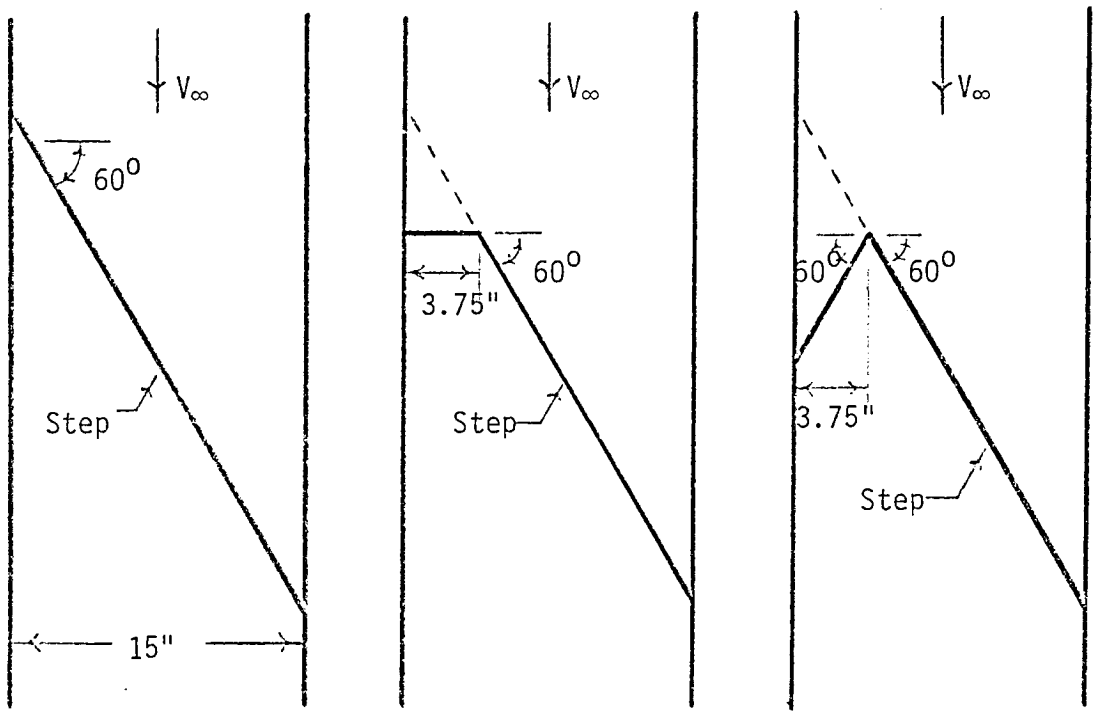

Nominal E.C. 0-Deg. E.C. -60-Deg. E.C.

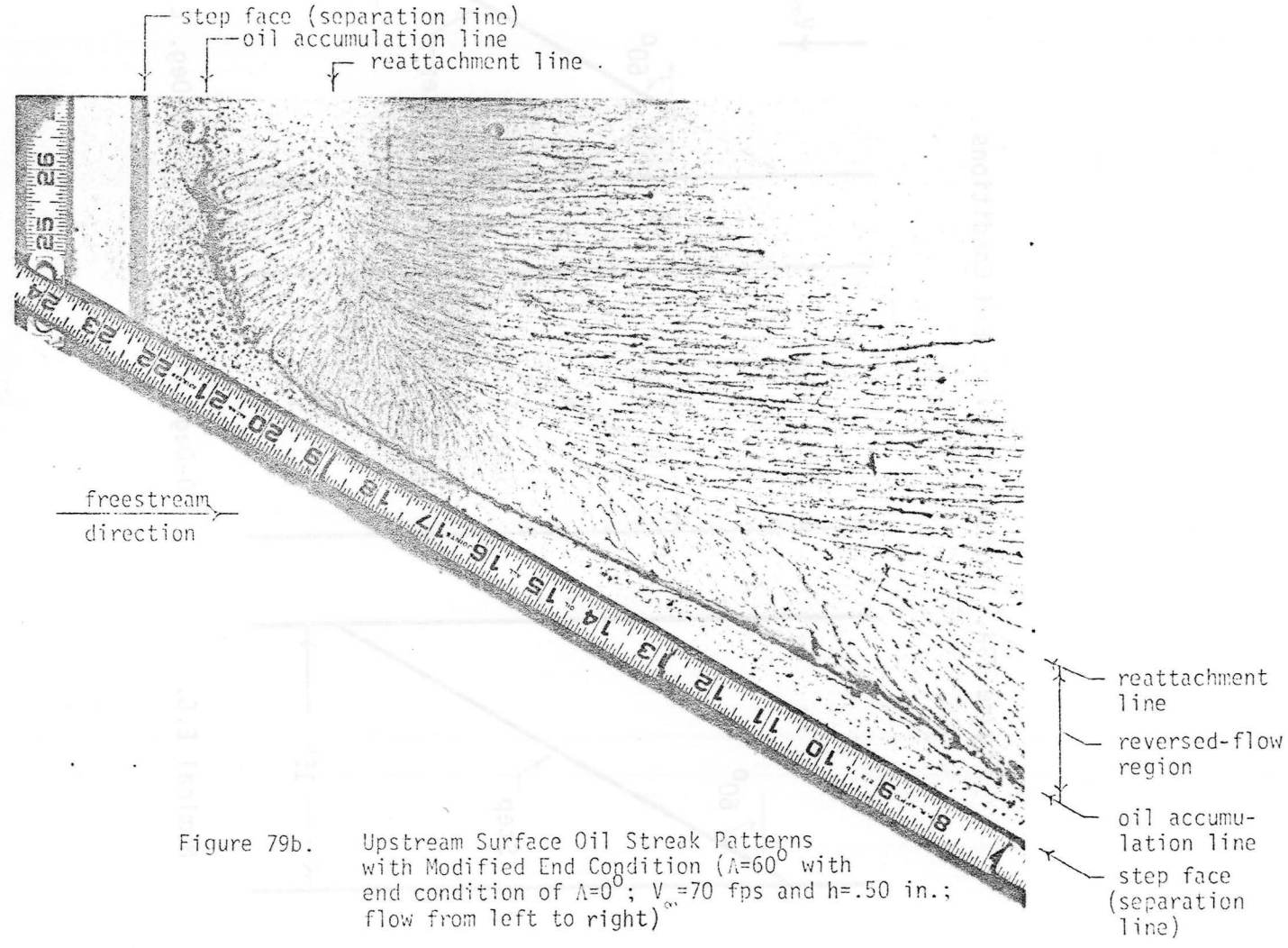

Figure 79b. Upstream Surface Oil Streak Patterns with Modified End Condition ($\Lambda=60^0$ with end condition of $\Lambda=0^0$; V_∞=70 fps and h=.50 in.; flow from left to right)

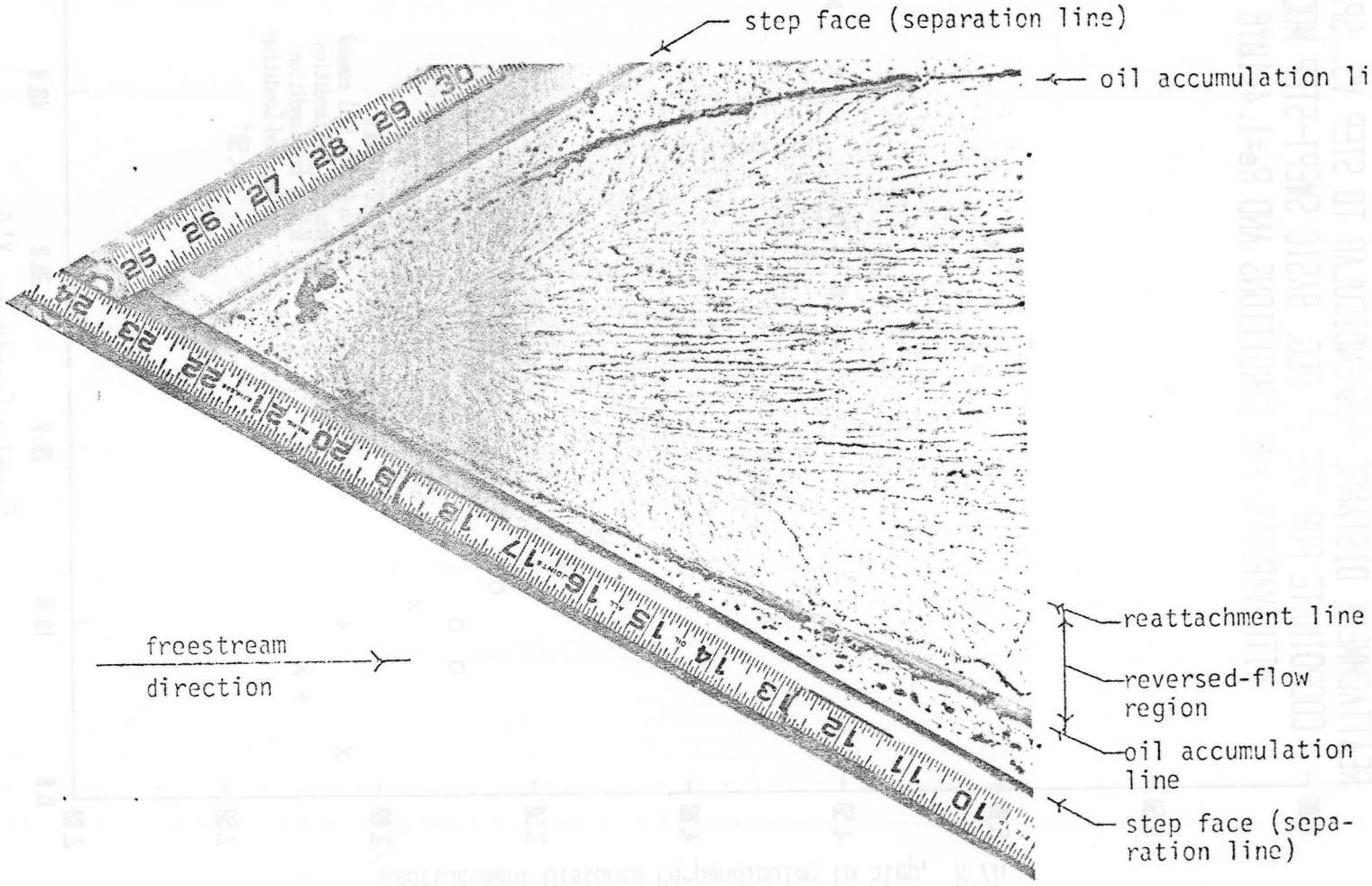

Figure 79c. Upstream Surface Oil Streak Patterns with Modified End Condition ($\Lambda=60^{o}$ with end condition of $\Lambda=-60^{o}$; $V_{\infty}=70$ fps and h=.50 in.; flow from left to right)

FIGURE 80.

REATTACHMENT DISTANCE PERPENDICULAR TO STEP VS. SPANWISE COORDINATE FOR THE 60-DEG. BASIC SWEPT-STEP MODEL WITH VARIOUS END CONDITIONS AND Re=1.4x10↑6

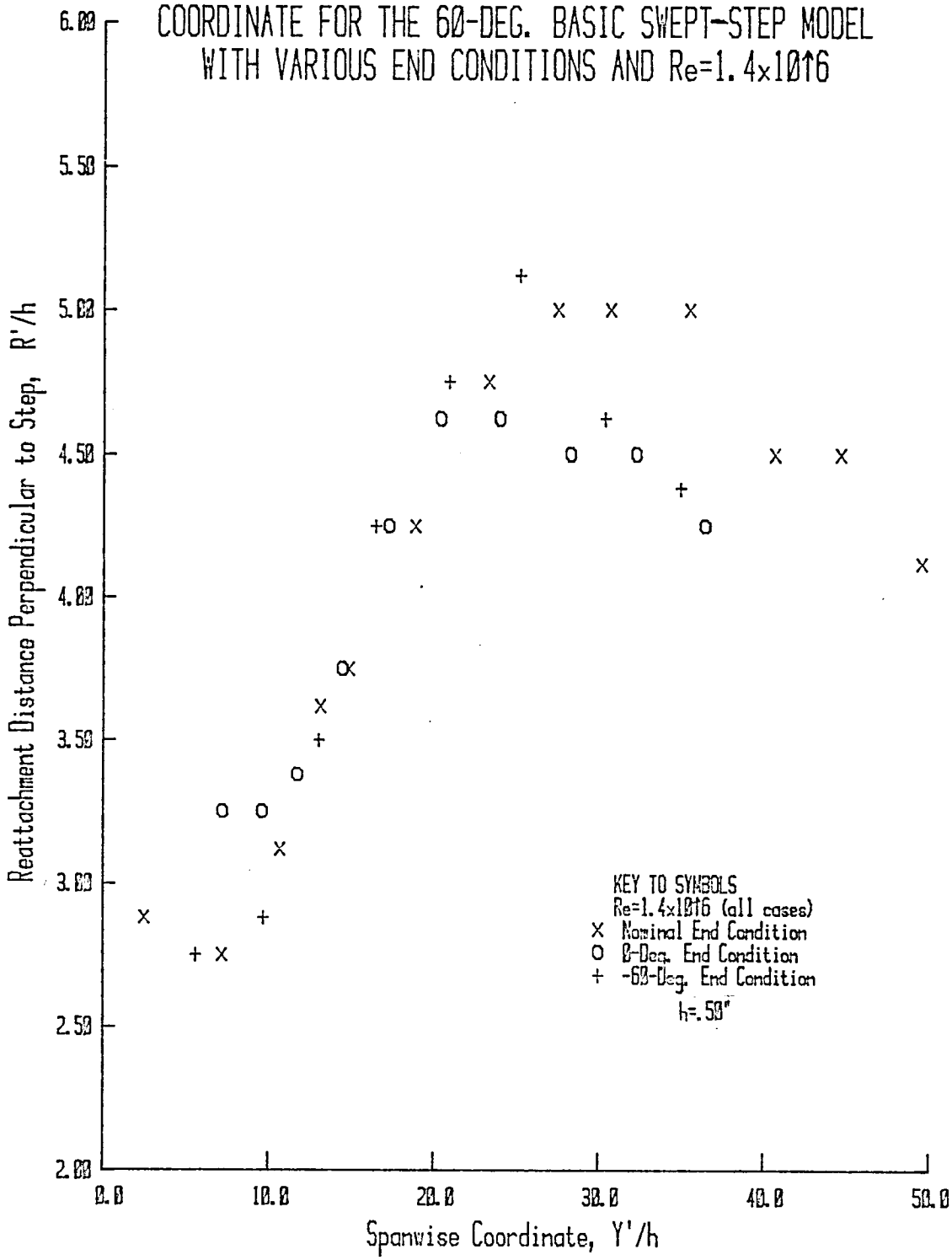

FIGURE 81.
SWIRL ANGLE VS. SPANWISE COORDINATE FOR THE 60-DEGREE BASIC SWEPT-STEP MODEL WITH VARIOUS END CONDITIONS

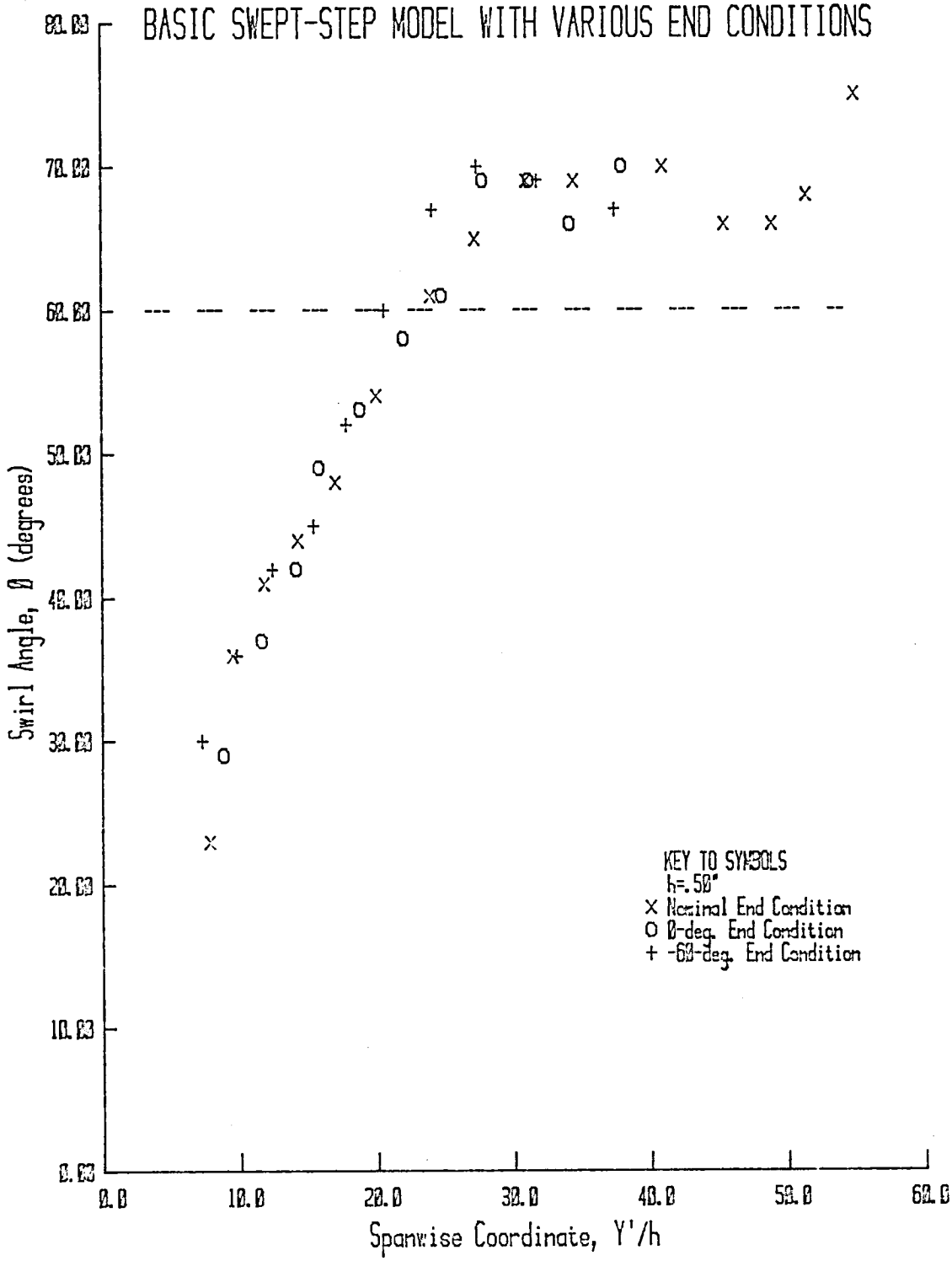

FIGURE 82. SPANWISE VARIATION IN Cp[base] FOR THE 60-DEGREE BASIC SWEPT-STEP MODEL WITH MODIFIED LATERAL END CONDITIONS

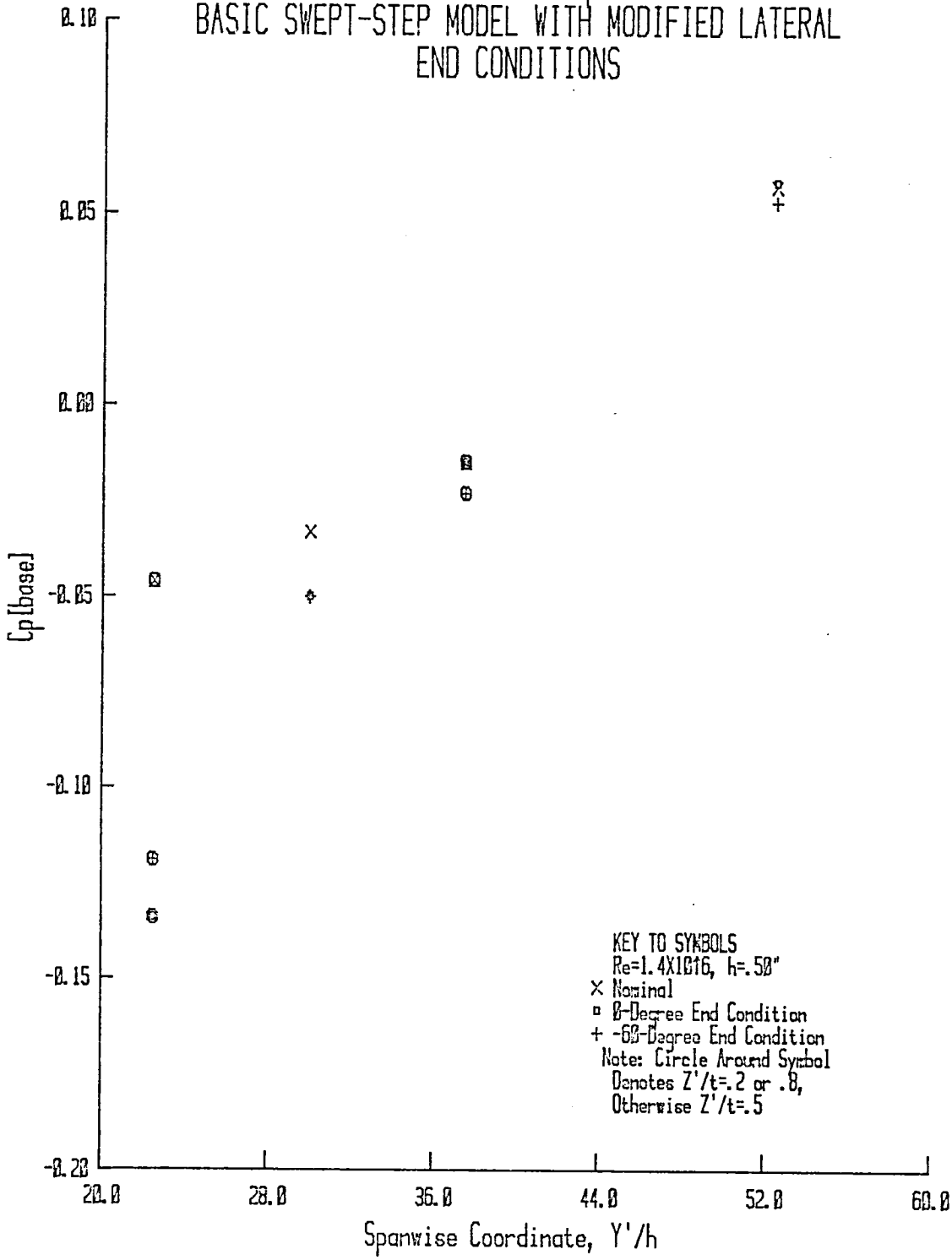

not dependent on the upstream spanwise end condition, but are primarily dependent on other parameters, such as h, Λ and Ar.

3.5.5. Base Geometric Modifications

Based on some of the methods for reducing drag discussed in Section 1.2, models were designed with the base modifications shown in Figure 8(c). The effect of these base modifications on the three-dimensional separated-flow region was determined from an examination of oil flow photographs and reattachment distance, swirl angle and surface pressure measurements. The base configurations examined were RC (rectangular cutout or recess), CC (circular cutout or recess), CL (conical step lip) and VT (vortex troughs on surface upstream of step).

Oil flow photographs for base configurations CC and VT are shown in Figures 83 and 84 for $\Lambda = 30°$. Figure 83 indicates the presence of a pair of secondary separated-flow regions at the base of the swept step with base configuration CC for h = .94". The direction of these secondary vortex flows is opposite that of the primary vortex. The presence of a secondary spanwise vortex flow directed opposite to that of the primary spanwise vortex flow was previously discussed in Section 3.3.3 for base configuration BB30 (30° swept basic base). However, for base configuration CC30, there exists one separated-flow region between the step and the upstream oil accumulation line and a second region between the two oil accumulation lines. The upstream oil accumulation line serves as a separation line

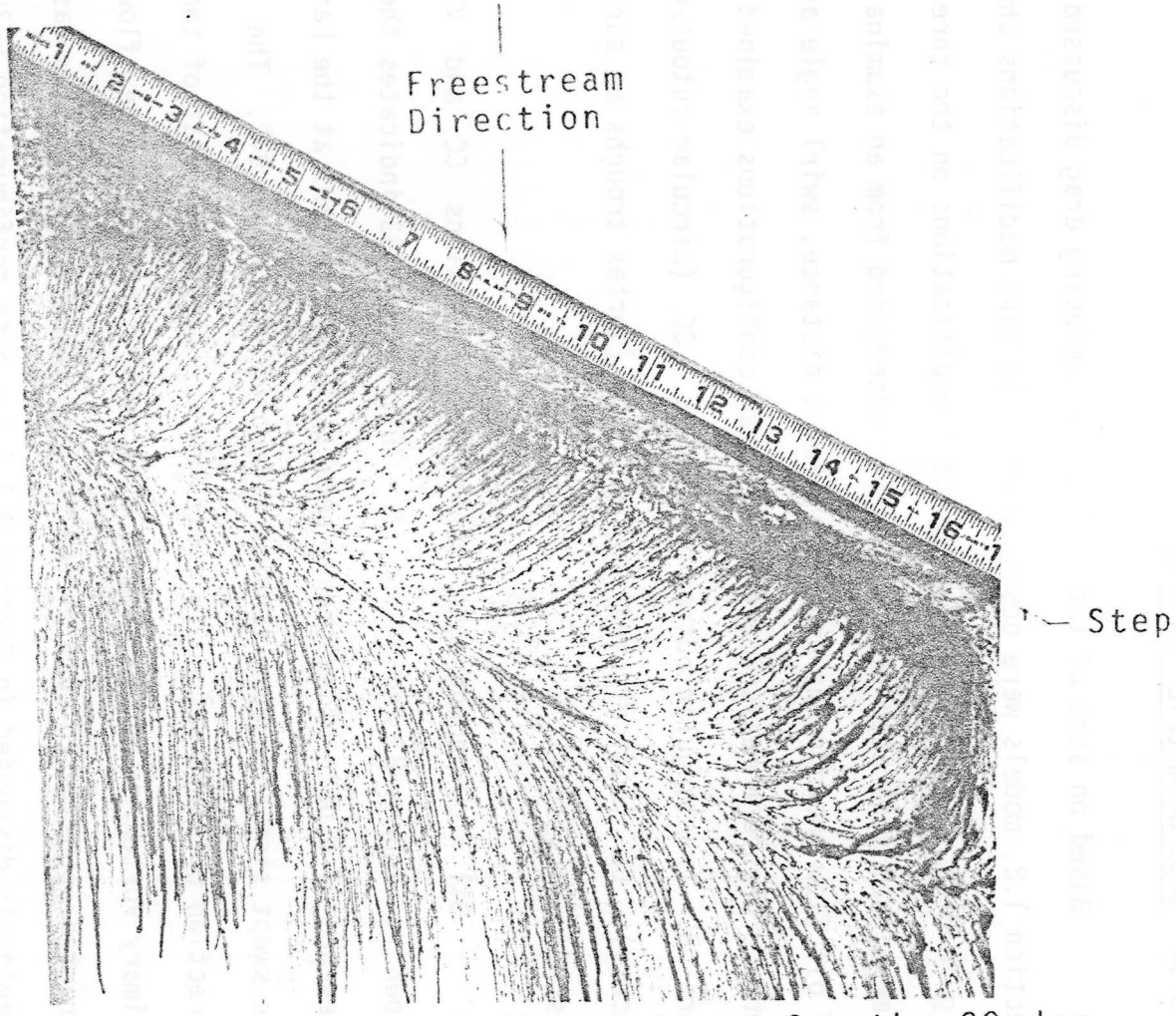

Figure 83. Surface Oil Flow Pattern for the 30-deg. Swept-Step Model with Base Modification CC (h=.94" and V_∞=70 fps)

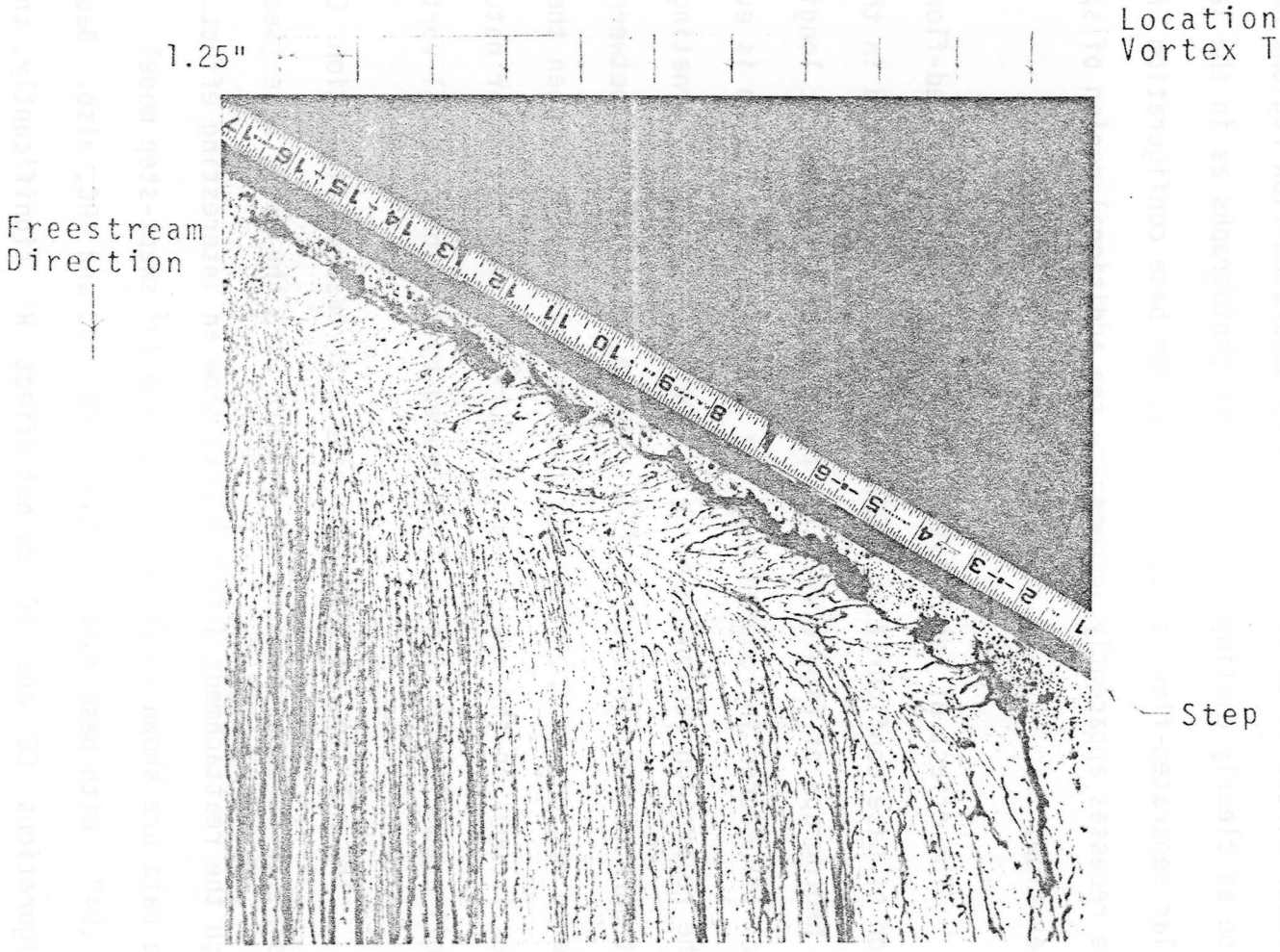

Figure 84. Surface Oil Flow Pattern for the 30-deg. Swept-Step Model with Vortex Troughs (h=.50" and V_∞=70 fps)

for the secondary vortex flows and the downstream oil accumulation line serves as a primary separation line and secondary reattachment line. The shear-stress lines in the secondary separated-flow regions may not be as clearly distinguishable in the photographs as in the laboratory. Similar separated-flow structures exist for base configuration RC30. These recesses apparently accommodate the additional region of spanwise vortex flow.

The effect of longitudinal vortices on the separated-flow region of base configuration VT30 (h = .44") is depicted in the oil flow photograph of Figure 84. The presence of the periodic longitudinal vortex structures introduced into the separated-flow region is evident in the relaxation region also, as determined from the alternating light-dark regions in the oil flow pattern. The distance between the darkened regions is approximately the lateral spacing between the vortex troughs on the upstream model surface. The irregular nature of the oil accumulation line is also caused by the longitudinal vortices.

The oil flow pattern generated with base configuration CL was similar in appearance to the pattern with the basic base (Section 3.3.3) though the reattachment distance data show an interesting effect. These data are shown in Figure 85 for the 30° swept-step model (h = .94") with base configurations BB, CC and RC, also. Base configurations CC and RC do not affect R' significantly, though configuration CL results in at least a 10% reduction. This result is in agreement with the findings of Wilson et al. (1979), who

FIGURE 85.
REATTACHMENT DISTANCE PERPENDICULAR TO STEP VS. SPANWISE COORDINATE FOR CONFIGURATIONS BB, CC, RC, AND CL OF THE 30-DEGREE SWEPT-STEP MODEL

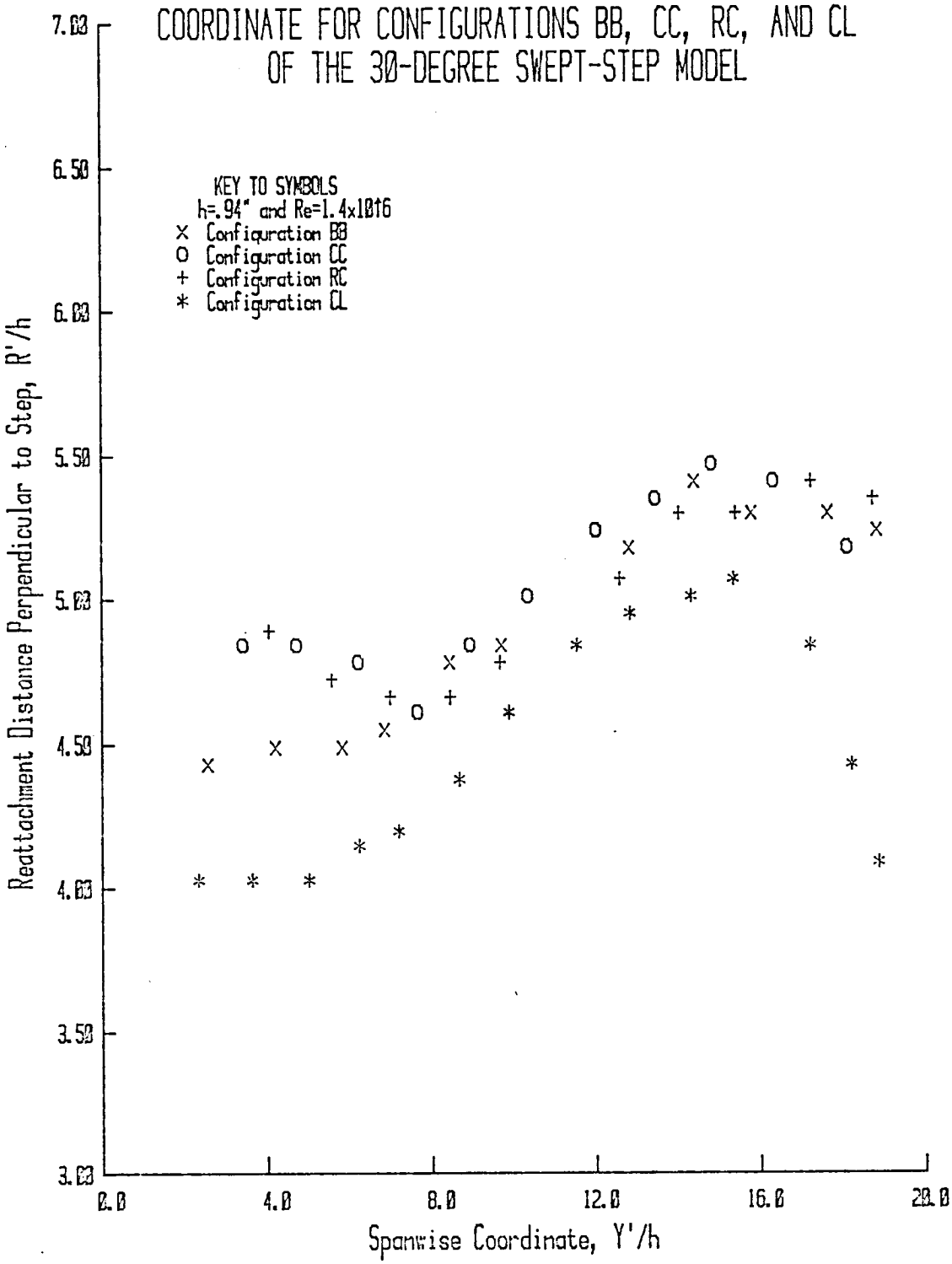

experimentally determined that the reattachment distance behind flat-crested (as opposed to sharp crested) hill models could be effectively reduced to zero as Re approached some "critical" value. The present research indicates that step lip curvature has an effect on flow reattachment distance—reducing it at $Re = 1.4 \times 10^6$ below that of the sharp-lipped model. Reynolds number effects on flow reattachment behind base configuration CL have not been examined, though, in effect, changes in the amount of lip curvature have, since the lip radius is ≈0 at one end and equal to .5" at the other end. The maximum reduction in R' was realized where lip radius was largest (near Y'/h = 18). However, end effects are somehow masked in this reduction.

Reattachment distance as a function of spanwise coordinate is compared in Figure 86 for base configurations BB30 (h = .50"), CL30 (h = .44") and VT30 (h = .44"). The reduction in R' achieved with the VT configuration is greater than that with the CL configuration—R' for configuration CL being approximately 20% less than nominal as compared to 30% less than nominal for configuration VT. The irregular shape of the R'-Y' profile is due to the interaction of the longitudinal vortices with the separated flow. It is this interaction that has resulted in the reduction in R' observed through energization of the separated flow. The effect of trough depth, included angle and spacing on R' has not been studied in the present research effort, but further optimization should be possible.

FIGURE 86.

REATTACHMENT DISTANCE PERPENDICULAR TO STEP VS. SPANWISE COORDINATE FOR CONFIGURATIONS BB, CL AND VT OF THE 30-DEGREE SWEPT-STEP MODEL WITH Re=1.4x10^6

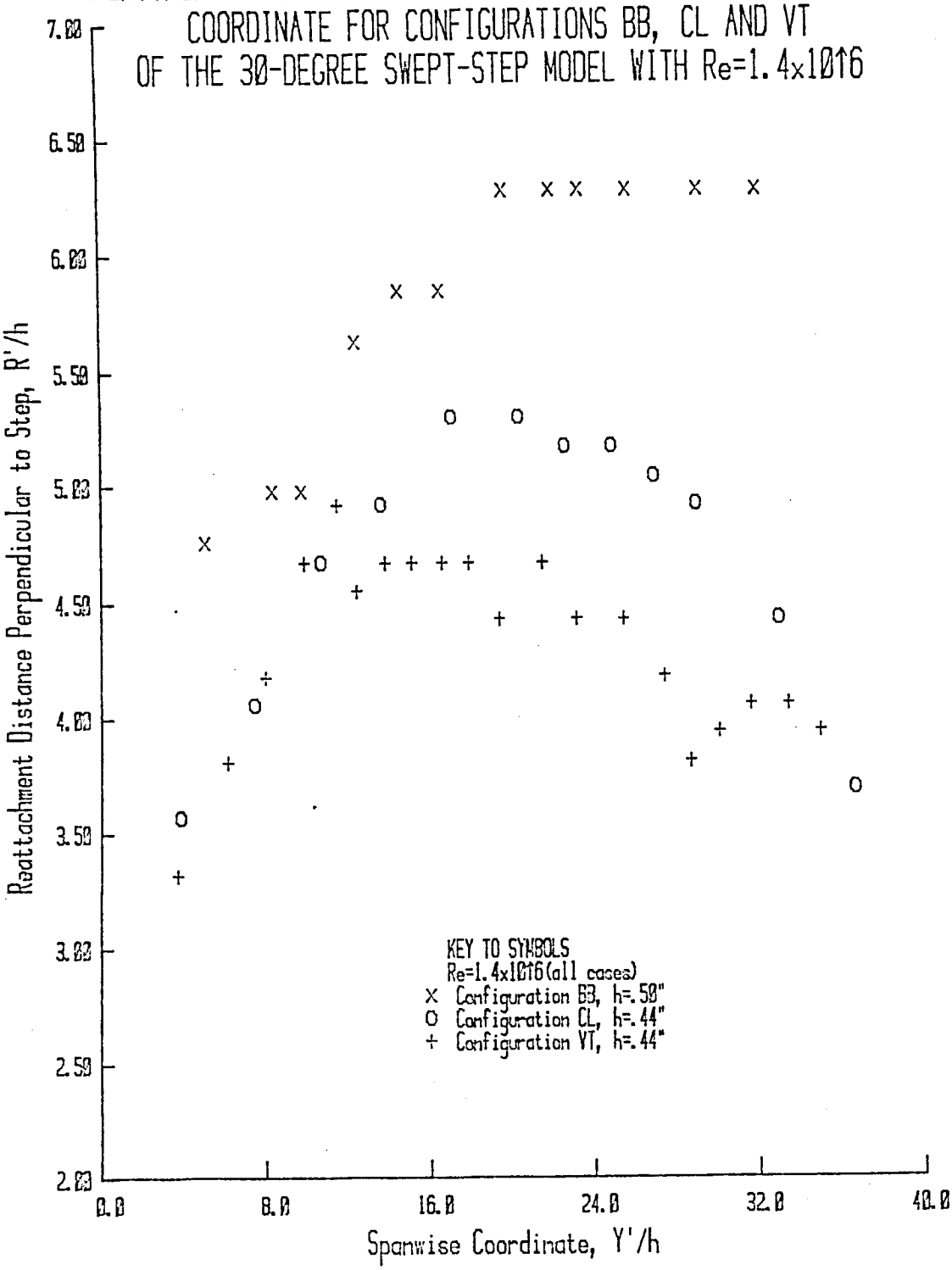

Swirl angle data are presented in Figure 87 for the 30° swept-step model with the base modifications under discussion. Again, as in the cases with the BB configurations, the approximate equality of Λ and ϕ is demonstrated.

The spanwise variation in C_p is presented in Figures 88 through 92 for base configurations RC (h = .94"), CC (h = .94"), CL (h = .50" and .94") and VT (h = .50"), respectively. These data are to be compared to the data of Figures 55 (h = .50") and 56 (h = .94") for the BB configuration. The only significant variation from the nominal data is observed for configurations CL and VT. Figures 90 and 91 indicate that surface pressures at X'/h = -1 for configuration CL are closer to the values in the near separated-flow region than in the nominal (BB) case. For the .94-in. step case of configuration CL, the pressures forward of the step and in the near separated-flow region are equal—as Figure 91 indicates. The finite lip radius effectively causes the separation line and the initial area expansion to be forward of the step face thereby moving the orifices at X'/h = 1 closer to the separated-flow region and its influence.

The significant difference between the ΔC_p data for configuration VT and the nominal case is the decreased value of the adverse pressure gradient at X'/h = 3.5. However, this is consistent with the reduction in R' experienced with this base modification.

FIGURE 87.

SWIRL ANGLE VS. SPANWISE COORDINATE FOR THE 30-DEGREE SWEPT-STEP MODEL WITH VARIOUS BASE MODIFICATIONS

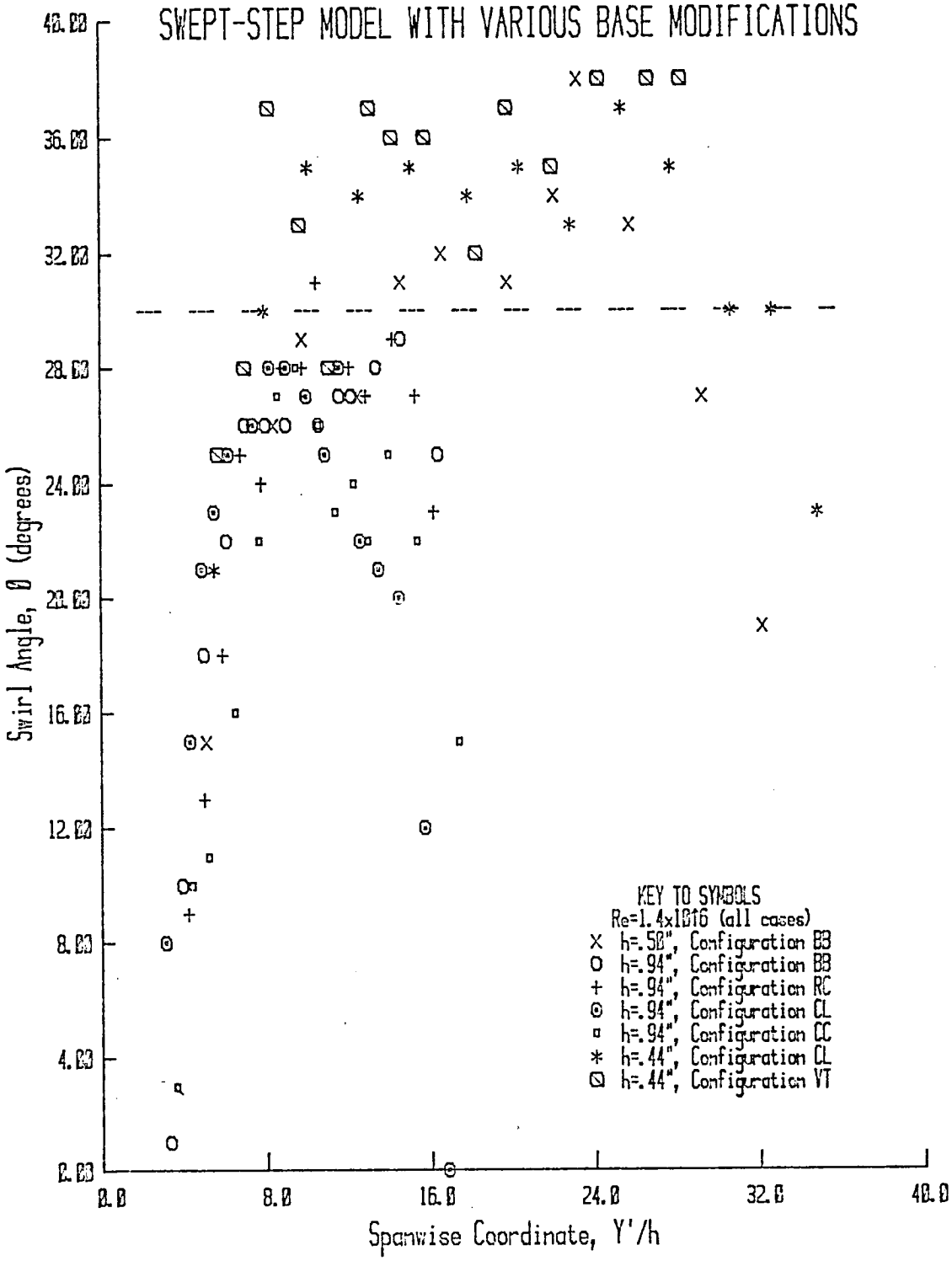

FIGURE 88.
SPANWISE VARIATION IN C_p AT VARIOUS LONGITUDINAL LOCATIONS FOR CONFIGURATION RC OF THE 30-DEG. SWEPT STEP WITH h=.94"

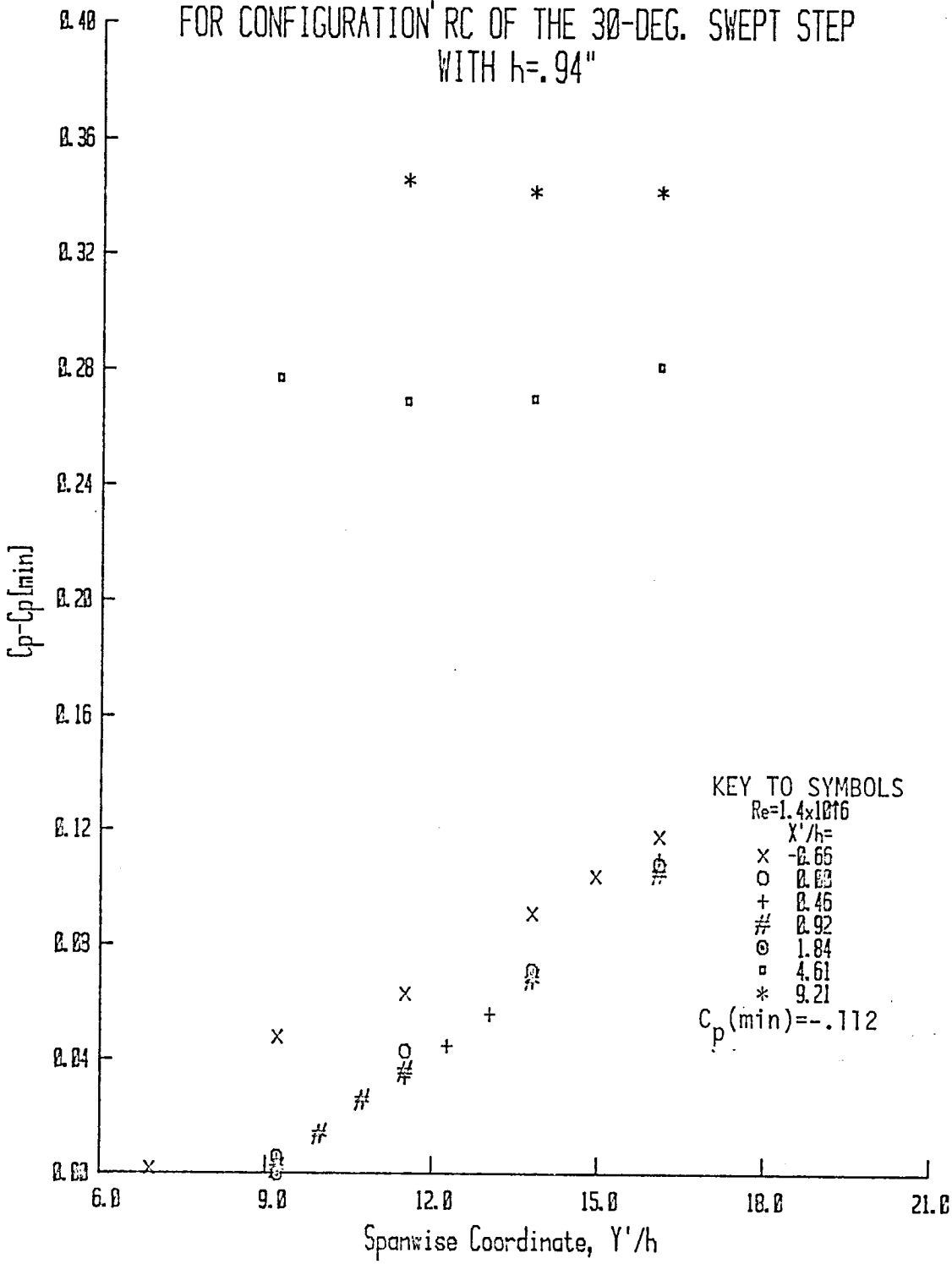

FIGURE 89.
SPANWISE VARIATION IN C_p AT VARIOUS LONGITUDINAL LOCATIONS FOR CONFIGURATION CC OF THE 30-DEG. SWEPT-STEP MODEL WITH h=.94"

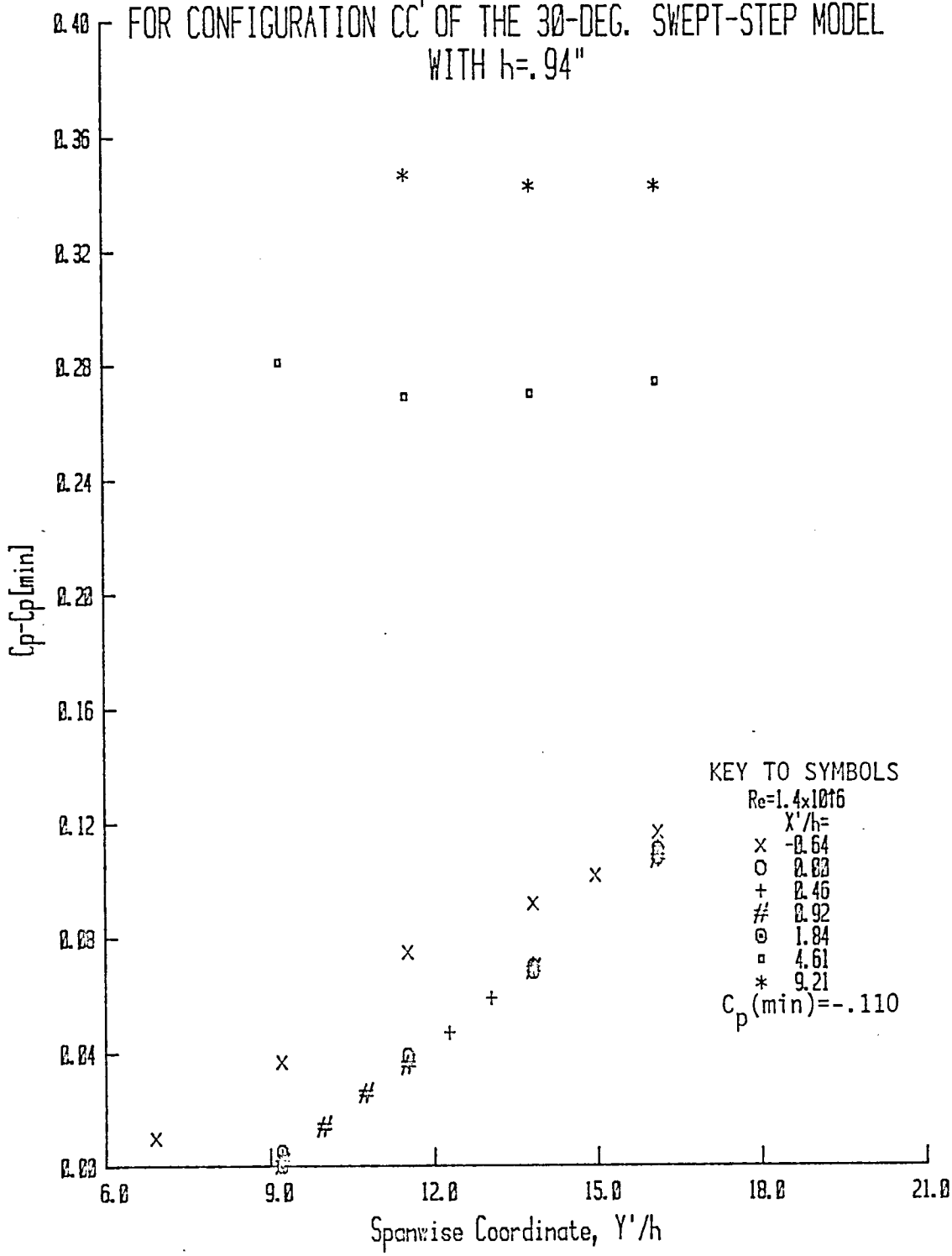

FIGURE 90.
SPANWISE VARIATION IN C_p AT VARIOUS LONGITUDINAL LOCATIONS FOR CONFIGURATION CL OF THE 30-DEG. SWEPT-STEP MODEL WITH h=.50"

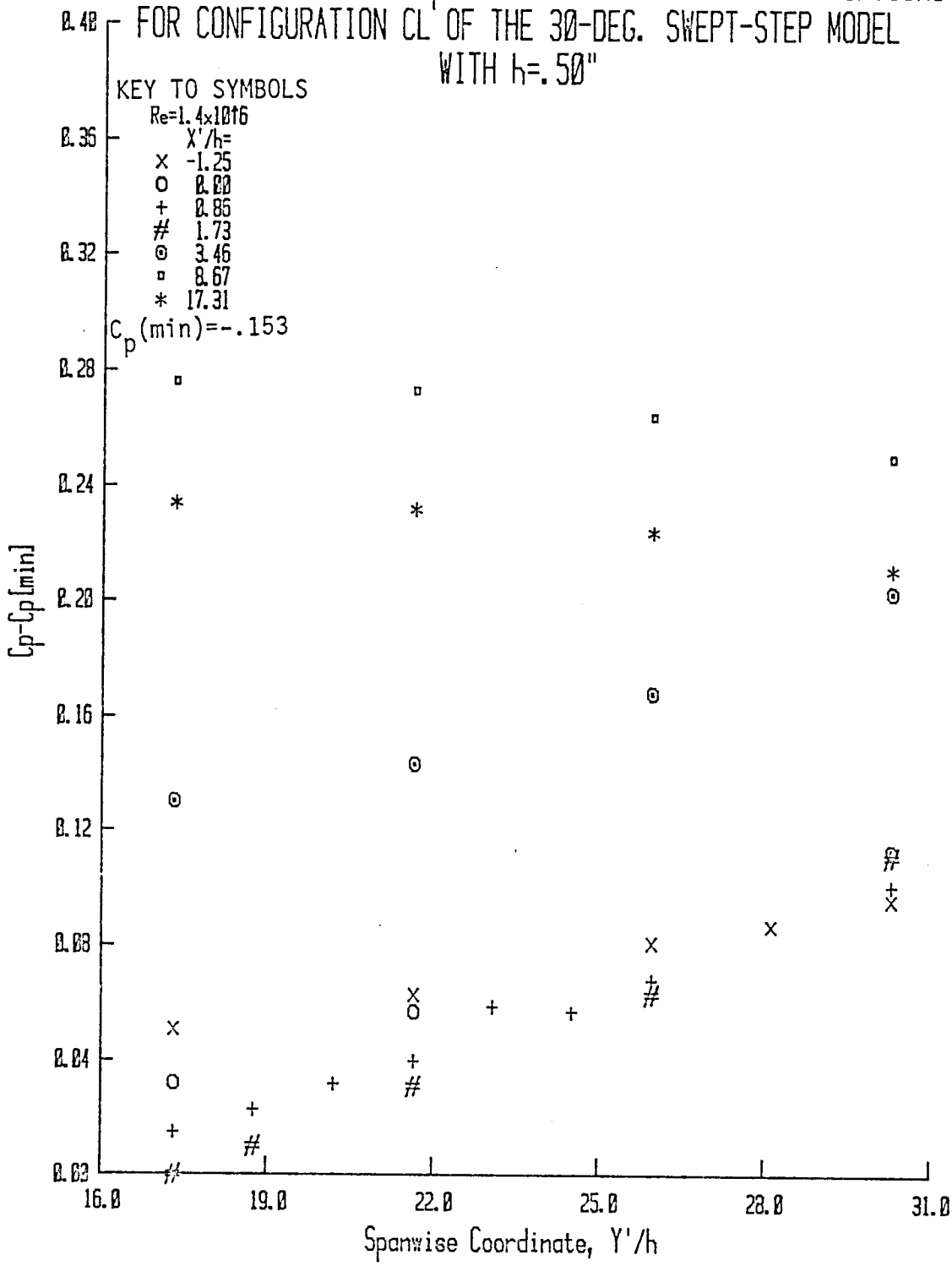

FIGURE 91.
SPANWISE VARIATION IN C_p AT VARIOUS LONGITUDINAL LOCATIONS FOR CONFIGURATION CL OF THE 30-DEG. SWEPT-STEP MODEL WITH h=.94"

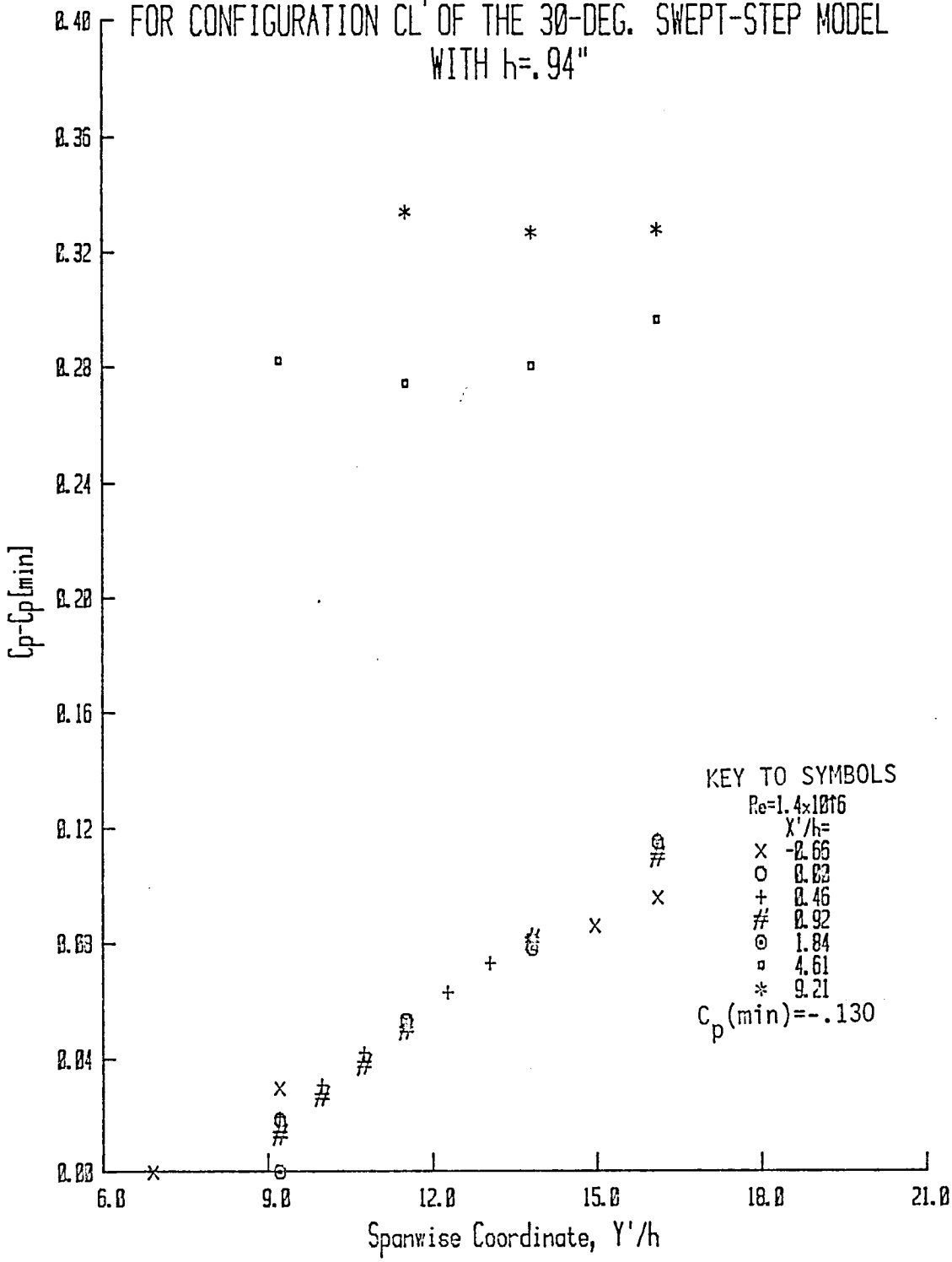

FIGURE 92.
SPANWISE VARIATION IN C_p AT VARIOUS LONGITUDINAL LOCATIONS FOR CONFIGURATION VT OF THE 30-DEG. SWEPT-STEP MODEL WITH h=.50"

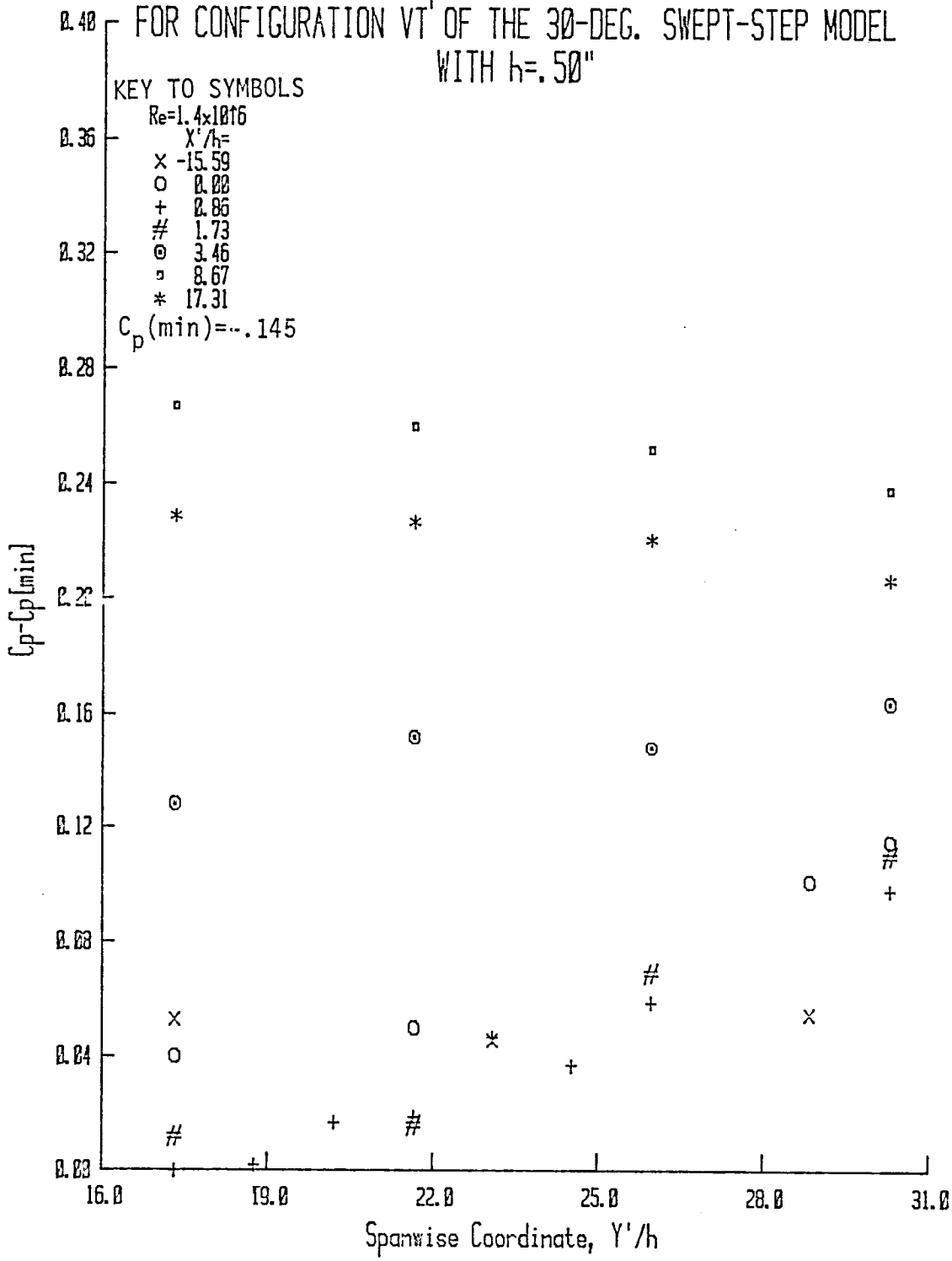

The spanwise variation in C_p[base] is displayed in Figure 93 for the 30° swept step with modified bases for h = .94". These data show no significant effect of base geometry on the base pressure, even for configuration CL with which a significant reduction in R' was achieved. This finding is in agreement with the conclusion stated by Breidenthal (1980) that "the global structure of the shear layer quickly forgets the initial perturbations, while the wake remembers them."

Preliminary base pressure measurements with the splitter plate downstream of the 30°, sept steps removed (swept-wake models) yield the results shown in Figure 94 in regard to base pressure increases over the nominal case (base drag reduction). These tentative results are consistent with the experience of Nash et al. (1963), who achieved a 10% increase in base pressure at M = .2 with a recessed base geometry. Due to the irregular nature of the C_p data for wake configuration VT30, no tentative conclusions could be drawn. This configuration will be instrumented with additional pressure orifices and will be retested along with the other swept-wake configurations, in a continuing study of three-dimensional separated flows and three-dimensional wake modification. The statement and experiences of Breidenthal (1980), who made three-dimensional base modifications to an unswept trailing edge and used a flow visualization method to study the effects, indicate that base geometric modifications can significantly

---

Breidenthal, R., "Response of Plane Shear Layers and Wakes to Strong Three-Dimensional Disturbances," Physics of Fluids, Vol. 23, No. 10, pp. 1929-1934, 1980.

FIGURE 93. SPANWISE VARIATION IN Cp[base] FOR THE 30-DEG. SWEPT-STEP MODELS OF CONFIGURATIONS BB, RC, CC AND CL WITH h=.94"

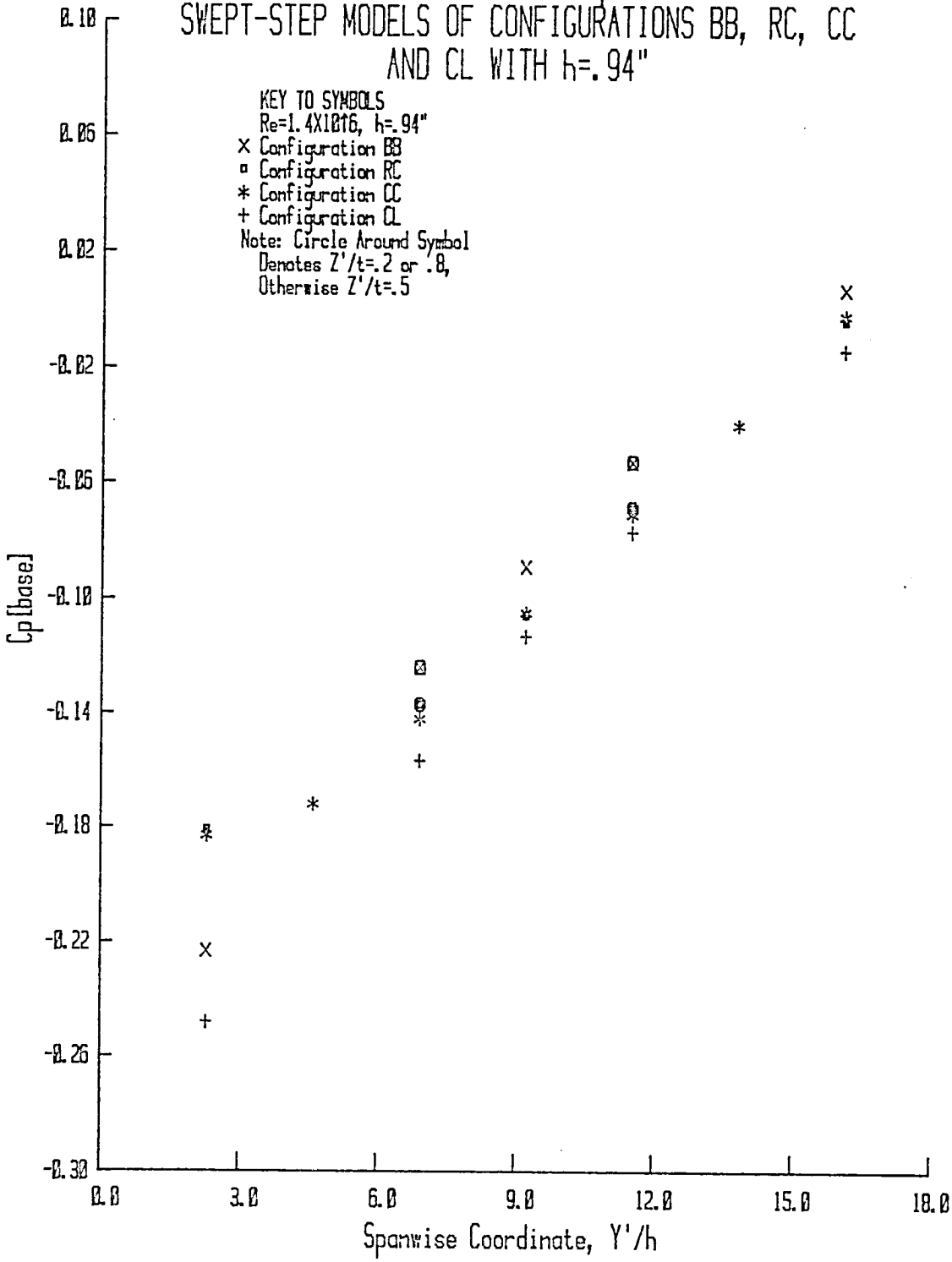

FIGURE 94. SPANWISE VARIATION IN Cp[base] FOR THE 30-DEG. SWEPT-WAKE MODELS OF CONFIGURATIONS BB, RC, AND CC

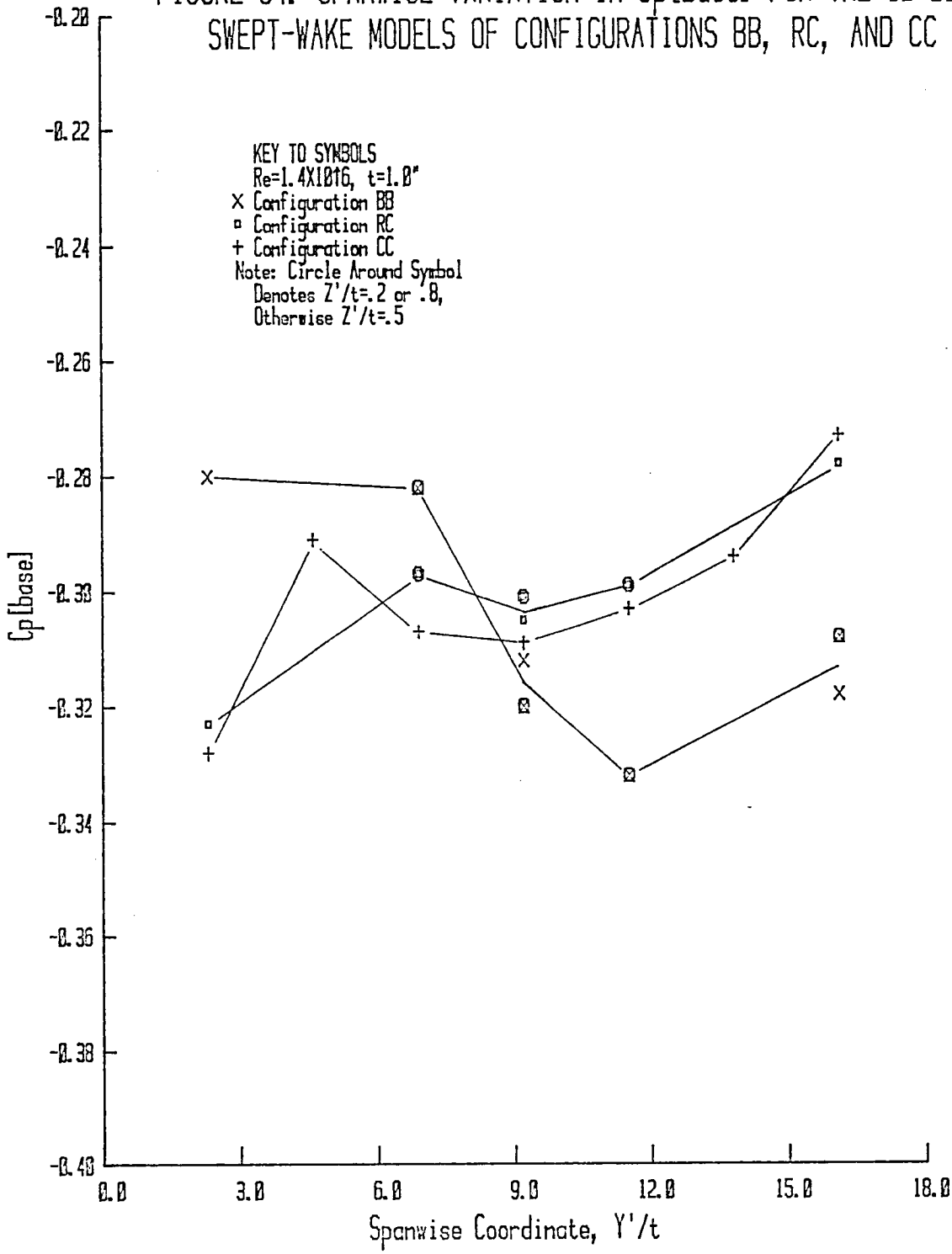

affect the wake. The success achieved by Gai and Sharma (1981) is also encouraging. These researchers obtained a 20 to 60% reduction in base drag by segmenting an unswept trailing edge.

3.5.6. Installation of Boundary-Layer Fences

The early use of part- and full-chord boundary-layer fences on swept airfoils at angle-of-attack [Dickson and Sutton (1955)] demonstrated the significant desirable effect these devices could have on span loading. In other instances, part-chord fences have been placed at the leading edge of swept airfoils to delay separation of the laminar boundary layer. [See Atkins (1961) and Schuringa (1972.] Additional uses of boundary-layer fences include obstruction of the spanwise movement of boundary-layer flow and delay of the development of the main part-span vortex sheet on swept airfoils [Kuchemann (1953)].

Dickson, J. K. and Sutton, F. B., The Effect of Wing Fences on the Longitudinal Characteristics of Mach Numbers up to 0.92 of a Wing-Fuselage-Tail Combination Having a 40° Sweptback Wing with NACA64A Thickness Distribution, NACA RM A55C30a, 1955.

Gai, S. L. and Sharma, S. D., "Experiments on the Reduction of Base Drag of a Blunt Trailing Edge Airfoil in Subsonic Flow," Aeronautical Journal, May, pp. 206-210, 1981.

Atkins, P. B., A Preliminary Wind Tunnel Investigation of the Control of Leading-Edge Separation on the Avro 707A, Australian Defense Scientific Service, Aeronautical Research Laboratories, Flight Technical Memorandum 12, 1961.

Schuringa, T., "Aerodynamics of Wing Stall of the Fokker F28," Proceedings of AGARD Conference No. 102 on Fluid Dynamics of Aircraft Stalling, AGARD-CP-102, 1972.

Kuchemann, D., "Types of Flow on Swept Wings," Journal of the Royal Aeronautical Society, Vol. 57, November, pp. 478-482, 1953.

In the present research, streamwise boundary-layer fences were installed in the separated-flow region of the 60° basic swept-step model (h = .5") to determine the effect on the spanwise vortex flow. The fence goemetries used are depicted in Figure 95. Fences were located at Y' = 5.6, 13.1, 20.6 and 28.1". Oil flow studies were performed and reattachment distance and surface pressure were measured.

The oil flow pattern obtained using fence #2 is shown in Figure 96. A similar pattern resulted from fence #1. The most significant features observed in the oil flow patterns are: (1) each fence-step junction serves as a vortex genesis location; (2) the secondary vortex flow is in the same direction as the primary vortex flow and (3) the fences turn the vortex flows toward the streamwise direction—causing vortex breakdown in the process. Reattachment distance data determined from oil flow patterns are displayed in Figure 97 for both fence geometries. The reattachment distance increases from a minimum value at each fence-step junction to a maximum value at the adjacent fence, where a new vortex originates. Each fence goemetry has essentially the same effect on the separated flow in terms of R'. An overall effect of the fences is to recuce the separated-flow region by over 50% for this particular spacing of fences. Other spacings examined resulted in the same general effect on the three-dimensional separated flow.

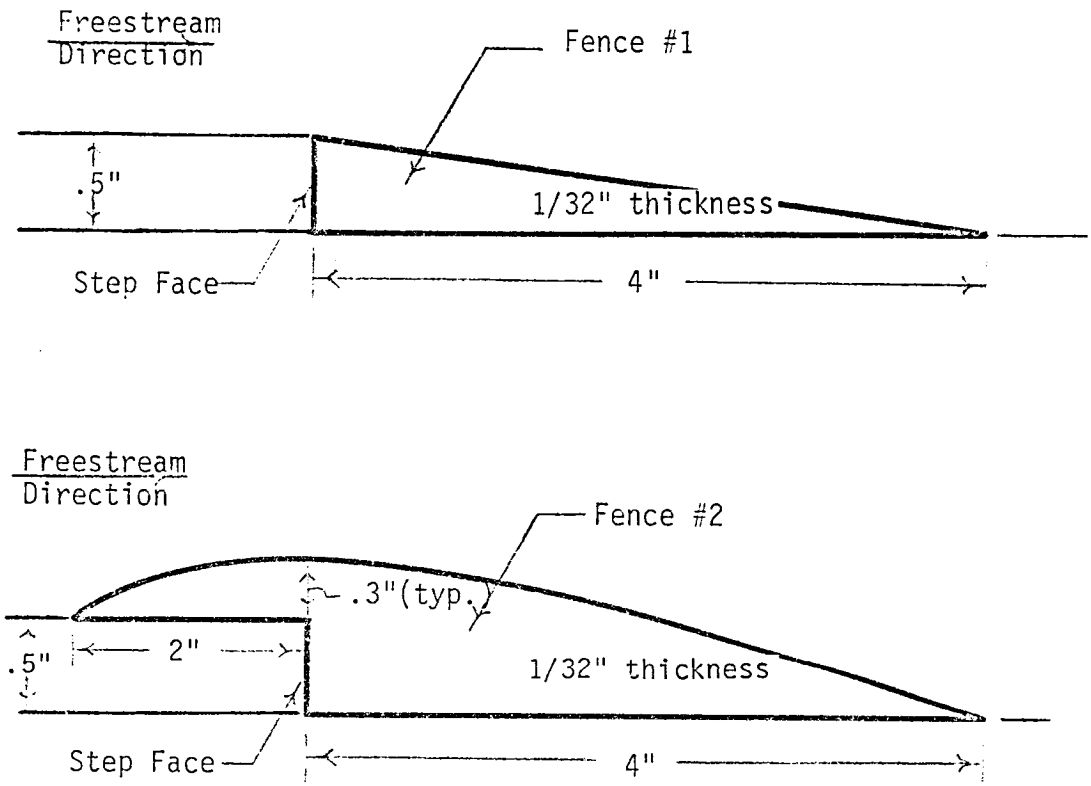

Figure 95. Sketch of Boundary Layer Fences

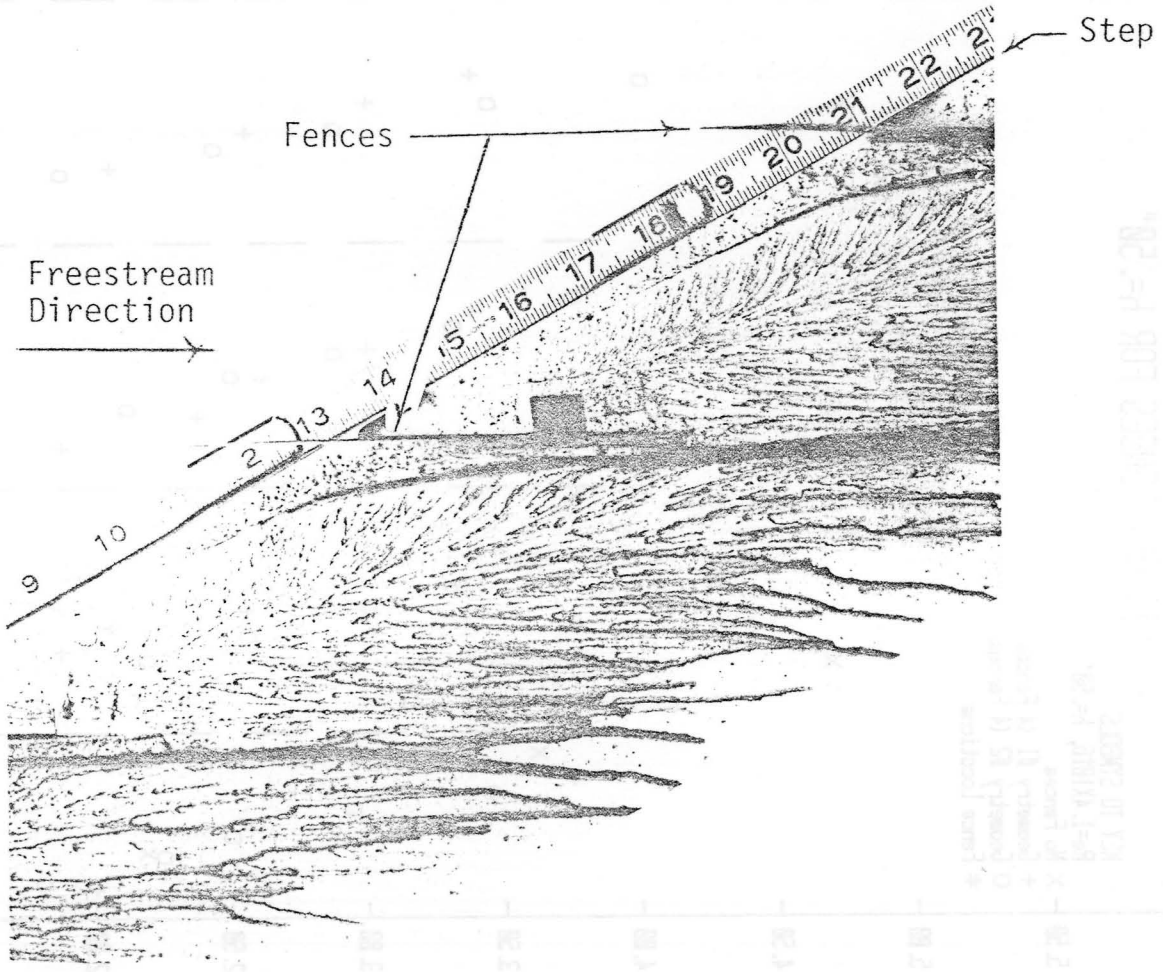

Figure 96. Surface Oil Flow Pattern for the 60-deg. Swept-Step Model with Four Boundary-Layer Fences (Geometry #2) Located at Y'=5.6, 13.1, 20.6 and 28.1 in. (h=.50" and V_∞=70 fps)

FIGURE 97. REATTACHMENT DISTANCE VS. SPANWISE COORDINATE FOR THE 60-DEG. BASIC SWEPT-STEP MODEL WITH AND WITHOUT FENCES FOR h=.50"

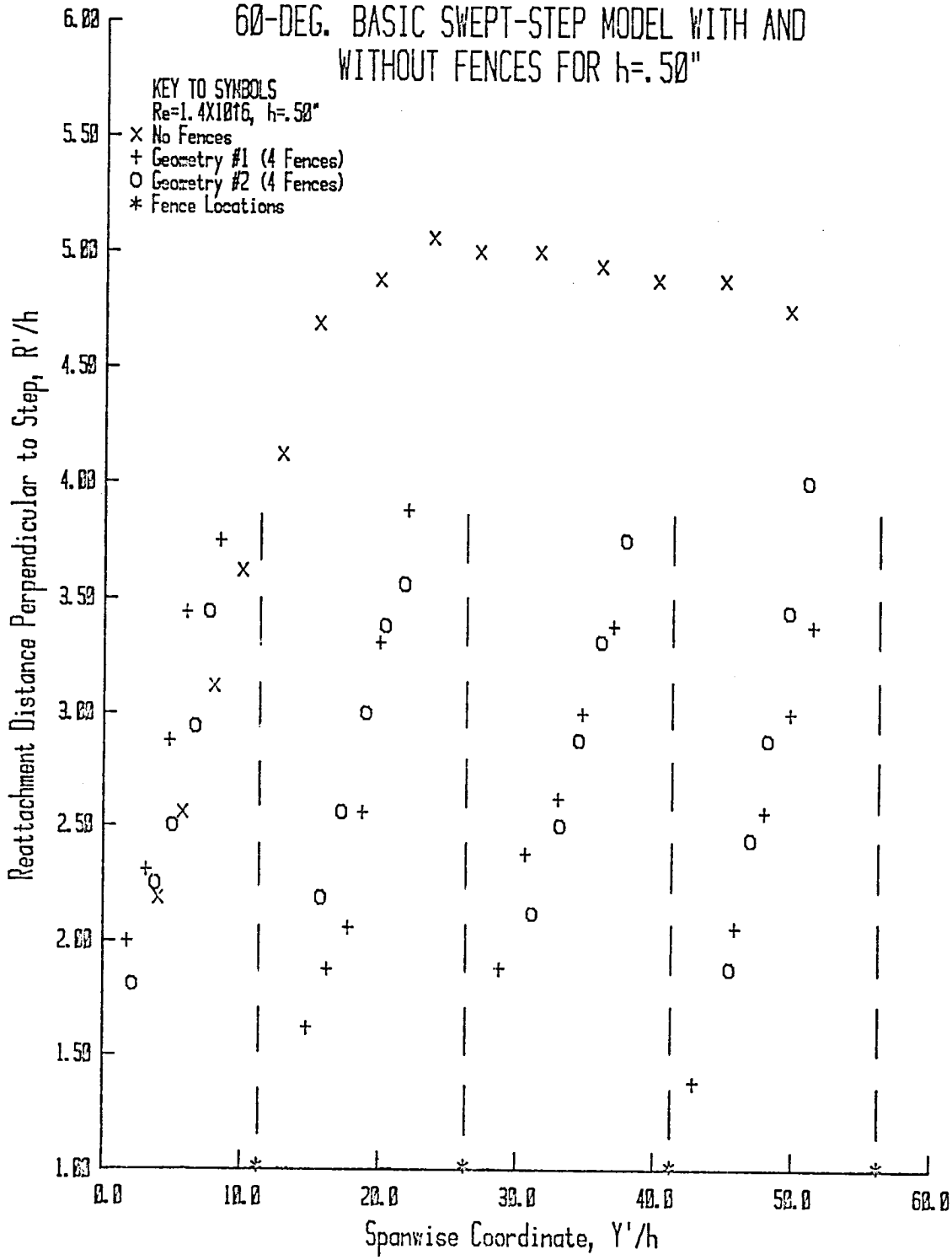

Base pressure coefficient data are compared in Figure 98 for the basic 60° swept-step model with and without fences. Fence locations are as previously stated. Base pressure shows a dependence on the proximity of the measurement location to the fence as is evident at Y'/h = 30. In order to study this dependence further, base pressure measurements were made at Y'/h = 22.5, 30.0, and 37.5 with fences (#1) located at Y'/h = 22.0 and 37.0 for one test then at 23.0 and 38.0 for another. Based on these tests, the following table was constructed to show the dependence of base pressure on spanwise distance from a fence at Y'/h = 22.0 with an adjacent fence at Y'/h = 37.

Table 7

Influence of Fences on Base Pressure

Distance from Fence in +Y' Direction (in.)	C_p[base]
0.50	-.554
3.25	-.111
4.25	-.087
7.00	-.029

The average base pressure over the 7"-span, as calculated from the data of Table 7, is -.156. This is to be compared to a value of -.026 for the model without fences. Then, average base C_p is considerably lower in the presence of fences—though base C_p is higher than nominal just to the left (from downstream viewpoint) of a fence.

Spanwise variation in surface pressure downstream of the step is presented in Figures 99 through 102 for fence geometries #1 and #2

FIGURE 98. BASE C_p VS. SPANWISE COORDINATE FOR THE BASIC 60-DEG. SWEPT-STEP MODEL WITH AND WITHOUT FENCES IN THE SEPARATED-FLOW REGION

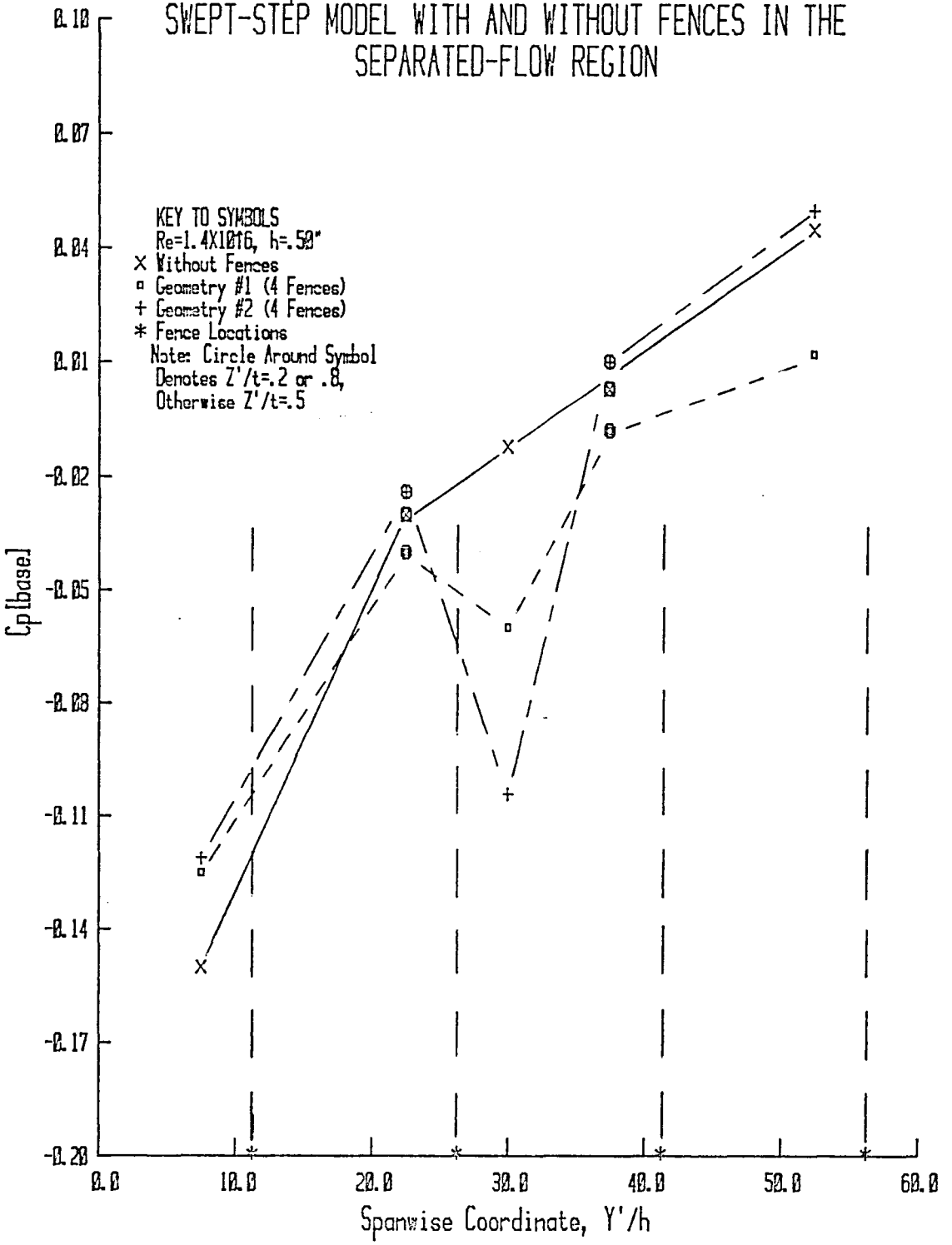

FIGURE 99. SPANWISE VARIATION IN C_p AT X'/h=.5 FOR THE 60-DEG. BASIC SWEPT-STEP MODEL WITH AND WITHOUT FENCES

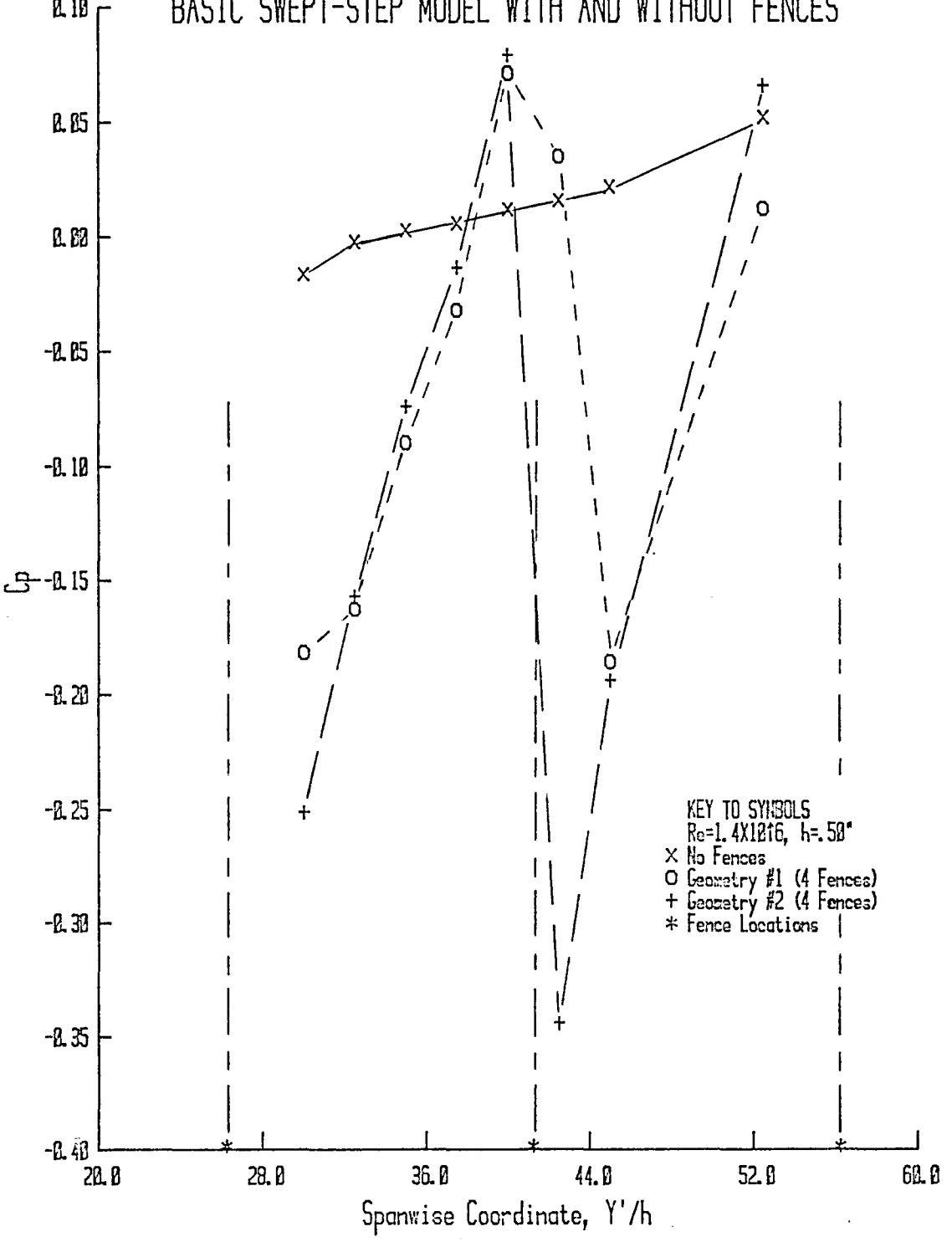

FIGURE 100. SPANWISE VARIATION IN C_p AT X'/h=1.0 FOR THE 60-DEG. BASIC SWEPT-STEP MODEL WITH AND WITHOUT FENCES

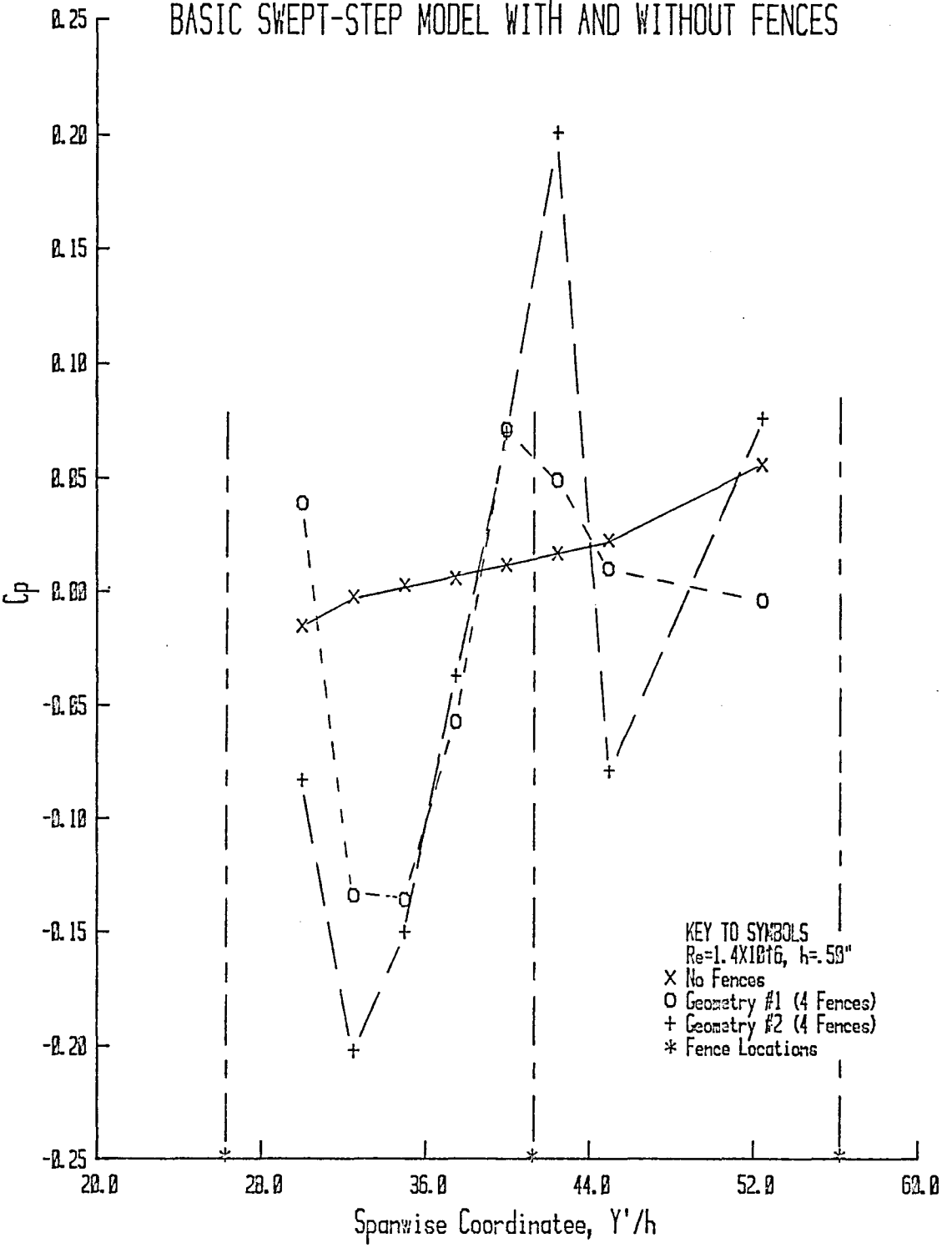

FIGURE 101. SPANWISE VARIATION IN C_p AT X'/h=2.0 FOR THE 60-DEG. BASIC SWEPT-STEP MODEL WITH AND WITHOUT FENCES

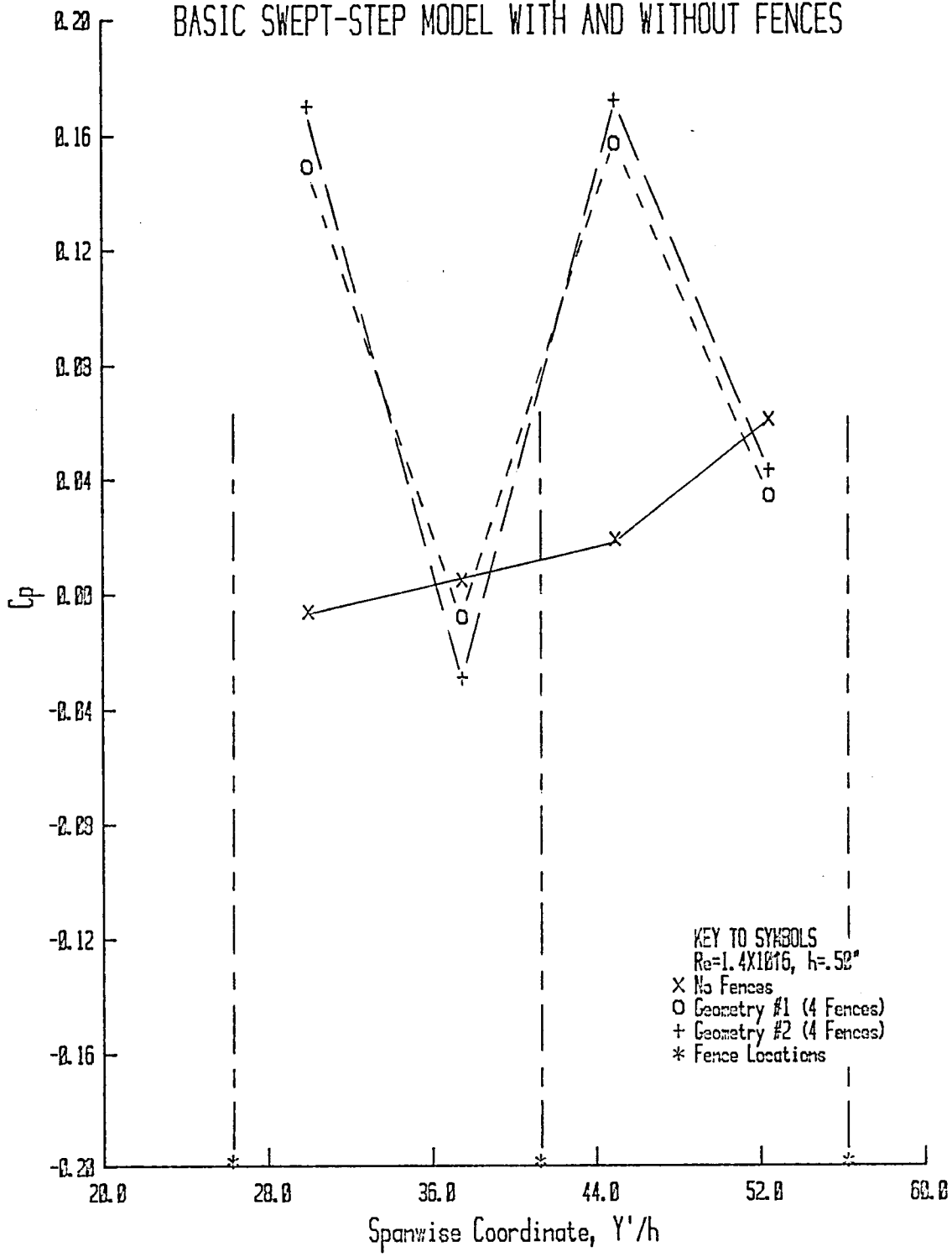

FIGURE 102. SPANWISE VARIATION IN C_p AT X'/h=5.0 FOR THE 60-DEG. BASIC SWEPT-STEP MODEL WITH AND WITHOUT FENCES

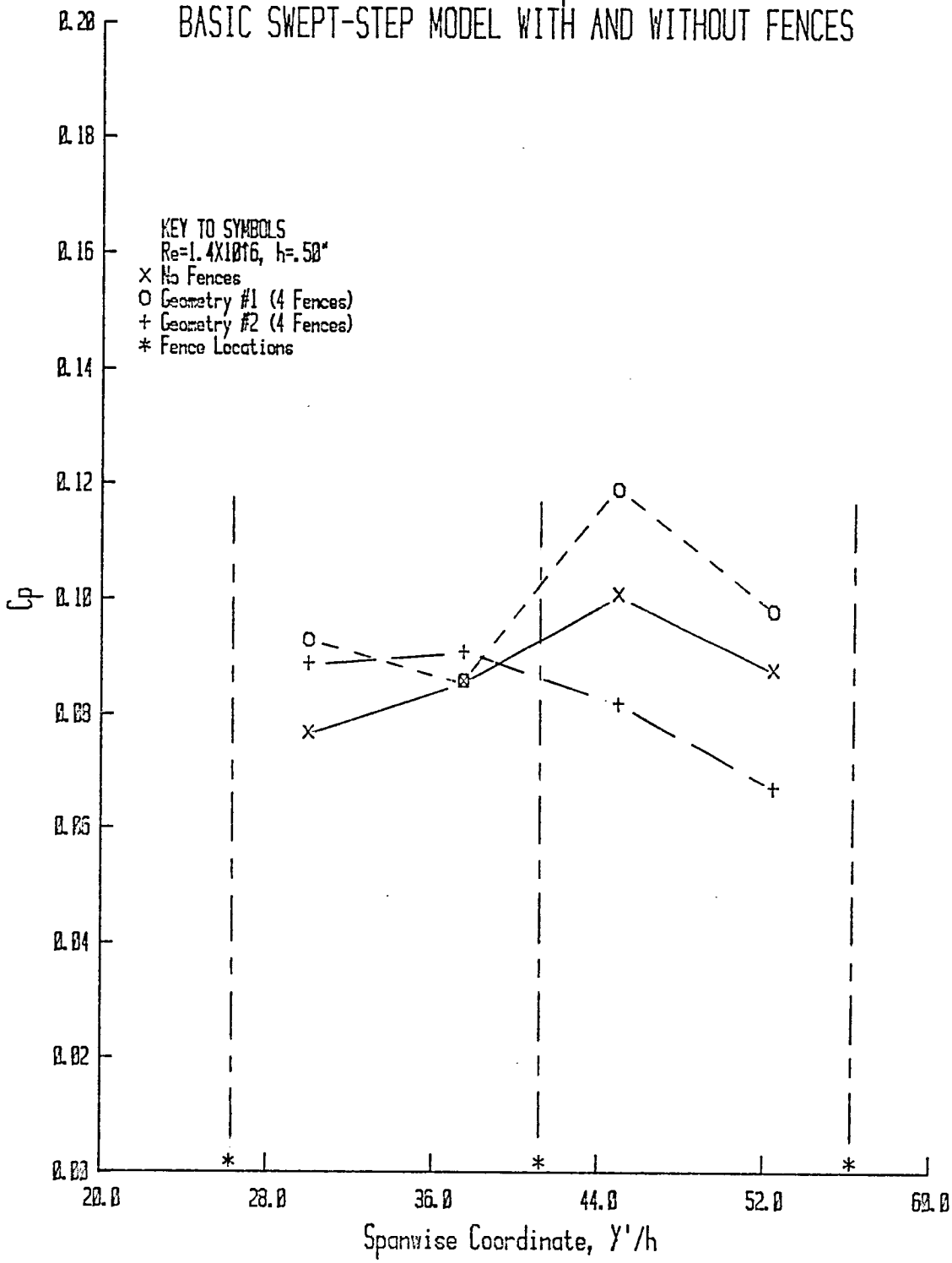

at $X'/h = .5, 1, 2$ and 5. Fence locations are labeled. It appears that average surface C_p near the step is less than nominal with the fences present—whether geometry #1 or #2. If this result was applied to the separated area at the trailing edge of the wings in Figure 1, one would expect higher lift and drag with the flap-track fairings attached, provided the fairings behave as boundary layer fences. The notes in Figure 1 indicate that higher lift was measured in the presence of the fairings. However, drag did not increase, but decreased. This suggests that the flap-track fairings decreased the vorticity shed by the wings at angle-of-attack, thus decreasing the momentum transferred to the wake. The general effect of fences placed in the three-dimensional near separated-flow region $(X'/h < 1)$ was to decrease base and surface pressure coefficient, independent of fence geometry (fence #1 or 2) and spacing. (Models with eight fences and two fences were tested also.) However, upon considering the entire separated-flow region $(0 < X'/h < 5)$, the addition of fences appear to result in an increase in surface pressure. Due to the limited number of orifices in the vicinity of the fences, a more definite conclusion cannot be drawn. Another approach is to mount a swept airfoil on a drag balance and perform tests with and without fences.

3.6. Attempted Measurements

Attempts to measure spanwise diffusion rates in the separated-flow region behind a swept step were not successful. In the first scheme, swept-step models were placed in a free-surface water channel. The

motion of dye released into the separated-flow region was recorded on by a motion-picture camera. However, the dye front dispersed too rapidly to obtain consistent measurements of the time required for it to travel a predetermined distance.

The second series of tests were conducted in the 15" Low Turbulence Wind Tunnel. A constant-temperature pulsed-wire probe with high overheat ratio was mounted near the model surface in the separated-flow region. A second hot-wire probe with low overheat was mounted on a traverse mechanism and served as the detector. However, even for separation distances between source and detector probes of .5 in., the heated fluid could not be detected—probably due to rapid entrainment by the streamwise flow and the highly unsteady nature of the spanwise flow. A similar arrangement used by Westphal et al. (1981) in two-dimensional separated flow is reported to be effective in situations where a substantial vertical velocity component is not present. The separated spanwise vortex flow fails to meet this criterion.

Westphal, R. V., "A New Probe for Measurement of Velocity and Wall Shear Stress in Unsteady, Reversing Flow," Transactions of the ASME, Vol. 103, September, pp. 478-482, 1981.

4.0. SUMMARY, CONCLUSIONS AND RECOMMENDATIONS

4.1. Summary of Research Program

Many of the practical problems related to aircraft design and development, as well as design problems in several other disciplines in engineering, involve flow separation. In addition, most turbulent boundary-layer flows contain three-dimensional effects. Three-dimensional effects in separated flows often result in the creation of a vortex system, such as the spanwise vortex flow of the present study.

The objectives of the present research were as follows:

(1) to conduct a phenomenological study of the effects of sweep on the separated flow downstream of a rearward-facing step—proceeding from the unswept (two-dimensional) case to a highly swept case ($\Lambda = 60°$);

(2) to examine three-dimensional shear-layer reattachment and

(3) to investigate the effect of base geometry on the flow physics in the three-dimensional separated-flow region and on base pressure.

A rearward-facing step geometry was chosen as the research model for the following reasons:

(1) among three-dimensional separated flows, the rearward-facing step is perhaps the simplest reattaching flow;

(2) the separation line is straight and fixed at the edge of the step;

(3) there is only one primary separated-flow region, instead of two, as in the flow over a surface-mounted obstacle and

(4) the streamlines are essentially parallel to the wall at the separation point.

Flow over rearward-facing step geometries is of considerable importance in several branches of engineering, including:

(1) the flow of air over spanwise joints on airfoils;

(2) flow in channels with a sudden enlargement;

(3) wind flow around buildings and

(4) the flow of water over an excrescence on the surface of a submarine.

Though a relatively large body of information exists for unswept rearward-facing steps, the swept-step case (with three-dimensional separated-flow region) has not received significant attention.

The present research on swept, rearward-facing steps was conducted in the NASA Langley Subsonic Low-Turbulence Wind Tunnel. The freestream velocity was varied between 25 and 105 fps. Models included step heights from .12 to 94 in. and sweep angles from 0° to 60°.

In addition to the base geometric modifications, end conditions were modified to determine their effect on the separated flow.

Various flow visualization techniques were utilized to obtain a qualitative understanding of the three-dimensional flow physics. These methods included smoke wire, oil drop and surface tufts. The quantitative data obtained included measurements of surface pressure, flow angularity, reattachment distance and swirl angle.

4.2. Significant Conclusions

Among the significant conclusions resulting from the present research are those discussed below.

4.2.1. Three-Dimensional Effects in the Unswept Case

There are large apparent three-dimensional effects in the unswept cases. Although there was no appreciable spanwise pressure gradient present, the oil flow pattern for $h = .94"$ $(AR = 16)$ indicated that the separated flow was two-dimensional only for a small region near midspan. An unswept model $(h = .5,\ AR = 30)$ produced similar oil flow patterns in the presence and absence of an appreciable spanwise pressure gradient (three-dimensional effects confined to $<8h$ from wall). These findings are inconsistent with the results of de Brederode and Bradshaw (1972) who have indicated that if $AR > 10$, the flow over the unswept step will be two-dimensional. Their conclusions were based primarily on oil flow photographs and "representative" base pressure measurements. It is possible that many

researchers do not check the spanwise uniformity of their flow, but just rely on the "AR > 10" criterion established by de Brederode and Bradshaw. At the very least, studies of flow over unswept steps should include an independent check of the two-dimensionality of the flow.

4.2.2. Model-Test Section Coupling

There is a coupling between the model and the test section which affected the flow structure in the secondary separated-flow region and values of pertinent parameters such as the spanwise pressure gradient. The direction of the secondary vortex flow was opposite that of the primary vortex flow for $\Lambda < 45°$ and in the same direction for $\Lambda = 45°$ and 60°. It was found that the level of the spanwise pressure gradient can be approximated using the assumptions and methods discussed in Appendix B. Related to this coupling is the experimental result that there is a definite (uncorrelated) dependence of $\Delta C_p[\max]$ on Ar, which further shows the need of including the proper test section geometry in any attempt to numerically compute flows over steps for comparison with experimental results.

4.2.3. Effects of Varying Spanwise End Conditions

Spanwise end conditions do not have a significant effect on the separated flow. An examination of base C_p, R' and ϕ with nominal, 0° and -60° end conditions led to these conclusions.

4.2.4. Applicability of the Independence Principle

The Independence Principle is valid up to $\Lambda \approx 38°$ for $h < .50"$. The reattachment distance data for $h < .50"$ supports the tentative conclusion that this principle may be valid for $\Lambda > 38°$ for $h/\delta << 1$. At the value of Λ where the Independence Principle becomes invalid, the cross- and axial-flow components of the freestream velocity can no longer be considered independently. The validity of this principle allows the application of two-dimensional analyses (in the proper coordinate system) of the separated flow associated with swept steps for $\Lambda << 38°$ and $h/\delta < 1$.

4.2.5. Sweep Angle-Swirl Angle Correlation

A correlation was found between the sweep angle and the swirl angle which can be explained using a "Vortex Spring Model" of the three-dimensional separated flow. This correlation has been developed in Appendix C with the result that $\phi \approx \Lambda$.

4.2.6. Effects of Base Modifications

Models with base configurations CL (conical lip) and VT (vortex troughs on surface upstream of step) displayed a significant effect on reattachment distance—a 20 to 30% reduction. However, no significant effect on base pressure was observed for any of the models with base modifications.

4.2.7. Effects of Boundary-Layer Fences

The effect of installing fences in the separated-flow region of the 60° swept step was to segment the region, resulting in the spanwise vortex flow being created and subsequently turned streamwise and attenuated at adjacent fences. Base pressure was decreased in the presence of fences as was surface pressure in the near-base region. However, the average C_p in the region $Y'/h < 5$ apparently increased in the presence of the fences, as compared to the same region on the model without fences.

4.3. Recommendations for Future Research

The following recommendations are made for future research:

(1) Study the effect of an imposed adverse pressure gradient on the three-dimensional separated flow associated with swept steps. (Swept joints on airfoils are usually in a region with an adverse pressure gradient, e.g., trailing-edge flap hinge lines.)

(2) Investigate additional means of controlling spanwise vortex flow in the three-dimensional separated-flow region in order to decrease detrimental effects of three-dimensional flow separation.

(3) Perform a survey of the three-dimensional separated flow using a nonobtrusive method in order to obtain velocity maps. Such a survey would confirm the existence of the

structures defined herein. As applied to the unswept step, such surveys would aid in a reconsideration of the claim of two-dimensional flow for AR > 10.

(4) Optimize the effects of vortex troughs and lip radius on the reattachment length associated with swept steps.

(5) Conduct flow visualization studies of flow over swept steps in a water channel. Such a facility would be more conducive to visualizing this unsteady flow.

(6) Develop a general three-dimensional code for subsonic laminar and turbulent flow over swept steps.

(7) Conduct research on swept wake modification with the goal of reducing base drag.

(8) Design a lifting airfoil with blunt swept trailing edge and appropriate spanwise vortex control device, which incurs no drag penalty as compared to the comparable airfoil with sharp trailing edge.

Present plans are for this author to continue research in the above areas.

REFERENCES

Abbott, D. E. and Kline, S. J. (1962): "Experimental Investigation of Subsonic Turbulent Flow Over Single and Double Backward Facing Steps," Journal of Basic Engineering, No. 9, pp. 317-325.

Armaly, B. F. and Durst, F. (1980): "Reattachment Length and Circulation Regions Downstream of a Two-Dimensional Single Backward-Facing Step," Momentum and Heat Transfer Processes in Recirculating Flows," ASME Winter Annual Meeting, Chicago, Illinois, 16-21 November, HTD-Vol. 13.

Ashkenas, H. and Riddell, F. R. (1955): Investigation of the Turbulent Boundary Layer on a Yawed Flat Plate, NACA TN 3383.

Atkins, P. B. (1961): A Preliminary Wind Tunnel Investigation of the Control of Leading-Edge Separation on the Avro 707A, Australian Defense Scientific Service, Aeronautical Research Laboratories, Flight Technical Memorandum 12.

Aung, W. and Goldstein, R. J. (1972): "Heat Transfer in Turbulent Separated Flow Downstream of a Rearward-Facing Step," Israel Journal of Technology, Vol. 10, Nos. 1-2, pp. 35-41.

Badrinarayanan, M. A. (1961): "An Experimental Investigation of Base Flows at Supersonic Speeds," Journal of the Royal Aeronautical Society, Vol. 65, pp. 475-482.

Billet, G. (1980): "Numerical Simulation of a Three-Dimensional Wall Separation," La Recherche Aerospatiale (English Edition), No. 4, pp. 11-23.

Bradshaw, P. (1971): "Calculation of Three-Dimensional Turbulent Boundary Layers," Journal of Fluid Mechanics, Vol. 46, p. 417.

Bradshaw, P. and Wong, F. Y. F. (1972): "The Reattachment and Relaxation of a Turbulent Shear Layer," Journal of Fluid Mechanics, Vol. 52, Part 1, pp. 113-135.

Breidenthal, R. (1980): "Response of Plane Shear Layers and Wakes to Strong Three-Dimensional Disturbances," Physics of Fluids, Vol. 23, No. 10, pp. 1929-1934.

Browand, F. K. (1966): "An Experimental Investigation of the Instability of an Incompressible, Separated Shear Layer," Journal of Fluid Mechanics, Vol. 26, Part 2, pp. 281-307.

Bushnell, D. M. and Morris, D. J. (1971): Shear-Stress, Eddy-Viscosity, and Mixing-Length Distributions in Hypersonic Turbulent Boundary Layers, NASA TM X-2310.

Carr, G. W. (1969): "The Study of Road Vehicle Aerodynamics Using Wind Tunnel Models," Proceedings of Symposium on Road Vehicle Aerodynamics, City University, London, Paper 14.

_____ (1973): "Aerodynamic Lift Characteristics of Cars," Proc. I. Mech. E., Vol. 187, 30/73, p. 333.

_____ (1974): Influence of Rear Body Shape on the Aerodynamic Characteristics of Saloon Cars, Motor Industry Research Association, Nuneaton, Warwickshire, Report No. 1974/2.

Chang, P. (1970): Separation of Flow, Pergamon Press, Inc.

_____ (1976): Control of Flow Separation, Hemisphere Publishing Corporation.

Chapman, D. R. (1955): Reduction of Profile Drag at Supersonic Velocities by the use of Airfoil Sections Having a Blunt Trailing Edge, NACA TN 3503.

Chapman, D. R. and Kester, R. H. (1952): Effect of Trailing-Edge Thickness on Lift at Supersonic Velociites, NACA RM A 52D17.

Crawford, D. R. (1967): Supersonic Separated Flow Downstream of a Backward-Facing Step, Ph.D. Dissertation, University of California at Berkeley, University Microfilms, Inc., Ann Arbor, Michigan.

Czarnecki, K. R. (1966): "The Problem of Roughness Drag at Supersonic Speeds," Conference on Aircraft Aerodynamics, NASA Langley Research Center, 23-25 May, pp. 455-468.

de Brederode, V., and Bradshaw, P. (1972): Three-Dimensional Flow in Nominally Two-Dimensional Separation Bubbles-Flow behind a Rearward Facing Step, Imperial College of Science and Technology, I. C. Aero Report 72-19.

Dickson, J. K. and Sutton, F. B. (1955): The Effect of Wing Fences on the Longitudinal Characteristics at Mach Numbers up to 0.92 of a Wing-Fuselage-Tail Combination Having a 40° Sweptback Wing with NACA64A Thickness Distribution, NACA RM A55C30a.

Eaton, J. K. (1980): Turbulent Flow Reattachment: An Experimental Study of the Flow and Structure Behind a Backward-Facing Step, Ph.D. Dissertation, Stanford University, University Microfilms International, Ann Arbor, Michigan.

Eaton, J. K. and Johnston, J. P. (1980): A Review of Research on Subsonic Turbulent Flow Reattachment, AIAA 13th Fluid and Plasma Dynamics Conference, 14-16 July 1980, Snowmass, Colorado, AIAA-80-1438.

Emmons, H. W. (1951): "The Laminar-Turbulent Transition in a Boundary Layer-Part I," Journal of Aeronautical Science, Vol. 18, pp. 490-498.

Farivar, D. (1981): "Turbulent Uniform Flow around Cylinders of Finite Length," AIAA Journal, Vol. 19, No. 3, pp. 275-281.

Friehe, C. A. (1980): "Vortex Shedding from Cylinders at Low Reynolds Numbers," Journal of Fluid Mechanics, Vol. 100, Part 2, pp. 237-241.

Gai, S. L. and Sharma, S. D. (1981): "Experiments on the Reduction of Base Drag of a Blunt Trailing Edge Airfoil in Subsonic Flow," Aeronautical Journal, May, pp. 206-210.

Ginoux, J. J. (1958): Experimental Evidence of Three-Dimensional Perturbations in the Reattachment of a Two-Dimensional Laminar Boundary Layer at M = 2.05, Training Center for Experimental Aerodynamics (Belgium), Tech. Note 1.

_____ (1961): Leading Edge Effect on Separated Supersonic Flows, Training Center for Experimental Aerodynamics, Belgium, Technical Note NR. 4.

Goradia, S. H., Mehta J. M. and Shrewsbury, G. S. (1977): Analysis of the Separated-Boundary-Layer Flow on the Surface and in the Wake of Blunt Trailing Edge Airfoils, NASA CR-145202 prepared by Lockheed-Georgia Company.

Griffin, O. M. and Ramberg, S. E. (1974): "The Vortex Street in the Wake of a Vibrating Cylinder," Journal of Fluid Mechanics, Vol. 66, pp. 553-578.

Hall, M. G. (1972): "Vortex Breakdown," Annual Review of Fluid Mechanics, Annual Review, Inc., Vol. 4.

Hanson, C. E. (1969): The Design and Construction of a Low-Noise, Low-Turbulence Wind Tunnel, Department of Mechanical Engineering, Massachusetts Institute of Technology, Report No. DSR 79611-1.

Harrowood, Paul (1967): Study of Vortex Motions in Wake Flows, Ph.D. Dissertation, North Carolina State University, University Microfilms, Inc., Ann Arbor, Michigan.

Hefner, J. N. and Bushnell, D. M. (1977): "An Overview of Concepts for Aircraft Drag Reduction," Special Course on Concepts for Drag Reduction, NATO Advisory Group for Aerospace Research and Development, AGARD Report No. 654.

Helms, V. T. III (1979): "Measuring Flow Angle and Mass Flow Rate in an Unknown Flowfield," Journal of Spacecraft and Rockets, Vol. 16, No. 1, pp. 20-26.

Hieser, G. and Whitcomb, C. F. (1948): Investigation of the Effects of a Nacelle on the Aerodynamic Characteristics of a Swept Wing and the Effects of Sweep on a Wing Alone, NACA TN 1709.

Hinze, J. O. (1975): Turbulence, McGraw Hill Book Company.

Hoerner, S. F. (1965): Fluid-Dynamic Drag, Hoerner Fluid Dynamics.

Holder, D. W. (1964): "The Transonic Flow Past Two-Dimensional Aerofoils," Journal of the Royal Aeronautical Society, Vol. 68, No. 644, pp. 501-516.

Hopkins, E. J., Keating, S. J., Jr. and Bandettini, A. (1960): Photographic Evidence of Streamwise Arrays of Vortices in Boundary-Layer Flow, NASA Ames Research Center, TN D-328.

Howe, John T. (1968): Some Fluid Mechanical Problems Related to Subsonic and Supersonic Aircraft, NASA SP-183.

Hucho, W. (1978): "The Aerodynamic Drag of Cars—Current Understanding, Unresolved Problems and Future Prospects," Aerodynamic Drag Mechanics of Bluff Bodies and Road Vehicles, Plenum Press, pp. 7-44.

Hunt, J. C., Abell, C. J., Peterka, J. A. and Woo, H. (1978): "Kinematical Studies of the Flows around Free or Surface-Mounted Obstacles; Applying Topology to Flow Visualization," Journal of Fluid Mechanics, Vol. 86, Part 1, pp. 179-200.

Inger, G. R. (1974): Three-Dimensional Distrubances in Reattaching Separated Flows, Department of Aerospace and Ocean Engineering, Virginia Polytechnic Institute and State University, Blacksburg, Virginia.

Jones, R. T. (1974): Effects of Sweepback on Boundary Layer and Separation, NACA TN 1402.

Kangovi, S. and Page, R. H. (1978): "Subsonic Turbulent Flow Past a Downstream Facing Annular Step," Proceedings of the Winter Annual Meeting, American Society of Mechanical Engineers, No. 78-WA/FE15.

Kasagi, N., Hirata, M. and Hiraoka, H. (1977): Large-Eddy Structures in Turbulent, Separated Flow Downstream of a Rearward-Facing Step, Symposium on Turbulent Shear Flows, University Park, Pennsylvania, 18-20 April.

Kim, J., Kline, S. J. and Johnston, J. P. (1979): "Investigation of a Reattaching Turbulent Shear Layer: Flow over a Backward-Facing Step," Proceedings of the Winter Annual Meeting, American Society of Mechanical Engineers, p. 41-48.

Kuchemann, D. (1953): "Types of Flow on Swept Wings," Journal of the Royal Aeronautical Society, Vol. 57, November, pp. 683-699.

Laine, S. (1972): A Theoretical Study of the Effect of a Step in a Flat Plate Upon the Laminar Boundary Layer, Helsinki U. of Technology, Doctor of Technology Thesis.

Maltby, R. L. (1962): Flow Visualization in Wind Tunnels Using Indicators, NATO Advisory Group for Aeronautical Research and Development, AGARDograph 70.

Merzkirch, W. (1974): Flow Visualization, Academic Press, Inc., p. 53.

Mirande, J. et Quelin, C. (1977): Analyse détaillée de la structure d'un ecoulement tridimensionnel, Rapport Technique 07-1977, ONERA.

Morel, T. (1977): Aerodynamic Drag on Bluff Body Shapes Characteristic of Hatch-Back Cars, Research Publication GMR-2581, General Motors Research Laboratories.

Morkovin, M. V. (1964): "Flow around Circular Cylinder-A Kaleidoscope of Challenging Fluid Phenomena," Symposium on Fully Separated Flows, ASME Fluids Engineering Division Conference, Philadelphia, PA, May 18-20, pp. 102-118.

Moss, W. D. and Baker, S. (1980): "Re-Circulating Flows Associated with Two-Dimensional Steps," The Aeronautical Quarterly, Vol. 31, Part 3, pp. 151-172.

Mullin, T., Greated, C. A. and Grant, I. (1980): "Pulsating Flow over a Step," The Physics of Fluids, Vol. 23, No. 4, pp. 669-674.

Narayanan, M. A., Khadgi, Y. N. and Viswanath, P. R. (1974): "Similarities in Pressure Distribution in Separated Flow behind Backward-Facing Steps," Aeronautical Quarterly, Vol. 25, pp. 305-312.

Nash, J. F. (1962): An Analysis of Two-Dimensional Turbulent Base Flow Including the Effect of the Approaching Boundary Layer, London, England: Ministry of Aviation, Aeronautical Research Council Reports and Memoranda No. 3344.

_____ (1965): A Discussion of Two-Dimensional Turbulent Base Flows, London, England: Ministry of Aviation, Aeronautical Research Council Reports and Memoranda Number 3468.

Nash, F. J., Quincey, V. G. and Callinan, J. (1963): Experiments on Two-Dimensional Base Flow at Subsonic and Transonic Speeds, National Physical Laboratory, Aerodynamics Division, NPL Aero. Report 1070-A.R.C. 25 070.

Nice, G. R., Tseng, W. and Moses, H. L. (1965): Separation of Turbulent, Incompressible Flow from a Curved, Backward-Facing Step, Gas Turbine Laboratory, Massachusetts Institute of Technology, Report No. 87.

Patterson, J. G. (1968): "Aerodynamic Design Features of the C-5A," Aircraft Engineering, June Issue, pp. 8-15.

Peake, D. J. and Tobak, M. (1980): Three-Dimensional Interactions and Vortical Flows with Emphasis on High Speeds, NASA Ames Research Center, NASA TM 81169.

Peake, D. J. and Tobak, M. (1982): Three-Dimensional Separation and Reattachment, AGARD Lecture Series No. 121 on High Angle of Attack Aerodynamics, 10-11 March, NASA Langley Research Center, Paper #1.

Pearcey, H. H. (1962): "The Aerodynamic Design of Section Shapes for Swept Wings," Advances in Aeronautical Sciences: Proceedings of the Second International Congress in the Aeronautical Sciences, (Zurich, 12-16 September 1960), Pergamon Press, pp. 277-322.

_____ (1958): A Method for the Prediction of the Onset of Buffeting and Other Separation Effects from Wind Tunnel Tests on Rigid Models, ARC 20, 631, AGARD Report Number 223.

Ram, V. V. and Wauschkuhn, P. (1975): "Turbulent Flow Connected with Separation and Reattachment," Boundary Layer Effects: Proceedings of the Fourth Data Exchange Agreement Meeting, Gottingen, West Germany, 2-3 June 1975, pp. 96-103.

Ramberg, S. E. (1978): The Influence of Yaw Angle upon the Vortex Wakes of Stationary and Vibrating Cylinders, Naval Research Laboratory, Washington, DC, NRL Memorandum Report 3822.

Roach, P. (1968): Numerical Solutions of Compressible and Incompressible Laminar Separated Flows, U. of Notre Dame, Ph. D. Dissertation.

Rockwell, D. and Knisely, C. (1980): "Observations of the Three-Dimensional Nature of Unstable Flow Past a Cavity," The Physics of Fluids, Vol. 23, No. 3, pp. 425-431.

Rom, J., Kronzon, Y. and Seginer, A. (1968): The Velocity, Pressure and Temperature Distribution in the Turbulent, Supersonic, Near Wake behind a 2-D Wedge-Flat Plate Model," Israel Journal of Technology, Vol. 6, pp. 84-94.

Roshko, A. (1980): The Plane Mixing Layer-Flow Visualization Results and Three-Dimensional Effects, International Conference on the Role of Coherent Structures in Modelling Turbulence and Mixing, Madrid, Spain, 25-27 June.

Schuringa, T. (1972): "Aerodynamics of Wing Stall of the Fokker F28," Proceedings of AGARD Conference No. 102 on Fluid Dynamics of Aircraft Stalling, AGARD-CP-102.

Sedney, R. (1981): A Flow Model for the Effect of a Slanted Base on Drag, Ballistic Research Labs., Aberdeen Proving Ground, MD, Technical Report ARBRL-TR-02341.

Settles, G. S. and Perkins, J. J. (1979): Investigation of Three-Dimensional Shock-Boundary Layer Interactions at Swept Compression Corners, Paper 79-1498, AIAA 12th Fluid and Plasma Dynamics Conference, July 23-25, Williamsburg, VA.

Thomson, D. K. and Morrison, D. F. (1971): "The Spacing, Position and Strength of Vortices in the Wake of Slender Cylindrical Bodies at Large Incidence," Journal of Fluid Mechanics, Vol. 50, Part 4, pp. 751-783.

Van Atta, C. W. (1968): "Experiments on Vortex Shedding from Yawed Circular Cylinders," AIAA Journal, Vol. 6, No. 5, pp. 931-933.

Werle, H. (1980): "Transition and Separation-Visualizations in the ONERA Water Tunnel," La Recherche Aerospatiale (English Edition), No. 5, pp. 35-49.

Werle, M. J., Vatsa, V. N. and Bertke, S. D. (1973): "Sweep Effects on Supersonic Separated Flows—A Numerical Study," AIAA Journal, Vol. 11, No. 12, pp. 1763-1765.

Westphal, R. V. (1981): "A New Probe for Measurement of Velocity and Wall Shear Stress in Unsteady, Reversing Flow," Transactions of the ASME, Vol. 103, September, pp. 478-482.

Whitcomb, R. T. (1974): Review of NASA Supercritical Airfoils, Presented at the 9th Congress of the International Council of the Aeronautical Sciences, Haifa, Israel, 25-30 August, ICAS Paper 74-10.

Wilson, D. J., Winkel, G. and Neiman, O. (1979): "Reynolds Number Effects on Flow Recirculation behind Two-Dimensional Obstacles in a Turbulent Boundary Layer," Proceedings of the Fifth International Conference on Wind Engineering, Fort Collins, Colorado, July, pp. 965-974.

Yevenko, V. I. and Anisin, A. K. (1978): "Effect of Surface Orientation on the Characteristics of Separated Flow," Heat Transfer-Soviet Research, Vol. 10, No. 5, pp. 16-19.

Young, A. D. and Patterson, J. H. (1981): Aircraft Excrescence Drag, AGARDograph No. 264.

Zumwalt, G. W. (1980): The Vortex Trough and Its Use an an Igniter for Supersonic Burning, Report to NASA Langley Research Center, Hypersonic Propulsion Branch.

APPENDIX A

SMOKE WIRE PHOTOGRAPHS FOR LAMINAR SWEPT-STEP AND SWEPT-WAKE FLOWS

Smoke flow photographs were taken for both laminar and turbulent flow over swept rearward-facing steps and plates with swept trailing-edges in the manner elucidated in Section 2.3. The dominant features observed in the laminar flow photographs for swept-step flow are: (1) laminar boundary layer approaching the step; (2) laminar separation from the step; (3) formation of eddies at step edge and (4) turbulence spots on downstream step surface in the relaxation region. Flow features observable in the photographs for the swept-wake case include: (1) oncoming laminar boundary layer; (2) flow transition in the Karman vortex street and (3) the three-dimensionality of the vortex street even for the unswept trailing edge.

Figure A1 depicts laminar flow over a two-dimensional rearward-facing step with $h = .31"$. Prominent flow features observeable in this photograph are the laminar state of the boundary layer at separation (smoke lines at the step face are parallel and steady) and the presence of turbulent or "Emmons" spots. Turbulent spots are a phenomenon

of natural transition. [See, e.g., Hinze (1975).] Turbulent spots are the results of flow disturbances at randomly located points in the boundary layer. Emmons (1951) has stated that these disturbances are propagated in the streamwise and spanwise directions and result in turbulent spots. These spots ultimately overlap and consequently, the entire boundary layer becomes turbulent.

The photos presented as Figure A2 and A3 are for $\Lambda = 30°$. Figure A2 also shows the presence of turbulent spots as well as another phenomenon, which is more pronounced in Figure A3—periodic shedding of eddies from the upper edge of the step face. These eddies appear to be a part of the transition process also—a phenomenon that occurs in the laminar flow region upstream of the turbulence spots and which minimally accentuates the growth of the turbulence spots. This phenomenon is seen to be even more pronounced in Figure A4 for $\Lambda = 60°$; however, it was not identifiable in any of the photos of flow over a two-dimensional step. In Figures A1 through A4, the test section is viewed from the side and the vertical smoke wire was used.

This phenomenon has previously been observed—at least by numericists. Roache (1968) computed a case for vortex shedding from a two-dimensional rearward-facing step in laminar incompressible flow

---

Hinze, J. O., Turbulence, McGraw Hill Book Company, 1975.

Emmons, H. W., "The Laminar-Turbulent Transition in a Boundary Layer-Part I," Journal of Aeronautical Science, Vol. 18, pp. 490-498, 1951.

Roache, P., Numerical Solutions of Compressible and Incompressible Laminar Separated Flows, University of Notre Dame, Ph. D. Dissertation, 1968.

Figure A1. Two-Dimensional Step

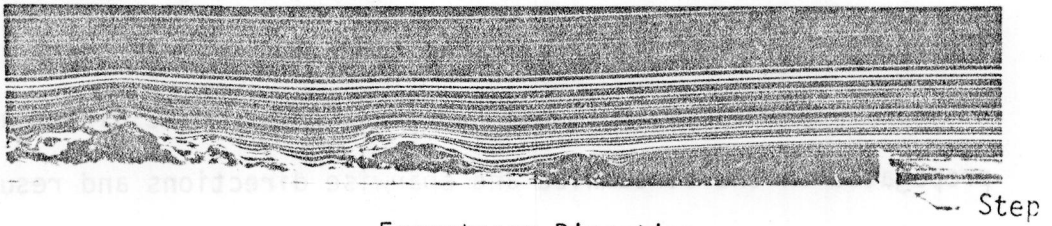

Figure A2. 30-deg. Swept Step

Figure A3. 30-deg. Swept Step

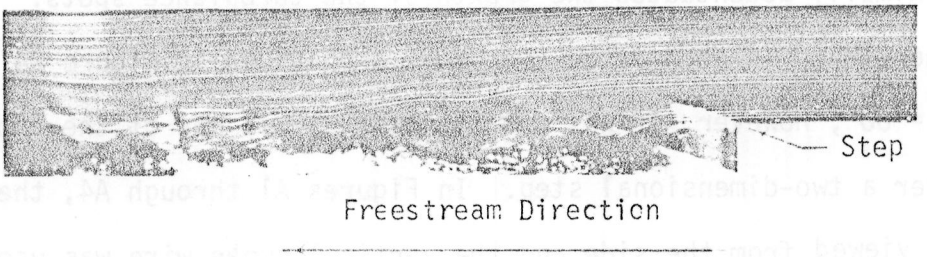

Figure A4. 60-deg. Swept Step

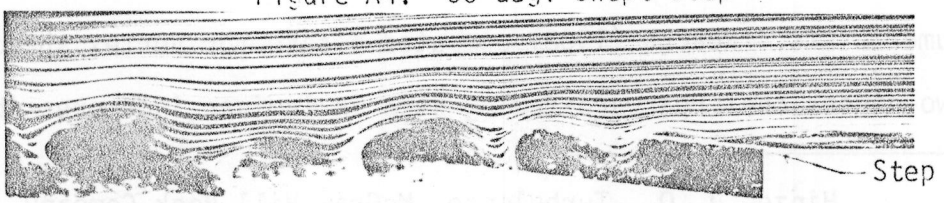

Figures A1 - A4. Flow Over Rearward-Facing Steps Visualized Using a Vertical Smoke Wire ($h=.31"$, $V_\infty=25$ fps and $Re=5 \times 10^5$)

with $\delta/h = 1$. Having obtained a steady flow solution, he then increased Re_x until unsteadiness was observed for which no solution was available. The unsteady "wake" behind the step was "open"—reattachment did not occur before the mesh boundary was reached.

Laine (1972) also studied the stability of laminar incompressible flow over a two-dimensional rearward-facing step. His assertion was that Roache's results applied to channel flow with an abrupt expansion of the flow section area rather than to flow over a flat plate with a step. Laine's aim was to examine the effect of a two-dimensional roughness element (rearward-facing step on flat plate) in incompressible flow on transition to a turbulent boundary layer. Laine's calculations showed that the flow remained steady at low Reynolds numbers but became unsteady at high values of Reynolds number. Thus, when the value of the Reynolds number was increased sufficiently, the flow became unsteady; the reattachment length varied periodically and vortex shedding occurred so that a row of eddies moved downstream. Laine's calculations predict shedding from steps for Re from 1 to 4×10^5 for δ/h between .7 and 1.0. Reynolds number for the cases shown in Figures A1 through A4 varies from 2.8×10^5 at midspan for $\Lambda = 0$ to 4.3×10^5 at midspan for $\Lambda = 60°$. However, δ/h for these cases is greater than 2. The apparent accentuation of the eddies with increasing sweep is probably due to Reynolds number effects.

Laine, Seppo K., A Theoretical Study of the Effect of a Step in a Flat Plate Upon the Laminar Boundary Layer, Helsinki University of Technology, Doctor of Technology Thesis, 1972.

Chang (1970) indicated that similar eddy shedding may be present at the trailing edge of a two-dimensional airfoil in subsonic flow. In this situation an array of eddies is generated which may prevent the fluid from closing up behind the body, result in higher drag and cause asymmetrical pressure distributions. The first observation is in agreement with Laine's data which indicated much greater reattachment distances for the cases with eddy shedding from the steps.

The top views of the flows presented in Figures A1 ($\Lambda = 0°$) and A2 and A3 ($\Lambda = 30°$) are shown in Figures A5 and A6 for $\Lambda = 0°$ and $\Lambda = 30°$, respectively. The horizontal smoke wire is located 1/2" downstream of the base of the two-dimensional step model and 2/5" downstream of the base of the 30° swept-step model.

Figure A5 indicates that the flow is highly three-dimensional at the base of the two-dimensional step. Even with an aspect ratio of 48, only for a small region near midspan do the smoke filaments initially move perpendicular to the step base. As one travels toward either wall from the midspan position, the flow is observed to be increasingly spanwise; hence, increasingly three-dimensional. This observation contradicts the assertion made by de Brederode and Bradshaw (1972) who have stated that two-dimensional flow can be expected in the separated-flow region for flow over an unswept rearward facing step with $AR > 10$.

The flow in the separated-flow region for the 30° swept case of Figure A6 generally appears to be directed either perpendicular to

Figures A5 and A6. Separated-Flow Region Aft of Rearward-Facing Steps Visualized Using a Horizontal Smoke Wire ($h=.31"$, $l_w=.5"$, $h_w \simeq 0$, $V_\infty=25$ fps and $Re=5 \times 10^5$)

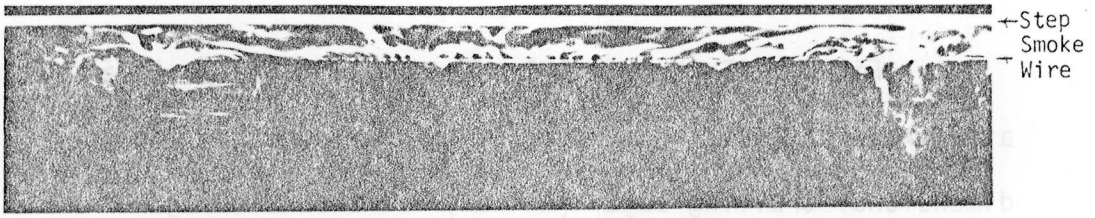

Figure A5. Two-Dimensional Step

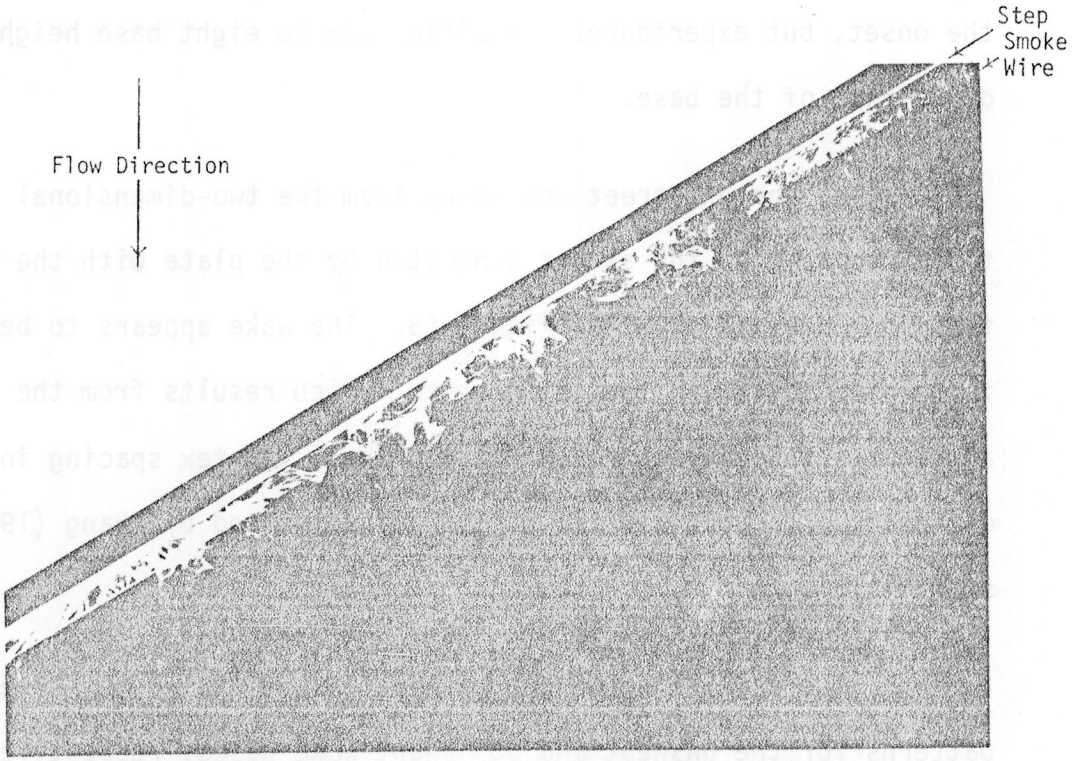

Figure A6. 30-deg. Swept Step

the step or spanwise from right to left in the photo. This is not unexpected in view of the results presented in Chapter 3. There also appears some indication of streamwise periodicity at midspan in the direction perpendicular to the step face. This possibly relates to the eddy shedding at the step face observed in previous photographs.

Figures A7 through A10 relate to flow over a flat plate with a thick swept trailing edge. The wake shed by the model with the two-dimensional trailing edge ($\Lambda = 0°$) is shown in Figure A7. The regular Karman vortex street is observable. The street is laminar at the onset, but experiences transition six to eight base heights downstream of the base.

The vortex street emanating from the two-dimensional base is to be compared to the street generated by the plate with the 30° swept trailing edge, as shown in Figure A8. The wake appears to be highly three-dimensional in the latter case, which results from the presence of a spanwise velocity component at the base. Vortex spacing in the two-dimensional case is similar to the values quoted by Chang (1970) for stability.

Figures A9 and A10 show a top view of the vortex street patterns for the unswept and 30° swept wake cases, respectively. The horizontal smoke wire locations are the same as in the corresponding rearward-facing step cases. Figure A9 shows the three-dimensionality of the wake generated by the two-dimensional trailing edge, which is the

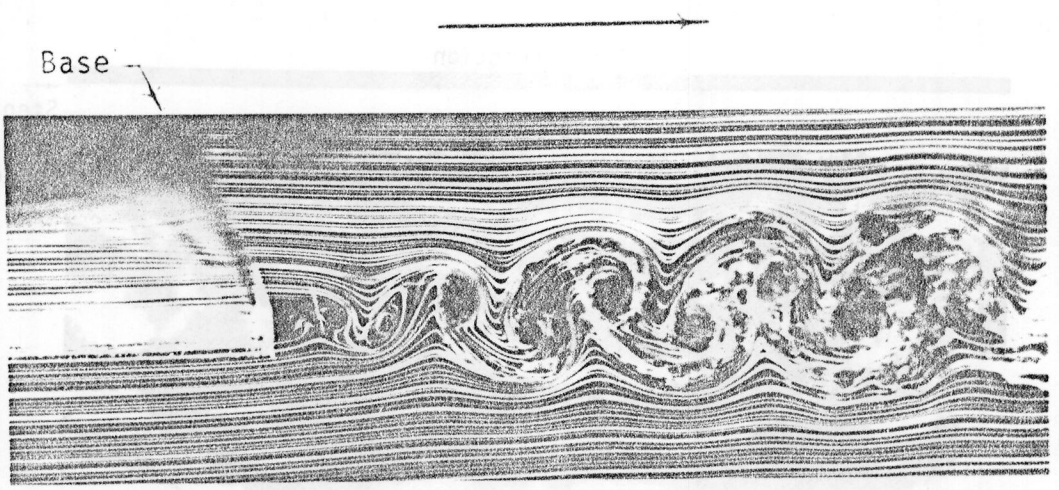

Figure A7. Laminar Near-Wake of the Basic Model with Unswept Trailing Edge Visualized Using a Vertical Smoke Wire (t=.5", V_∞=25 fps and Re=5 x 10^5)

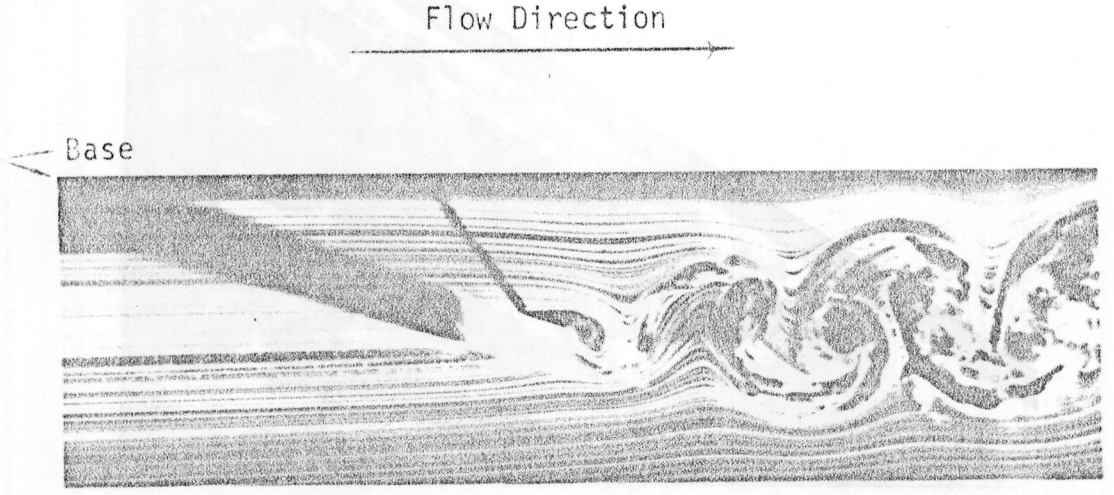

Figure A8. Laminar Near-Wake of the Basic Model with 30-deg. Swept Trailing Edge Visualized Using a Vertical Smoke Wire (t=.5", V_∞=25 fps and Re=5 x 10^5)

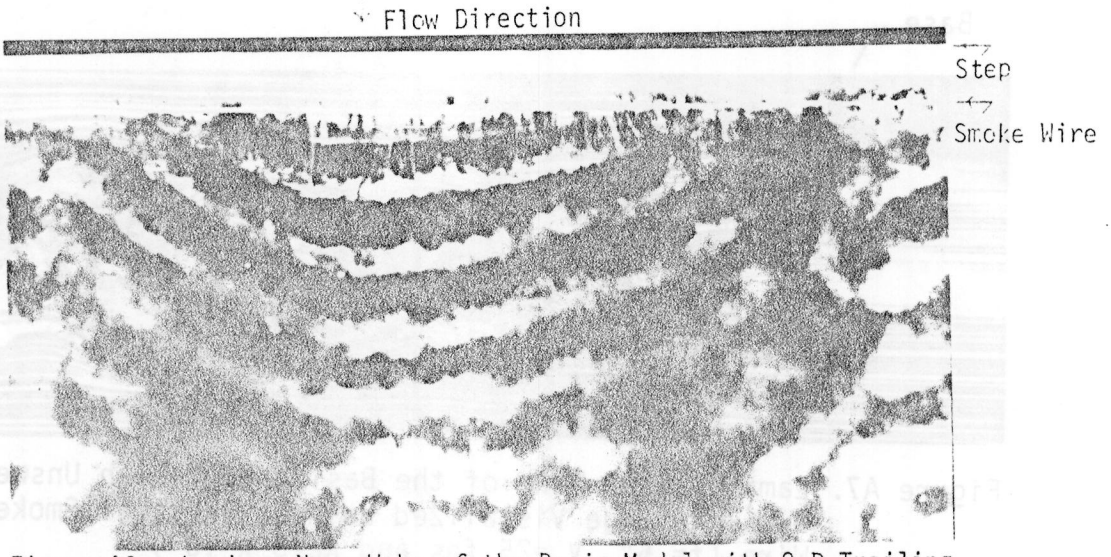

Figure A9. Laminar Near-Wake of the Basic Model with 2-D Trailing Edge Visualized Using a Horizontal Smoke Wire ($t = .5"$, $l_w = .5"$, $V_\infty = 25$ fps, $Re = 5 \times 10^5$)

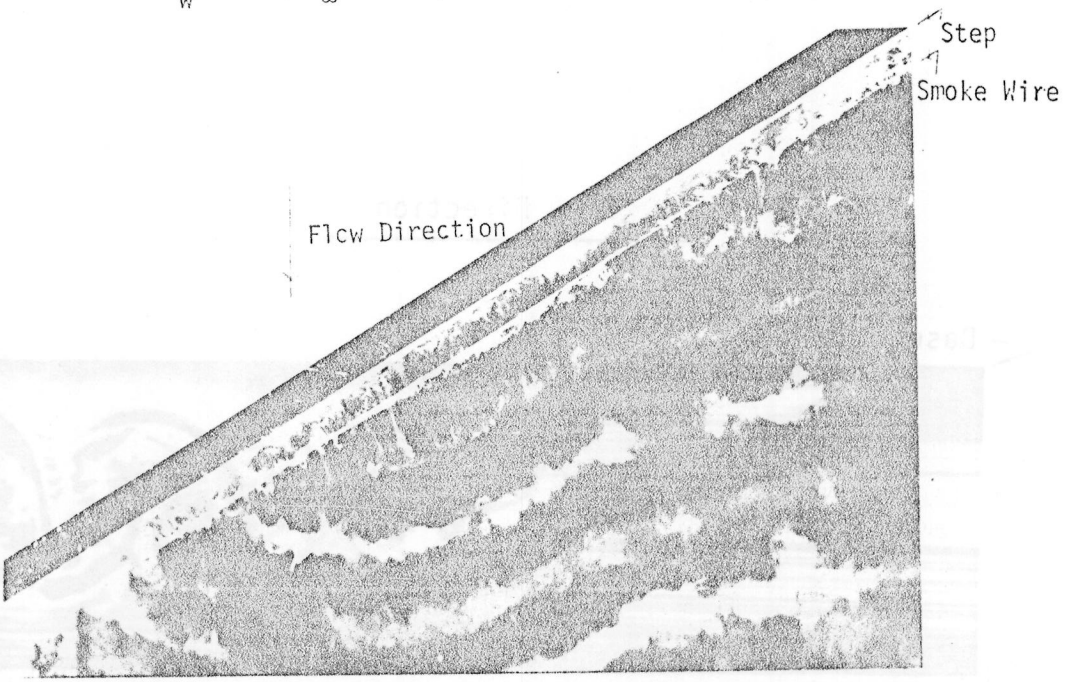

Figure A10. Laminar Near-Wake of the Basic Model with 30-deg. Swept Trailing-Edge Visualized Using a Horizontal Smoke Wire ($t=.5"$, $l_w=.4"$, $V_\infty=25$ fps and $Re=5 \times 10^5$)

result of end effects. The ratio of base thickness to test section width is 30.

The development of a formation region for the bow-shaped vortices of Figure A9 is interesting. Each vortex appears to originate at midspan where a central formation region bifurcates and the two resulting formation regions move toward the tunnel walls. Ideally, one would expect the vortex formation region to span the tunnel along the base of the two-dimensional trailing edge, and the vortex cores to be parallel to the base of the model.

For the swept trailing-edge model shown in Figure A10, a single, finite vortex formation region appears to originate at the upstream tunnel wall-trailing edge junction for each vortex, and then move spanwise along the base. As the vortices comprising the vortex street move downstream from the trailing edge, the vortex lines increasingly become perpendicular to the tunnel walls.

Of future interest might be the variation of Strouhal number with sweep and free-end effects. Free-end effects would be obtained by examining the shedding characteristics of half-span models. It is possible that the wealth of information on vortex shedding from swept and unswept circular cylinders might be helpful—at least from a qualitative standpoint—in understanding the many aspects of vortex shedding by swept trailing edges. For example, Thompson and

Morrison (1971) studied the arrangement of the vortices in the wake of swept cylindrical bodies. Ramberg (1978) investigated the applicability of the Independence Principle in correlating vortex wake phenomena for swept cylinders. Van Atta (1968) measured the effect of sweep on Strouhal number at constant Reynolds number. Friehe (1980) researched the Strouhal number-Reynolds number relationship for two-dimensional cylinders. Farivar (1981) examined free-end effects on shedding from two-dimensional cylinders. Most of these studies were performed in low-speed flows.

Thompson, K. D. and Morrison, D. F., "The Spacing, Position and Strength of Vortices in the Wake of Slender Cylindrical Bodies at Large Incidence," Journal of Fluid Mechanics, Vol. 50, Part 4, pp. 751-783, 1971.

Ramberg, S. E., The Influence of Yaw Angle upon the Vortex Wakes of Stationary and Vibrating Cylinders, Naval Research Laboratory, Washington, DC, NRL Memorandum Report 3822, 1978.

Van Atta, C. W., "Experiments on Vortex Shedding from Yawed Circular Cylinders," AIAA Journal, Vol. 6, No. 5, pp. 931-933, 1968.

Friehe, C. A., "Vortex Shedding from Cylinders at Low Reynolds Numbers," Journal of Fluid Mechanics, Vol. 100, Part 2, pp. 237-241, 1980.

Farivar, D., "Turbulent Uniform Flow around Cylinders of Finite Length," AIAA Journal, Vol. 19, No. 3, pp. 275-281, 1981.

APPENDIX B

COUPLING BETWEEN MODELS AND TEST SECTION

Often, results are published relating to flow over rearward facing steps when the actual test configuration more accurately corresponds to channel flow with an abrupt expansion of the flow area. This observation applies to the present research as well.

Upon viewing the surface pressure measurements for the separated-flow region of the present basic swept-step configurations, it is evident that an appreciable spanwise pressure gradient exists for $\Lambda = 30°$ and $60°$. An attempt was made to calculate the level of this pressure gradient for the following four specific cases: $\Lambda = 30°$ and $60°$ for $h = .50"$ and $.94"$.

A simple calculation procedure is described below. From the measured velocity at the leading edge of the model the velocity in a series of successive planes perpendicular to the tunnel walls and downstream of the upstream step-wall junction was calculated using area ratios. The change in pressure coefficient between successive planes was determined from Bernoulli's relation in the form

$$C_{p_2} - C_{p_1} = \frac{V_1^2 - V_2^2}{V_\infty^2}$$

where the subscript "2" designates a plane downstream of that designated by the subscript "1." From this equation, the spanwise pressure gradient at the base of the model was calculated as a function of spanwise position.

Two models were considered for the calculations. Model 1 represented a sudden increase in flow area. The reduction in flow area primarily due to the separated boundary layer was included in Model 2. The reattachment distances used in the present calculations were the measured data of Chapter 3. The results are presented in Figures B1 through B4 for the cases previously discussed. The spanwise pressure gradient levels labeled "average from graph" are primarily from Figure 58 of Section 3.4.2.

It can be concluded that the spanwise pressure gradient present in the separated-flow region of a swept rearward-facing step mounted in a typical test section is primarily due to the area expansion. The level of the pressure gradient depends on the specific area ratios involved, hence, on test section dimensions and step height. It has been demonstrated that a simple one-dimensional inviscid flow calculation procedure can be used to roughly predict the level of the pressure gradient.

The solution to this problem is to use compensating roof steps in the manner of Narayanan et al. (1974). Surface pressures measured with and without a swept roof step are presented in Section 3.5.2 for the basic 30° swept-step model with $h = .94"$. When compensating

Figure B1.

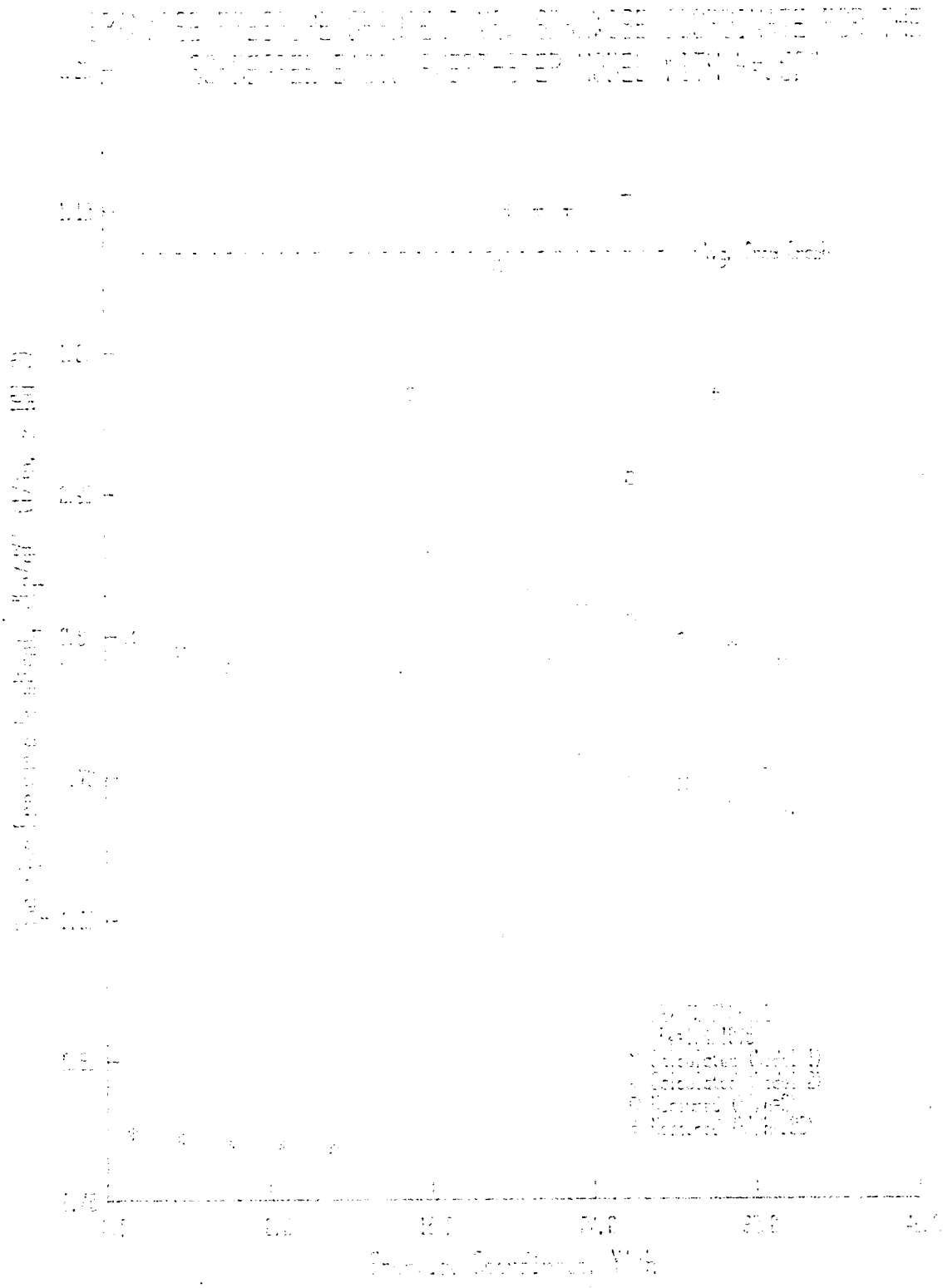

Figure B2.

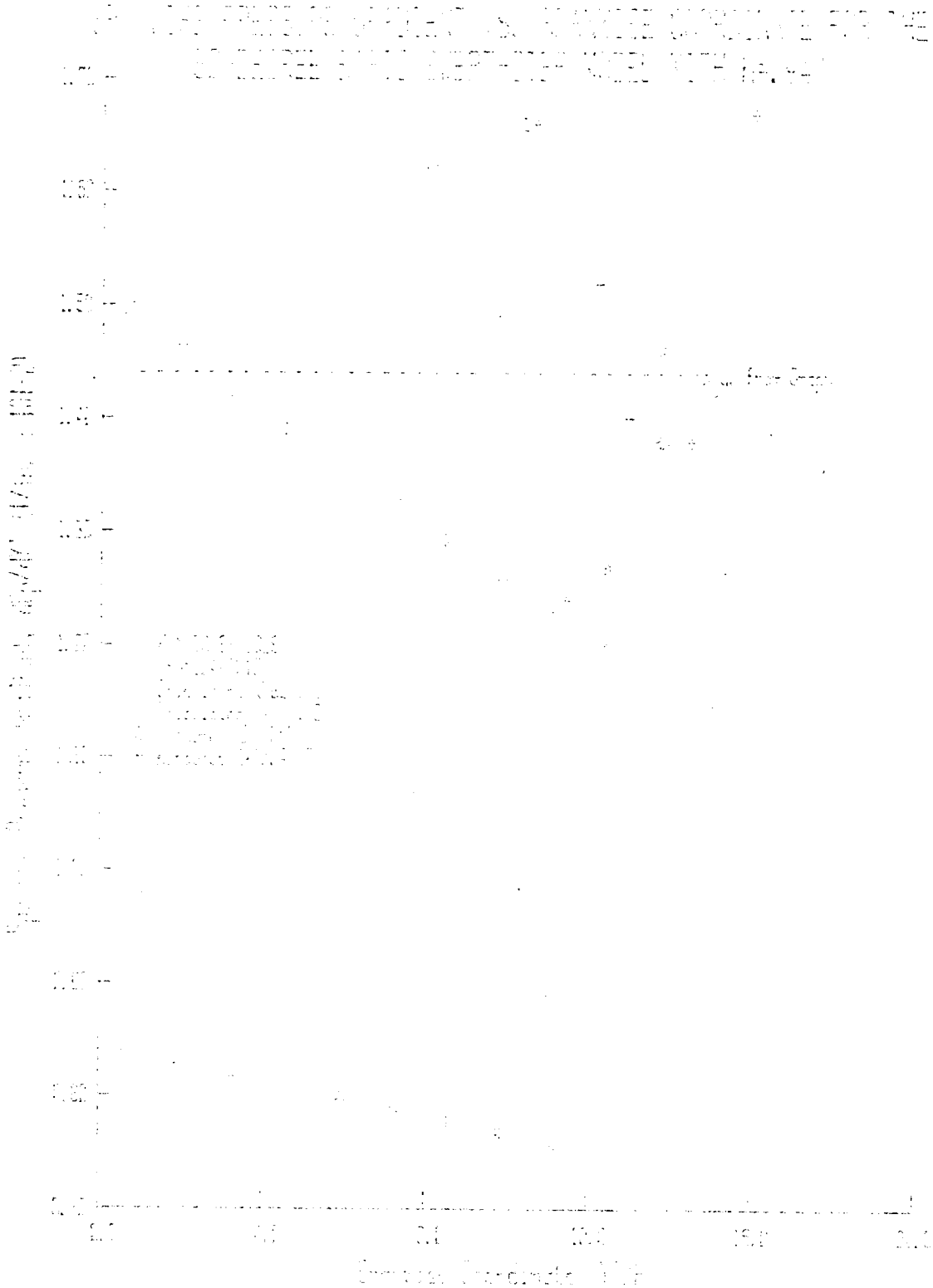

Figure B3.

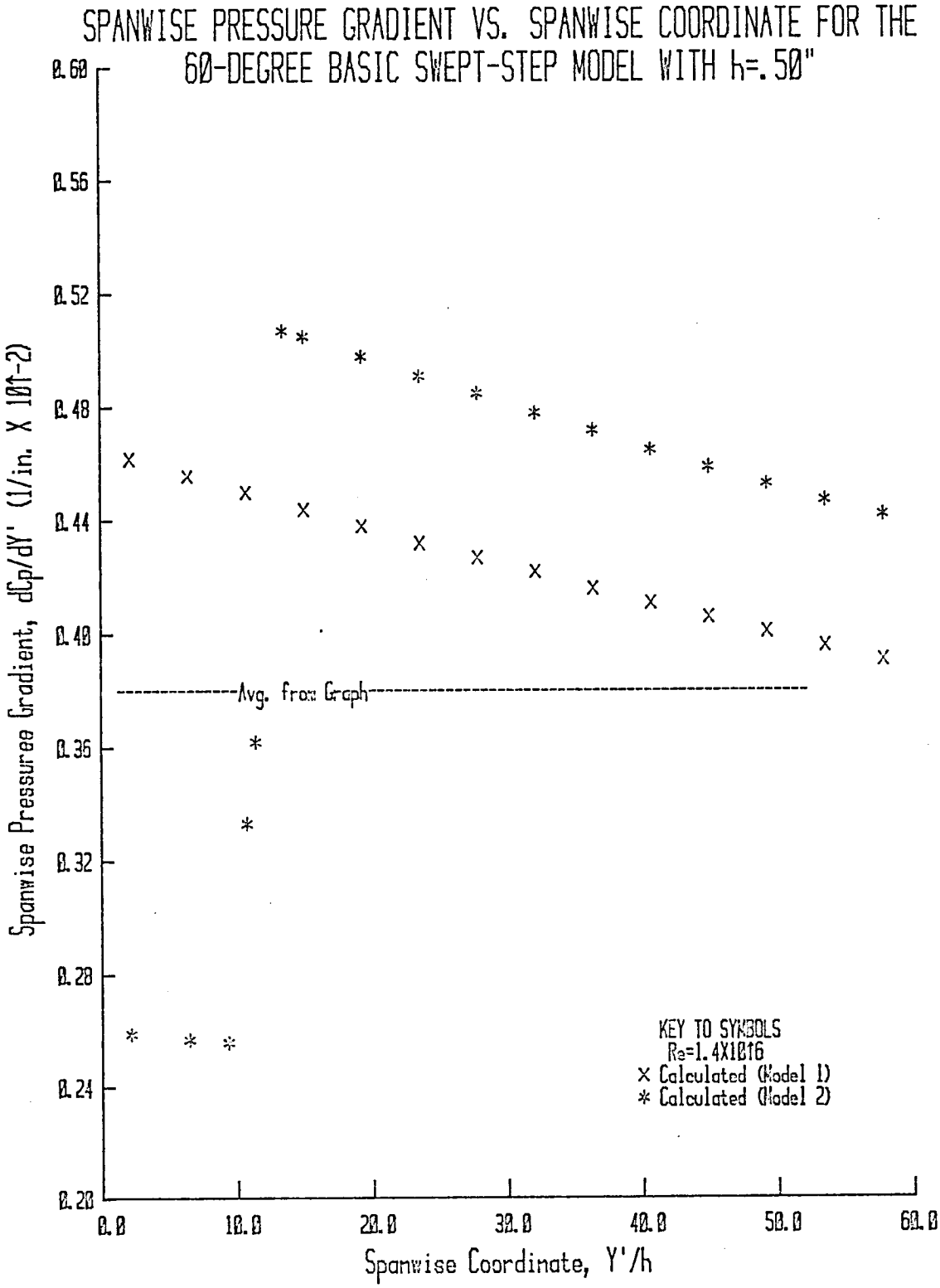
SPANWISE PRESSURE GRADIENT VS. SPANWISE COORDINATE FOR THE 60-DEGREE BASIC SWEPT-STEP MODEL WITH h=.50"
Spanwise Pressure Gradient, dCp/dY' (1/in. X 10↑-2)
0.60
0.56
0.52
0.48
0.44
0.40
0.36
0.32
0.28
0.24
0.20
Avg. from Graph
KEY TO SYMBOLS
Re=1.4X10↑6
× Calculated (Model 1)
* Calculated (Model 2)
0.0
10.0
20.0
30.0
40.0
50.0
60.0
Spanwise Coordinate, Y'/h

Figure B4.

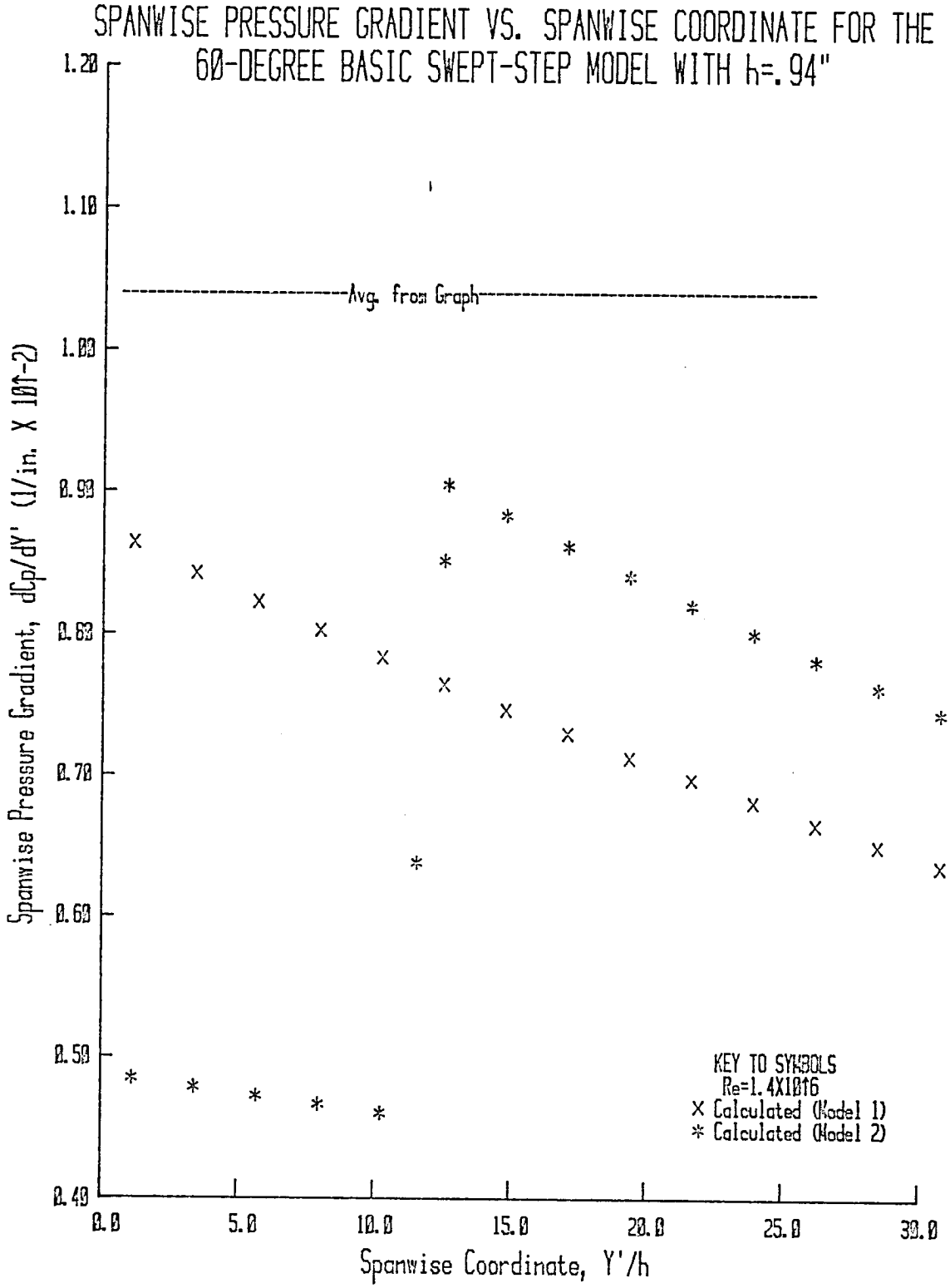
SPANWISE PRESSURE GRADIENT VS. SPANWISE COORDINATE FOR THE 60-DEGREE BASIC SWEPT-STEP MODEL WITH h=.94"
Avg. from Graph
Spanwise Pressure Gradient, dCp/dY' (1/in. X 10↑-2)
Spanwise Coordinate, Y'/h
1.20
1.10
1.00
0.90
0.80
0.70
0.60
0.50
0.40
0.0
5.0
10.0
15.0
20.0
25.0
30.0
KEY TO SYMBOLS
Re=1.4X10↑6
X Calculated (Model 1)
* Calculated (Model 2)

roof steps are not used, the results usually do not genuinely pertain to flow over rearward-facing steps.

The effect of the subject coupling on physical features of the flow in the separated region is discussed herein in Sections 3.3.3 and 3.5.2.

APPENDIX C

CORRELATION BETWEEN SWIRL ANGLE AND SWEEP ANGLE

It is evident from the swirl angle data presented in Section 3.4.4 that there is a direct relationship between swirl angle and sweep angle. The explanation for the apparent equality of swirl angle and sweep angle does not follow as easily—the reason is not obvious to a casual examiner. Therefore, an attempt was made to predict swirl angle based on the measured pressure distribution, Bernoulli's equation, the Independence Principle and a "Spring Vortex Model."

The mean velocity in the inviscid region at the location of the reference static pressure orifice, $(V_m)_{ref}$, was resolved into components u and w as shown in Figure C1. The w component was assumed to remain constant as one proceeds downstream pass the step (based on the Independence Principle as discussed in Section 3.3.3). The u component was altered based on Bernoulli's equation and the applicable measured pressure distribution. The flow angle, ϕ', at the reference pressure location was assumed to be equal to Λ, i.e., two-dimensional flow.

From Bernoulli's equation,

$$P_{x'} - P_{ref} = 1/2\,\rho\,[u^2 - u_{x'}^2] \qquad (C1)$$

Figure C1.

Definition of Pertinent Parameters Relating to Swirl Angle-Sweep Angle Correlation.

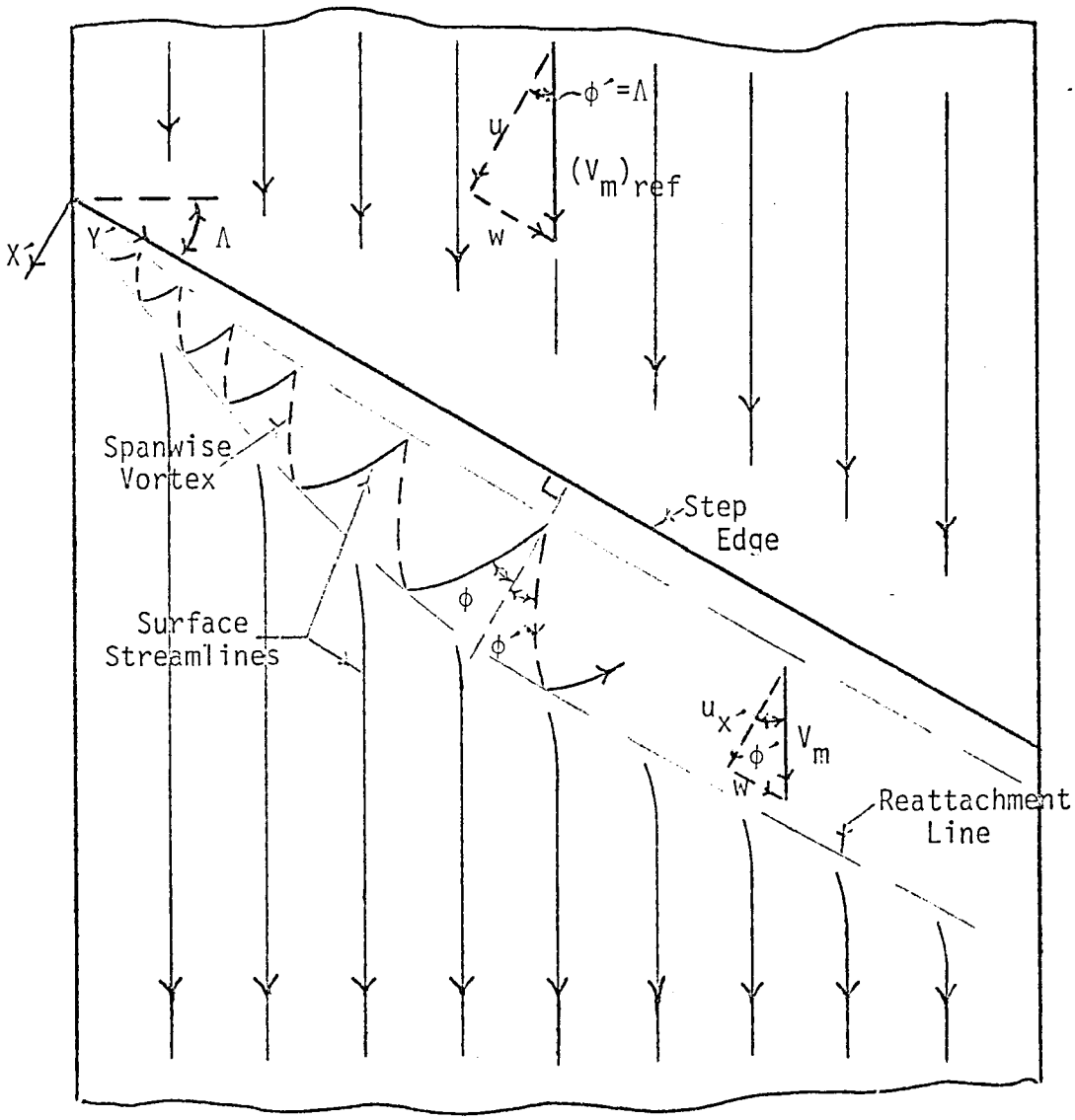

and the defining relation for the pressure coefficient,

$$C_p = (P_{x'} - P_{ref})/1/2\,\rho V_\infty^2 \qquad (C2)$$

where $P_{x'}$ is the measured static pressure at some specified X' position, P_{ref} is the static pressure at the reference location, $u_{x'}$ is the velocity component normal to the step in the inviscid region at X' and V_∞ is the freestream velocity measured at the leading edge of the model. From Equations (C1) and (C2) one can obtain

$$u_{x'} = [u^2 - V_\infty^2\, C_p]^{1/2} \qquad (C3)$$

which allows one to write

$$\phi' = \tan^{-1}[(V_m)_{ref} \sin \Lambda/(u^2 - V_\infty^2\, C_p)^{1/2}] \qquad (C4)$$

Values calculated from Equation (C4) for the inviscid flow angle, ϕ', are presented in Figure C2. One can readily observe that in the region $0 < X' < 6h$ for $\Lambda = 15°$ and $30°$, the flow angle is nearly equal to the sweep angle. Also, for $\Lambda = 60°$, the values shown in Figure C2 are in the same range as those experimentally observed for the swirl angle.

The inviscid flow angle can be related to the swirl angle through a "Vortex Spring Model." The inviscid flow angle just above the

Figure C2.

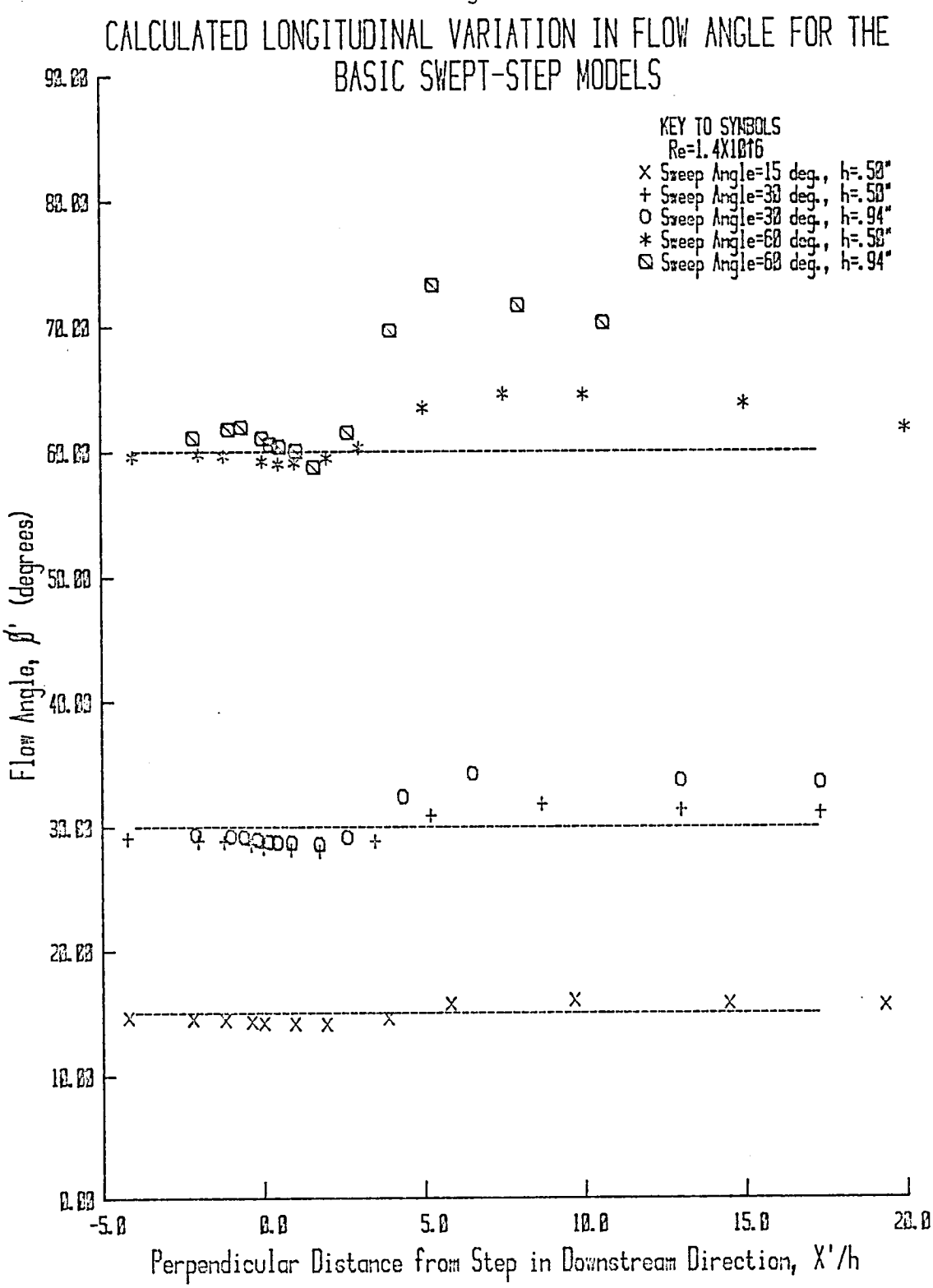
CALCULATED LONGITUDINAL VARIATION IN FLOW ANGLE FOR THE BASIC SWEPT-STEP MODELS
KEY TO SYMBOLS
Re=1.4X10^6
× Sweep Angle=15 deg., h=.50"
+ Sweep Angle=30 deg., h=.50"
O Sweep Angle=30 deg., h=.94"
* Sweep Angle=60 deg., h=.50"
⊠ Sweep Angle=60 deg., h=.94"
Flow Angle, β' (degrees)
90.00
80.00
70.00
60.00
50.00
40.00
30.00
20.00
10.00
0.00
-5.0
0.0
5.0
10.0
15.0
20.0
Perpendicular Distance from Step in Downstream Direction, X'/h

plane of dividing streamlines is assumed to be equal to the flow angle in the vortex just beneath this plane. Then, based on the Spring Vortex Model, ϕ' is equal to the flow angle on the surface—the swirl angle, ϕ.

Therefore, the experimental observation that the swirl angle is essentially equal to the sweep angle has been verified subject to the assumptions previously stated.